

**Hydro-chemical Characterization of Lower and Middle
Teesta Basin, Sikkim Himalaya**

A Thesis Submitted

To

Sikkim University



In Partial Fulfilment of the Requirement for the

Degree of Doctor of Philosophy

By

Paolenmang Haokip

Department of Geology
School of Physical Sciences
Sikkim University

November 2023

ABSTRACT

Purpose: In the present research work, the Teesta River of Sikkim Himalaya, India, was selected for hydrogeochemical characterization studies owing to its importance nationally as well as internationally because it flows through Sikkim and West Bengal in India as well as in Bangladesh and for various uses of its water. The study's goal is to describe the hydro-chemical characteristics of the Lower and Middle Teesta River to know the near source characteristics. The primary objectives are morphometric analysis of the sub-watershed in the study area for earth's natural processes, to investigate the spatio-temporal variability of hydrochemical characteristics and to find the impact of Land Use/Land Cover changes and anthropogenic activities on the water quality in the study area.

Methods and Materials: To achieve the first objective of the study, various datasets have been utilized which include (a) Advanced Spaceborne Thermal Emission and reflection Radiometer - Digital Elevation Model (ASTER DEM) data of 30 m spatial resolution for drainage generation; (b) Sentinel-2A of 10 m spatial resolution (band 2, 3, 4 and 8) to generate land cover details of the study area using supervised classification and to validate the drainage network derived from ASTER DEM; also ancillary datasets such as Geological Map from Bhukosh, GSI to understand the geology, Watershed Map published by Soil and Land Use Survey of India (SLUSI) to validate the watershed which have been generated. Additional information of the study area was collected during field survey. In this study, morphometric parameters such as linear, areal and relief were generated using ASTER DEM with Spatial Analyst Tools (ArcGIS 10.2). For land cover classification (LC) of the study area, multispectral Sentinel-2A data of S2MS12A product type with 10 m spatial

resolution acquired on 16 December, 2018 was used. And to generate soil erosion susceptibility map w.r.t water quality for natural hazards Multi-Criteria Analysis (MCA) method was adopted.

For hydrochemical characterization water samples were collected during both the pre-monsoon and post-monsoon seasons for two years, 2019 and 2021. To collect water samples, pre-cleaned HDPE bottles with a capacity of 1 liter were utilized, following the procedures outlined in APHA (2005). The collected water samples were transported to the laboratory for further analysis. Each sample was divided into two portions (acidified and non-acidified) – 500 ml each and stored refrigerator under 4° Celsius separately for further chemical analysis. A total of 236 samples were collected for two seasons (pre-monsoon and post-monsoon) for two years, 2019 and 2021 from 59 locations in the study area.

Physiochemical parameters such as pH, Temperature, Electrical conductivity (EC), Total dissolved solids (TDS), Turbidity (NTU) and Dissolved Oxygen (DO) were measure on the site of the study area using portable hydro-physiochemical analyzer, Horiba -U50.

Major ions such as F^- , Cl^- , NO_3^- , Alkalinity, Na^+ , K^+ , Ca^{2+} , and Mg^{2+} , and heavy metals such as Mn, Fe, Ni, Cu, Zn, As, Ba and U were analyzed at laboratory using analytical instruments such as Ion Chromatography (IC) and Inductively Coupled Plasma Mass Spectrometry (ICP-MS) whereas, alkalinity was measured using titration method. To analyze the water quality w.r.t heavy metals pollution water indices such as Heavy Metal Pollution Index (HPI), Contamination Factor (CF) and Heavy Metal Index (HEI) method was used.

To understand the impact of Land/Land Cover changes and anthropogenic activities LULC Map of Rani Khola watershed area was generated from multispectral Sentinel-2A data of S2MS12A product type with 10 m spatial resolution and various Google Earth scenes for particular location within the study area was utilized.

To identify the principal components of hydro-chemical data and deduce the main factors controlling water quality, multivariate statistical analyses, such as Pearson's correlation analysis, and Principal Component Analyses (PCA), were employed.

Findings: This study offers a detailed evaluation of the geochemical characteristics and the processes that exert control over the chemical composition of the Teesta River in the Sikkim Himalaya. By analyzing morphometric parameters and integrating land use/land cover (LU/LC) data, the study identifies areas susceptible to erosion, which subsequently have a discernible impact, either direct or indirect, on the river's hydrochemical composition. The dominant major ions in the water follow a specific order, with $\text{Ca}^{2+} > \text{Na}^+ > \text{Mg}^{2+} > \text{K}^+$ for cations and $\text{HCO}_3^- > \text{SO}_4^{2-} > \text{NO}_3^- > \text{Cl}^-$ for anions. Notably, hydrochemical attributes exhibit marked spatio-temporal variations, as depicted by the descriptive statistical data. Piper Diagram and Durov Plot. classified the different types of water in the study area respectively Ca-HCO₃ type, followed by a Mixed Ca-Mg-Cl type and HCO₃-Ca type and Calcite Gypsum water type in both seasons for each year. Furthermore, an assessment of the Water Quality Index and various parameters related to irrigation quality, all based on major ions, underscores that the river's water quality rates as excellent to good, suitable for both domestic use and irrigation. Factors controlling the water quality was depicted by Gibbs Diagram and Na-normalized molar ratios mixing diagram.

Analysis of the Rani Khola watershed, a part of our study area, from 2010 to 2021, reveals notable changes in Land Use and Land Cover (LU/LC). Notably, there's an increase of 0.93% in Agricultural and 0.8% in Built-up Areas, while Water Bodies decrease by 0.03% and Forest Area by 1.7%. Google Earth images of locations, Ranipool, Kumrek, and Majitar at the lower part of Teesta River change in land-use, including the emergence of small-scale industries. The development of these industries raises concerns about potential pollution impacting the region's hydrochemistry. An analysis of Heavy Metal Pollution Indices (HPI, CF & HEI) identifies heavy metal contamination in the lower portion of the study area, emphasizing the environmental challenges in the region. Lastly, PCA analysis validates the hydrochemistry in the area is influenced by both natural (erosion, weathering) and anthropogenic factors (industrial processes, land use changes). This complex interplay dictates water quality.

Conclusion: The following conclusion are drawn from the present study:

- Morphometric parameters analysis along with LU/LC of the study area helps in finding soil erosion susceptibility zone which may contributes to hydro-chemical characteristics.
- Hydro-chemical attributes exhibit perceptible spatio-temporal variations in the study area as indicated by descriptive statistical analysis.
- The order of dominance of major ions follows $\text{Ca}^{2+} > \text{Na}^{+} > \text{Mg}^{2+} > \text{K}^{+}$ for cations, and $\text{HCO}_3^{-} > \text{SO}_4^{2-} > \text{NO}_3^{-} > \text{Cl}^{-}$ for anions.

- Piper Diagram and Durov Plot. classified the different types of water in the study area respectively Ca-HCO₃ type, followed by a Mixed Ca-Mg-Cl type and HCO₃-Ca type and Calcite Gypsum water type in both seasons for each year.
- Gibbs Diagram and Na-normalized molar ratios mixing diagram which depicted the factors controlling the hydrochemistry in the study area shows that the water chemistry is controlled by rock weathering.
- The Water Quality Index (drinking purpose) results indicate that the water quality is excellent for domestic use in terms of major ion concentration.
- The water quality assessment of the Teesta River reveals a spectrum that spans from excellent to suitable for agricultural purposes, as evidenced by the outcomes of multiple comprehensive indices. These indices, including the Permeability Index, Kelly's Index, Wilcox Diagram, and Residual Sodium Carbonate, collectively provide a thorough evaluation of the Teesta River in the context of agriculture.
- Heavy Metal Pollution Index (HPI) is a comprehensive metric that amalgamates the influence of individual heavy metals, on the overall water quality. Similarly, the Contamination Factor (CF) and Heavy Metal Evaluation Index (HEI) offer additional dimensions of assessment. The results derived from these indices reveal that certain samples from the lower Teesta River exhibit noteworthy variations in heavy metal pollution levels during the pre-monsoon season.
- The analysis of LU/LC patterns within the Rani Khola watershed, situated within the study area, unveils significant changes over the decade from 2010 to 2021. Notably, there is a discernible increase in the extent of Agricultural and Built-up Areas by 0.93% and 0.8%, respectively. In contrast, there has been a marginal

reduction in Water Bodies and a more substantial decline in Forest Area, shrinking by 0.03% and 1.7%, respectively, during this period. A closer examination through Google Earth image comparisons for areas such as Ranipool, Kumrek, and Majitar at the lower region of Teesta River brings transformations in land use. These changes are particularly evident in the emergence of new small-scale industrial ventures within the region. The development of these industries raises concerns as they have the potential to introduce pollutants into the water chemistry of the area.

- The PCA analysis indicates that hydrochemical parameters in the study area result from the interplay of natural and anthropogenic factors. Natural processes, such as erosion and weathering, release solutes into the water, influencing its composition. Anthropogenic activities, such as industrial processes and land use changes, introduce pollutants and alter the water's natural attributes. This complex interaction of natural and human-induced factors collectively dictates the hydrochemistry of the area.

Keywords: Teesta Basin, Hydro-chemistry, Major ion, Heavy metals, Morphometry, Soil erosion, LULC, Sikkim Himalaya.

DECLARATION

I hereby confirm that I conducted the research for my Ph.D. thesis, titled "Hydro-chemical Characterization of Teesta Basin, Sikkim Himalaya," as a part of the requirements for the Doctor of Philosophy (Geology) degree at Sikkim University. This research was conducted under the guidance of Dr. Md. Abdullah Khan, as my supervisor.

I also attest that the content of this thesis has not been previously submitted for any degree or diploma at Sikkim University or any other institution. To the best of my knowledge, there is no material in this thesis that has been published or authored by another person, except when appropriate acknowledgments are provided within the thesis text. Additionally, this thesis does not contain any material that violates copyright.

Furthermore, I affirm that the content of this thesis is primarily based on my fieldwork and information gathered from previously published literature, which has been appropriately cited in the references. It is an original work and not a partial or complete copy of any prior reports. I am submitting this thesis to the Department of Geology at Sikkim University as part of the requirements for obtaining a Doctor of Philosophy in Geology.

Date : 7th November 2023

Place : Gangtok

**Paolenmang Haokip
16/Ph.D./GEO/03
Department of Geology
Sikkim University**

ACKNOWLEDGEMENT

I wish to convey my profound appreciation to my supervisor Dr. Md. Abdullah Khan without whom this academic endeavor of mine would not have been possible. I am so grateful for his guidance and support throughout my research work. I would like to sincerely thank the Department of Geology, Sikkim University, Gangtok, Sikkim for giving me this opportunity to carry out this Ph.D. work.

I would like to thank Dr. Rakesh Kumar Ranjan, Head of the Department of Geology, Sikkim University, for providing departmental facilities. I also acknowledge my gratitude to Prof. Anil Kumar Misra, Professor, for all valuable suggestions, encouragement from time to time for completing this research work.

I am grateful to the faculty members of the Department of Geology, Sikkim University namely Prof. Vikram Gupta, Dr. Nischal Wanjari, Dr. Anand G. Badekar and Om Prakash Kaptan for their encouragement and valuable suggestions.

I am greatly indebted to Dr. Horthing V. Zimik, Scientist C, CSIR-NIO, Goa for helping me throughout my analysis and interpretation. I cannot express my feelings in words to acknowledge his guidance and support which he has rendered on me during my research work.

I would also like to show my deep gratitude to Mr. Bhanu Manger, Mr. Dinesh Rai and Mr. Abhishek Rai, Lab Attendant, Department of Geology, for helping me with all my laboratory work.

I would also like to thank my friends and colleagues, Mr. Raj Kumar Priya and Miss Tanya Srivastava for their valuable suggestions and support throughout the research work.

I am also grateful to Stuti Borgohain, Khushboo Sharma, Kriti Rai, Deepika Dutta, Priyanka Kumari, Kuldeep Dutta, Rajeev Rajak, Maadhushree Phukan, Lalit Pokhrel and Sargam Lohar who have always been by my side at the time of need, encouraging me, motivating, and supporting me whenever needed. I would also like to thank other staff members of Sikkim University for their help and support.

I specially thank DST's Center of Excellence Department of Geology, Sikkim University for providing access to the laboratory facilities for analyzing my water samples.

I am sincerely thankful to UGC for providing financial assistance (Non-NET Fellowship) without which this research would not have been possible. I would also like to acknowledge the Forest Department, Government of Sikkim and the Indian Army for their help and permission to carry out the field work in the North Sikkim. Gratitude is also extended to Soil and Land Survey of India, Bhukosh, Geological Survey of India for providing necessary ancillary maps for the course of my research work.

I sincerely would express my deepest respect and gratitude to my parents and family whose keen help and encouragement supported me at every stage, without their blessings nothing would have been possible for me. And last but not the least, I would like to thank Lord Almighty for all His blessings and guidance. Grateful for everything.

Date : 7th November, 2023
Place : Gangtok

Paolenmang Haokip

माइल, सामदुर, तादोंग - 737102
गंगटोक, सिक्किम, भारत
फोन-03592-251212, 251415, 251656
फैक्स - 251067
वेबसाइट - www.cus.ac.in



सिक्किम विश्वविद्यालय SIKKIM UNIVERSITY

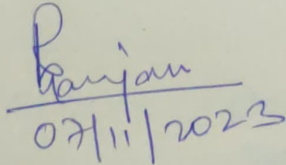
6th Mile, Samdur, Tadong-737102
Gangtok, Sikkim, India
Ph. 03592-251212, 251415, 251656
Telefax : 251067
Website : www.cus.ac.in

(भारत के संसद के अधिनियम द्वारा वर्ष 2007 में स्थापित और नैक (एनएएसी) द्वारा वर्ष 2015 में प्रत्यायित केंद्रीय विश्वविद्यालय)
(A central university established by an Act of Parliament of India in 2007 and accredited by NAAC in 2015)

Date: 7 November 2023

CERTIFICATE

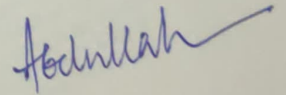
This is to certify that the thesis work entitled "*Hydro-chemical Characterization of Lower and Middle Teesta Basin, Sikkim Himalaya*" has been carried out in the Department of Geology, Sikkim University by **Mr. Paolenmang Haokip** for the partial fulfillment of the award of degree of **Doctor of Philosophy (Geology)**. This work is original and has not been submitted in part or full, for any other degree or diploma in any University/Institution.


07/11/2023

(Dr. Rakesh Kumar Ranjan)

Head
Associate Professor
Department of Geology
Sikkim University

अध्यक्ष/प्रभारी
Head/In-charge
शु-विज्ञान विभाग
Department of Geology
सिक्किम विश्वविद्यालय
Sikkim University



(Dr. Md. Abdullah Khan)

Supervisor
Assistant Professor
Department of Geology
Sikkim University

Assistant Professor
Department of Geology
School of Physical Sciences
SIKKIM UNIVERSITY
Gangtok, Sikkim

6 माइल, सामदुर, तादोंग -737102
गंगटोक, सिक्किम, भारत
फोन-03592-251212, 251415, 251656
टेलीफैक्स -251067
वेबसाइट - www.cus.ac.in



6th Mile, Samdur, Tadong -737102
Gangtok, Sikkim, India
Ph. 03592-251212, 251415, 251656
Telefax: 251067
Website: www.cus.ac.in

सिक्किम विश्वविद्यालय SIKKIM UNIVERSITY

(भारत के संसद के अधिनियम द्वारा वर्ष 2007 में स्थापित और नैक (एनएएसी) द्वारा वर्ष 2015 में प्रत्यायित केंद्रीय विश्वविद्यालय)
(A central university established by an Act of Parliament of India in 2007 and accredited by NAAC in 2015)

Date: 06/11/2023

PLAGIARISM CHECK REPORT

This is to certify that the plagiarism check has been carried out for the following Ph.D. Thesis with the help of **DrillBit Software**, and the result is **2%** similarity which is within the permissible limit (below 10% tolerance rate) as per the norms of Sikkim University.

“Hydro-chemical Characterization of Lower and Middle Teesta Basin, Sikkim Himalaya”

Submitted by Mr. Paolenmang Haokip under the supervision of **Dr. Md. Abdullah Khan**, Assistant Professor, Department of Geology, School of Physical Sciences, Sikkim University, Gangtok, Sikkim.

(Mr. Paolenmang Haokip)

Signature of Research Scholar

(Dr. Md. Abdullah Khan)

Signature of Supervisor

Vetted by Librarian

Assistant Professor
Department of Geology
School of Physical Sciences
SIKKIM UNIVERSITY
Gangtok, Sikkim

पुस्तकालयाध्यक्ष
LIBRARIAN
केन्द्रीय पुस्तकालय Central Library
सिक्किम विश्वविद्यालय
SIKKIM UNIVERSITY

TABLE OF CONTENTS

	Page No
Abstract	i-vi
Declaration	vii
Acknowledgement	viii-ix
Certificates	x-xi
Table of Contents	xii-xiii
List of Tables	xiv-xv
List of Figures	xvi-xviii
Chapter 1 Introduction	1-35
1.1 Geographical Overview of the Teesta River Basin	5
1.2 Human Settlements and Land Use	10
1.3 Hydrology of the River Teesta	10
1.4 Chemical Components of River Water	12
1.5 Spatial Distribution of Chemical Constituents	13
1.6 Sources and Origins of Chemical Contaminants	15
1.7 Ecological and Environmental Implications	17
1.8 Hydro chemical faces and evolution of the Teesta River	19
1.9 Impact of human activities on the hydrochemistry of the Teesta Basin	21
1.10 Isotopic Signatures and Their Implications	22
1.11 Water Quality Index	24
1.12 Management strategies for improving the Teesta Basin's water quality	31
1.13 Statement of the Problem	33
1.14 Research Gap	34
1.15 Aims and Objectives	35

Chapter 2	Review of Literature	35-67
Chapter 3	Method and Material	68-86
3.1	Introduction	68
3.2	Study area	68
3.3	Field surveys and collecting samples	71
3.4	Analytical data analysis	74
3.5	Preliminary survey	75
3.6	Hydro-chemical analysis	77
3.7	Erosion susceptibility test	82
3.8	Multivariate statistical analysis	84
Chapter 4	Result and Discussion	87-167
4.1	Introduction	87
4.2	Soil erosion susceptibility	87
4.3	Assessment of major ions of Teesta River	100
4.4	Hydro-chemical facies	105
4.5	Factors controlling Hydro-chemistry	111
4.6	Water Quality Assessment	118
4.7	Assessment of Heavy metals of Teesta River	129
4.8	Comparison of LU/LC in Rani Khola Watershed	139
4.9	Multivariate Statistical Analysis of Teesta River	146
4.9	Discussion	164
Chapter 5	Conclusion	168-170
	References	171-185
	Appendix	186-198

List of Tables

	Page No
Table 1: Water Quality Ranges	25
Table 2: Weighing parameters related to water quality	26
Table 3: Preliminary survey of the study area during the initial period of research	76
Table 4: Estimations of drainage morphometry linear parameters	82
Table 5: Estimations of drainage morphometry areal parameters	83
Table 6: Estimation of drainage morphometry relief aspects	84
Table 7: Number of Streams of the study area	89
Table 8: Stream Length of the study area	90
Table 9: Morphometry based watershed prioritization for erosion susceptibility of study area.	92
Table 10: Accuracy assessment of supervised land cover classification of study area.	95
Table 11: LULC based watershed prioritization for erosion susceptibility of study area	96
Table 12: Watershed prioritization for erosion susceptibility of study area based on the combined influences of morphometry and land cover.	96
Table 13: Descriptive statistical representation of major ions conc. in the Teesta river basin, shown in mg/L (2019)	100
Table 14: Descriptive statistical representation of major ions conc. in the Teesta river basin, shown in mg/L (2021)	101
Table 15: Descriptive statistical graphical presentation using bar graph for Spatio-temporal variation of major ions, & pH	103
Table 16: Concentration of ions, standard limit and weight index for WQI	118
Table 17: Descriptive statistical representation for concentration of Heavy Metals in the Teesta River basin (2019)	130
Table 18: Descriptive statistical representation for concentration of Heavy Metals in the Teesta River basin (2019)	132
Table 19: Heavy Metal concentration with permissible limit of BIS and WHO	134
Table 20: KMO and Bartlett's test for PrM hydro-chemistry data 2019	156

Table 21: Loadings of experimental variables on the first 5 PCs for PrM hydro-chemistry data 2019.	156
Table 22: KMO and Bartlett's test for PoM hydro-chemistry data 2019	158
Table 23: Loadings of experimental variables on the first 5 PCs for PoM hydro-chemistry data 2019.	158
Table 24: KMO and Bartlett's test for PrM hydro-chemistry data 2021.	160
Table 25: Loadings of experimental variables on the first 6 PCs for PrM hydro-chemistry data 2021.	160
Table 26: KMO and Bartlett's test for PoM hydro-chemistry data 2021	162
Table 27: Loadings of experimental variables on the first 7 PCs for PoM hydro-chemistry data 2021	162

List of Figures

	Page No
Figure 1-1: Geographical Overview of the Teesta Basin	06
Figure 1-2: Geological map of the study area along with sampling locations	08
Figure 1-3: Ecological and Environment	18
Figure 1-4: Isotopic signatures of river water	23
Figure 3-1: Study area map	70
Figure 3-2: Flow chart methodology for hydrochemistry analysis	72
Figure 3-3: Flow chart methodology for prioritization analysis	74
Figure 4-1: Drainage Map of study area	89
Figure 4-2: Erosion Susceptibility map based on drainage morphometry	91
Figure 4-3: LULC Map of study area	93
Figure 4-4: Erosion Susceptibility map based on land cover	97
Figure 4-5: Erosion Susceptibility map Based on Morphometry and Land Cover	99
Figure 4-6: Box plot graphical representation of major ions conc. for PrM & PoM 2019	100
Figure 4-7: Box plot graphical representation of major ions conc. for PrM & PoM 2021	102
Figure 4-8: Piper's trilinear diagram, showing the relationship between dissolved ions and hydrochemical facies in the Teesta river basin (2019)	106
Figure 4-9: Piper's trilinear diagram, showing the relationship between dissolved ions and hydro chemical facies in the Teesta river basin (2021)	107

Figure 4-10: Durov diagram 2019, showing the hydrochemical facies in the Teesta river basin	109
Figure 4-11: Durov diagram 2021, showing the hydrochemical facies in the Teesta River basin	110
Figure 4-12: 2019 Gibb's Diagram of the study area	112
Figure 4-13: 2021 Gibb's Diagram of the study area	112
Figure 4-14: Bivariate Na-normalized molar ratios mixing diagram for 2019.	114
Figure 4-15: Bivariate Na-normalized molar ratios mixing diagram for 2021	114
Figure 4-16: Scatter plot of Cl^- vs $\text{Na}^+ + \text{K}^+$ in a) upstream and b) downstream for all waters	115
Figure 4-17: Scatter plot of HCO_3^- vs $\text{Mg}^{2++}\text{Ca}^{2+}$ in a) upstream b) downstream c) $\text{HCO}_3^- + \text{SO}_4^{2-}$ vs $\text{Ca}^{2++}\text{Mg}^{2+}$ for all waters.	117
Figure 4-18: WQI index of the study area	119
Figure 4-19: WQI in 2019 of the study area	120
Figure 4-20: WQI in 2021 of the study area	121
Figure 4-21: Graphical representation of Wilcox diagram showing the relationship between %Na vs EC in the Teesta River basin (2019)	123
Figure 4-22: Graphical representation of Wilcox diagram showing the relationship between %Na vs EC in the Teesta river basin (2021)	124
Figure 4-23: RSC score of the study area	125
Figure 4-24: Permeability Index of the study area	127
Figure 4-25: Kelly's Index of the study area	128
Figure 4-26: Box plot graphical representation of Heavy Metals in Teesta Basin River in 2019	131

Figure 4-27: Box plot graphical representation of Heavy Metals in Teesta Basin River in 2019	132
Figure 4-28: Heavy Pollution Index of the study area	134
Figure 4-29: Contamination factor representation of the study area	135
Figure 4-30: Heavy Metal Evaluation Index of the study area	137
Figure 4-31: LULC Map of Rani Khola Watershed 2000	139
Figure 4-32: LULC Map of Rani Khola Watershed 2010	139
Figure 4-33: Graphical representation of LULC within Rani Khola watershed from 2000 to 2010	140
Figure 4-34: Comparison of Ranipool Landuse Map using Google Earth in 2006 & 2021	141
Figure 4-35: Comparison of Kumrek Landuse Map using Google Earth in 2006 & 2021	143
Figure 4-36: Comparison of Majitar Landuse Map using Google Earth in 2006 & 2021	144
Figure 4-37: Correlation matrix heatmap of 2019 major ions.	146
Figure 4-38: Correlation matrix heatmap of 2021 major ions.	148
Figure 4-39: Correlation matrix heatmap of 2019 trace elements	150
Figure 4-40: Correlation matrix heatmap of 2021 trace elements	152

CHAPTER 1

INTRODUCTION

Introduction

The existence of life on Earth depends on water, making it an essential and irreplaceable resource. It may be found in a variety of states, including the gaseous form in the atmosphere, the liquid state in river channels and subterranean aquifers, and the solid state as snow and glaciers atop mountain peaks and polar ice caps. The location determines not only the amount but also the quality of its occurrences, and these differences might be rather significant.

The state of natural water resources all over the world has been gradually altering as a consequence of slow adjustments in the global climate as well as an increase in the amount of activity generated by people. (Tsering et al., 2019) This is due to the fact that the quantity of activity caused by humans has been slowly increasing. According to the findings of a research that WHO (World Health Organization) commissioned, there are about 1.1 billion individuals who having no access to water that is suitable for drinking. The Himalayan glaciers are melting, which is a direct consequence of climate change on a worldwide scale, is having a detectable influence on the chemical composition of the Himalayan rivers as well as the quantity of pollution produced by dangerous metals. This is due to the fact that the melting of glaciers in the Himalayas is a direct result of global climate change. Because river water is the major source of freshwater for all living things, including people and animals, the availability and quality of river water are two key indicators that must be monitored closely. This is true for both civilization and ecosystems.

Groundwater is an abundant source of water that may be used for agricultural, residential, and drinking purposes, which is crucial for the formation of sustainable societies. Groundwater can be found in underground aquifers. (Islam et al., 2018) At this moment in time, irrigation accounts for forty percent of the world's total consumption of groundwater, while residential uses account for seventy percent of the world's total use of groundwater. As a consequence of the worsening state of the surface water sources, the population has been forced to become more dependent on the water that is found deep inside the earth (groundwater). Because of this, groundwater resources all over the world have been exposed to excessive extraction, which has resulted in their deterioration. This is a direct consequence of the situation. (Pant et al., 2021) However, the chemistry of groundwater is determined in part by the geological make-up of the area, the weathering of rocks, the quality of the water that is used to refill the aquifer, and other sources. Chemical study of water has the potential to provide light on the nature of water in connection to geology, climate, sources, and uses of water. Specifically, the primary ions that may be found in water may be of assistance in describing the geochemical processes that have an effect on the groundwater's quality.

The hydro-chemical characteristics the river's water is an important factor to consider from both an ecological and economic point of view. The total dissolved concentration components the river water is primary factor that determines whether or not the water is suitable for use in residential settings. (Khatri et al., 2023) Ions that have dissolved in water, the most common dissolved elements in river water are magnesium (Mg^{2+}), sodium (Na^+), and potassium (K^+), calcium (Ca^{2+}) as well as bicarbonate (HCO_3), carbonate (CO_3), sulphate (SO_4^{2-}), chloride (Cl^-), and nitrate (NO_3), The natural and artificial interferences in the watershed may be reflected in the chemical characteristics

of the river area. For example, the predominant riverine source Ca^{2+} , Mg^{2+} , SO_4^{2-} , and HCO_3^- is natural, but the primary source of NH_4^+ and NO_3^- is generated by human activity. Given that the Amazon, Ganges-Brahmaputra, Yellow, Nile, Indus, Mississippi, Mekong, Tigris, and Yangtze rivers all originated on the Tibetan plateau, Since the 1980s, scientists have studied and recorded the chemical signals and variables that govern the hydrochemistry of the world's main rivers. (Bishwakarma et al., 2022) Rock weathering, precipitation, and the crystallization of evaporation are the three processes that have the most influence on the natural hydrochemistry of surface waters. In addition to this, groundwater discharge and both natural processes and human activities significantly alter the hydro chemical composition of surface water. Electrical conductivity (EC), total dissolved solids (TDS), main ions, organic matter, nutritional content, and extra soluble trace elements are some of the broad criteria used to characterize water quality. These parameters are crucial in establishing the overall quality of water used for irrigation. However, TDS, EC, and main ions have been widely utilized as significant benchmarks for assessing the quality of irrigation water. Indeed, in irrigation water, salinity & ion toxicity are major issues (F. T. Ahmed et al., 2021). The ideal conditions for plant growth and soil permeability demand an appropriate amount of water that has a manageable salinity as well as ion toxicity level. The salinity danger, magnesium hazards, as well as sodium hazards are the three most significant salt issues in irrigation water. High levels of salt in irrigation water may harm vegetation. (Bishwakarma et al., 2022) For example, irrigation water with over sixty percent salt may degrade the physical characteristics of the soil. Alkali soils may occur when high Na% combines with carbonate. Similarly, high Ca^{2+} and Mg^{2+} concentrations in irrigation water may modify salinity, raise soil pH, influence the degree of permeability characteristics of soil's root zone, and diminish

phosphorous nutrient availability.

The Himalayan region stands as an ecological treasure trove, possessing a unique blend of biodiversity, hydrological resources, and cultural diversity. Amongst the many rivers that meander through this formidable terrain, the Teesta River emerges as a vital lifeline for the inhabitants of Sikkim, a picturesque Indian state nestled in the Eastern Himalaya. The Teesta Basin, comprising its Lower and Middle regions, plays a pivotal role in establishing the region's ecological and economic conditions. It is within this geographical context that we embark upon an exploration of paramount significance - the hydro-chemical characterization of the Lower and Middle Teesta Basin. The Teesta River, originating from the pristine glacial sources of the Greater Himalayas, traverses its course through steep valleys and dense forests, carrying the legacy of its ecological interactions. In its journey, the river interacts with diverse geological formations, ecosystems, as well as human activities, which all contributes to the chemical makeup of its waters. Understanding this intricate interplay between geology, ecology, and human interventions is essential not only for the sustenance of the local communities but also for the preservation of the Himalayan ecosystem.

The Lower and Middle Teesta Basin, extending from the high-altitude reaches of North Sikkim to the subtropical lowlands of West Bengal, represents a microcosm of the broader challenges facing the Himalayan region. This region is marked by unique hydro-geological features, including active seismic zones, diverse lithological formations, and a rich biodiversity, all of which converge to influence the hydro-chemical composition of the Teesta River. The region's delicate environment is also under increasing pressure from global warming, human interference, and rising human needs. The research aims to

elucidate the complex interplay between hydrological and chemical factors affecting the Teesta River's lower and middle basin. It aims to unravel the unique hydro-chemical signatures of the river, delineate the sources and fate of various chemical constituents, and assess the implications of these findings on both aquatic ecosystems and human communities. By undertaking this study, we seek to add to scientific knowledge of the Himalayan aquatic systems, provide insights into sustainable resource management, and facilitate informed decision-making for the preservation of this fragile yet vital ecosystem. we delve into the depths of hydro-chemical analysis, traversing the diverse landscapes of the Lower and Middle Teesta Basin to understand its water chemistry and the controlling factors. Through rigorous scientific inquiry, we aspire to not only illuminate the ecological intricacies of this region but also advocate for responsible stewardship of the invaluable natural resources it holds.

1.1 Geographical Overview of the Teesta River Basin

The Teesta River Basin, nestled at the centre of the Sikkim Himalaya, is a region of unparalleled geographical diversity and ecological significance. Spanning an area of approximately 12,000 square kilometres, this basin extends from its headwaters in the northern reaches of Sikkim, near the pristine Tsolamo Lake, to its confluence with the Brahmaputra River in the plains of West Bengal, India, and Bangladesh. This geographical expanse encompasses a range of elevations, geological formations, and climatic zones, contributing to the unique hydro-chemical characteristics of the Teesta River.

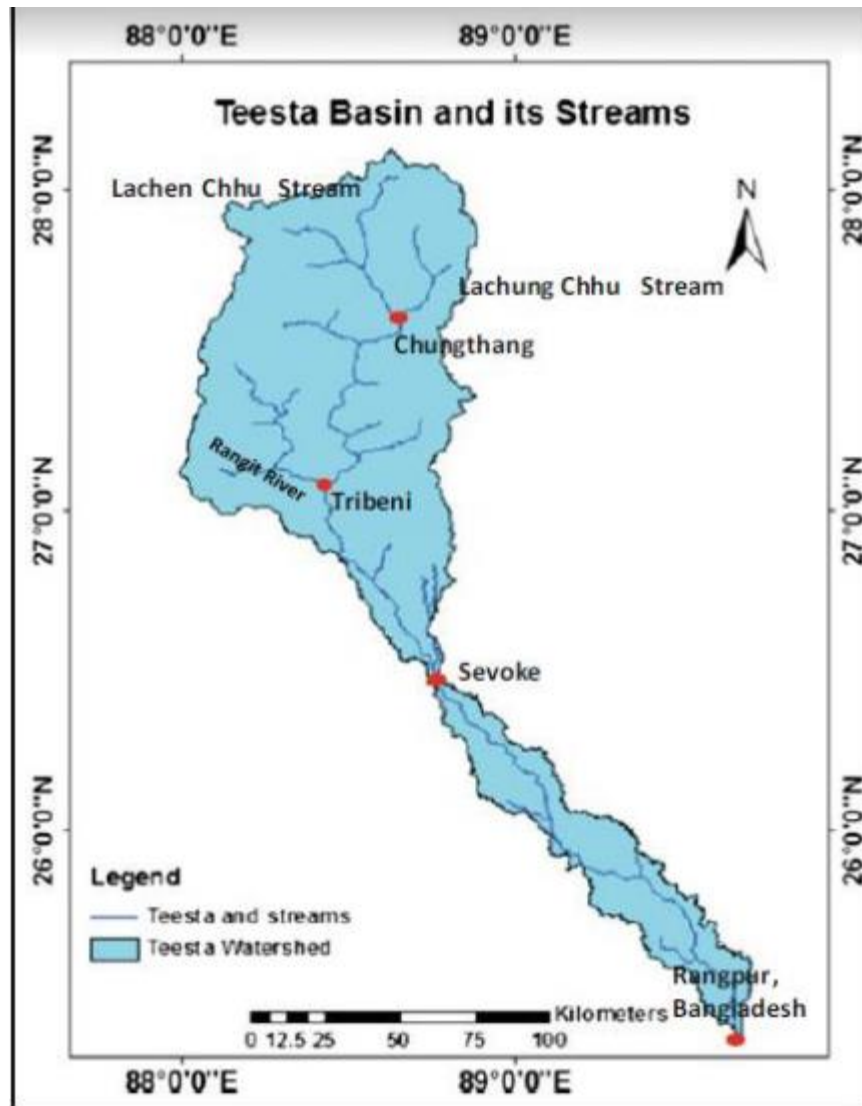


Figure 1-1: *Geographical Overview of the Teesta Basin Goyal, M. K., & Goswami, U. P. (2018)*

In the Himalayas, the Teesta basin is particularly vulnerable owing to erosion, the possibility of landslides, and the frequency of flash floods. Annual monsoon rainfall in the basin may range from 200 mm to more than 600 mm, and the rainfall variability in the basin is particularly high because of the substantial differences in height. (Pal et al., 2016) In compared to the plain one-half of the basin, the mountain section the basin's is subject to much more precipitation. When one considers the influence that variations in

height have on the distribution of rainfall; it is easy to see that foothill regions get a lot of it. From that point on, the amount of rainfall will begin to lessen as the height will have dropped from 2000-2400 m to 600-800 m. (Khan & Ali, 2019) The river basin produces the biggest quantity of silt by volume among the Himalayan Rivers (98.40 cum/ha/year). Additionally, the rate of average annual denudation is the greatest (9.8 mm/yr) among the Himalayan Rivers. These features provide an indication of the behavior of the basin and its vulnerability to natural disasters.

1.1.1 Topography

The Teesta Basin's topography is characterized by extreme variations in altitude. It begins in the Greater Himalayas' high-altitude areas, where glaciers feed the river with pristine meltwater. The river then descends rapidly through steep valleys and gorges, transitioning into the temperate and subtropical zones as it flows southward. This diverse topography profoundly influences the basin's hydrology and the chemical composition of its waters.

1.1.2 Geological Formations

The basin is situated in a seismically active zone, which has shaped its geological diversity. It encompasses a mosaic of rock types, including sedimentary, metamorphic, and igneous formations. These geological substrates influence the mineral content and chemical constituents found in the Teesta River water.

The regional geological setting of the Sikkim Himalaya is prominently manifested by the Teesta gorge, which serves as a major geological feature in the area, with the river flowing predominantly from north to south. This geological setting is

further characterized by a generalized stratigraphic succession, providing insights into the rock formations present in the region.

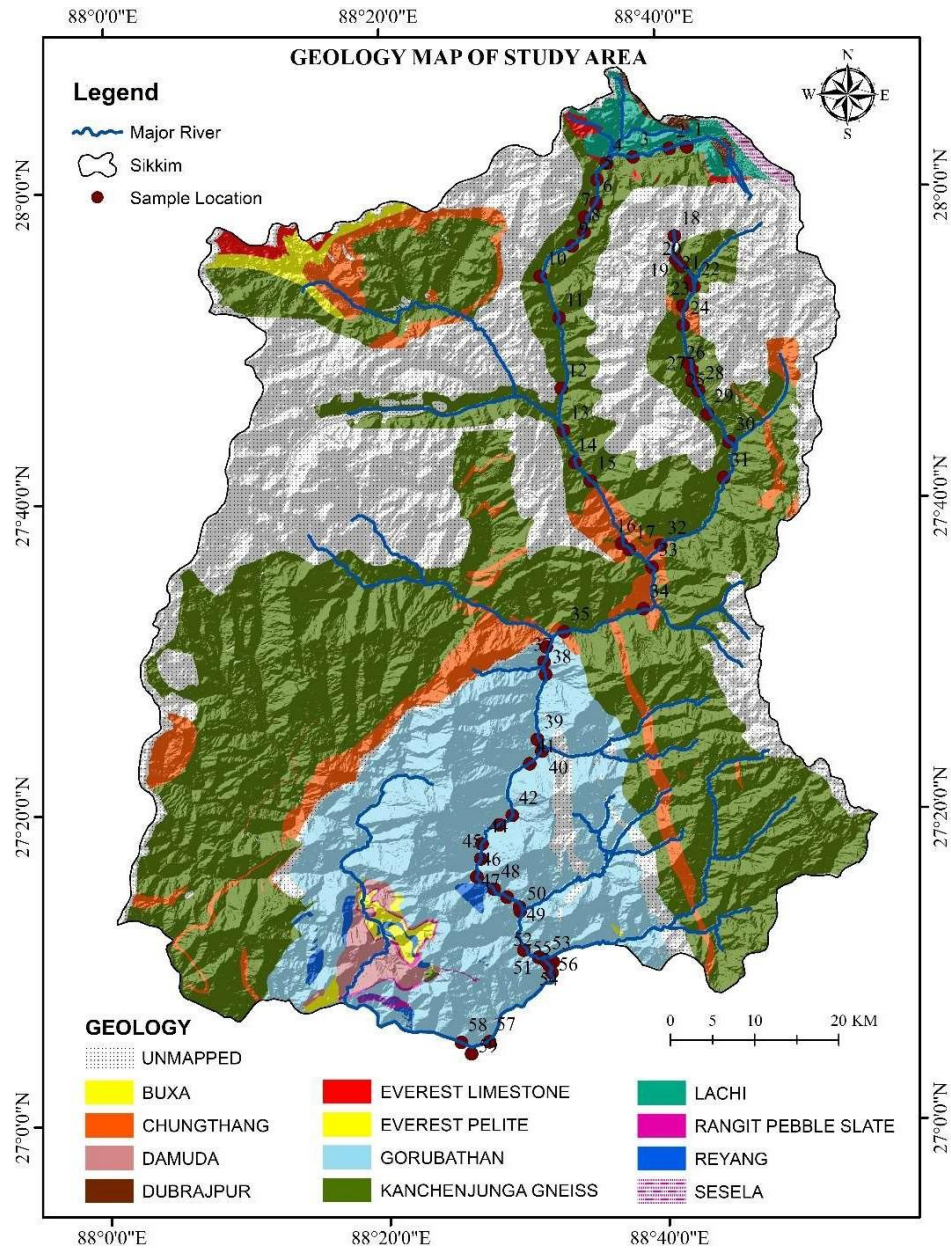


Figure 1-2: Geological map of Sikkim along with the sampling location (Bhukosh, GSI)

In the Axial Zone of North Sikkim, the Central Crystalline take centre stage, comprising calc-granulites, schist, & quartzite are all part of a high-grade meta-

sedimentary sequence. These rock formations are accompanied by gneisses/migmatites and are punctuated by various granitic intrusions. The exposure of the Central Crystalline in this region showcases their significant influence on the overall geological composition.

Within the Teesta basin's southern region in Sikkim, the geological landscape is characterized by a distinct lithological assemblage. The low-grade Pelite-Psammitic assemblage, known as Dalings, dominates this area. It is succeeded by an alternating sequence of sandstone, shale, and coal, collectively referred to as the Gondwana assemblage. The Gondwana rocks are interspersed with notable structural dislocations, adding to the geological complexity of the region. These geological characteristics are crucial to the hydrological dynamics of the river Teesta, and they also contribute to the overall stratigraphy.

Moving further south, a significant tectonic feature, the Main Boundary Fault, separates the Gondwana rocks from the Shiwalik formations. This fault zone acts as a distinct boundary demarcating the geological units and their associated characteristics.

Overall, the regional geological set-up of the Sikkim Himalaya, as exemplified by the Teesta gorge and the stratigraphic succession, highlights the interplay of various rock formations, structural dislocations, and tectonic activity. Understanding these geological aspects is essential for comprehending the Hydrogeochemical dynamics and processes occurring within the Teesta River and its surrounding area.

1.1.3 Climatic Zones

The Teesta Basin straddles various climatic zones, ranging from alpine and sub-alpine climates at the higher altitudes to subtropical and tropical climates lower down

regions. These climatic variations govern the river's flow regime, precipitation patterns, and the sources of both natural and anthropogenic inputs to its chemical composition.

1.1.4 Vegetation and Biodiversity

The basin is adorned with lush vegetation and supports a rich biodiversity. Dense forests, alpine meadows, and wetlands are interspersed throughout the region. The unique flora and fauna contribute to organic matter and nutrient inputs into the river, influencing its hydro-chemical composition.

1.2 Human Settlements and Land Use

The Teesta Basin is not only a vital ecological zone but also home to numerous communities. Human activities, including agriculture, hydropower generation, and urbanization, have intensified in recent years. These activities introduce various chemicals and pollutants into the river, affecting its chemical makeup.

Understanding the geographical intricacies of the Teesta Basin is essential for comprehending the hydro-chemical characteristics of its waters. This diversity, from the glacier-clad peaks from the north to fertile southern plains, creates a dynamic and complex environment where geological, ecological, and human factors converge to influence the Teesta River's chemical makeup. In the subsequent sections of this thesis, we delve deeper into these factors to decipher the hydro-chemical signatures of this vital Himalayan River system.

1.3 Hydrology of the River Teesta

The river Teesta's hydrology is a multifaceted system, reflecting the intricate

dynamics of a river that courses through the diverse landscapes of the Sikkim Himalaya. It exhibits a wide array of flow patterns, driven by its unique geographical characteristics and climatic influences. (Bishwakarma et al., 2022) At its inception, the Teesta originates from the glacial meltwaters of the Greater Himalayas, contributing cold and turbid water to its headwaters. As the river progresses downstream, its flow becomes increasingly regulated, influenced by the confluence of various tributaries and geological features. These flow patterns encompass both high and low flow regimes, each with distinct implications for the river's hydro-chemical composition.

The discharge of the Teesta River presents notable variations throughout the year, underscoring the river's seasonal dynamics. June to September, the monsoon season, is the time of highest discharge. During this time, heavy rainfall and the accelerated melting of seasonal snow significantly augment the river's flow. (Mandal & Chakrabarty, 2016) As a result, the Teesta fills with water, which often causes an increase in sediment movement and changes in the river's chemical composition. In contrast, the dry season, extending from October to May, witnesses a marked reduction in discharge. Reduced precipitation, coupled with diminished snowmelt, contributes to lower flow rates, thereby altering the hydro-chemical characteristics of the river. These seasonal variations in flow have significant ecological and the Teesta Basin's socioeconomic effects. They influence the availability of water resources for various uses, including agriculture, hydropower generation, and domestic consumption. (M. J. Islam et al., 2019) Furthermore, the changing flow regimes can impact the river's aquatic ecosystems, including fish populations and riparian habitats, as well as the transportation of sediments and nutrients downstream. Understanding these hydrological intricacies is crucial for comprehending

the hydro-chemical dynamics of the Teesta River and for devising strategies to manage and conserve this vital Himalayan watercourse. In the subsequent sections of this thesis, we delve deeper into the hydro-chemical aspects of the Teesta River to elucidate its complex interactions with the surrounding environment.

1.4 Chemical Components of River Water

River water's chemical makeup is a multifaceted interplay of natural processes & anthropogenic influences, and it serves as a critical aspect of understanding the hydro-chemical dynamics of the River Teesta in the Lower and Middle Basin of the Sikkim Himalaya. Among the primary chemical components are ions, such as chloride (Cl^-), sodium (Na^+), calcium (Ca^{2+}), and magnesium (Mg^{2+}). These ions, originating from the dissolution of minerals in the surrounding geological formations, contribute to the ionic characteristics of river water. (Zhang et al., 2021) Their concentrations can vary significantly and play pivotal roles in shaping water quality, ecosystem health, and the water's appropriateness for different uses. In addition to ions, river water contains essential nutrients like nitrogen compounds (nitrate and ammonia) and phosphorus compounds (phosphate). These nutrients are derived from both natural sources, such as decaying organic matter, and human activities, notably agriculture and wastewater discharge. Their presence influences the growth of algae and aquatic plants, exerting a profound influence on the quality of water and the overall health of the marine environment.

Trace metals including iron (Fe), manganese (Mn), and zinc (Zn) may be found in abundance in river water. These elements originate from geological sources and atmospheric deposition. While they are present in small concentrations, they can have

significant ecological implications, with elevated levels potentially posing toxicity risks to aquatic organisms and, in some cases, human well-being if drinking water is consumed or irrigation. Organic matter, comprising plant and animal residues and dissolved organic compounds, can influence the colour, taste, and odor of river water. Moreover, it plays a role in the river's ability to transport and bind with other chemical constituents, affecting water chemistry and quality.

pH and alkalinity are fundamental chemical parameters that impact river water. pH measures the acidity or alkalinity of the water, while alkalinity refers to its capacity to neutralize acids. These parameters can be influenced by geological characteristics, land use, and the presence of specific ions, further shaping the river's chemical composition. Furthermore, river water can contain pollutants and contaminants introduced through human activities, encompassing heavy metals, pesticides, industrial chemicals, and pharmaceuticals. Protecting the Teesta River Basin's water quality and ecosystem requires vigilant monitoring and management of these pollutants.

A comprehensive understanding of these chemical components in the Lower and Middle Teesta Basin is essential for assessing the ecological health of the river, its suitability for various uses, and its susceptibility to pollution. Analyzing these constituents and their variations provides invaluable insights into the river's hydro-chemical characteristics, forming the bedrock for informed management and conservation efforts in this ecologically significant Himalayan region.

1.5 Spatial Distribution of Chemical Constituents

Understanding the geographical distribution of chemical components within the

Lower and Middle Teesta Basin is paramount for deciphering the intricate hydro-chemical dynamics of this Himalayan River system. This section delves into the nuanced variations of chemical parameters across different sampling locations within the basin, shedding light on how geological, ecological, and anthropogenic factors converge to shape the river's chemical composition. The spatial distribution of chemical constituents often exhibits distinct gradients from upstream to downstream. In the headwaters of North Sikkim, closer to the river's glacial source, the water is characterized by lower temperatures and carries a heavier load of suspended sediments. As the river courses downstream, it encounters tributaries and undergoes mixing processes, leading to shifts in the concentrations of ions, nutrients, and other chemical constituents.

Altitudinal variations within the basin also exert a significant influence on the river's chemical composition. At higher elevations, such as near the glacier-fed sources, the river may exhibit lower pH values because of the existence of acidic soils as well as organic stuff. Conversely, lower elevations in the subtropical regions may display higher alkalinity. Geological variables have an important influence in shaping the spatial distribution of chemical constituents. Distinct rock types release specific minerals and ions into the river water. Areas with limestone formations, for instance, may lead to higher levels of calcium and carbonate ions. The presence of diverse ecosystems within the basin, including forests, wetlands, and aquatic habitats, can significantly impact chemical constituents' spatial distribution. Vegetation can introduce organic matter and nutrients into the water, influencing its chemistry. Moreover, microbial processes within aquatic environments can further modify nutrient concentrations. Human activities, ranging from agriculture and urbanization to industrial discharge, introduce chemical constituents into

the river at specific locations. These anthropogenic inputs can result in localized hotspots of contamination, therefore influencing the dispersal of pollution and toxins across the environment. The selection of monitoring and sampling points within the basin is of utmost importance for accurately characterizing spatial variations. Different sampling locations, including main stem sites, tributary sites, and areas in proximity to human settlements or industrial zones, offer diverse hydro-chemical profiles.

Through a meticulous examination of the geographical distribution of chemical constituents across the Lower and Middle Teesta Basin, this research seeks to identify patterns, hotspots, and trends that provide critical insights into the river's hydro-chemical behavior. Such knowledge not only aids in understanding the basin's ecological diversity but also informs targeted management and conservation efforts. In subsequent sections, we delve deeper into the sources, consequences, and management implications of these spatial variations in the Teesta River's chemical composition.

1.6 Sources and Origins of Chemical Contaminants

Understanding the sources and origins of chemical contaminants within the Lower and Middle Teesta Basin is pivotal for comprehending the complexities of the river's hydro-chemical composition and for devising effective strategies for environmental protection and remediation. One significant contributor to chemical contaminants is natural sources. In the Teesta Basin, natural sources of these contaminants arise primarily from geological processes. Geological formations, prevalent within the basin, release trace elements and minerals into the river water, significantly contributing to its chemical composition. The dissolution of rocks, including those rich in iron, manganese, and other elements, can elevate their concentrations in the water. Additionally, microbial

transformations of organic matter within the river can produce chemical by-products that influence water chemistry, adding to the intricate blend of constituents.

However, human activities in the basin play a pivotal role in introducing chemical contaminants into the Teesta River. Urbanization within the basin's vicinity leads to the discharge of pollutants like heavy metals, organic contaminants, and nutrients through storm water runoff and wastewater effluents. Industrial activities, particularly in urban areas, release a diverse range of chemical contaminants, including heavy metals, industrial chemicals, and pharmaceuticals. These activities collectively pose substantial risks to water quality and ecosystem health. Another noteworthy factor influencing chemical contaminants is land use changes, particularly deforestation. Such changes can lead to increased erosion and sedimentation due to the removal of vegetation and disruption of natural ecosystems. This alteration in land use can significantly affect the river's chemical makeup. Additionally, deforestation can elevate nutrient levels in the water, as it disrupts the natural nutrient cycling processes within forested areas. The atmosphere also plays a role in introducing chemical contaminants into the Teesta River. Airborne pollutants, such as heavy metals and acidic compounds, can be transported over long distances and subsequently deposited into the river and its catchment area. This process can be influenced by regional and global factors, including industrial emissions and prevailing weather patterns. Lastly, invasive species and alterations in ecological dynamics can impact water chemistry. The introduction of invasive species, particularly invasive plants, can disrupt nutrient cycling and organic matter decomposition rates, leading to changes in water chemistry that can have cascading effects throughout the ecosystem. Understanding these multifaceted sources and origins of chemical

contaminants is essential for mitigating their impacts and implementing effective management strategies for preserving the environmental and the condition of the Teesta River's lower and middle basin water supplies.

1.7 Ecological and Environmental Implications

The hydro-chemical properties of the Teesta River in the Lower and Middle Basin have profound implications for the river's aquatic ecosystems and the surrounding environment. These implications extend to various facets of the river's ecology, with far-reaching consequences. Firstly, aquatic ecosystems within the Teesta River are significantly influenced by its hydro-chemical composition. Variations in water chemistry, including nutrient levels, pH, and the presence of contaminants, play pivotal roles in shaping the composition and abundance of aquatic flora and fauna. Elevated nutrient concentrations, for instance, can lead to excessive algal growth, potentially causing algal blooms. Such blooms can result in oxygen depletion, harming fish populations and other aquatic life, disrupting the balance within these ecosystems.

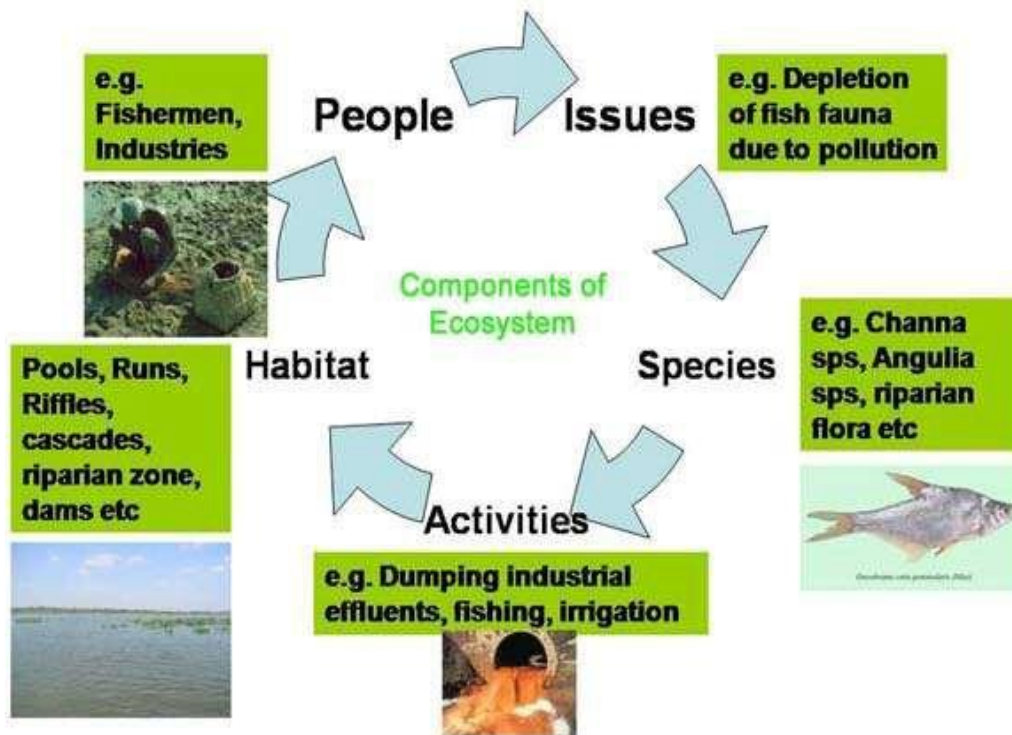


Figure 1-3: *Ecological and Environment (Heda, N. (2007))*

The implications are not confined solely to aquatic ecosystems but also extend to the biodiversity of the Teesta Basin. The region is characterized by a varied and high species diversity, both aquatic and terrestrial. Changes in water chemistry can disrupt the ecological balance and habitats that are crucial for these species. Altered pH levels and the presence of contaminants can directly impact the health of aquatic organisms. This is particularly concerning for sensitive species, such as amphibians and certain fish species, which may experience reduced populations and compromised health. Water quality is another pivotal aspect affected by the Teesta River's hydro-chemical makeup. It's not only fish that rely on the river's high-quality water but additionally for human consumption as well as agriculture in the neighboring areas. Variations in chemical constituents,

particularly the presence of pollutants and contaminants, can render the water unsuitable for these purposes. People living along the river, on which they depend for both drinking water and agricultural irrigation, are at serious danger as a result of this, potentially resulting in adverse health effects and decreased agricultural productivity.

Moreover, alterations in the Teesta River's hydro chemical composition can influence sediment transport dynamics. Changes in flow patterns, often associated with shifts in water chemistry, can affect sediment deposition and erosion rates within the river. This, in turn, has implications for riverbed stability, erosion control, and the maintenance of riparian habitats. In summation, the hydro-chemical characteristics of the Teesta River are intricately linked to the ecological and environmental health of the region. These characteristics influence structure and operation of aquatic ecosystems, impact biodiversity, affect water quality for both ecosystems and human communities, and play a role in sediment transport processes. Recognizing these implications is vital for informed decision-making and the development of strategies aimed at preserving and restoring the ecological integrity of the Teesta River and its surrounding environment.

1.8 Hydro chemical faces and evolution of the Teesta River

Analyzing the hydro chemical faces of the River Teesta in the Lower and Middle Basin of the Sikkim Himalaya offers a profound understanding of its geological, hydrological, and environmental history. (Singh et al., 2023) These faces, characterized by unique combinations and concentrations of major ions, provide a window into the prevailing geochemical processes within the river system. For example, the river may exhibit a bicarbonate-type faces, dominated by ions like bicarbonate (HCO_3^-) and calcium (Ca^{2+}), or a sulphate-type faces featuring elevated sulphate (SO_4^{2-}) and magnesium (Mg^{2+})

concentrations. These distinctions in faces highlight the complex interplay of geological, climatic, and anthropogenic factors that have influenced the river's chemical composition.

Temporal changes in hydro chemical faces further illuminate the Teesta River's evolving chemistry. The river experiences shift in faces over time due to a myriad of factors, including seasonal variations, changes in precipitation patterns, and shifts in the contribution of groundwater to the river flow. (Kaushik et al., 2023) These temporal variations provide crucial insights into the dynamic nature of the river's hydro-chemical processes. Geological and geological characteristics are instrumental in forming the hydro chemical sides of the Teesta River. The unique rock formations within the basin release specific ions into the river water, leaving their chemical signature. Minerals and trace elements found in the water are influenced even more by geological processes like weathering as well as erosion. (Kaushik et al., 2023) Climate and hydrological factors are intrinsic to the evolution of hydro chemical faces. The availability of water from various sources, including glacial meltwater, rainfall, and groundwater, significantly affects the river's ion composition. Seasonal fluctuations in temperature and precipitation alter the solubility of minerals and drive chemical reactions within the basin.

Human interactions within the Teesta Basin, ranging from agricultural practices to urbanization and industrialization, introduce a multitude of ions and pollutants into the river. These anthropogenic influences can disrupt the river's hydro chemical faces, posing challenges to water quality and the overall health of its ecosystem. (Ma et al., 2021) By scrutinizing the hydro chemical faces and their evolution in the Teesta River, this research seeks to uncover the river's historical and contemporary processes. It provides a lens through which to observe the intricate interplay of geological, hydrological, climatic, and

anthropogenic factors that have shaped the river's chemical composition over time. Furthermore, it lays the foundation for understanding how these processes may continue to evolve, due to the ongoing impacts of human activity and environmental change. (Ghimire et al., 2021) In the subsequent sections, we delve deeper into the specific hydrochemical faces observed in the Teesta River and their broader implications for the ecosystem and environment.

1.9 Impact of human activities on the hydrochemistry of the Teesta Basin

The Teesta Basin, nestled in the Sikkim Himalaya, is subject to a complex interplay of human activities that leave a substantial imprint on its hydrochemistry. Human interventions have become a defining factor in the evolution of the river's chemical composition, shaping the quality and sustainability of this vital water resource. Agriculture, a fundamental livelihood has two roles in the region's hydrochemistry. While it sustains communities, it is also one of the most significant contributors to changes in the river's chemical makeup. The widespread use of insecticides and fertilizers in farming practices introduces elevated levels of nitrogen and phosphorus compounds into the river. When these nutrients find their way into the water, they can catalyze nutrient enrichment, potentially giving rise to harmful algal blooms and degrading overall water quality.

Urbanization and industrialization within the basin bring forth their own set of challenges to the river's hydrochemistry. Urban centers and industrial activities introduce pollutants, including heavy metals, oils, and a myriad of chemicals, into the river through urban runoff. This localized contamination poses significant risks to both the aquatic ecosystems and the communities that rely on the river for various purposes. (S. Gupta et al., 2016) Furthermore, the increase in impervious surfaces due to urban expansion can

alter the hydrological dynamics, affecting the flow and distribution of chemical constituents within the river. These human activities collectively underscore the intricate relationship between society and the Teesta River's hydrochemistry. The consequences of nutrient enrichment, pollutant introduction, and altered flow patterns are far-reaching, impacting not only water purity as well as the ecological river's and the area's health well-being of the communities it serves. (Lü & An, 2023) Understanding and mitigating these human-induced changes is paramount So that the Teesta Basin's water may be managed properly and the environment can be protected. In the subsequent sections, we delve into specific examples and implications of these impacts on the river's hydrochemistry and broader ecosystem.

1.10 Isotopic Signatures and Their Implications

Isotopic analysis stands as a formidable tool in unravelling the intricate hydrochemical complexities of the Lower along with Middle Basins of the river Teesta. Through the examination of isotopic signatures, particularly those of stable hydrogen (δD) and oxygen ($\delta^{18}O$) isotopes, we gain profound insights into the river's hydrological dynamics and their far-reaching implications. (Ali et. al., 2020) One of the primary applications of isotopic analysis lies in tracing the origins of the river's water sources. By scrutinizing isotopic compositions, researchers can distinguish between contributions from various sources, including glacial meltwater, precipitation, and groundwater. These sources each bear their own unique isotopic fingerprints, enabling us to discern their respective roles and fluctuations in the river's flow.

Furthermore, isotopic signatures unveil the story of seasonal variations within the Teesta River. During the monsoon season, characterized by heavy rainfall, the isotopic

ratios within the river's water exhibit discernible shifts. This temporal transformation of isotopic composition provides invaluable insights into the ebb and flow of water sources and their relative impacts on the river's hydrochemistry throughout the year. (Song et al., 2021) Beyond source identification and seasonal patterns, isotopic analysis is instrumental in illuminating the intricate pathways through which water navigates the Teesta Basin. Whether it's the journey of water from its glacial origins to the river's flow or the intricate interactions between surface water and groundwater, isotopic signatures serve as tracers, unravelling these hydrological mysteries.

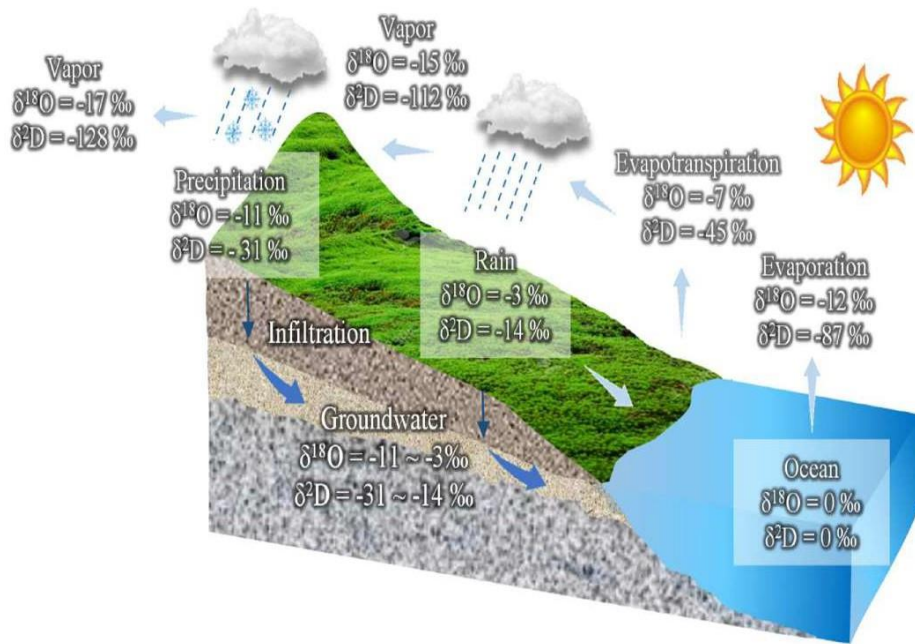


Figure 1-4: Isotopic Signature of river water. (after Hoefs, 1997 & Coplen et al. 2000)

Ultimately, the implications of isotopic signatures extend beyond mere scientific curiosity. They offer a deeper understanding of the Teesta River's hydrological cycle, influencing not only its water quality but also its availability and sustainability. Moreover, this knowledge contributes to the broader context of environmental issues and climate

change conservation in the fragile Himalayan ecosystem. In the subsequent sections, we delve into specific applications of isotopic analysis and their implications for the Teesta River's hydro-chemical dynamics.

1.11 Water Quality Index

G. S. (2013) Indexes are essentially a numerical method for deriving a single value taken from a collection of different test results. Water quality in a given lake, river, or stream is represented by an index value. Observing ecological changes in water requires long-term monitoring of water quality. The Water Quality Index is one method that may be used to track and evaluate progress over time. Additionally, it may provide as a useful gauge of watershed health over time. The Water Quality Index (WQI) has two potential applications: monitoring the development of a given water supply through time, or making direct comparisons between several water sources locally, regionally, or globally.

These days, one way that water quality is measured is via the Water Quality Index (WQI). If one segment of a river is healthy to swim in, one may deduce this from the aggregate results of nine different tests conducted on the river.

There are nine exams in the WQI:

- Dissolved Oxygen
- Fecal Coliform
- pH
- BOD (Biochemical Oxygen Demand)
- Temperature

- Total Phosphate
- Nitrates
- Turbidity
- Total Solids

The results of the nine tests are recorded when they have been completed, and then they are moved to a graph of a weighted curve where a number is calculated from them. At each stage of the process, Multiplying the numerical value (also called the Q-value) by the "weighting factor." The dissolved oxygen test, for instance, has a somewhat high weighting factor (.17), which is due to the fact that it is more relevant than the other tests in assessing the overall water quality. After that, the nine values that were determined are combined together to provide a final water quality index (WQI). One hundred is the maximum possible rating that may be given to a body of water.

Table 1: Water Quality Ranges (G. S. 2013)

Index Ranges	Water Quality
0-25	Very bad
25-50	Bad
50-70	Medium
70-90	Good
90-100	Excellent

Parts of Water Quality Index

The standard for water quality is split in half.

- The Q-value
- Weighting factor

Q- Value

In comparison to a scale of 100 for a single metric, it indicates the water's quality. The parameter of the Q-Value indicates the general quality of the water according to the specified measure.

- 100 = Excellent
- 1 = Very bad

Weighing Factor

This determines how much the feature contributes to water quality as a whole.

Table 2: Weighing parameters related to water quality

Parameters	Weight Factors
DO	0.17
FAECAL COLIFORM	0.16
BOD	0.11
pH	0.11
NITRATE	0.10
PHOSPHATE	0.10
TEMPRATURE	0.10
TURBIDITY	0.08
TOTAL DISSOLVED SOLIDS	0.07

1.11.1 The Water Quality Index's parameters

- **Biochemical Oxygen Demand (BOD):**

The Oxygen Demand in Biochemistry, often known as BOD, is a measurement that determines how much food there is in water for bacteria to consume. In the process of their respiration, bacteria use organic materials, and in the process, they extract water oxygen. BOD testing offers a general estimate of the amount of waste that can be broken down biologically that is found in the water. The majority of the components that make up biodegradable trash are organic waste products like grass clippings, leaves, and manure. It is stated in milligrams per litre.

- **Dissolved Oxygen (DO):**

The test known as "dissolved oxygen" determines how much of the oxygen that is necessary for living is really dissolving in water. Fish, insects, and other organisms can breathe in this oxygen and species that make their home in the water have access to. The majority of plants and animals that live in water need oxygen in order to thrive; in fact, fish will perish if the dissolved oxygen levels in the water drop too low. The presence of low quantities of dissolved oxygen in water is an indication that the water may be polluted. It indicates that if a body of water has a high level of oxygen dissolved in it, then the water's quality is deemed to be excellent in relation to the value of the dissolved oxygen in the water. But if a body of water has a low amount of liquid oxygen, then the amount of oxygen in the water is deemed to be poor in relation to the value of the dissolved oxygen in the water.

- **Nitrate:**

An essential macronutrient in water, nitrates are a measure of nitrogen in its oxidised state. Nitrates come from the word "nitrous," which means "to oxidise." Nitrates have the potential to create health problems in humans due to the fact that nitrites, which are produced when nitrates are broken down by the intestines into nitrites, inhibit the capacity of the red blood cells to transport oxygen. Nitrites, like nitrates, have been shown to cause fish to suffer from significant ailments.

- **pH:**

The amount of acid that is present in the water is measured by its pH level. The pH of the surrounding environment might have a huge influence on majority of aquatic life forms. Generally speaking, the acidity of the water will be increased to some degree if it contains a significant amount of organic pollutants. It is said to have a neutral pH level of 7 when the measurement is taken from water. Water is termed acidic if its pH level falls below 7, while alkaline water is defined as having a pH value that is larger than 7.

- **Temperature:**

The water's temperature in a river is of critical importance because it has such a significant effect on the river's physical, biological, and chemical features. The majority of the animal and plant life that lives in water can only survive within a narrow temperature range, and very few of these species are able to adapt to dramatic shifts in this variable. The temperature of the water should be measured using the same thermometer at the actual testing location and a second, comparable location one mile

upstream. When measuring the temperature upstream, care should be made to guarantee that the amount of sunlight and the river's depth are equivalent to the location where the first test was conducted.

- **Total Dissolved Solids**

This represents the number of solids that have dispersed into the river's water. Salts, certain chemical components, as well as a wide range of other materials, such as nutrients to poisonous chemicals, are included in this category. For there to be aquatic life, there must always be a certain amount of the minerals in the water. Both excessively high and inadequately low concentrations of total dissolved solids may stifle development, which in turn can cause the demise of a great deal of aquatic species.

- **Turbidity**

Turbidity is defined as the amount of light that is scattered across a column of water as a result of the presence of suspended materials. When the turbidity of the water is high, it will seem to be cloudier. When water reaches a certain level of turbidity, it no longer has the capacity to sustain a diverse range of plants along with other aquatic organisms.

1.11.2 Assessment of water quality and suitability for drinking and irrigation

One of the most important chemicals in the world is water. A water body's production is determined by its physicochemical properties. Water of higher grade has appropriate physical, chemical, and biological properties. However, some association between these measures was feasible, and the significant one might be used to suggest water quality. An ensemble of a water's physical, chemical, as well as biological (including bacteriological) characteristics is referred to as its quality. region of water in

particular. (Amin et al., 2020) Water quality provides data on the condition of bodies of water and helps formulate strategies for improved watershed and water resource management. Changes in the nature of freshwater environments may result in fast changes in biodiversity composition. Physical and chemical characteristics of a body of water are used to determine its level of pollution and whether or not it is suitable for certain types of aquatic life. (Sharma & Goyal, 2020) Water quality might deteriorate due to seasonal or yearly variations in fresh water supply. Therefore, monitoring water quality is essential for activities requiring the use of bodies of water for pollution control, sewage reservoir management, fisheries management, and impoundments.

Analyzing the Teesta River's water quality across its Lower and Middle Basin is essential, directly impacting both the health of ecosystems and the well-being of the communities reliant on this vital resource. This evaluation entails a thorough analysis of diverse physicochemical parameters, pH, turbidity, dissolved oxygen (DO), conductivity of electricity (EC), and other parameters and concentrations of various ions such as nitrates, phosphates, heavy metals, and organic pollutants. When taken as a whole, these details allow for an accurate depiction of the chemical and physical properties of river water.

The standard of our drinking water, this assessment assumes paramount importance. It involves rigorous scrutiny to ensure that the water meets the stringent standards necessary to safeguard public health. Factors such as pH, DO, and the absence of contaminants such as heavy metals, pesticides, and pathogens are essential criteria for determining suitability. Any deviations from these standards can pose significant risks to human health, potentially leading to waterborne diseases and long-term health concerns.

Therefore, this evaluation considers not only the water quality as it is at the moment but also considers the long-term security of the water supply.

Taking a look at the irrigation water quality, a lifeline for many in the Teesta Basin, is equally important. The appropriateness of irrigation using river water hinges on parameters like that salinity, nutrient concentrations, and pH. High salinity levels, for instance, can hinder crop growth and productivity. Nutrient concentrations must also strike a delicate balance to ensure optimal plant growth without leading to excessive nutrient runoff, which can degrade downstream water bodies. A proper evaluation of these parameters guides sustainable agricultural practices and resource management, helping to maintain agricultural productivity and reduce environmental impacts. In summary, the Teesta River's water quality evaluation is a multifaceted undertaking with profound implications for both ecosystems and human communities. Whether for drinking water or agricultural irrigation, rigorous evaluation ensures the responsible utilization of this critical resource, safeguarding health, sustaining livelihoods, and preserving the fragile Himalayan ecosystem. Subsequent sections delve into the specific findings and management strategies arising from this assessment.

1.12 Management strategies for improving the Teesta Basin's water quality

Preserving and enhancing the quality of water in the Teesta Basin is imperative for the well-being of both ecosystems and communities relying on this essential resource. A comprehensive approach to water quality management encompasses diverse strategies that address both natural processes and human-induced factors affecting the river system. An essential strategy involves the restoration and conservation of riparian zones along the Teesta River. These zones act as natural buffers, mitigating pollution by filtering

sediments and absorbing excess nutrients before they enter the water. Establishing and maintaining vegetative cover in riparian areas can effectively reduce the influx of pollutants and enhance the overall health of the river ecosystem.

Furthermore, sustainable land-use practices play a pivotal role. Implementing best management practices in agriculture, such as precision farming techniques and reduced fertilizer application, can curtail nutrient runoff into the river. Promoting sustainable land management practices and soil conservation measures can significantly reduce erosion and sedimentation, further enhancing water quality. Effective wastewater treatment and management systems are imperative for reducing the discharge of pollutants into the Teesta River. Implementing advanced wastewater treatment technologies in urban and industrial areas can significantly reduce the introduction of contaminants into the river, safeguarding water quality for downstream users. Engaging local communities in water quality management is also vital. Community-based monitoring and awareness programs can empower residents to take an active role in protecting their water resources. Education and outreach initiatives can promote responsible water use and discourage harmful practices that degrade the standard of water.

Additionally, Water quality development and enforcement regulations and standards are crucial. Measures to reduce pollution from both point and non-point sources should be included into regulatory frameworks, ensuring that industrial discharges, agricultural runoff, and other potential pollution sources adhere to stringent water quality guidelines. Monitoring and research are ongoing processes that inform and adapt management strategies. Regular water quality monitoring and assessment programs provide critical data for identifying emerging issues and tracking the effectiveness of

implemented measures. Research initiatives also contribute to a deeper understanding of the river's hydro-chemical dynamics, facilitating evidence-based decision-making. In summary, managing and improving water quality in the Teesta Basin necessitates a multi-pronged approach that addresses ecological, agricultural, industrial, and societal aspects. Through riparian zone restoration, sustainable land-use practices, wastewater management, community engagement, regulatory frameworks, and ongoing monitoring and research, a concerted effort can be made to safeguard and improve the health of the Teesta River and the communities it sustains.

1.13 Statement of the Problem

In the present research work, the Teesta River of Sikkim Himalaya, India, was selected for hydrogeochemical characterization studies owing to its importance nationally as well as internationally because it flows through Sikkim and West Bengal in India as well as in Bangladesh and for various uses of its water. The Sikkim Himalaya's Teesta River is prone to various environmental issues due to its natural characteristics and human activities. The natural calamities such as landslides, soil erosion, run off, snow fall, etc. which leads to losses or contaminated water its chemical compositions. The anthropogenic activities such as human activities and recent development of small-scale pharmaceuticals factories along the course of the river in the downstream of the study area could also contribute to the changes in the chemical characteristics of river water. Furthermore, the deposition of animal wastes, the presence of human fecal matter, and the industrial waste may contribute to the introduction of nutrient and toxic substances into the river valley.

Geologically, heavy metals contamination in the river water is bigger possibility due to rock-water interaction and metal mineralization. Therefore, while Teesta River flows from its pristine source to the confluence at Melli, South Sikkim, the quality of water and nature of the streams become altered continuously by both natural and anthropogenic changes.

Rivers being dynamic systems serves to transport or store contaminants which are brought into from outside sources. If contaminants are readily transported, the rivers provide a means by which contaminants can migrate and adversely impact downstream. Again, when contaminants are stored, it may result in adverse localized problems or form a contaminant reservoir which may be released at a later time (Solo Gabriele, 1995). Therefore, it becomes imperative to understand the underlying hydrogeochemical processes which actually control the transport and fate of contaminants in the river.

1.14 Research Gap

1. Though Teesta River, the major river which originate from Sikkim, India covering the state of West Bengal, India, and Bangladesh which flows into Bay of Bengal it lacks comprehensive water characteristic analysis in the Sikkim part of Teesta River.
2. Lack of reports on heavy metal pollution on the water quality.
3. Lack of studies in impact of Land use/Land Cover changes, anthropogenic activities and natural processes on the river water quality

1.15 Aim and Objectives

The primary goal of this research is to perform Hydro chemical analysis in Teesta Basin and find out the anthropogenic impact activities as well as natural processes on water chemistry.

The research has highlighted the following goals to be addressed in light of the different hydro-geochemical features throughout the Sikkim Himalaya region of the Teesta River.

1. Morphometric analysis and prioritization of sub-watershed in the study area for natural processes.
2. Spatio-temporal variability of hydrochemical characteristics of the river water.
3. To find the impact of Land Use/Land Cover changes and anthropogenic activities on water quality of river.

CHAPTER 2

REVIEW OF LITERATURE

The study titled "Morphometry and land cover-based multi-criteria analysis for assessing the soil erosion susceptibility of the Jhelum River watershed in the western Himalayas" offers a comprehensive examination of soil erosion risk in a critical ecological region. To assess the susceptibility of sub watersheds to soil erosion using GIS, this research combines information on morphometric characteristics and land cover into a multi-criteria analysis framework. By employing such a multifaceted methodology, the study presents a nuanced and in-depth understanding of the complex interplay between topography, vegetation, and erosion susceptibility, it is crucial for managing western Himalayan water and land resources efficiently. This research not only contributes to the scientific knowledge of soil erosion dynamics but also provides valuable insights for sustainable land-use planning and conservation efforts in this ecologically sensitive area Altaf et. al (2014).

The study titled "Quantitative geomorphometric and land cover-based micro-watershed prioritization in the Tons river basin of the Lesser Himalaya, with a focus on the Tons sub-watershed in the Mussoorie Hills," showcases an intricate analysis of micro-watershed prioritization, employing a multi-criteria approach and GIS techniques. The research meticulously evaluates and ranks the sub-watersheds, including data on topography and other geomorphological features. It does this by analyzing the sensitivity and risk of natural resource deterioration in the Himalayan environment. Not only does this research deepen our appreciation for the nuances of micro-watershed management,

but it also provides essential insights for informed decision-making in land-use planning and resource conservation efforts in the Tons river basin. Such detailed research is invaluable for preserving the ecological balance and Advocating for the advancement of sustainable development within the geographical expanse of the Lesser Himalayas area. According to Chauhan et al. (2015), the authors assert the following.

The research titled "Multi-criteria-based sub-basin prioritization and its risk assessment of erosion susceptibility in the Kansai-Kumari catchment area, India" delves into a comprehensive analysis of sub-basin prioritization using a multi-criteria approach and GIS technology. Focused on the Kansai-Kumari area in West Bengal, the study meticulously assesses and ranks sub-watersheds, offering valuable insights into erosion susceptibility. By combining quantitative criteria and geographical information systems, the research provides a detailed understanding of erosion risk, particularly in these sub-watersheds. This work is pivotal in informing land and water resource management decisions in the region, emphasizing the need for proactive measures to combat erosion and safeguard the natural environment, the Kansai-Kumari catchment region, helping immensely with sustainable development and land-use planning in 2018, Bhattacharya et al.

The study titled "Water quality evaluation of Himalayan Rivers in the Kumaun region, Uttarakhand, India," features an in-depth analysis of the water quality in the Kumaun area. Water quality may be measured using the Water Quality Index (WQI) or the Integrated Water Quality Index (IWQ), the research delves into the complex dynamics affecting the rivers of this ecologically vital region. Water quality in these Himalayan rivers has been deteriorating for several reasons, which are acknowledged, including

eutrophication, the impacts of tourism, as well as anthropogenic and geogenic processes. This work is instrumental in shedding light on the environmental challenges faced by this unique and sensitive ecosystem, providing essential data to guide conservation and policy efforts aimed at preserving the pristine waters of Uttarakhand's Kumaun region Seth et. al (2014).

The study titled "Spatiotemporal variations of hydro geochemistry and its controlling factors in the Gandaki River Basin, Central Himalaya, Nepal" provides a comprehensive examination of the hydro geochemistry within this ecologically significant region. This research examines the Central Himalayan Gandaki River Basin and its intricate hydro chemical makeup. While most of the region's water is still OK for human consumption and agricultural irrigation, the research did identify some very serious safety issues in a few spots. This work offers valuable insights into the spatiotemporal dynamics of hydro geochemistry and the factors influencing it, emphasizing the significance of water quality monitoring and management in Nepal's Central Himalaya for environmental protection and sustainable development and the well-being of local communities Pant et. al (2018).

The study titled "A GIS-based assessment of water quality pollution indices for heavy metal contamination in Tuticorin Corporation, Tamil Nadu, India" presents a comprehensive analysis of the heavy metal pollution situation in Tuticorin Corporation, located in Tamil Nadu. The Heavy Metal Contamination Index (HPI), the Heavy Metal Evaluation Index (HEI), and the Dissolved Oxygen Content (DOC) are only some of the indicators used to assess water quality contamination in this research utilizing a Geographic Information System (GIS). The results of this investigation clarify the many

ways in which heavy metal contamination in the area is caused by contaminant processes originating in chemical industry, landfill leachate, as well as the municipal sewage system. This research not only enhances our understanding of water quality issues but also provides crucial insights for effective pollution management and policy decisions, highlighting the need of acting to lessen the negative effects that urban and industrial development have on Tuticorin, Tamil Nadu, India's water resources Al and Selvam (2015).

The study titled "Assessment of heavy-metal pollution in three different Indian water bodies through a combination of multivariate analysis and water pollution indices" provides an in-depth look at the metal pollution in the rivers Indus, Sutlej, and Beas. Worrying information is uncovered by calculating water quality indices and heavy metal pollution indices. The research shows that the Beas and Sutlej Rivers' heavy metal contents are much higher than the safe levels recommended by the WHO. Extremely high amounts of heavy metal pollution are seen in the Sutlej River, making it stand out as the most severely impacted. This work underscores the urgent need for heightened attention to water quality management and pollution control measures in these vital Indian water bodies, as their contamination poses a substantial risk to both the environment and public health Kumar et. al (2020).

The investigation of hydro-geochemical studies, which specifically examine the main ion composition, toxicity, mobility, and bioavailability of trace elements in river systems, plays a critical role in comprehending the fundamental principles that govern biogeochemical processes. The investigation of this particular subject matter has been thoroughly examined in rivers around the globe. The origins of the hydro geochemistry

of natural waterways may be attributed to the pioneering research conducted by V.I. Vernadsky throughout the 1930s. Shvartsev et al. (2006) and Chudaev et al. (2013) assert that Vernadsky established the fundamental principles of aqueous geochemistry in his publication titled "The History of Natural Waters," which was released from 1933 to 1936.

Vernadsky's research offered a comprehensive examination of the widespread presence of water, the establishment of water equilibrium inside the Earth's crust, and the interphase movement of chemical components. Furthermore, his research has been crucial in laying the foundation for the emergence of new study domains, including environmental hydro geochemistry, organic hydro geochemistry, and microbiology.

Over the last several decades, there has been a notable escalation in human-induced stress on river ecosystems, resulting in an upward trajectory of pollution levels. Consequently, a significant amount of study has been undertaken in the realm of environmental hydro geochemistry with the aim of comprehending, evaluating, and alleviating river contamination, along with other origins of natural water pollution. A comprehensive collection of scholarly material pertaining to the hydro geochemistry of rivers around the globe is readily accessible. However, this analysis has only mentioned and addressed a limited number of books in various areas.

Hydrochemistry of rivers

Tsering et. al (2019) focuses on the Teesta River's weathering processes for the first time using primary ion data. Water samples were gathered in Sikkim, Himalaya, India, along the Teesta River. There was discussion of the typical chemical composition of rivers

worldwide as well as evaluation of major and minor ions against recommended thresholds for purity. Novel Understandings in Hydrology: All streams have a preponderance of Ca, Mg, and HCO_3^- , which indicates the Teesta River's carbonate weathering. However, the correlation between the growth in Silicon (Si) and the rise in the Na/Ca ratio downstream suggests that silicate weathering predominated in the Teesta River lowlands. The pace at which silicates are weathered is dependent on a number of factors, including but not limited to gradient, contact length, temperature, and vegetation. The increased cation concentration was counterbalanced by SO_4 , which came from the reaction of H_2SO_4 and H_2CO_3 with carbonates and silicates. Evaporite dissolution is the primary process that governs the Teesta River's principal ion chemistry, after rock weathering (carbonate-silicate weathering). The Rangpur region exhibits hydrogeological activity due to ion exchange and dissolution processes. Dolomite and limestone dissolve to create Ca^{2+} , Mg^{2+} , and HCO_3^- .

(Su et al., 2022) Concerns about public health and water supply stem from an understanding of the major variables affecting the chemical characteristic. Additionally, it aids in protecting surface water from the effects of human activity. We use principal component analysis as well as hydro chemical analysis on a total of 33 samples collected from rivers in the Muling-Xingkai Plain to learn more about the hydro chemical process of river water and the key drivers influencing chemical compositions. The types of HCO_3^- , Ca and combined HCO_3^- Ca ·Na are what define river water, according to the results. However, Cl^- is the predominant anion in certain samples with a rather high nitrate level.

(Roy et al., 2018) utilizes water quality measures and employs multivariate analysis to examine the land use fingerprints of a tidal river that is experiencing a decline

in health as a result of human-induced disturbances. Hydro-chemical and anthropogenic processes were evaluated and quantified using a number of statistical methods (factor analysis, bio-geo-chemical fingerprints, factor analysis, and hierarchical cluster analysis). The system's ion concentrations were studied employing these methods to analyze what influences people.

The results show that the indicators of water quality fluctuate significantly across space and time ($p < 0.05$). The stream's solute concentrations are lowest in the stream's middle section, where ag and sewage runoff meet. The agricultural areas exhibit elevated levels of dissolved oxygen (DO), sodium ions (Na^+), and potassium ions (K^+). This may be caused by the closeness of shrimp wastewater effluents and the effect of tidal spill-over. The urban locations exhibit elevated levels of salinity, electrical conductivity (EC), chloride (Cl^-), bicarbonate (HCO_3^-), nitrate (NO_3^-), phosphate (PO_4^{3-}), and total suspended solids (TSS). These findings suggest that the land use in these areas is primarily characterized by the direct release of organic waste from households into the water bodies. The author suggests that these dying tidal river basins might be a great source of surface water to complement the region's high-quality water supply, especially in light of the recent pattern of rising precipitation and declining ground water tables.

In 2019 April–May and September–October saw the completion of a thorough examination of the Yellow River main stem. (Han et al., 2022) In order to illustrate the three states of natural and artificial impacts, Cluster analysis of ion composition data was used to divide the Yellow River into three sections. According to the results of the hydro-chemical investigation, the concentrations of ions and nutrients were first found to be low in Region I, to be larger in Region II, and to have consistently stayed high in Region III.

Second, the movement of phosphorus in the Yellow River Basin is controlled primarily by sediment adsorption as well as rainfall runoff erosion. point source pollution primarily supplies nitrogen in the spring, although point and nonpoint sources also contribute to the total amount of nitrogen in the fall; and Three sources of pollution were eventually qualitatively analyzed using six indicators: Na^+ , K^+ , Mg^{2+} , Cl^- , SO_4^{2-} , and HCO_3^- . This group of tracers was divided into point source and nonpoint source categories: K^+ , Mg^{2+} , and HCO_3^- , and Na^+ , Cl^- , and SO_4^{2-} . The findings have significant ramifications for Yellow River Basin water resource management, which enhance our knowledge of the application of the hydro chemical characteristic's technique.

(Jiang, 2020) Sought to examine regional differences in hydro chemical river features and water quality. The Tuo River in central Suzhou, Northern Anhui, China, as well as the Bian River on the outskirts of the city were selected for this investigation. The geochemical characteristics of surface water in the study area were evaluated using the Piper trigram, the Gibbs diagram, and the hydrogen as well as oxygen isotope concentration features. The water quality was then assessed using a revised fuzzy comprehensive evaluation method. The results showed that the two rivers' hydro chemical compositions belonged to the SO_4^{2-} Cl^- Na^+ category. Moreover, in the Bian River, found on the outskirts of the city, the concentrations of Na^+ , K^+ , SO_4^{2-} , Cl^- , Ca^{2+} , and total phosphorus (TP) were substantially higher than those detected in the Tuo River, found in the city's heart (ANOVA, $p < 0.001$).

(Wiejaczka et al., 2018) The article explains how a recently built reservoir affects the hydrochemistry of water in the Teesta River (a tributary of the Brahmaputra) as it flows through the Himalayas. Field study was carried out from 2013 to 2015 during the

post-monsoon season. The Teesta River in the Darjeeling Himalaya served as the site for five separate sample and measurement stations covering 43 km. Water samples taken both above and below the reservoir throughout the river's longitudinal profile show that the reservoir significantly decreased the concentrations of most basic ions (Cl^- , K^+ , Na^+ , Mg^{2+} , NO_3^- , and PO_4^{3-}). Only Ca^{2+} , SO_4^{2-} , and NH_4^+ had an inverse trend. The dam has no effect on F- concentrations. Cu, Ni, Zn, Cr, Cd, and Sr, among the hardest metals, are created in a somewhat enriched state by the reservoir. The lower enrichment of Teesta water below the dam is reflective of the metals' ability to self-purify in the water of the Teesta Reservoir. Just 15 kilometers upstream from where the Teesta River begins to flow out of the Himalayas, environmental factors often normalize changes in physicochemical quality and ion concentrations generated by the reservoir.

(Das et al., 2021) The solute sources, weathering patterns, and acids involved in these processes have been constrained by studying the spatial distribution of dissolved main ions and carbon isotopic compositions in the Teesta River, a significant tributary of the Brahmaputra River. Mixing diagrams and piper plots of significant ions show that the weathering of silicates and carbonates provides a significant solute supply. The Teesta samples had an average sulfate content of $92 \pm 47 \mu\text{M}$, which is much higher than the atmospheric deposition concentration in this basin, which was previously believed to be about $5 \mu\text{M}$. The dissolved inorganic fractions' carbon isotopic compositions ($\delta^{13}\text{CDIC}$) range from -11.87‰ to -3.82‰ (mean: $-7\text{‰} \pm 2\text{‰}$). The Teesta River watershed experiences chemical weathering due to the contribution of both H_2SO_4 and H_2CO_3 acids, as shown by comparing the trends of $\delta^{13}\text{CDIC} - \text{SO}_4 / (\text{SO}_4 + \text{HCO}_3) - \text{HCO}_3 / (\text{Ca} + \text{Mg})$ with their corresponding values anticipated for acid-mediated

weathering. The influence of sulfuric (H_2SO_4) and carbonic (H_2CO_3) acids on the Teesta water chemistry has been measured using $\delta^{13}\text{CDIC}$ data and inversion modeling of key ions. In this basin, the average proportion of cations obtained through H_2CO_3 -mediated weathering of carbonates (0.27 ± 0.14) as well as silicates (0.20 ± 0.09) is similar to that of H_2SO_4 -mediated weathering of carbonates (0.38 ± 0.18) and silicates (0.15 ± 0.11). According to these findings the Teesta River's CO_2 intake (via silicate weathering mediated by H_2CO_3) and release (by carbonate weathering mediated by H_2SO_4) are in balance.

(Refat Nasher & Humayan Ahmed, 2021) Investigations on the hydro-geochemical and groundwater geochemistry were conducted in three distinct Bangladeshi river basins. The BGS website was the source of the data. To learn more about the hydro-geochemical and geochemical processes that take place in groundwater, researchers in Bangladesh analyzed 113 samples taken from 10-274 meters deep in a variety of Ganges-Brahmaputra-Meghna (GBM) river basins. Groundwater concentrations of Ca^{2+} , Mg^{2+} , Na^+ , K^+ , Zn^{2+} , Cl^- , HCO_3^- , and SO_4^{2-} were considered for the studies. In the Ganges, Brahmaputra, and Meghna basins, the primary cations are ranked as follows: $\text{K}^+ > \text{Mg}^{2+} > \text{Zn}^{2+} > \text{Na}^+ > \text{Ca}^{2+}$, $\text{Ca}^{2+} > \text{Na}^+ > \text{Mg}^{2+} > \text{K}^+$, and $\text{Mg}^{2+} > \text{Zn}^{2+} > \text{Na}^+ > \text{Ca}^{2+}$. The Ganges, Brahmaputra, and Meghna basins rank $\text{Cl}^- > \text{SO}_4^{2-} > \text{HCO}_3^-$, $\text{Cl}^- > \text{HCO}_3^- > \text{SO}_4^{2-} > \text{HCO}_3^-$, correspondingly, in terms of the ions that matter. Experiments used factor analysis as well as bivariate plot interpretation. Carbonate weathering is the exception to the rule that silicate weathering, ion exchange, as well as saltwater intrusion are the primary processes in the Ganges basin. In all three basins, the Cl^- above SO_4^{2-} showed human effects into groundwater.

(Ribinu et al., 2023) The research team in Kerala, India, emphasize on chemical and physical properties of the groundwater in the Thoothapuzha River basin. Over the course of the PRM and POM seasons, a total of 54 groundwater samples were collected from the research region. The features of groundwater couldn't be understood without first establishing its hydro-chemical composition. which included of things like acidity, conductivity, and pH total hardness, salinity, alkalinity, Na^+ , K^+ , Ca^{2+} , Mg^{2+} , SO_4^{3-} , Fe , Cl^- , NO_3^- , and total dissolved solids (TDS). The relationship between chemical components and water quality was established by scientific methods for analytical data. Ca-HCO_3 and mixed Ca-Mg-Cl were the main facies found in the samples. In the combined Ca-Na-HCO_3 and Ca-Cl , Na-Cl facies, only few examples have been found. According to Gibbs plots, evaporation as well as rock-water interactions are the primary processes that regulate water's chemical composition. Ca^{2+} , Mg^{2+} , Na^+ , and K^+ are associated, which indicates that ion exchange controls how much of each ion is present in groundwater. More so than carbonate and evaporite dissolution, silicate weathering is a major contributor. In addition, the correlation analysis shows that anthropogenic sources, silicate weathering, and reverse ion exchange regulate the water chemistry.

(V. Gupta et al., 2022) This research looked at the relationship between landslip occurrence and meteorological and geomorphic variables in the Teesta River valley in the Sikkim Himalaya. These variables included rainfall pattern, valley floor width to valley height ratio, channel steepness index, and stream length gradient index. The main cause of landslides in the Higher Himalaya is found to be tectonic activity at higher levels, which is disguised by an orographic barrier to the north of the Main Central Thrust.

However, it has been shown that the increasing tectonic activity and the increased rainfall along the Main Central Thrust go hand in hand. Landslides in the Lesser Himalaya are mostly triggered by precipitation, and their locations are largely governed by the lithology of the terrain.

(Tsering et al., 2019) Based on the first major ion measurements, this article discusses weathering along the Teesta River. Water samples from the Teesta River have been collected in the Indian state of Sikkim Himalaya. Methods for determining whether or not a river's concentration of a given chemical relative to recommended limits were followed were described, as were the typical chemical make-up of rivers throughout the globe. All streams' prevalence of Ca, Mg, and HCO_3^- is indicative of the Teesta River's carbonate weathering. While Si concentrations rose with distance from the river's mouth, the Na/Ca ratio rose as well, suggesting that silicate weathering was more widespread in the Teesta river delta. For silicate weathering to occur at a given rate, a number of important elements must be balanced, including gradient, contact length, temperature, as well as vegetation. The SO_4 that resulted from the reaction of H_2SO_4 and H_2CO_3 with carbonates and silicates counterbalanced the increased concentration of cations. The Teesta River's primary ion chemistry is primarily controlled by rock weathering, also known as carbonate-silicate weathering, which is followed by evaporate dissolution.

(Tiwari et al., n.d.) This research analyses the hydro-chemical mechanisms that shape the primary ion chemistry of the water in the catchment basin of the Teesta River in the Eastern Himalayas. The pH of the water in the Teesta River basin was between 7 and 9. The Teesta watershed water composition showed that the predominant hydro-

chemical facies was Ca-Mg-HCO³, and the leading ionic species were HCO³⁻, Ca²⁺, Na⁺, Mg²⁺, and SO₄²⁻. Increased contributions from (Ca²⁺ + Mg²⁺) and HCO³⁻ to TZ⁺ and TZ⁻, as well as high ionic ratios of (Ca²⁺ + Mg²⁺)/ (Na⁺ + K⁺), HCO³⁻/ (Cl⁻ + SO₄²⁻), as well as low (Na⁺ + K⁺)/TZ⁺ ratios, suggest that carbonate weathering is a major contributor to the ionic composition of water in the Teesta basin. It seems that during water-rock interaction, both carbonate and sulphate phase minerals may be dissolved by water due to their under-saturation. All of the analyzed water quality indicators had concentrations far below the safe thresholds for use in drinking and irrigation.

(Chakrabarty et al., 2023) The Teesta River is heavily impacted by human involvement on many levels. This aspect made the evaluation of the riverine ecology much more necessary. The lower Teesta River watershed was chosen for this research in response to increased dam construction and growing human habitation. An indicator of biotic integrity based on fish was established using the seven sample locations that were selected. The evaluation of the three areas used as examples—Rungpo, Rishikhola, and Gajoldoba—is "Acceptable." The greatest difference across the sample locations was driven by the proportion of predators and the number of lithophilic spawners. Considering riparian impacts and physical habitat characteristics, a generic model was developed to predict the fish-based measure of biotic integrity over place and time. It is anticipated that both the upper Teesta River basin as well as the lower Teesta River will be given an "Acceptable" rating. On the plains, on the other hand, the status of "Impaired" is predicted. and there is a good correlation between the established fish-based measure of biotic integrity index and the stream water index, indicating sufficient ecological conditions.

(Saha, Reza, & Roy, 2019) The existence of many deserted channels with varying levels of deterioration suggests significant Teesta River movements. The groundwater's pH ranges from 6.20 to 7.40, indicating that the aquifers under study are somewhat acidic to alkaline. Major cations' mean abundance is $\text{Na}^+ > \text{Ca}^{+2} > \text{Mg}^{+2} > \text{K}^+$, whereas major anions' mean abundance is $\text{HCO}_3^- > \text{Cl}^- > \text{SO}_4^{-2}$. In anions, SO_4^{-2} is a minor ingredient and HCO_3^- is the most prevalent, Whereas Na^+ predominates and K^+ plays a minor role among the cations. Anion facies of groundwater include bicarbonate, bicarbonate-chloride, and bicarbonate, whereas cation facies include sodium, sodium-magnesium, sodium-calcium, as well as sodium-calcium-magnesium. Given that just three samples had potassium levels over the maximum permissible limit, the groundwater in the research region may be used for both residential and commercial reasons without risk. Overall hardness, SAR, RSC, PI, SSP, as well as MH values for the groundwater in the studied region, are favorable, indicating that it may be utilized for irrigation.

(Das et al., 2022) However, despite the links between climate change and water management, there needs to be more effort to analyze the impacts of climate change over the transboundary Teesta River basin. This is even though changing climatic conditions can trigger significant changes in eco-hydrological as well as socio-political-economic setups. We analyzed temperature, precipitation, potential evapotranspiration, and water availability changes for 1.5 and 2 degrees Celsius warming levels to provide the best management suggestions for the whole transboundary Teesta River basin. For this aim, we used the CMIP6 ensemble median, the average of five models with their biases considered. Based on these findings, we may anticipate a significant rise in future temperatures and monsoon rainfall. Except during the time just before the monsoons, the

evaporation paradox is projected to be witnessed soon, increasing water availability. If these trends persist, melting snow, receding glaciers, and increased flooding might damage the ecosystem.

(Sharma & Goyal, 2020) temperature, precipitation, and climatic extremes (23 indicators) were analyzed for shifts in the Eastern Himalayan Teesta River basin between 1951 and 2100. In this study, we used projections from four distinct GCMs and two different concentration scenarios (RCP4.5 and RCP8.5). Significant differences were discovered between the anticipated and actual climates in terms of temperature, precipitation, and patterns of climatic extremes. Overall, it was discovered that there is warming and an increase in precipitation, the increase from RCP4.5 to RCP8.5. Under RCP8.5, average maximum and minimum temperatures in the basin are expected to rise by 0.54 °C, 1.18 °C, and 1.92 °C from the 1951–2010 period, and by 0.5 °C, 1.2 °C, and 2 °C from 2011–2040 to 2070 and 2100, respectively. Increases in precipitation are predicted throughout both the monsoon and off-monsoon seasons; however, estimates are fraught with uncertainty. RCPs anticipate a significant rise in precipitation indices during the 21st century, to name a few, we have RX1day, RX5day, R10, R20, CWD, as well as R95p. Warm evenings, days, summer days, as well as tropical nights are expected to increase, whereas cold evenings, cool days, frost days, as well as ice days are expected to decrease as a result of RCPs. Furthermore, there may be problems with water supply as a consequence of a sharp decline in the contribution of snowfall to precipitation. Furthermore, the findings coincide with earlier research conducted in and around the basin.

(Mandal & Chakrabarty, 2016) The Teesta Watershed in Sikkim's Darjeeling Himalaya region is likely to see flash floods. The purpose of this research is to create a model for simulating surface runoff in the upper Teesta Basin, an area prone to destructive floods. First, the stream flow response at the watershed's outflow is predicted in advance of an excess rainfall event, and then a central unit hydrograph is created. This method was developed for use in the geospatial editing and processing of meteorological as well as morphological data. Runoff volume and peak discharge evaluation over time data from the India Meteorological Department's rainfall time series was used. In addition to meteorological data, background information was gathered on topography, drainage systems, land cover, and geology. HECRAS and HEC-HMS software were used to analyze the various hydraulic models and determine the possibility of flash floods. This process was crucial in achieving the desired outcome.

(Talukdar et al., 2020) Using cutting-edge innovative ensemble machine learning methods, Finding and predicting flood-prone areas along the Teesta River is the focus of this research. In order to get highly accurate and trustworthy results, the study developed bagging ensembles using the random forest (RF), M5P, random tree (RT), and REP tree algorithms. We selected 12 parameters that are considered conditioning factors and 413 locations with a history or current occurrence of flooding to include in our models. The influence of the factors leading to floods was evaluated using the statistical method of Information Gain Ratio. The ROC was utilised by the author to check the flood-prone models. To compare the flood susceptibility models, the Friedman test, Wilcoxon signed-rank test, Kruskal-Wallis test, as well as Kolmogorov-Smirnov test were all combined for the first time. According to the results, all algorithms anticipated that an area larger than

800 km³ would be very vulnerable to flooding. According to the ROC curve, all of the models produced area under the curves that were more than 0.85, suggesting very accurate flood models.

(Paul et al., 2019) The hydro morphological state of a river system is indicative of the quality of its habitat and is affected by both natural and anthropogenic forces. The research focuses on the Teesta River Valley in the Himalayan Indian state of Sikkim. The Teesta and the primary tributary that flows into it from the right, the Rangit, make up this river network. The upper and lower dams of each river comprise the examined portions. A thorough field survey is used to evaluate the river's hydro-morphological condition. In addition, a River Habitat Survey was conducted in 2015 throughout the winter, particularly during periods of low river water flow. Studying rivers' hydro-morphological characteristics is crucial to this investigation, such as the Teesta and Rangit, which are situated both above and below the locations of significant dams. The magnitude of the hydro-morphological characteristics found in the higher and lower dams was also compared in this research. The results of the Habitat Quality Assessment (HQA) as well as the Habitat Modification Score (HMS) show that the dam has not significantly impacted the river's hydro morphological quality. Enough hydro morphological elements are present in the dams in the analyzed river basin to further support the naturalness of the river system.

(Shit et al., 2019) The primary goals of the research were to assess the drinking water's hydro-chemical and hydro-biological quality and to examine household water consumption patterns in the Indian state of Sikkim. Through surveys and interviews with 98 families in three main Sikkim towns—Gangtok, Ravangla, and Pelling—the pattern

of water usage and socioeconomic level were ascertained. The World Health Organization and the Bureau of Indian Standards both concluded that the hydro chemical parameters of the drinking water were well within acceptable ranges. Eighty-two percent, forty-seven percent, fifty-five percent, and seventy-five percent of the water samples tested positive for total coliforms, *Escherichia coli*, *Enterococcus* spp., *Salmonella* spp., *Staphylococcus aureus*, as well as *Pseudomonas aeruginosa*, respectively. A thorough household survey, however, indicates that during the monsoon season, around 43% of participants had water-borne illnesses. 60% of individuals would rather boil or purify their water before drinking it because of this.

(Ansari & Ahmad, 2019) Utilizing a variety of hydro-chemical data from the Himalayan streams, an examination of the hydro-geochemical processes has been conducted in this study. Results showed that the nature of the bedrock affected the chemistry of glacial streams, with many glaciers exhibiting greater ($\text{Ca}^{+2} + \text{Mg}^{+2}$) than ($\text{Na}^{+} + \text{K}^{+}$) concentrations. Greater silicate weathering than in the higher Himalayan rivers is shown by the intermediate and lower altitude rivers' small drop in ($\text{Ca}^{+2} + \text{Mg}^{+2}/\text{Na}^{+} + \text{K}^{+}$). The glaciers and other streams seem to follow a certain pattern according to Piper's (1944) graphic. At medium and lower elevations, streams with diverse types of fluids are seen, whereas Ca-HCO₃-type streams predominate in glacier streams. It was found that the glaciers and other streams exhibit a unique pattern of ($\text{Ca}^{+2} + \text{Mg}^{+2}$)/ SO_4^{-2} ratios. The sulfate minerals, such as anhydrite and gypsum, are potential sources of dissolution; sulfide oxidation is a potential secondary source. Water in glacier streams showed electrical conductivity to have a direct connection with snout height and an inverse

relationship with length. Since glaciers are becoming smaller, their shorter length and greater snout height enrich the solute in meltwater streams.

(S. Gupta et al., 2016) The primary goals of this study are to analyze the water quality for agricultural as well as human use using hydrogeochemical analysis of water samples from the Rangit river basin. River water has an ionic strength that ranges from neutral to slightly alkaline, with K^+ , Ca^{2+} , HCO_3^- , and SO_4^{2-} dominating. The predominant hydro chemical facies in river water upstream is $K^+-Ca^{2+}-Mg^{2+}-HCO_3^-$, whereas downstream river segments are dominated by the $Ca^{2+}-K^+-Mg^{2+}-HCO_3^-$ water type. The process of solute acquisition is mostly governed by the weathering of minerals that form rocks. The low ratio of $(Na^+ + K^+/TZ^+)$ and the large equivalent ratios of $(Ca^{2+} + Mg^{2+}) / (Na^+ + K^+)$ show that silicate weathering contributes somewhat to the overall chemical composition of river water. According to the Water Quality Index rating, the vast majority of the analyzed river water is very good to very good for human consumption and domestic usage. Based on its EC content, SAR, as well as RSC values, river water is a good to excellent source of irrigation water for agricultural purposes.

(Kaushik et al., 2023) Recent research has shown that the Himalayan region's surface water chemical composition is influenced by the increased melting of glaciers brought on by climate change. The dynamics of chemical weathering in the Ladakh region are poorly known since there are no available in situ datasets. The goal of this study is to learn more about how the Lato and Stok catchments affect the chemical make-up of the meltwater that eventually makes its way into the Indus River and its tributary in the Western Himalayas. Glacial catchments of the Indus River, the Chabe Nama, the Lato, and the Stok rivers in Ladakh were all sampled. The meltwater samples' varying ionic

trend and slightly alkaline pH (7.3–8.5) revealed the unique weathering processes and geology of the Upper Indus Basin (UIB). On the other hand, smaller glacierized catchments (Stok) have a lower average value of 6.69 t/km²/year, while the average is 15.7 t/km²/year in larger glacierized catchments (Lato). In both catchments, CWR is rather high compared to the silicate weathering rate (SWR). The Lato as well as Stok glacierized catchments in Ladakh now have in situ datasets for stream water chemical properties, which will aid in the promotion of healthy ecosystems and livelihoods in the UIB.

(Schneider & Avellan, 2019) While some of the lakes are utilized for religious purposes and are regarded as holy, others serve as sources of drinking water. The chemical makeup of the lake water might provide some insight on the cause of the anomalies, the level of pollution, and the consequences of human activities. Six prominent and holy lakes in Sikkim were studied, and their water chemistry was analyzed and critically examined: Gurudongmar, Lamapokhari, Kheheopalri, Karthok, Menmecho, and Kupup. These lakes provided samples of water, which were then chemically analyzed. To determine if the lakes are appropriate for residential and agricultural use, these water samples' general quality characteristics were analyzed and compared to standards established by the WHO and the Bureau of Indian Standards. Findings have shown that these lakes' lake water quality differs depending on a variety of chemical factors. Calcium (Ca), dissolved oxygen (DO), as well as total dissolved solids (TDS) concentrations in lake water samples, have been looked into, and shown to have links to both natural and human-caused elements. This study advocated for preserving the natural state of these sacred lakes and investigated possible causes for their peculiar chemical composition.

(Sonker et al., 2023) The active tectonic processes and surface and subsurface faults that disturb the basin's drainage system's pattern are the foundation for this research. Indicators of neotectonic activity are derived from the morphological features and drainage patterns seen in the morphometric drainage basin areas. This study focuses on the Sikkim, Himalayan state located in the Upper Teesta River basin. The Upper Teesta River basin drainage order was made using Arc GIS software. using ALOS PALSAR DEM for the purpose of morphometric and morph tectonic investigation. The basin is said to drain in the sixth position. An asymmetry factor of 45.66, an elongation ratio of 0.55, a transverse topographical asymmetry of 0.25, a mountain-front sinuosity of 0.94, and a valley floor width to valley height ratio of 0.44 were calculated. All criteria point to tectonic activity in the Upper Teesta River Basin, as shown by these data. An indicator of the basin's stream gradient, calculated to be >500 , demonstrates the tectonic activity of the examined region. 50 years of seismic data (1971–2020) are used to verify this study. Because of this, geospatial tools are crucial for determining if a region is neotectonically active.

(Rahman, 2023) Changes in land use and land cover (LULC) in tandem with climate variability and variability cause significant water balance adjustments in the Teesta basin, which is shared by Bangladesh as well as India. This in-depth study examines how future changes to the LULC and climate will interact to affect runoff in the basin. By using a cellular automata model, he was confident in his ability to predict LULC in 2020 and in future years between 2050 and 2080. For both the historical era (1995-2014) and the two future decades (2050s (2035-2064) and 2080s (2071-2100)), we used the semi-distributed Soil Water Assessment Tool (SWAT) hydrological model.

Eight GCMs run under SSP245 and SSP585, two Socioeconomic Pathways (SSPs), which apply the SWAT model. From 2000 to 2010, the study indicates substantial changes in LULC, with changes continuing until 2020, including expansions in both farmland (0.49%) and populated areas (1.67%).

(Adhikari & Kamle, 2021) The Teesta River, which flows across international borders between Bangladesh and India, often experiences both flooding and drought. In this section, we'll talk about the conflict over the Teesta River, which has been raging between the two countries for over thirty years due to competing claims and for which there is currently no suitable framework for cooperative administration and efficient governance. Within the basin of this river, conflicts related to ecology, socioeconomics, and geopolitics have been exacerbated by the long-standing dispute and the disregard for sustainable management of Teesta water. The purpose of this chapter is to analyze the complex issues surrounding the Teesta River water conflict within the context provided and provide solutions to resolve the conflict amicably by addressing the issues resulting from the competing claims. According to the results of the investigation, the Interim Deal must be revised into a permanent Teesta River Water Treaty if the issue is ever to be resolved. The implementation of an ITRWM system for the whole Teesta River basin would also be extremely helpful in ending the protracted conflict.

(Rai & Khawas, 2023) Sikkim, India is a state in the Eastern Himalayas, and this research examines the potential for conflict and disputes to arise from plans for large-scale hydropower production in the Upper Tista River Basin. However, as a consequence of global warming, hydropower projects in the Eastern Himalayan area of Sikkim have become a contentious paradigm for regional development. The study draws attention to

possible problems and disputes between local opposition to hydropower projects and plans for limiting the effects of global warming. The dispute and collaboration in the Upper Tista River basin before and after hydropower development are critically examined in this research. Indeed, during the last several years, the area has seen how the Hydro Power Project has threatened social and environmental security. The research also examines the many ways in which local politicians, NGOs, dam developers, and those impacted by dams have a role in supporting and opposing the hydroelectric dam projects in the area. The research examines the environmental hazards and damages that are being made worse Environmental security framework to assess the threats posed to the upper Tista watershed in the Sikkim Himalaya (India) by hydropower development as well as climate change.

(Jana et al., 2016) Splitting its way between India and Bangladesh, the Teesta River has a dual current, this work examine this estimating issue. A variety of control structures govern the flows through the two channels, and Indirect indicators of flow include water level and the size of regulation structures. A multiplier known as a hydrological constant is included in the computing formula for the measurement. Results from empirical research show that the computational formula for the two channels is presently using the wrong multipliers. The author provides a methodology to estimate the correction factor for this reason, considering a number of important factors. The assumptions may be validated by using the model's diagnostic tests. Additionally, provide a consistent, nonparametric estimate of the required component. When a major stream flow is redirected via a canal, its measured volume (cumec) drops from 100 to 76. This is shown by an analysis of historical flow data. The governments of Bangladesh and India

would be better able to apply and oversee any water sharing deal if they adjusted the emerging metrics based on this conclusion.

(Akhter et al., 2019) To analyze as well as predict mid-line channel shifting and spatial and temporal changes of channel morphology in the Teesta River in Bangladesh from 1972 to 2031, this study makes use of a geographic information system (GIS), a spatial autocorrelation index, and an autoregressive integrated moving average (ARIMA) model. The findings demonstrate that the spatial changes throughout the channel reach (as shown by the various bar area forms) are predominantly influenced by differences in river banks. In contrast, the temporal changes in channel shifting rates are primarily affected by excessive sedimentation in the river flow route. There is a moderate correlation ($R^2 = 0.50$; $p < 0.05$) between the sinuosity index and time, a sign of rapid sedimentation and a change in river flow caused by bank erosion. The relationship between the bar area and the braided index shows a strong positive correlation ($R^2 = 0.96$, $p < 0.01$). Based on the ARIMA model findings, the greatest mid-line channel shifting is predicted to happen in a rightward direction between 2017 and 2024, and a leftward direction between 2024 and 2031. When the bar area is reduced, the channel's spatial pattern seems to grow, according to the findings of the spatial autocorrelation.

(Kashyap & Behera, 2023) The author computes geomorphic matrices consisting of topographic variables, for an in-depth look at where landslides have occurred throughout time and space, geographers use a variety of tools, including longitudinal and topographic swath profiles, channel steepness indices, and stream length gradient indices. Geospatial correlations were found between the exhumation and erosion rates of the watershed under study and the strength of the gradient of rainfall and topographic

characteristics. According to our data, Landslides are most common in the 24-28 degree slope, 800-1000 meter relief, and 1500-1700 meter elevation ranges that coincide with the 2500-2700 mm/year rainfall intensity of the Teesta river watershed. Increased tectonic activity in the northern Higher Himalaya is the primary source of landslides along the orographic barrier to the north of the Main Central Thrust (MCT) and Main Boundary Thrust (MBT). The MCT-MBT structural affinity is mostly determined by rainfall intensity, however landslides are controlled and often initiated by litho-tectonics. The discovery made by the author indicates that erosion rates are more varied in space and often surpass long-term exhumation rates. Although recent landslides seem to have had a significant influence on these rates, The MCT Zone watershed has the greatest erosion rates, at 5 mm/year. Teesta watershed erosion and long-term exhumation, however, do not seem to be much impacted by variations in rainfall rates.

(Mishra & Rai, 2019) Evaluating temperature variations is essential to understanding these areas' physiography. The Upper Teesta basin is remarkable because it combines the subtropical climate of the south with the arctic environment of the north. Northern Sikkim, where the Teesta River flows, has heavy snowfall and near-freezing temperatures for at least three months out of the year (November - January). The whole region of Sikkim is covered by the upper Teesta River basin, which determines how people live and work depending on the water's availability. The atmosphere's temperature greatly affects the make-up of streams and the total amount of water they carry. The average monthly temperatures were produced using data from NCEP and the India Meteorological Department, which were then analyzed using kurtosis, skewness, and Z-distribution visualization in a GIS context. While keeping in harmony with the local

climate, it offers a strategic perspective for the appropriate use of river water. The outcome shows how the river's course has changed in relation to the pattern of climatic variability, necessitating sustainable management of this water resource.

(Z. Ahmed et al., 2022) Using a mix of sociological and geographic data, this study analyses the effects of water withdrawals in the upper Teesta River basin on land use and livelihoods in the lower basin. Analysis of accretion and riverbank erosion trends suggests that accretion rates are increasing relative to riverbank erosion. A self-administered questionnaire was used to perform a home survey with 450 participants (200 farmers and 250 fishermen). The majority of farmers (65.5%) and fishermen (76.8%), according to survey data, believe that they have suffered damage as a consequence of upstream barrage building. Water shortage is experienced by most farmers and fishers, especially during the dry season. They discovered that many individuals in the research sector are open to switching careers. In addition, participants noted that a large number of locals are now either relocating or wanting to relocate. According to the research, farmers who experience a shortage of water in their region are more likely to relocate than their peers, whereas farmers who have difficulties with their crops are less inclined to move. However, the consequences of fishing, receiving assistance during a crisis, and upstream barrages all strongly predict changes in the profession of fishermen.

(Ghosh & Chakraborty, 2022) The study area of the eastern Himalayan foothill alluvial plain included around 75 km of the Teesta River. However, there is a lack of historical gauge data, which makes it difficult to examine the effect of dams on streamflow and silt in the rivers of the Himalayas. The author used a straightforward strategy, collecting in-situ sediment samples every year from 1987-2017, to recreate the

development of river landforms before the construction of dams and barrages. To better understand the pre-, syn-, and post-dam river sediment-transport pattern, we conduct a particle size study of the deposited silt. The 23 landforms studied have been divided into three groups based on when they were formed: (i) before 1997, when dams and barrage interventions were not yet in place; (ii) during upstream dam construction, between 1998 and 2010 (TML); and (iii) after 2010, when upstream dams and the barrage were both in place. Across 116 samples from TML and TNL silt, a smaller mean grain size may be attributed to the reservoir sequestration of coarser grains. The cleanest river state is characterized by the coarsest TOL material, which has a fining tendency downstream.

(Saha, Reza, Selim Reza, et al., 2019) Human activities have an effect on the Tista River's hydrochemistry, and this research looks at that effect, where it runs across plain terrain before entering the Brahmaputra River in Rangpur Division, Bangladesh. Fieldwork was completed in July of 2014. Sampling was carried out at four sites along a longitudinal segment of the Tista and Brahmaputra rivers (near the Tista river's mouth). Major ion compositions (cations Ca^{+2} , Mg^{+2} , Na^+ , K^+ , and anions HCO_3^{1-} , Cl^{1-} , and SO_4^{2-}) were used to examine the Tista River's water quality by analyzing its hydro chemical characteristics. The maximum amount of arsenic in any of the water samples was below the 10 g/L threshold set by the World Health Organization. Dewatering (removing water from the river for irrigation purposes), the geological formations the Tista River flows through, and human activities all contribute to the river's water changing hydro chemical facies. This indicates that the hydrochemistry of the Tista River is affected by both chemical weathering of rocks as well as groundwater discharge.

(Talukdar et al., 2021) Therefore, the likelihood of LULC fragmentation in the Teesta River Basin (TRB), Bangladesh, may be estimated utilizing multitemporal datasets in a GIS environment by using bagging, random forest (RF), random subspace (RSS), as well as their ensemble model. The FRAGSTATS programme was used to transform the LULC maps into a landscape and class matrix. These matrices comprised measures such as the aggregation index (AI), the contagion index (%) (CONTAG), the perimeter area ratio (P/A ratio), the area of a class, the percentage of a landscape, the density of patches, the total edge (TE), the biggest shape index (LSI), and the size of the center of a shape. Machine learning methods such as decision trees, as well as support vector machines, are used in sensitivity models. we evaluated the effect of several parameters on the fragmentation probability modelling. While the percentage of land covered by buildings increased by 1.45% between 2010 and 2019, There was a sharp drop of 6.21 percent in the proportion of water and 14.59 percent in the proportion of undeveloped land. Results showed that as levels of human intervention in the TRB have grown, so too has the dominance of the agricultural region.

(Das et al., 2022) However, the transboundary Teesta River basin, where changing climatic conditions can cause significant changes in eco-hydrological and socio-political as well as economic setups, has yet to receive nearly enough attention for analysis of the effects of climate change. To better manage the transboundary Teesta River basin, we investigated temperature, precipitation, potential evapotranspiration, as well as water availability changes under 1.5 and 2 C warming scenarios. Through the CMIP6 Coupled Model Intercomparison Project, we averaged the findings of five models that had their biases considered. According to the data, both the average temperature and the average

amount of monsoon rain are anticipated to rise significantly in the next years. The conundrum of evaporation, which leads to an increase in water availability, is predicted to persist for the foreseeable future, with the exception of the pre-monsoon season. By melting snow, causing glacial retreat, and causing floods, these processes might continue and result in environmental deterioration.

(Giri, 2020) This study's goal was to determine the Teesta River's Water Quality Index, which flows through Sikkim, India. In this research, the State Pollution Control Board's laboratory in Sikkim examined water quality parameters (physio-chemical parameters) during the months of June and October 2018. pH, turbidity, DO, BOD, electrical conductivity, hardness, alkalinity, TDS, chloride, and calcium are among the several parameters that are examined. In the lab, procedures recommended by the American Public Health Association (APHA) were followed. Nine monitoring stations along the Teesta River in Sikkim's East District provided the water samples for this investigation. The Weighted Arithmetic Index Technique was used to calculate the WQI. According to the results of the calculations, the Water Quality Index (WQI) measurements varied from 138 to 421 in June and from 85.13 to 391.45 in October. In June and October of 2018, respectively, Singtam and Majhitar achieved the highest WQI values. The station where the highest WQI was recorded is located in East Sikkim's industrial belt as well as a heavily inhabited area. Therefore, the river needs careful management and treatment to preserve water quality and decrease pollution.

(Sikkim, 2020) The purpose of this work was to use Geographic Information Systems (GIS) to map the spatial distribution of important indicators of water quality over the whole length of East Sikkim's Teesta River. For the purpose of the research, a total of

nine different spots were chosen to collect samples of water, and various physicochemical characteristics were measured at each spot using established protocols. According to the findings of this investigation, several sample stations, such as Singtam, Majhitar, and Rangpo, exhibited a high concentration of pH (that is, an acidic character). Other metrics, such as conductivity, hardness, and total dissolved solids, all exhibited an upward trend, this is closely associated with the quality of the available water. We made riverbank maps using Arc-Gis's Inverse Distance Weighted (IDW) feature.

(Talukdar et al., 2020) This study's goal was to precisely identify potentially flooded locations along the Teesta River and make flood forecasts using cutting-edge, novel ensemble machine learning algorithms. Ensembles of bagging are created by combining the random forest (RF), M5P, random tree (RT), as well as REP tree algorithms, the author was able to get results that were both trustworthy and highly accurate. For the aim of flood risk modelling, 413 locations of past and current flooding and twelve elements considered conditioning factors were identified. The Information Gain Ratio is a statistical tool used to measure the relative importance of different factors in causing floods. The receiver operating characteristic (ROC) curve was used to validate the flood-vulnerable models in the investigation. The results showed that over 800 km² were projected by all algorithms to be very high flood vulnerability zones. Every model obtained an area under the curve (AUC) of more than 0.85, suggesting extremely accurate flood models, according to the ROC curve. M5P bagging beat RF, REP tree, and RT bagging in terms of flood vulnerability models.

(M. Islam et al., 2015) The study's goal was to look at the Tista River's surface water quality at Kaunia point during both the dry (December–February) and wet

(September–November) months of 2013–2014. Five locations along the Tista River were used to collect water samples: There is St. 1 and St. 2 and St. 3 and St. 4 and St. 5 and so on. The study indicated that during the wet season, the average transparency was 13.28 cm, whereas during the dry season, it was 32.31 cm, with a temperature range of 25.86 to 18.180 C. Wet season measurements include: 84 and 145.67 $\mu\text{S cm}^{-1}$ for electrical conductivity (EC), 7.72 and 8.03 for pH, 5.35 and 5.37 mg l^{-1} for dissolve oxygen (DO), and 1.64 and 1.89 mg l^{-1} for biochemical oxygen demand (BOD). Measurements of total dissolved solids (TDS) showed a range from 53.2 to 73.86 mg l^{-1} during the wet and dry seasons, respectively. The alkalinity was measured at 40.94 mg l^{-1} during the rainy season and 43.4 mg l^{-1} during the dry season, while the hardness was measured at 98.47 and 102.46 mg l^{-1} at the same times. The majority of the criteria for the Tista River's water quality being conducive to aquatic life have been met, including fish, have been met, according to the study. However, the primary causes of the deterioration of aquatic life and water quality may be agricultural runoff and waste products produced by human activity.

(Saha, 2022) This investigation makes use of information on the quality of the water in the Tista alluvial fan collected over the summer. The long-term weathering of the sediments is responsible for the lower pH values in the groundwater, This point to carbonic acid's chemical decomposition and the absence of alkaline minerals in the aquifer. In conclusion, the Scholler diagram plot shows that during the summer months, Na is the most abundant cation among K, Ca, and Mg, and that HCO_3^{1-} is the most abundant anion in the groundwater under investigation. The summertime groundwater samples belong to the NaHCO_3 type. It is determined that the primary hydro chemical

mechanism influencing the hydro geochemistry of the Tista alluvial plain is reverse ion exchange. The groundwater exhibits transient hardness, as shown by the mean total hardness value of 104.92 mg/L and a very significant positive correlation between total hardness and the HCO_3^{1-} anion. The PCA estimates that 76.035% of the total variance can be explained by focusing on only three factors. The groundwater samples are separated into two categories using CA's clustering techniques: cluster-1 and cluster-2. Sundarganj Upazila, where three groundwater stations are situated, has elevated total dissolved solids (TDS) readings, which are typical of Cluster-1. Ten groundwater wells with high concentrations of K, Ca, Na, and SO^4 make up Cluster 2.

(Mondal et al., 2020) assessed the flood vulnerability of riverside communities. They used a comprehensive risk evaluation structure, combining flood risk, likelihood of flooding, and in-depth interviews with 377 people living along the Bangladeshi side of the Teesta River. The study also included interviews with key opinion leaders, creating a composite index to compare flood danger aspects. Findings indicated that midstream and upstream areas on the right bank of the Teesta River faced the highest flood risk. Vulnerability and competence had a strong negative connection, while exposure and vulnerability showed no clear relationships. Household preparedness had a significant impact on people's flood perception in a multivariate study. This empirical methodology may be applicable to assess flood risk in other areas, especially when data is limited.

CHAPTER 3

METHODS AND MATERIALS

3.1 Introduction

This research encompasses various aspects of hydro-geochemistry pertaining to the Teesta River, Sikkim Himalaya. It encompasses the study of drainage morphometry and prioritization of sub-watershed for natural processes, examination of water chemistry, as well as generating water quality index for drinking and agricultural purposes. Changes in land cover and land use as well as the effects of human activities on water quality are included in the analysis.

The study employs different methods, which can be classified into different categories: a) conducting field surveys and collecting samples, b) collecting satellite images and generating study maps through geospatial software's c) performing laboratory investigations, and d) analyzing and compiling the obtained results.

3.2 Study Area

The study area for the "Hydro-chemical Characterization of Lower and Middle Teesta Basin, Sikkim Himalaya" encompasses the Lower and Middle Teesta River Basin, and also to the upper part of Teesta River in Sikkim to understand the hydrochemistry of it, so sample locations for the present studies encompasses from the source to the mouth of Teesta River located in the northeastern region of the Indian state of Sikkim, within the Himalayan mountain range. This region includes a diverse landscape of rivers, streams, and lake sources, making it a crucial area for the investigation of hydro-chemical properties and water quality assessment. The study will cover various sites and locations within this basin to obtain a comprehensive understanding of the hydro-geochemical

characteristics.

Sikkim, located in the Eastern Himalaya, occupies the geographical coordinates of $27^{\circ} 04' 46''$ to $28^{\circ} 07' 48''$ N latitude and $88^{\circ} 00' 58''$ to $88^{\circ} 55' 25''$ E longitude, encompassing a total area of 7,096 square kilometers. One of the defining features of this region is its intricate drainage system, predominantly shaped by the Teesta River. According to Meetei et al. (2007) and Wiejaczka et al. (2014), this river system drains the whole of Sikkim from its source in the Teesta Khangse glaciers in the northwest of the state, at an altitude of 7,127 meters above sea level.

Flowing southward, the Teesta River courses through Sikkim before continuing its journey into West Bengal and eventually Bangladesh. Along the way, it converges with numerous small tributaries, nourished by glacier meltwater and precipitation. The significance of the Teesta River cannot be overstated; In the areas it flows through, its water is used for drinking, farming, and industrial purposes. The river also helps meet the energy demands of the places it flows through by providing hydropower. Thus, the Teesta River stands as a lifeline for both Sikkim and the downstream regions it benefits, exemplifying the vital role that water resources play in sustaining life and facilitating development in this part of the Eastern Himalaya.

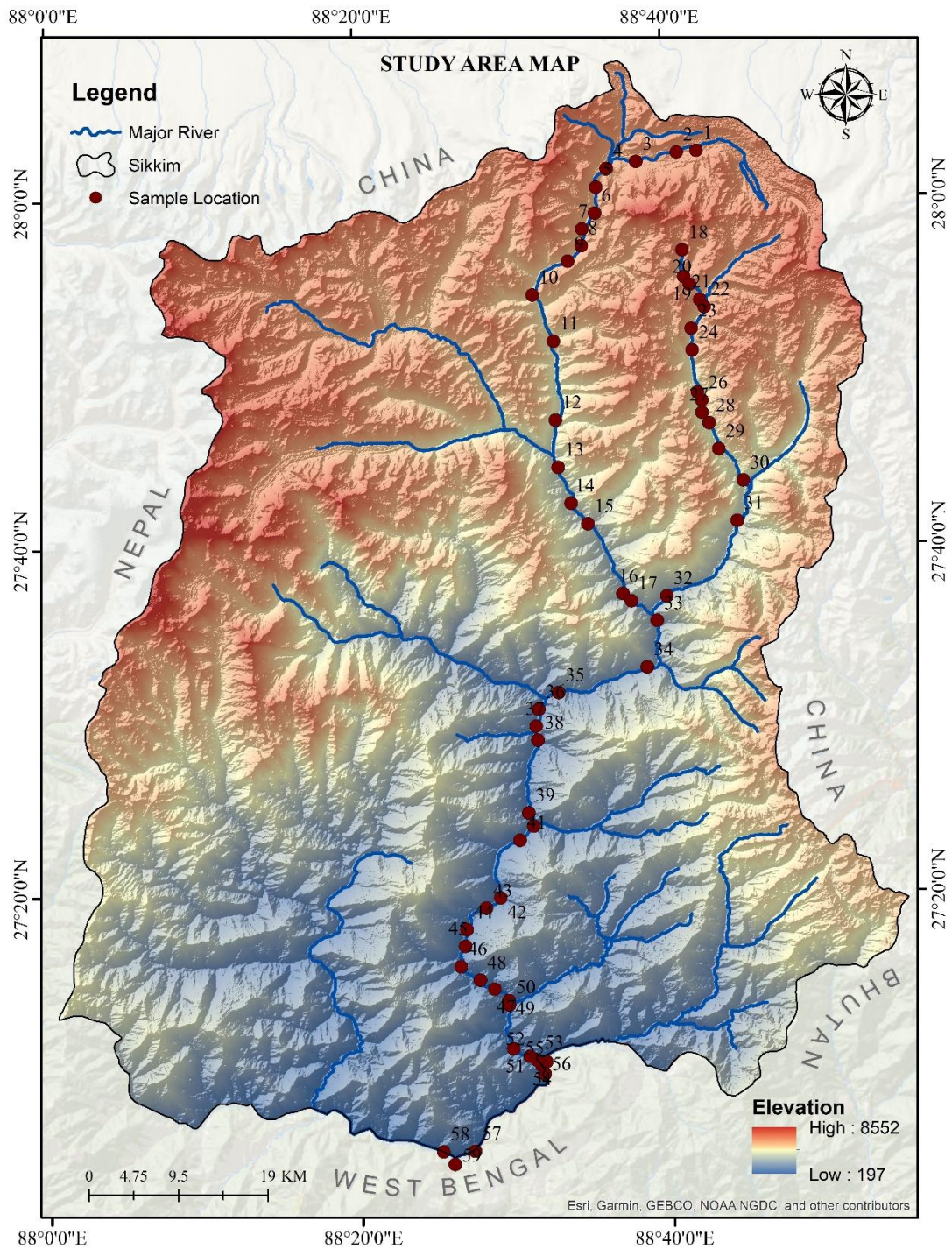


Figure 3-1: Study area map

3.3 Field surveys and collecting samples

The sample size for the hydro-chemical characterization study of the Teesta Basin in Sikkim Himalaya encompassed data collected a total of 236 samples for two seasons, pre-monsoon and post monsoon for two years, 2019 and 2021 from 59 locations in the study area. This extensive dataset allowed for a robust and representative analysis of ion concentrations and water quality parameters across the study area. Such a substantial sample size enhances the statistical significance of the findings, enabling a comprehensive understanding of the seasonal variations and trends in the hydro-chemical composition of the basin's water sources.

a) Field work and sampling

During the present research period collection of water samples for hydro-chemical characterization was performed during pre-monsoon and post monsoon for the year 2019 and 2021. To collect water samples, pre-cleaned HDPE bottles with a capacity of 1 liter were utilized, following the procedures outlined in APHA (2005). For further study, the obtained water samples were taken to a lab. Each sample was divided into two portions (acidified and non-acidified) – 500 ml each and stored refrigerator under 4° Celsius separately for further chemical analysis. A total of 236 samples were collected for two seasons (pre-monsoon and post-monsoon) for two years, 2019 and 2021 from 59 locations in the study area.

At the sampling location, a portable hydro-physiochemical analyzer, the Horiba - U50, was used to assess pH, temperature, electrical conductivity (EC), total dissolved solids (TDS), turbidity (NTU), and dissolved oxygen (DO). In the lab, analytical instruments

like Ion Chromatography (IC), Model: Metrohm Ico IC and Inductively Coupled Plasma Mass Spectrometry (ICP-MS), Model: Agilent 7800 were used to analyze major ions like F^- , Cl^- , NO_3^- , Na^+ , K^+ , Ca^+ and Mg^+ and heavy metals such as Mn, Fe, Ni, Cu, Zn, As, Ba and U, while alkalinity was measured through titration method in the laboratory. A detailed flow chart methodology for hydrochemical analysis is presented in **Figure 3-2**.

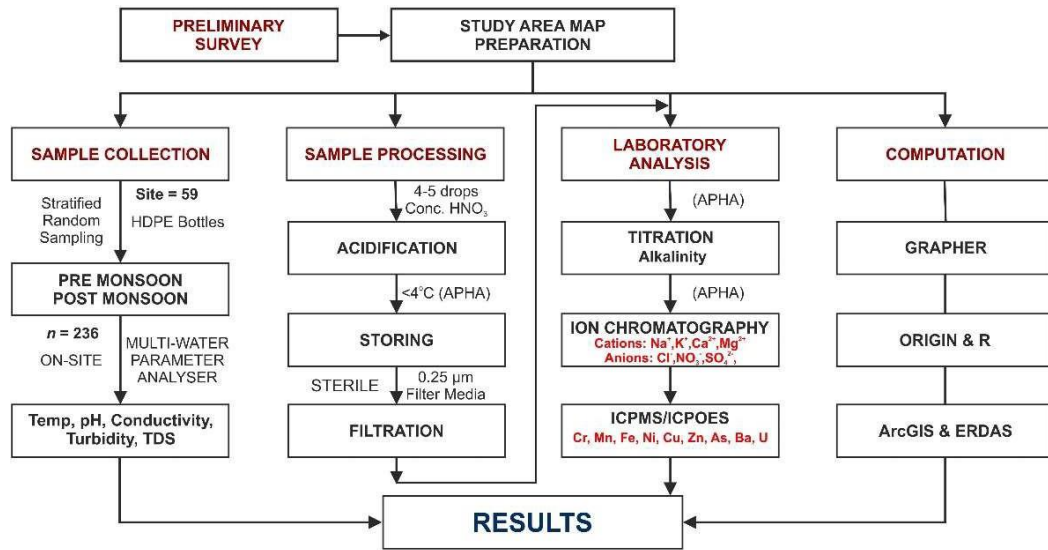


Figure 3-2: Flow chart methodology for hydrochemistry analysis

b) Collecting satellite images and generating study maps through geospatial software's

To generate study area for morphometry and land cover-based prioritization for erosion susceptibility various datasets were accumulated. The first dataset was ASTER DEM (Advanced Space borne Thermal Emission and Reflection Radiometer), obtained from <https://asterweb.jpl.nasa.gov/data.asp>, with a cell size of 30 meters. The second dataset was Sentinel-2A, acquired from <https://sentinel.esa.int/web/sentinel/sentinel-data-access>, with a pixel size of 10 meters, specifically considering bands 2, 3, 4, and 8. To determine the land use and land cover details of the study area, a supervised classification

method was employed. The watershed map published by the Soil and Land Use Survey of India (SLUSI) from <https://slusi.dacnet.nic.in/> was downloaded and used to validate the watershed boundary and drainage network, which were generated using ASTER DEM. Additionally, ancillary data sets such as the Geological map from Bhukosh (<http://bhukosh.gsi.gov.in/Bhukosh/Public>) provided by the Geological Survey of India (GSI) were utilized to understand the geology and interpret areas prone to soil erosion. Morphometric parameters for linear, areal and relief based were generated using ASTER DEM with Spatial Analyst Tools (ArcGIS 10.2). For the land cover classification, the study utilized multispectral Sentinel-2A data of S2MS12A product type with a spatial resolution of 10 meters. The data, acquired on 16 December 2018, had already undergone geometric correction. To facilitate the classification process, the data was prepared by stacking the 10-meter resolution bands (2, 3, 4, and 8). The Maximum Likelihood Classification (MLC) method was employed for the land cover classification, and the processing was carried out using ERDAS IMAGINE 14. A total of seven land classes were identified. A detailed flow chart methodology for morphometry and land cover-based prioritization for erosion susceptibility is presented in **Figure 3-3**.

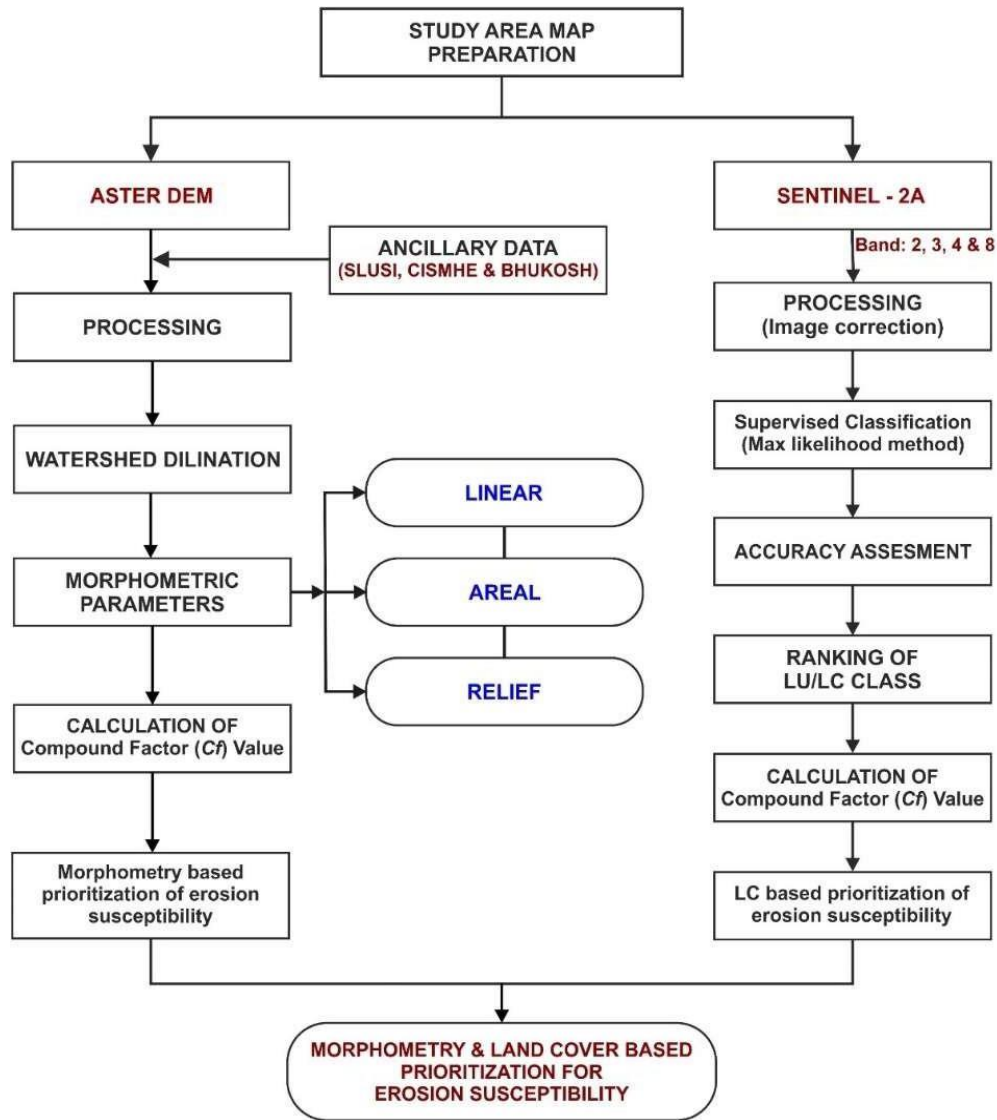


Figure 3-3: Flow chart methodology for prioritization analysis

3.4 Analytical Data Analysis

In the hydro-chemical characterization study of the Lower and Middle Teesta Basin in the Sikkim Himalaya, both major ions and trace ions are systematically sampled and analyzed to comprehensively assess water quality. Following standard sample techniques, we collect major ions such as calcium (Ca^{2+}), magnesium (Mg^{2+}), sodium

(Na⁺), potassium (K⁺), bicarbonate (HCO₃⁻), sulphate (SO₄²⁻), chloride (Cl⁻), and nitrate (NO₃⁻). These protocols involve using clean, acid-washed containers, filtering samples if necessary, and adding stabilizing agents like sulfuric acid (H₂SO₄) to prevent alterations in pH during storage. In parallel, trace ions of interest, such as iron (Fe), manganese (Mn), copper (Cu), zinc (Zn), lead (Pb), arsenic (As), mercury (Hg), and chromium (Cr), are sampled with meticulous attention to trace metal-clean techniques. This includes filtration, acidification with nitric acid (HNO₃) for preservation, and the use of specialized containers to minimize contamination risks. Quality control measures, including blank samples and stringent equipment cleaning, are implemented for trace ion sampling. Subsequently, both major ions and trace elements are analyzed in the laboratory using suitable analytical methods, such as ion chromatography and atomic absorption spectrometry. The results of these analyses provide valuable insights into water quality and the potential sources of ions within the Lower and Middle Teesta Basin, facilitating a hydro-chemical assessment.

3.5 Preliminary Survey

A preliminary survey, also known as a reconnaissance survey, plays a crucial role as the initial step in various research, planning, and investigative endeavors. This preliminary phase involves the identification and selection of potential study sites or project areas, considering factors like geographical location, accessibility, and relevance to research objectives. Limited data collection occurs during this stage, encompassing the gathering of existing literature, maps, and historical data pertaining to the study area. Additionally, site reconnaissance entails physical visits to selected sites to provide

firsthand insights through observations of the natural environment, infrastructure, and potential challenges or opportunities. In the present study a preliminary field survey was conducted for physio-hydrochemical in the research area during the initial stage, the following table represented the result of analysis during the field work.

Table 3: Preliminary survey of the study area during the initial period of research

Sub Watershed	Temp	pH	EC (uS/cm)	Turbidity (NTU)	DO (mg/L)	TDS (mg/L)
SW1	26.68	6.5	51.56	12.5	6.35	29
SW1	24.37	5.5	52.17	16.5	12.63	30
SW1	23.07	5.5	52.77	17.1	11.93	31
SW1	21.57	7.3	41.82	16	6.96	23
SW2	14.38	6.1	56.67	14.2	10.04	34
SW2	14.14	7	58.78	12.6	10.79	36
SW3	17.59	7.8	70.77	9.71	9.56	46
SW3	21.06	7.7	73.96	30.6	9.84	49
SW4	9.85	7.4	96	25.4	9.05	72
SW4	10.14	7.6	93.79	25.1	7.49	68
SW5	14.24	7.2	87.14	44.1	8.13	61
SW5	13.12	7.5	89.82	79.4	7.17	64
SW6	14.72	7	78.26	15.7	12.42	54
SW6	15.67	7.2	75	14.1	11.13	51
SW7	21.06	7.9	65.88	32.1	7.13	42
SW8	26	6.9	62.4	5.27	6.83	39

The above **Table 3** provides a complete summary of water quality metrics in several sub- watersheds. significant variances across sub-watersheds are noted during the preliminary survey, reflecting a variety of environmental circumstances. Sub-watershed SW1, for example, has moderate temperatures (ranging from 21.57°C to 26.68°C) and mildly acidic to neutral pH values (ranging from 5.47 to 7.29). SW2, on the other hand,

has lower temperatures (averaging approximately 14.26°C) and varying pH values (from 6.07 to 6.97), as well as increased turbidity, indicating poor water quality. SW3 has a slightly alkaline pH range (7.72 to 7.77) with varied amounts of conductivity, turbidity, oxygen dissolved in the water, and TDS. SW4 and SW5 have lower pH & higher TDS levels, reflecting a variety of geological and human factors. SW6, SW7, and SW8 exhibit a variety of properties, including dissolved oxygen levels, turbidity, & electrical conductivity, highlighting the complicated nature of water quality within the sub-watersheds.

3.6 HYDRO CHEMICAL ANALYSIS

3.6.1 Water Quality Index (Drinking Purposes):

As a means of evaluating the hydro chemical safety of surface water samples for human consumption (Sahu and Sikdar 2008; Yidana and Yidana 2010; Edet et al. 2013). Adimalla et al. (2018b) and Sutadian et al. (2016) propose a parameter that combines the effects of all ions.

The following procedures were used to determine the water quality index (WQI):

$$HEI = \sum_{i=1}^n \frac{H_c}{H_{mac}} \quad W_r = \frac{wi}{\sum_{n=1}^n wi},$$

$$qi = \frac{C_i}{S_i} \times 100,$$

$$SI = W_r \times qi,$$

$$WQI = \sum_{n=1}^n SI,$$

W_r = Relative weight,

W_i = unit weight,

Qi= quality rating scale,
Ci= concentration of the parameter,
Si= standard limit,
SI= water quality sub index.

3.6.2 Wilcox Diagram

Electrical Conductivity (EC) and Sodium Percentage (Na%) are crucial parameters when evaluating water quality for agricultural irrigation. The salinity of water, often indicated by EC, plays a significant role in determining its suitability for irrigation purposes. High salinity levels in irrigation water can create a physiological drought condition in plants by reducing the soil's permeability, which, in turn, affects plant growth and crop yield (Ayers and Westcot, 1985).

One of the commonly used methods to assess the potential hazard of sodium in irrigation water is the Sodium Percentage (Na%) formula, which was initially proposed by Wilcox in 1955 known as Wilcox Diagram. The Na% is calculated using the following equation:

$$\%Na = \frac{[Na^+ + K^+]}{[Ca^{2+} + Mg^{2+} + Na^{2+} + K^+]} \times 100$$

In this equation, the concentrations of Na, Ca, and Mg ions are measured in meq/l. The resulting Na% value indicates the proportion of sodium relative to the total exchangeable cations (Na, Ca, and Mg).

A high Na% value in irrigation water implies an increased sodium hazard, which can have detrimental effects on soil structure and plant growth. Monitoring and managing EC and Na% are vital components of ensuring the quality and effectiveness of irrigation water for agricultural purposes. Proper water quality assessment helps prevent soil degradation and

ensures optimal crop growth, which is essential for sustainable agriculture (Ayers and Westcot, 1985).

3.6.3 Residual Sodium Carbonate

Residual Sodium Carbonate (RSC) is a pivotal parameter when evaluating the appropriateness of water for irrigation practices (Eaton, 1950). The RSC is calculated using the following equation, determined based on the concentrations of various ions, all measured in meq/l.

$$RSC = [HCO_3^- + CO_3^-] - [Ca^{2+} + Mg^{2+}]$$

RSC index for irrigation water serves as a valuable indicator of the alkalinity hazard posed to soil. When water contains elevated levels of dissolved sodium compared to dissolved calcium and magnesium, it can lead to adverse effects. In such cases, the soil is prone to swelling and dispersion, resulting in a significant reduction in its capacity for water infiltration (Karanth, 1989).

3.6.4 Permeability Index:

The concentration Ca^{2+} and Mg^{2+} react with water rich in HCO_3^- and CO_3^- . As a consequence, calcite and magnesite cation precipitates form, increasing salt danger by adsorption onto clay surfaces. This hinders root growth, prevents water from reaching the soil, and so on (Todd and Mays, 2005).

To get the permeability index (PI), the following equation was used:

$$PI = \frac{Na^+ + \sqrt{HCO_3^-}}{(Ca^{2+} + Mg^{2+} + Na^+)} \times 100$$

3.6.5 Kelly's Index:

Kelley's ratio, which compares sodium to calcium and magnesium, is used to rank irrigation water quality (Kelley, 1940). It is to estimate the level of Sodium concentration.

The following formula is used to calculate KI:

$$KI = \frac{Na^+}{Ca^{2+} + Mg^{2+}}$$

3.6.6 Heavy Metal Pollution Index:

For each criterion used to create the index, water pollution levels were assigned weights using the HPI approach. (Horton 1965; Reddy 1995; Mohan et al. 1996).

Unit weight (Wi)

$$w_i = \frac{k}{S_i}$$

k= constant=1, S_i = Standard limit

Sub Index value (Qi)

$$Qi = \sum_{i=1}^n \frac{(Mi(-)Ii)}{(Si - Ii)} * 100$$

Mi= Monitored Value

Ii= Ideal value

Si= Standard Limit

3.6.7 Contamination Factor:

Multiple quality criteria may have a negative impact on drinking water, and the contamination factor index summarizes these impacts (Backman et al. 1997).

$$Cd = \sum_{i=1}^n C_{fi}$$

Where

$$C_{fi} = (C_{Ai} / C_{Ni}) - 1$$

C_{fi} = contamination factor

C_{Ai} = Analytical Value

C_{Ni} = permissible limit

3.6.8 Heavy Metal Evaluation Index:

The Heavy Metals Quality of Water Index (HEI) is an expression of the following (Edet and Offiong, 2002):

$$HEI = \sum_{i=1}^n \frac{H_c}{H_{mac}}$$

H_c = monitored value

H_{mac} = permissible limit of parameters

3.7 Erosion susceptibility test

Table 4: Estimations of drainage morphometry, linear parameters

ESTIMATION OF LINEAR PARAMETERS			
Sl. No	Parameters	Formula/Definition	References
1	Stream order(μ)	Ranking hierarchically	Strahler (1964)
2	Stream length (L_μ)	Total length of the stream segments of that particular order	Horton (1945)
3	Mean stream length (L)	$L = \sum L_\mu / N_\mu$	Strahler (1964)
4	Stream length ratio (R_l)	$R_l = L / L_{(\mu-1)}$ Where L = The mean length of all stream segments of a given order(μ) $L_{(\mu-1)}$ = The mean length of all stream segments of one order less to given order(μ)	Horton (1945)
5	Bifurcation ratio (R_b)	$R_b = N_\mu / N_{(\mu+1)}$ Where N_μ = Total number of stream segments of the order “ μ ” $N_{(\mu+1)}$ = number of stream segments of the next higher order	Schumm (1956)
6	Drainage density (D_d)	$D_d = \sum L_\mu / A$ Where, $\sum L_\mu$ = Total length of the stream segments of all orders A = area of the river basin or grid (km^2)	Horton (1932)
7	Texture ratio	Number of stream segments of all order present in per perimeter of that area	Horton (1945)
8	Length of overland flow (L_o)	$L_o = 1/2D_d$ Where D_d = drainage density of basin	Horton (1945)

Important morphometric elements for comprehending the Teesta Basin's hydrological system are summarized in the table (Table 4). It includes Schumm's (1956) and Horton's (1932) Drainage Density (Dd), Texture Ratio, as well as Length of Overland Flow (Lo), as well as Strahler's (1964) Stream Order (μ), Stream Length (L), Mean Stream Length (L), Stream Length Ratio (Rl), and Bifurcation Ratio (Rb). These characteristics provide

essential insights into the flow hierarchy, distribution patterns, and surface runoff dynamics of the basin, and serve as the foundation for extensive basin research.

Table 5: Estimations of drainage morphometry, areal parameters

ESTIMATION OF AREAL PARAMETERS			
1	Circularity ratio (R_c)	$R_c = 4\pi A/P^2$ Where A = area of the basin (km^2), P = perimeter (km)	Miller (1953) Strahler (1964)
2	Elongation ratio (R_e)	$R_e = D/L = \frac{1.2\sqrt{A}}{L}$ Where D = diameter of a circle of the same area (A) as the basin, A = Area of the basin (km^2), L = Basin length (km)	Schumm(1956)
3	Form Factor (F_f)	$F_f = A/L^2$ Where A = area of the basin (km^2), L = Basin length (km)	Horton (1932, 1945)
4	Compactness constant (C_c)	Ratio between basin perimeters to the perimeter of a circle to the same area	Horton (1945)
5	Drainage texture (T)	$T = D_d \times F_f$ Where D_d = drainage density, F_s = stream frequency	Horton (1945)
6	Shape factor (B_s)	$B_s = L^2/A$ Where L = Basin length (km), A = area of the Basin (Km^2)	Horton (1932)
7	Constant of channel maintenance (C)	$C = 1/D_d$ Where D_d = drainage density of basin	Schumm (1956)
8	Drainage Frequency (F_μ)	$F_\mu = N_\mu / A$	Horton (1932)

Above table (**Table 5**) shows geometric characteristics needed to evaluate the Teesta Basin's form and structure. It measures basin roundness, elongation, compactness, and perimeter in respect to an equivalent circle using Circularity Ratio (R_c), Elongation Ratio (R_e), Form Factor (F_f), and Compactness Constant (C_c). These characteristics include Drainage Texture (T) for network complexity, form Factor (B_s) for basin form, and Constant of Channel Maintenance (C) for channel maintenance. These measures provide brief geometric insights into the basin, which are crucial for hydrological knowledge and conservation initiatives.

Table 6: Estimation of drainage morphometry, relief aspects

ESTIMATION OF RELIEF ASPECTS			
1	Basin Relief (R)	$R=H-h$ Where H= maximum elevation (m), h = minimum elevation (m)	Handley and Schumm (1961)
2	Relief Ratio (R_r)	$R_r = R/L$ Where R = Basin relief, L= longest axis of the major river (Basin length) in km	Schumm (1956)

The above table (**Table 6**) lists critical relief estimate criteria for analyzing Teesta Basin topography. Basin Relief (R), determined as the difference between the highest (H) and lowest (h) heights according to Handley and Schumm (1961), indicates vertical variation in the basin. Schumm (1956)'s Relief Ratio (R_r) shows basin relief in proportion to its longest axis (L), revealing its relief patterns. These estimates are essential for understanding the basin's topology, geological analysis, and landscape protection.

3.8 MULTIVARIATE STATISTICAL ANALYSIS

3.8.1 Correlation Matrix

Correlation studies play a pivotal role in the assessment of the relative concentration of various pollutants in water, offering essential insights for the development of effective water quality management plans (Sharma 2011). From a statistical perspective, correlation analysis unveils the connections between different variables, with the correlation coefficient serving as a quantitative measure of the extent of these connections (Milana et al. 2013). Essentially, the correlation coefficient reveals how one variable's behavior is linked to changes in another associated variable. Mathematically, the correlation coefficient (r_{xy}) between two variables, x and y, is expressed as follows:

$$r_{xy} = \frac{\sum (x_i - \bar{x})(y_i - \bar{y})}{\sqrt{\sum (x_i - \bar{x})^2} \sqrt{\sum (y_i - \bar{y})^2}}$$

where \bar{x} and \bar{y} represent the mean values of the x and y variables. To conduct the correlation studies in this study, the SPSS software was employed. Pearson's correlation test was applied to the dataset, generating the Pearson's product moment correlation coefficients, denoted as 'r'. These 'r' values signify the linear relationship between different pairs of water quality variables (Seth et al. 2014).

In essence, an 'r' value close to 0 indicates minimal dependence between the variables, while values approaching +1 or -1 signify a strong and near-linear interdependence between the variables (Seth 2014 and Mudgal et al. 2009). This in-depth analysis of correlations is invaluable for discerning how changes in one variable relate to corresponding changes in another, providing essential insights for effective water quality management and decision-making.

3.8.2 Principal Component Analysis (PCA)

Principal Component Analysis, also known as PCA, is a popular dimensionality reduction along with feature extraction approach in data analysis as well as machine learning. It aids in the transformation of high-dimensional data into lower-dimensional data while maintaining the majority of the critical information. PCA finds the data's principal components, which are vectors with opposite angles reflecting the directions of highest variation.

Formulating Mathematically:

Let's take a look at a dataset that is represented by an $n \times p$ matrix X, where p is the number of variables and n is the number of observations. The initial phase in PCA is to standardize the data for each feature by dividing by the normal deviation (σ)

and subtracting the mean (μ):

$$Z = \frac{(X - \mu)}{\sigma}$$

The covariance matrix C of the standardized data is then calculated via PCA:

$$C = \frac{1}{n} Z^T Z$$

where the transform of the standardized data matrix Z is indicated by the symbol Z^T .

The covariance matrix V is then divided into eigenvalues ($\lambda_1, \lambda_2, \dots, \lambda_p$) and associated eigenvectors (V_1, V_2, \dots, V_p) via PCA. The main elements of the data are represented by these eigenvectors.

The percentage of variation explained by each primary component v_i is provided by:

$$\text{Proportion of Variance}(v_i) = \frac{\lambda_i}{\sum_{j=1}^p \lambda_j}$$

By choosing the top k principal components (where $k < p$), PCA enables dimensionality reduction by capturing the majority of variation. By projecting the standardized data matrix Z onto the top k main components, the reduced data matrix X' is produced:

$$X' = ZV_k$$

where V_k is a matrix with the top k eigenvectors as column.

PCA significantly reduces the number of features while keeping the fundamental patterns and connections within the data, enabling complicated datasets simpler to see and analyses.

In the present study PCA is run with SPSS 24 statistical software.

CHAPTER 4

RESULTS AND DISCUSSION

4.1 Introduction

In this section, a dual-phase study was performed to evaluate the water quality & hydrological processes of the Teesta Basin. To create a baseline knowledge, the main study used several indices such as a Water Quality Index (WQI), Permeability Index, which is as well as Heavy Metal Pollution Index, along with morphometric data. Following that, to ascertain the framework of water quality data and discern the primary factors governing water quality, a combination of multivariate statistical techniques, including Pearson's correlation analysis, Hierarchical Cluster Analysis (HCA), and Principal Component Analysis (PCA), were applied. This integrated approach gave a comprehensive view of the Teesta River Basin's water resources while supporting focused conservation efforts and long-term management policies.

4.2 Soil erosion prioritization

The drainage map of the study area shows the complex network of streams and rivers that drain it. Water flows via sub-watersheds SW1–SW8 to a common outlet. According to the Strahler stream ordering system, Second-order streams are the result of a convergence of first-order streams at the headwaters, which amalgamate to form higher-order streams. The region's plentiful rainfall may explain the research area's high drainage density, indicating a thick canal network. This assessment helps detect flood-prone areas, manage water pollution, develop water resources, and assess land use changes on drainage patterns. Watercourses run southwesterly, the Teesta River being the major river, and flood-prone locations are shown on the map. The map lacks flow rates, water quality ratings, and dams, which may be accessible from government agencies or research

organizations.

4.2.1 Stream Order

The hierarchical position of streams is a crucial factor for comprehending the drainage characteristics within a given watershed. This parameter was determined by employing the stream order model introduced by Strahler in 1957. In the case of the Teesta River basin, it is classified as a 6th order basin. Further details regarding the sub-watershed area, stream order, and the total count of streams per order and per sub-watershed can be found in Table 7 and Figure 4-1. These insights reveal that the Teesta River basin comprises a total of 838 streams, with the highest number of streams, 186, observed in SW-8 and the lowest in SW-2.

Among these streams, approximately 75.63% (633) are categorized as 1st order streams, 18.52% as 2nd order, 4.42% as 3rd order, 0.95% as 4th order, 0.48% as 5th order, and a mere 0.12% as 6th order streams. An intriguing observation is that the number of streams tends to decrease as the stream order increases, indicating a declining frequency of streams with higher stream orders. Such a stream arrangement is characteristic of basins where the flow direction typically follows the path from higher altitudes to lower altitudes, a feature that has been exemplified in the Teesta River basin (Strahler, 1957).

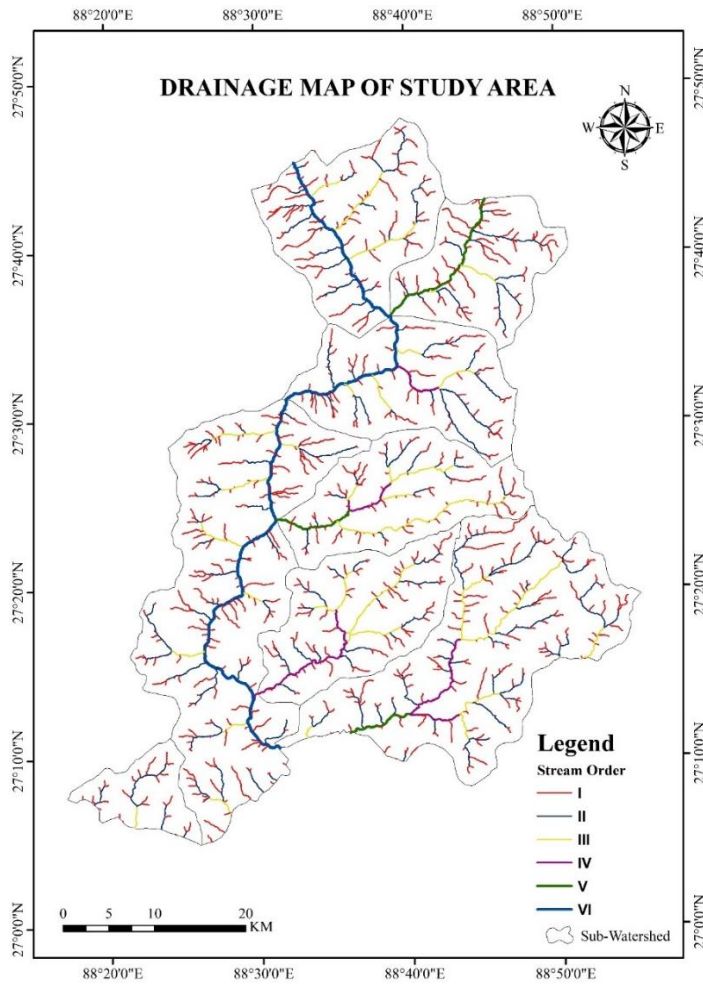


Figure 4-1: Drainage Map of study area
Table 7: Number of Streams of the study area.

Sl. No	Sub Watershed	Area (km ²)	Number of Streams						Total
			I	II	III	IV	V	VI	
1	SW1	599.86	82	34	8		1	1	126
2	SW2	81.77	22	5	1				28
3	SW3	270.95	72	18	5	1	1		97
4	SW4	294.04	96	19	4	1			120
5	SW5	200.47	53	12	3	1			69
6	SW6	245.95	85	17	6	2	1		111
7	SW7	252.27	77	19	4	1			101
8	SW8	508.73	146	31	6	2	1		186
Total			633	155	37	8	4	1	838
Percentage (%)			75.63	18.52	4.42	0.95	0.48	0.12	100

4.2.2 Stream Length

This parameter, calculated in line with Horton's second law (Horton, 1945), indicates that total stream length decreases as stream order increases. In essence, it means that the longest cumulative stream length is usually linked with the lowest stream order. The results, found in Table 8 and Figure 4-1, confirm that the study area aligns with Horton's law.

Among the basin's total stream length, which accounts to 1577.39 km (with the highest cumulative stream length observed in SW-1 and the lowest in SW-2), the distribution is consistent with Horton's law. Specifically, the 1st order streams account for the highest total stream length of 777.69 km, followed by 2nd order streams with a combined length of 409.94 km, 3rd order streams with 205.0 km, 4th order streams with 89.8 km, 5th order streams with 58.19 km, and the 6th order streams with the lowest total length. This variation can be ascribed to differences in slope steepness, lithological variations, and the flow from high-altitude to lower-altitude regions (Horton, 1945).

Table 8: Stream Length of the study area.

Sl. No	Sub Watershed	Area	Stream Length in Km						Total	
			I	II	III	IV	V	VI		
1	SW1	599.86	202.92	88.71	37.83			18.71	36.27	384.44
2	SW2	81.77	21.09	11.92	2.53					35.54
3	SW3	270.95	77.66	53.97	15.56	11.65	21.77			180.61
4	SW4	294.04	100.44	52.92	24.50	21.06				198.92
5	SW5	200.47	79.47	31.15	12.82	11.05				134.49
6	SW6	245.95	67.35	27.35	40.86	7.63	9.77			152.96
7	SW7	252.27	71.02	41.83	28.57	19.47				160.89
8	SW8	508.73	157.74	102.09	42.83	18.94	7.94			329.54
Total		2454.03	777.69	409.94	205.50	89.80	58.19	36.27		1577.39
Percentage (%)			49.30	25.99	13.03	5.69	3.69	2.30		100.00

4.2.3 Sub-watersheds prioritization based on morphometric parameters

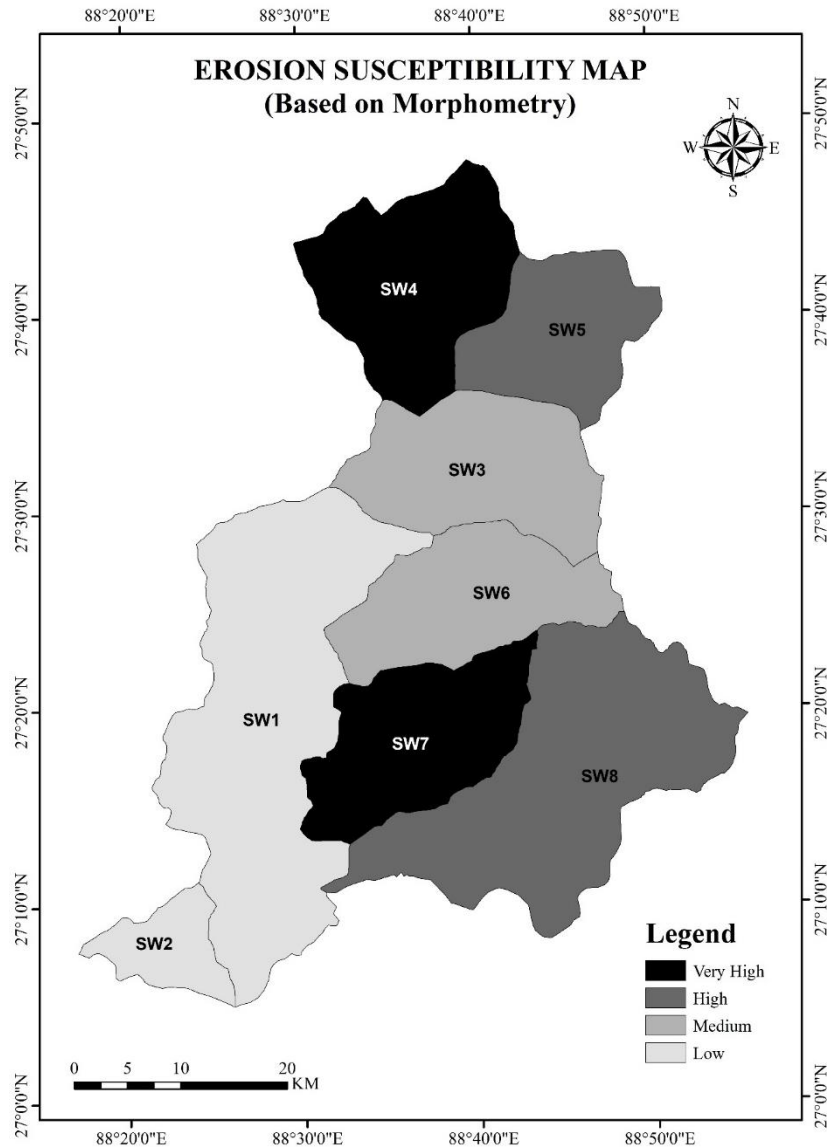


Figure 4-2: Erosion Susceptibility map based on drainage morphometry

Table 9 and Figure 4-2 provide insights into the erosion susceptibility of sub-watersheds based on morphometric characteristics. The results categorize the sub-watersheds into different priority levels. SW-4 and SW-7 are classified as "very high priority" due to their C_p values of 4.62 and 6.12, respectively. SW-5 and SW-8 fall into the "high priority" category with C_p values of 6.25 and 6.62. SW-6 and SW-3 are considered "medium priority" sub-watersheds, characterized by C_p values of 6.87 and 7. SW-1 and SW-2 are

labeled as "low priority" sub-watersheds, with Cp values of 8.12 and 8.37.

The significance of SW4, SW7, SW8, and SW5 lies due the contribution to soil erosion in the watershed. This is primarily due to their steep slopes, which play a pivotal role in erosional and geomorphic processes, leading to higher erosion susceptibility. SW3 and SW6 are placed in the medium priority category, attributed to their moderate slopes and lower drainage density. In contrast, SW1 and SW2 are considered low priority in terms of erosion susceptibility, mainly because they have less steep slopes compared to the other sub-watersheds.

Table 9: Morphometry based watershed prioritization for erosion susceptibility of study area.

Subwatershed	Linear Parameters					Shape (Areal parameters)					Relief	Cp Value	Erosion Susceptibility	
	D _d	F _u	R _b	L _o	T	R _c	R _f	R _e	C _c	B _s	C	H		
SW1	0.64	0.21	3.3	0.32	0.85	0.35	0.24	0.56	1.70	4.11	3.3	3510	8.125	Low Priority
Rank	6	8	7	4	7	1	1	1	8	8	7	7		
SW2	0.43	0.34	4.7	0.22	0.62	0.50	0.32	0.64	1.41	3.13	4.7	2008	8.375	Low Priority
Rank	8	7	1	8	8	3	8	8	6	1	1	8		
SW3	0.67	0.36	3.4	0.33	1.31	0.62	0.27	0.59	1.27	3.69	3.4	4495	7	Medium Priority
Rank	3	5	6	3	5	6	6	6	3	5	6	2		
SW4	0.68	0.41	4.6	0.34	1.63	0.68	0.27	0.58	1.21	3.73	4.6	3973	4.625	Very High Priority
Rank	1	2	2	2	1	8	5	3	1	6	2	4		
SW5	0.67	0.34	3.8	0.34	1.10	0.64	0.28	0.60	1.25	3.54	3.8	3907	6.625	High Priority
Rank	2	6	4	1	6	7	7	7	2	2	4	5		
SW6	0.62	0.45	3.21	0.31	1.49	0.55	0.27	0.59	1.34	3.64	3.21	4558	6.875	Medium Priority
Rank	7	1	8	7	2	4	4	5	5	3	8	1		
SW7	0.64	0.4	4.27	0.32	1.35	0.57	0.27	0.59	1.33	3.65	4.27	3731	6.125	Very High Priority
Rank	5	3	3	5	4	5	3	4	4	4	3	6		
SW8	0.65	0.37	3.72	0.32	1.48	0.40	0.25	0.56	1.57	4.02	3.72	4395	6.25	High Priority
Rank	4	4	5	6	3	2	2	2	7	7	5	3		

4.2.4 Sub-watersheds prioritization based on land cover parameters

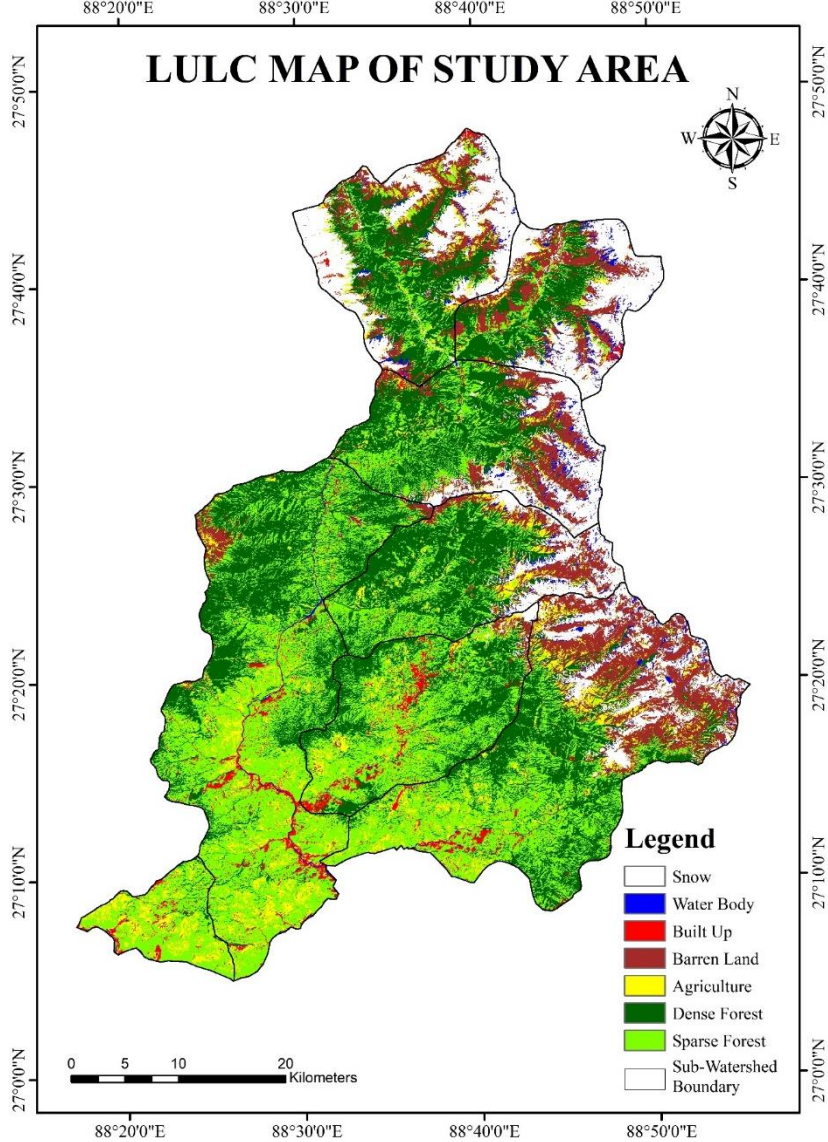


Figure 4-3: LULC Map of study area

The study area was categorized into seven primary land cover classes, namely water bodies, dense forests, sparse forests, snow, barren lands, agricultural areas, and built-up regions (Figure 4-3). The classification of these land cover types was primarily based on their significant contribution to accelerating land degradation, particularly erosion. A ground verification exercise, conducted as a post-classification step, involved

the collection of 349 ground truth samples.

The Maximum Likelihood Classification (MLC) exhibited an overall accuracy of 95.98% (Table 9), accompanied by a Kappa coefficient of 0.98. This level of accuracy falls within the acceptable range (>80%) recommended for erosion risk assessment utilizing land cover classes (Foody, 2002). To prioritize each sub-watershed, ranks were assigned based on the potential of specific land cover types to trigger erosion. Subsequently, compound values were computed, taking into account the land cover category ranking. Higher priority was assigned to sub-watersheds with smaller snow-covered areas, cultivation zones, lower vegetative cover, and larger barren lands, whereas the lowest priority was given to those with larger snow-covered areas, cultivation zones, greater vegetative cover, and extensive built-up regions. The summarized statistics for land cover categories, Cp values, and prioritization of sub-watersheds are presented in Table 11.

The land cover distribution indicated that water bodies, comprising perennial rivers, streams, lakes, and ponds, covered 40.03 km² (1.63% of the area). Dense forests, characterized by a 40% tree canopy density, dominated the land cover, occupying 778.63 km² (31.73%). Sparse forests, encompassing shrubs, agroforestry areas, and lands with tree canopy densities ranging from 10% to 40%, covered 764.45 km² (31.15%). Snow-covered areas accounted for 331.38 km² (13.5%), while barren lands, consisting of sediments, exposed rocks, landslide zones, and degraded forest regions, covered 296.2 km² (12.08%). Agricultural lands occupied 181.22 km² (7.38%), and built-up areas shared 62.11 km² (2.53%).

The analysis of compound values, as illustrated in Table 10, revealed that sub-

watersheds SW-3, SW-4, and SW-5, with Cp values of 3.83, 4, and 4, respectively, were assigned a "very high priority" ranking. SW-8 and SW-6, with Cp values of 4.33 and 4.5, respectively, were classified as "high priority" sub-watersheds. SW-1 and SW-7, with Cp values of 5.33 and 5.5, respectively, were designated as "medium priority." Meanwhile, SW-2, with a Cp value of 5.83, was allocated a "low priority" ranking (Figure 4-4).

Table 10: Accuracy assessment of supervised land cover classification of study area.

Reference data								Ground Truth Total	User's Accuracy
	DF	S	W	B	Ag	SF	BL		
Classification data									
DF	45				2		2	49	98
SW		50						50	100
W	1		50					51	98.03
B				45		2	2	49	100
Ag					50			50	100
SF						46	4	50	100
BL							49	50	98
<i>Column Total</i>	46	50	50	46	52	48	57	349	
<i>Producer's Accuracy</i>	90	100	100	90	100	192	98		
Overall accuracy $[(45 + 50 + 50 + 45 + 50 + 46 + 49)/349] \times 100 = 95.98 \%$									
DF Dense Forest, S Snow, W waterbody, B Built-up, Ag Agriculture, SF Sparse forest, BL Barren Land									

Table 11: LULC based watershed prioritization for erosion susceptibility of study area.

Subwatershed	Snow	Builtup	Barren Land	Agriculture	Dense Forest	Sparse Forest	C_p Value	Erosion Susceptibility
SW-1	0.00	4.47	1.94	8.21	33.81	50.29	5.33	Medium
Rank	1	6	7	6	5	7		
SW-2	0.00	5.98	1.20	25.87	4.40	62.25	5.83	Low
Rank	2	8	8	8	1	8		
SW-3	20.63	0.73	17.43	3.35	37.81	17.19	3.83	very High
Rank	6	3	3	1	7	3		
SW-4	34.61	0.74	16.88	4.73	30.57	10.53	4	very High
Rank	7	4	4	3	4	2		
SW-5	36.60	0.49	23.58	4.00	24.52	7.03	4	very high
Rank	8	2	1	2	2	1		
SW-6	14.86	0.40	11.53	5.36	45.22	20.92	4.5	High
Rank	5	1	5	4	8	4		
SW-7	0.67	5.92	2.26	7.46	36.10	46.40	5.5	Medium
Rank	3	7	6	5	6	6		
SW-8	12.21	1.83	20.71	8.69	25.25	29.83	4.33	High
Rank	4	5	2	7	3	5		

Table 12: Watershed prioritization for erosion susceptibility of study area based on the combined influences of morphometry and land cover.

SW	Morphometric Parameters												Land Cover						C_p Value	Erosion Susceptibility
	Linear parameters				Shape (Areal parameters)					Relief			S	B	BL	Ag	DF	SF		
	D_d	F_u	R_b	L_o	T	R_c	R_f	R_e	C_c	B_s	C	H								
SW1	6	8	7	4	7	1	1	1	8	8	7	7	1	6	7	6	5	7	5.39	7
SW2	8	7	1	8	8	3	8	8	6	1	1	8	2	8	8	8	1	8	5.67	8
SW3	3	5	6	3	5	6	6	6	3	5	6	2	6	3	3	1	7	3	4.39	4
SW4	1	2	2	2	1	8	5	3	1	6	2	4	7	4	4	3	4	2	3.39	1
SW5	2	6	4	1	6	7	7	7	2	2	4	5	8	2	1	2	2	1	4	2
SW6	7	1	8	7	2	4	4	5	5	3	8	1	5	1	5	4	8	4	4.56	5
SW7	5	3	3	5	4	5	3	4	4	4	3	6	3	7	6	5	6	6	4.56	6
SW8	4	4	5	6	3	2	2	2	7	7	5	3	4	5	2	7	3	5	4.22	3

SW Sub-watershed, D_d Drainage density, F_u Stream frequency, L_o Length of overland flow, T Drainage Texture, R_c Circularity ratio, R_f Form factor, R_e Elongation ratio, C_c Compactness coefficient, B_s Basin shape, C Constant of channel maintenance, H Basin relief, DF Dense Forest, S Snow, W waterbody, B Built-up, Ag Agriculture, SF Sparse forest, BL Barren Land

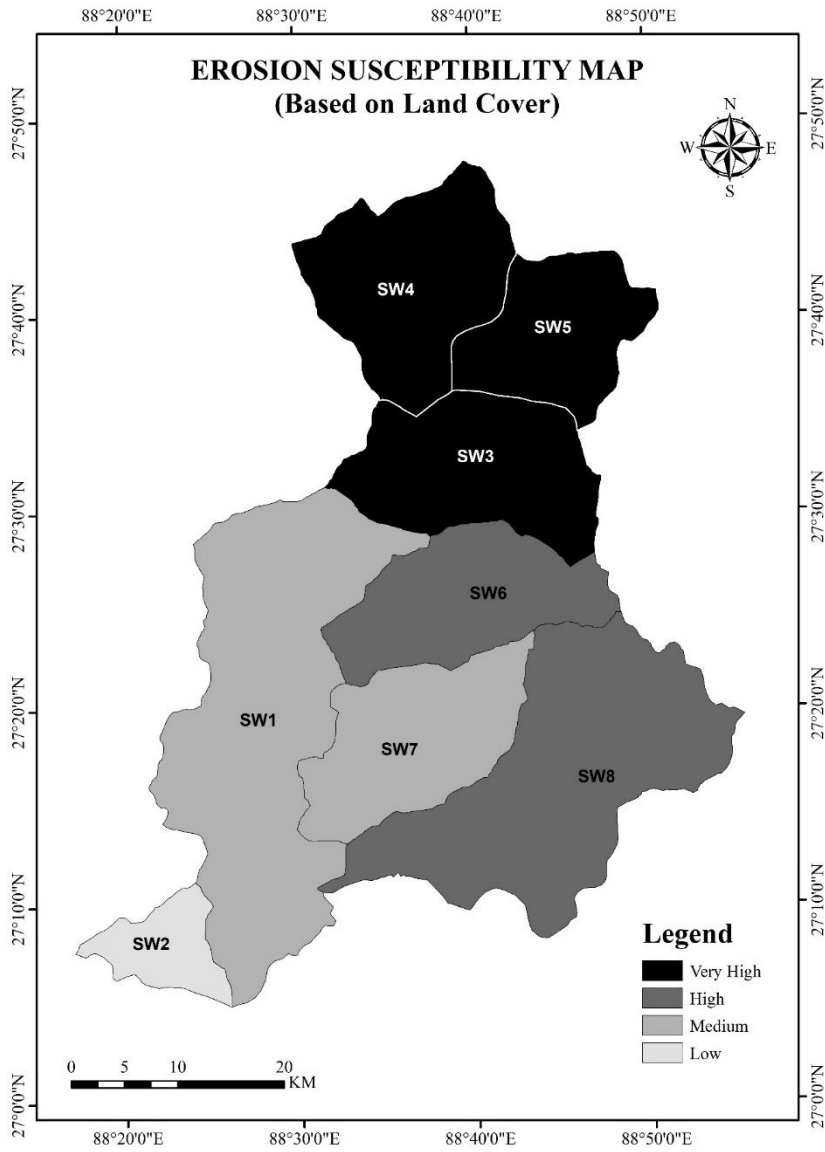


Figure 4-4: Erosion Susceptibility map based on land cover

4.2.5 Erosion Susceptibility map Based on Morphometry and Land Cover

In the final phase analysis, we undertook a comprehensive Multi-Criteria Analysis (MCA) that took into consideration the distinctive rankings assigned to various morphometric and land cover parameters. This holistic evaluation led to the classification of the sub-watersheds into eight distinct categories, which were designated as 1, 2, 3, 4, 5, 6, 7, and 8.

The results, presented in both Table 12 and Figure 4-5, yielded several key insights into the vulnerability of these sub-watersheds. SW4 and SW5, characterized by the low Cp values (3.39 and 4), emerged as the most susceptible to erosion, which is ranked as 1 and 2. These rankings underscore the urgency and priority for implementing erosion control measures in these sub-watersheds. Following closely in the vulnerability spectrum, SW-8 and SW-3, Cp values of 4.22 and 4.39, respectively, were identified as the third and fourth most vulnerable sub-watersheds. They were aptly assigned rankings of 3 and 4, signifying the need for proactive measures to mitigate erosion risks.

Slightly further down the hierarchy, SW-6 and SW-7 shared a similar level of vulnerability, with both exhibiting identical Cp values of 4.56. As a result, they were classified as "medium priority" sub-watersheds, securing rankings of 5 and 6. In this context, the emphasis would be on maintaining a vigilant stance to prevent further exacerbation of erosion. On the other end of the spectrum, SW-2 and SW-1, with Cp values of 5.39 and 5.67, were identified as the sub-watersheds displaying the lowest susceptibility to erosion. Consequently, they were ranked at 8 and 7, reflecting the relatively lower urgency for immediate erosion control measures.

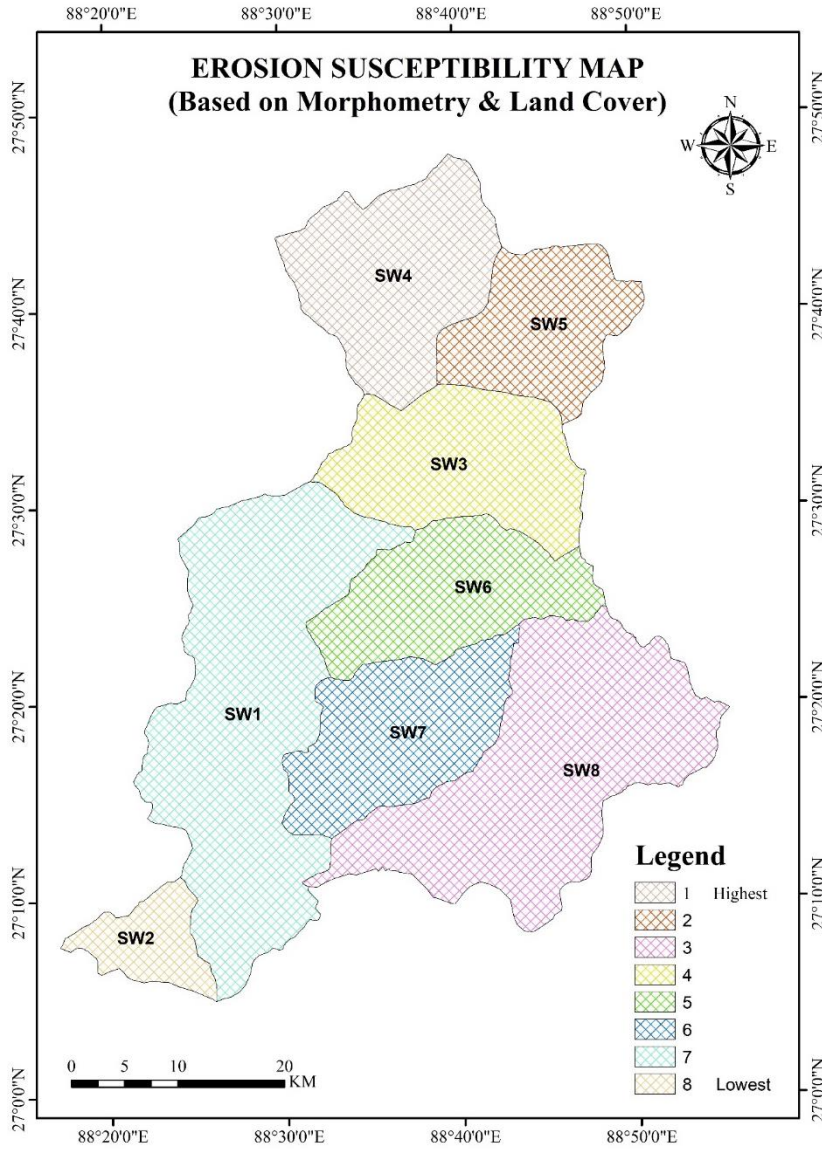


Figure 4-5: Erosion Susceptibility map Based on Morphometry and Land Cover

4.3 Assessment of major ions of Teesta River.

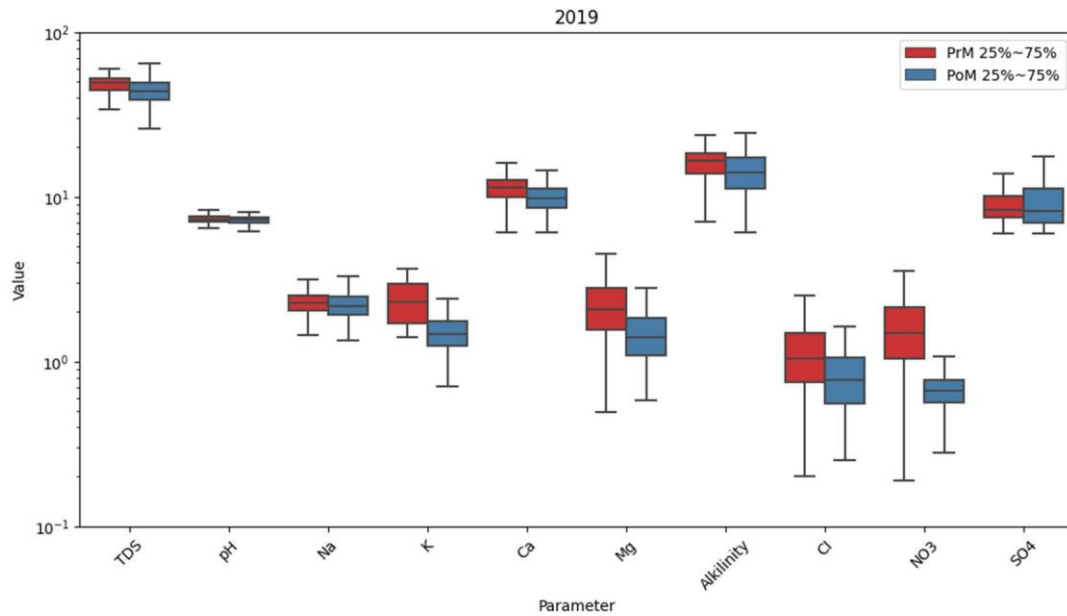


Figure 4-6: Box plot graphical representation of major ion concentration for PrM & PoM 2019.

Table 13: Descriptive statistical representation of major ions concentration in the Teesta river basin, shown in mg/L(2021)

		TDS	pH	Na	K	Ca	Mg	Alkalinity	F	Cl	NO ₃	SO ₄
2019 PrM	<i>Min</i>	34	6.44	1.44	0.46	6.06	0.49	6.10	0.01	0.20	0.19	6.01
	<i>Max</i>	60	8.32	3.17	4.64	18.13	5.53	23.64	0.23	5.51	5.56	13.93
	<i>Mean</i>	48	7.29	2.29	1.81	11.49	2.23	16.20	0.08	1.15	1.68	8.83
	<i>Median</i>	50	7.33	2.26	1.40	11.31	1.92	16.78	0.04	0.93	1.32	7.93
	<i>SD</i>	6.68	0.33	0.43	1.20	2.84	1.40	4.33	0.07	0.92	1.06	1.92
2019 PoM	<i>Min</i>	26	5.48	1.35	0.71	6.11	0.58	6.10	0.11	0.25	0.18	6.00
	<i>Max</i>	68	7.89	4.31	5.40	18.46	4.80	24.40	0.31	2.62	2.07	19.49
	<i>Mean</i>	43	7.22	2.22	1.53	10.16	1.53	15.13	0.20	0.88	0.67	9.10
	<i>Median</i>	44	7.30	2.10	1.43	9.45	1.27	12.96	0.20	0.66	0.66	7.29
	<i>SD</i>	9.95	0.53	0.63	0.85	3.08	0.83	5.09	0.04	0.59	0.38	3.83

The table 13 represents the descriptive statistical data of physio-chemical ion

concentration of the water sample in 2019 for two different seasons: the PrM (Pre-Monsoon) and the PoM (Post-Monsoon). Some of the critical indicators covered in the report are Total Dissolved Solids (TDS), pH, Sodium (Na), Potassium (K), Calcium (Ca), Magnesium (Mg), Alkalinity, Fluoride (F), Chloride (Cl), Nitrate (NO₃), and Sulphate (SO₄). Each parameter's minimum, maximum, mean, median, as well as standard deviation are shown in the table. Notably, PrM has somewhat higher TDS levels (mean of 48) than PoM (mean of 43), suggesting a minor difference in dissolved solids content. Both sources have pH values that are rather neutral, with PrM ranging from 5.48 to 8.32 and PoM ranging from 5.48 to 7.89. The sodium concentration of PoM (mean of 2.22) exceeds that of PrM (mean of 2.29), whereas the potassium content of PrM (mean of 1.81) is greater than that of PoM (mean of 1.53). Furthermore, PrM had greater calcium, magnesium, and alkalinity levels than PoM, indicating differences in mineral composition between the two sources. The descriptive statistical representation shows that spatio-temporal variation for premonsoon and postmonsoon of 2019 major ions concentrations in the study area

Table 14: Descriptive statistical representation of major ions concentration in the Teesta river basin, shown in mg/L (2021)

		TDS	pH	Na	K	Ca	Mg	Alkalinity	F	Cl	NO3	SO4
2021 PrM	Min	34	6.38	1.44	0.45	5.20	0.47	6.10	0.01	0.01	0.18	5.92
	Max	62	8.56	3.35	5.06	18.87	6.07	24.40	0.25	6.84	6.18	15.06
	Mean	47	7.29	2.29	1.79	11.51	2.21	16.11	0.08	1.14	1.67	8.86
	Median	50	7.30	2.26	1.35	11.25	1.85	18.30	0.04	0.93	1.27	7.93
	SD	7.19	0.35	0.48	1.22	2.95	1.44	4.65	0.07	1.04	1.12	1.99
2021 PoM	Min	27	5.47	1.02	0.68	5.99	0.49	6.10	0.08	0.25	0.17	4.95
	Max	68	7.94	4.55	6.58	18.56	5.82	24.40	0.31	2.96	3.25	19.60
	Mean	44	7.22	2.21	1.54	10.10	1.53	15.05	0.20	0.87	0.68	9.14
	Median	43	7.35	2.05	1.41	9.46	1.29	12.20	0.20	0.68	0.66	7.58
	SD	10	0.57	0.67	0.97	3.16	0.91	5.33	0.05	0.64	0.46	3.90

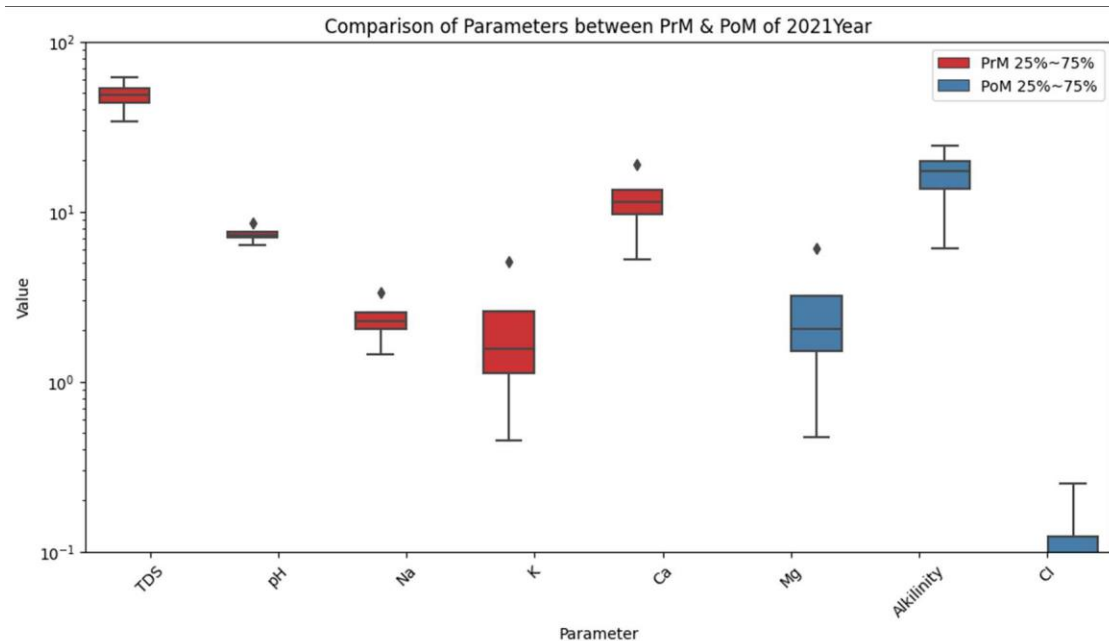
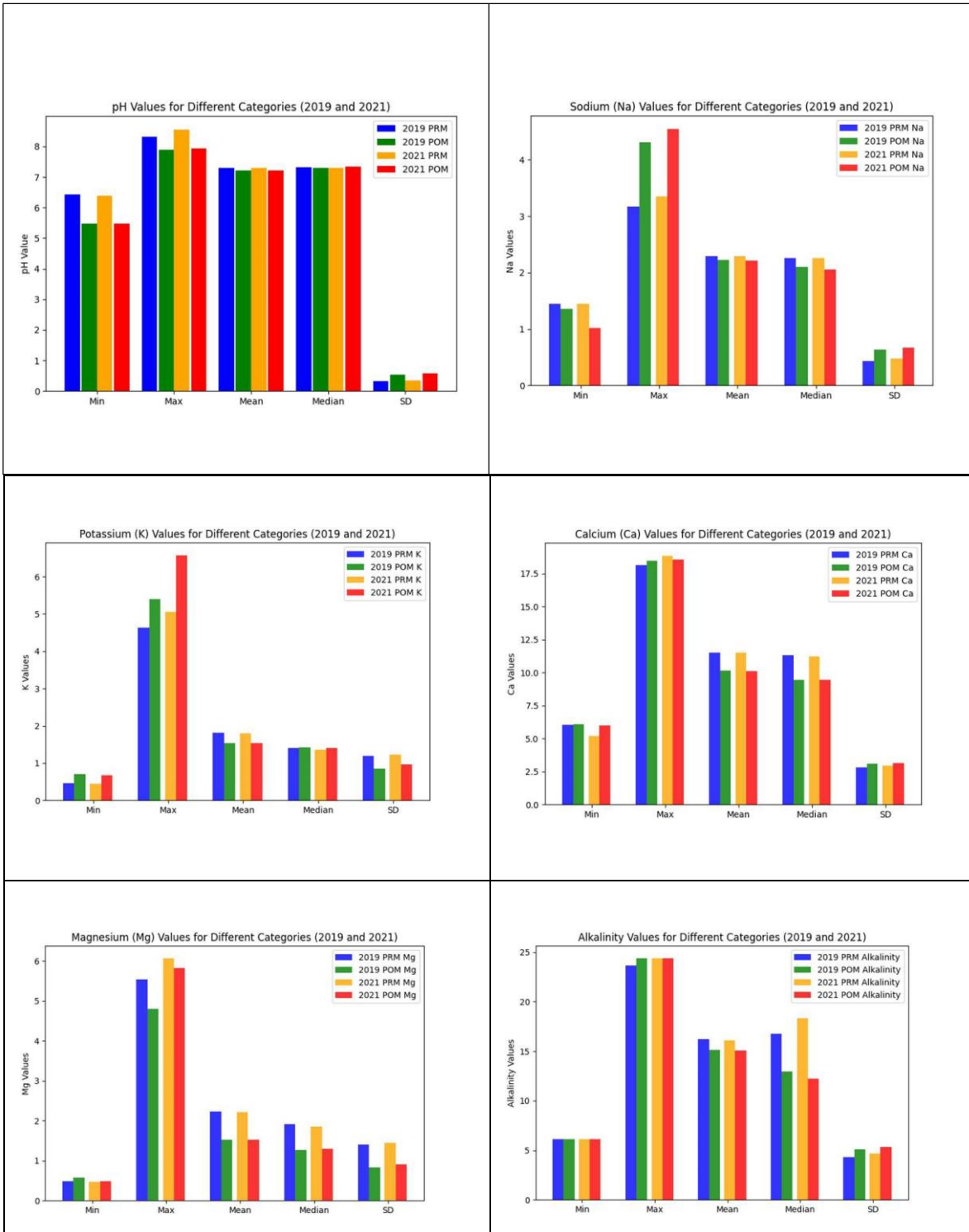


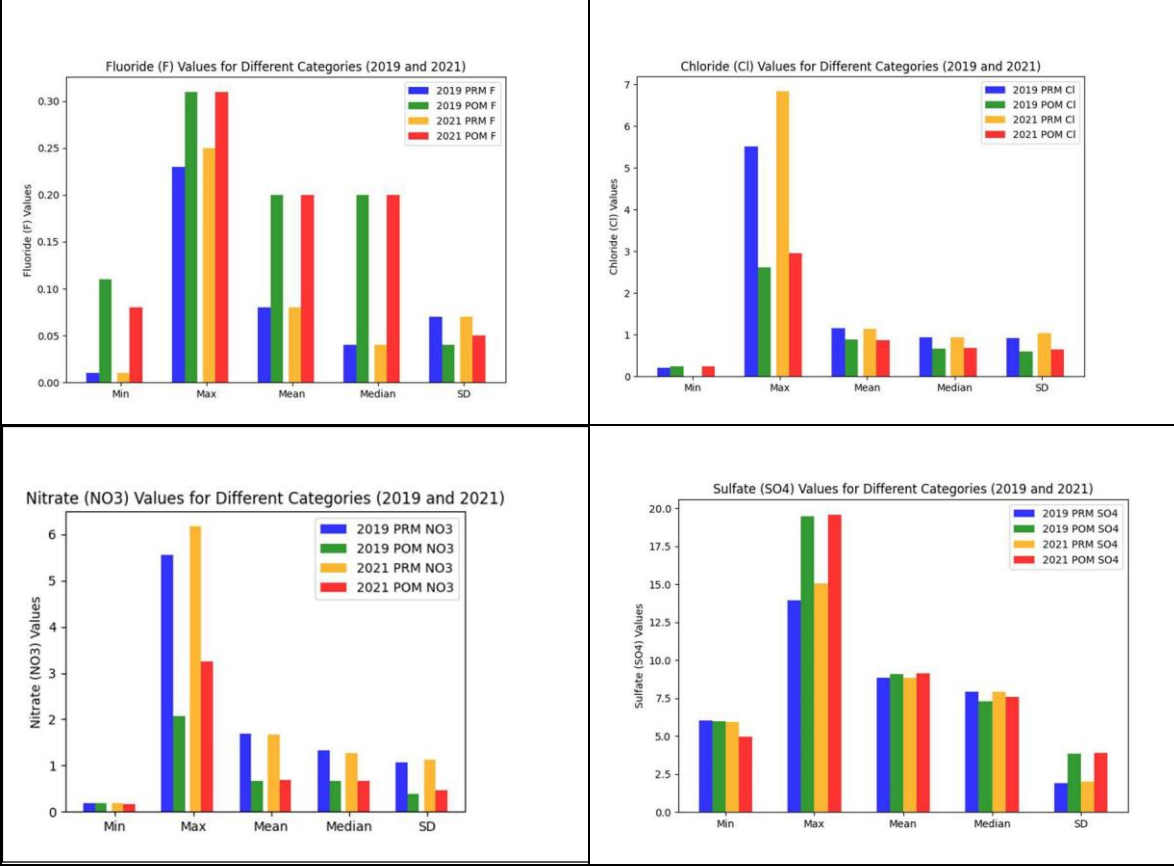
Figure 4-7: Box plot graphical representation of major ions concentration for PrM & PoM of 2021.

From the above table 14 & figure 4-7 it is observable that the complete study of water quality indicators measured in 2021 at the PrM (Pre-monsoon) & PoM (Post-monsoon). Total Dissolved Solids (TDS), pH, Sodium (Na), Potassium (K), Calcium (Ca), and Magnesium (Mg), as well as Alkalinity, Fluoride (F), Chloride (Cl), Nitrate (NO₃), and Sulphate (SO₄), are investigated for their lowest, maximum, mean, median, and standard deviation values. The dissolved solid concentration is indicated by TDS values ranging from 34 to 62 in PrM. The pH values at PrM and PoM remain generally neutral, ranging between 6.38 and 8.56 and 5.47 and 7.94, respectively. Notably, PrM has a higher mean sodium content (2.29) than PoM (2.21), although PoM has a slightly greater potassium content (1.54) than PrM (1.79). Calcium and magnesium levels are largely stable across both sources. The data also shows changes in chloride, nitrate, and sulphate levels, emphasizing the different composition of each of these ions in the water sources. The descriptive statistical representation shows that spatio-temporal variation for premonsoon

and postmonsoon of 2021 major ions concentrations in the study area

Table 15: Descriptive statistical graphical presentation using bar graph for Spatio-temporal variation of major ions, & pH, major ions conc. shown in mg/L.





4.4 HYDROCHEMICAL FACIES:

Hydrogeochemical facies layouts are graphical representations that attempt to explain the differences, similarities, and interpretation of various water types and evolutionary patterns in a given location. The use of graphical representation approaches is crucial for understanding diverse geochemical processes and for researching the impacts of mixing water within distinct lithological frameworks

4.4.1 Piper Diagram Analysis

Anion and cation compositions are shown on different ternary diagrams in Piper diagrams (1944), and the positions are projected into a quadrilinear, diamond-shaped grid (Fig. 4-8). The diagram's point locations disclose broad water compositions, infer a source, and demonstrate mixing. Piper's (1944) diagrams were also used to analyze the major ion data from the Teesta River. The general positions of the dots on the diagram suggest a source mineral and reveal the makeup of the water. The distribution of the points shows the variation in the composition of the water. In order to assess the hydro-chemical facies in water, the principal cations and anions, such as Ca^{2+} , Na^+ , Cl^- , SO_4^{2-} , and HCO_3^- , were plotted in mg/L using a Piper diagram for both seasons. Such an investigation considers the geochemical circumstances as well as the chemical processes that are active in the current lithological environment. Using the major cations (calcium, magnesium, sodium, and potassium) as well as anions (bicarbonate, sulphate, and chloride), Piper diagram provides a comprehensive picture of water types throughout the study area. The diagram depicts the cation and anion fields, which represent the most abundant ions, while the center field displays water samples to determine their type. In limestone-rich locations, the most common water type is calcium-

bicarbonate (Ca-HCO₃). Other common types include sodium-chloride (Na-Cl) in coastal areas, mixed calcium-sodium-bicarbonate (Ca-Na- HCO₃) where water types mix, mixed calcium-magnesium-chloride (Ca-Mg-Cl) in salt deposit regions, and sodium-bicarbonate (Na-HCO₃) in saline groundwater areas

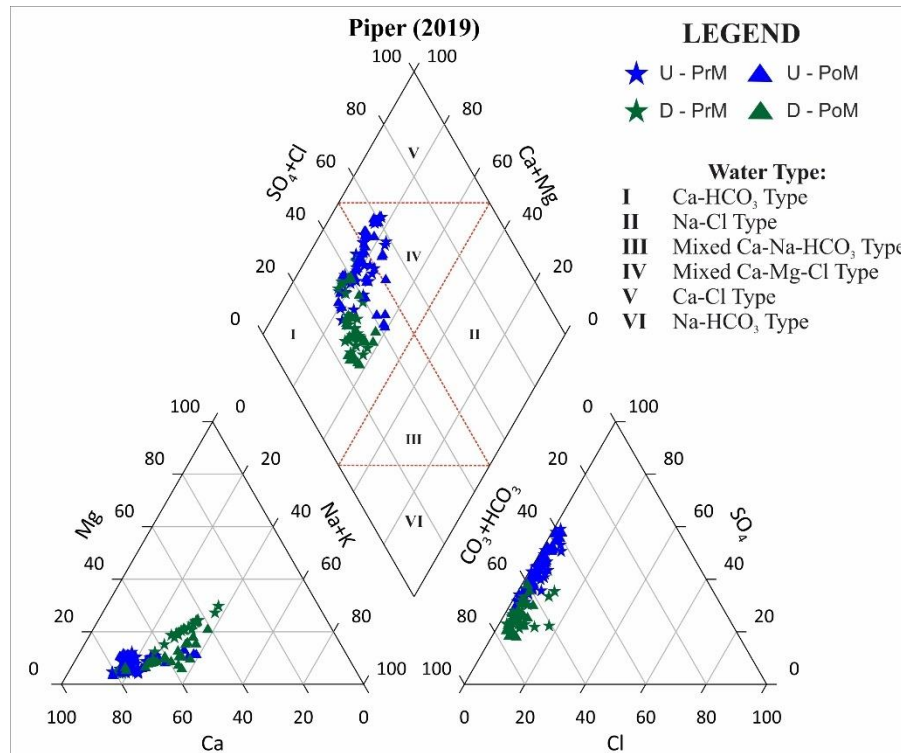


Figure 4-8: Piper's trilinear diagram, showing the relationship between dissolved ions and hydrochemical facies in the Teesta river basin (2019)

In the present study, the Piper diagram for 2019 (Figure 4-8) inferred that the water type is mainly composed of Ca-HCO₃ Water Type at the downstream during pre-monsoon and post-monsoon and a combination of water type of Ca-HCO₃ and Mixed Ca-Mg-Cl Type was inferred at upstream for both the seasons.

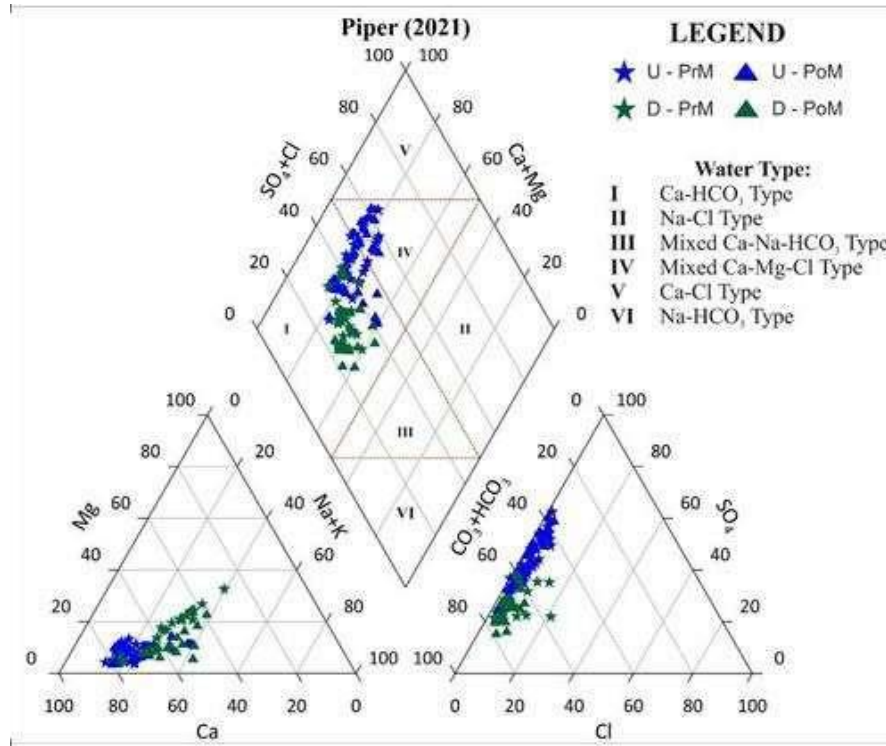


Figure 4-9: Piper's trilinear diagram, showing the relationship between dissolved ions and hydro chemical facies in the Teesta river basin (2021)

The 2021 Piper diagram (Figure 4-9) classifies primary cations (Ca, Mg, Na, K) as well as anions (HCO₃, SO₄, Cl). The hydro-chemical facies are mainly dominated by calcium-bicarbonate (Ca- HCO₃) water type during pre-monsoon in the downstream of the study area, while in the upstream of the study area during the hydro-chemical facies is jointly contributed by Ca-CHO₃ water type and Mixed Ca-Mg-Cl water type.

4.4.2 Durov Plot

Durov plot is a significant graphical structure that gives better data on the hydro-chemical portrayal and possible geochemical processes (mixing, cation exchange, reverse ion exchange dissolution) influencing the water quality of the area. This diagram is a composite plot consisting of two ternary diagrams where the milli equivalents percentages of the cations concentration were plotted against that of anions concentration; sides form a central rectangular, binary plot of total cation vs. total anion concentrations. This diagram is useful in indicating the samples with similar chemical composition as well as determines a useful relationship among different water samples. The Durov plot depicts the dominant hydro-chemical facies in the research region, highlighting a reverse cation and exchange processes. This demonstrates that several factors have substantial influence on the water chemical composition, including salt water intrusion, ion exchange mechanism, and carbonate mineral dissolution. While other facies such as calcite and gypsum dissolution, $\text{HCO}_3\text{-Ca}$ infiltration waters, $\text{HCO}_3\text{-Na}$ cation exchange water. The Durov plot may be used to identify the water sources, asses possible contamination hazards, and develop effective management plans for water chemistry of the region.

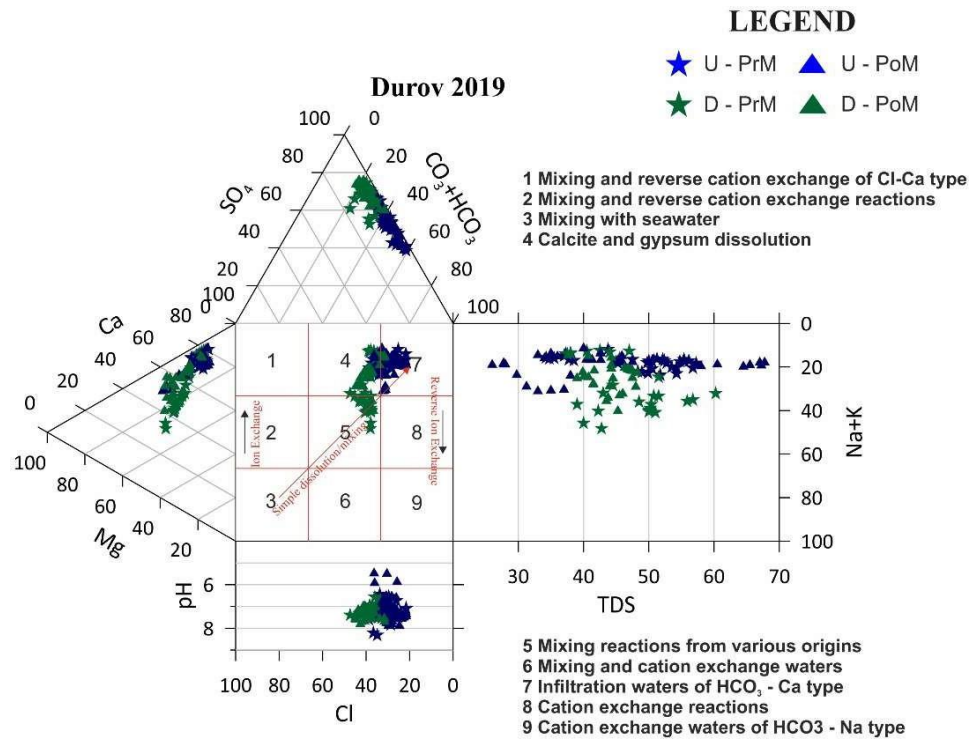


Figure 4-10: Durov diagram 2019, showing the hydrochemical facies in the Teesta river basin.

The 2019 Durov plot (Figure 4-10) depicts the dominant hydro chemical facies in the research region, highlighting a combination of calcite-gypsum dissolution and infiltration water of HCO_3^- - Ca types during pre-monsoon and post-monsoon at the downstream of the river. Whereas, mixing reactions from various origin and calcium-gypsum types during pre-monsoon and post-monsoon at the upstream of the river water.

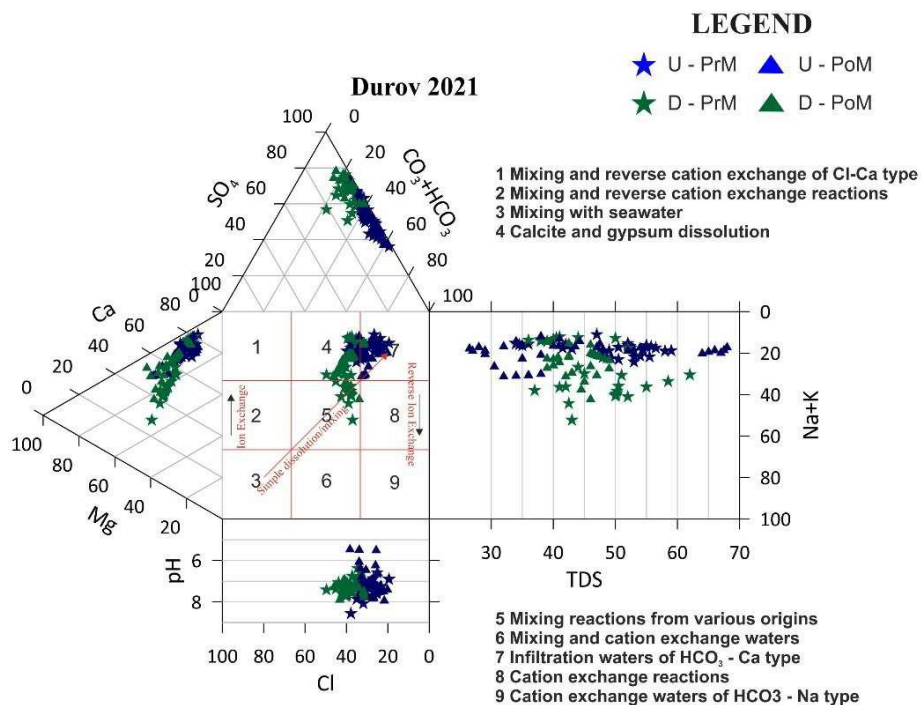


Figure 4-11: Durov diagram 2021, showing the hydrochemical facies in the Teesta River basin

According to the 2021 Durov plot (Figure4-11), the dominate hydro chemical facies in the study area is a combination of calcite-gypsum dissolution and mixing reaction from various origins during pre-monsoon and post-monsoon at the upstream of the study area. Whereas, the dominate hydro chemical facies during pre-monsoon and post-monsoon at downstream is a combination of calcite-gypsum dissolution and infiltration water of HCO₃ - Ca types of the study area

4.5 FACTORS CONTROLLING HYDRO-CHEMISTRY

4.5.1 Gibbs Diagram

The Gibbs plot provides a clear interpretation of hydro chemical processes including evaporation, precipitation, and rock-water interaction. Gibbs proved that plotting total dissolved solid versus $\text{Na}^{2+}/(\text{Na}+\text{Ca}^{2+})$ and $\text{Cl}/(\text{Cl}+\text{HCO}_3)$ would provide details about the mechanism governing the chemistry of water. The three primary variables that together influence the chemistry of water are (1) rock dominance, (2) precipitation dominance, and (3) evaporation dominance.

Research conducted in various other regions of the Himalayas has confirmed that the primary factor influencing the ionic composition of water bodies is the rock dominance. In the particular study area, extensive interactions between water and rock over an extended period, including percolation and flow through rocky lithological formations, have led to a notable increase in solute concentration. The major ion concentration significantly governs the water quality in the area. In the present study, Gibbs's diagram shows that all samples for premonsoon and postmonsoon for both the year 2019 and 2021 fall under the rock dominance category shown in **Figure 4-12, 4-13**. This study indicates that the primary controlling factors of hydrochemistry for Teesta River is governed by rock dominance.

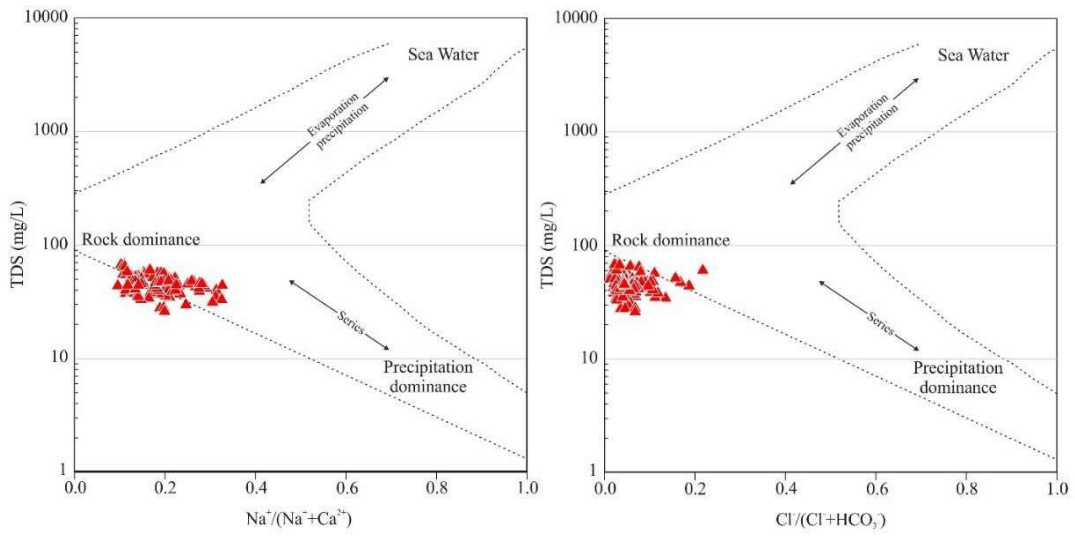


Figure 4-12: 2019 Gibb's Diagram

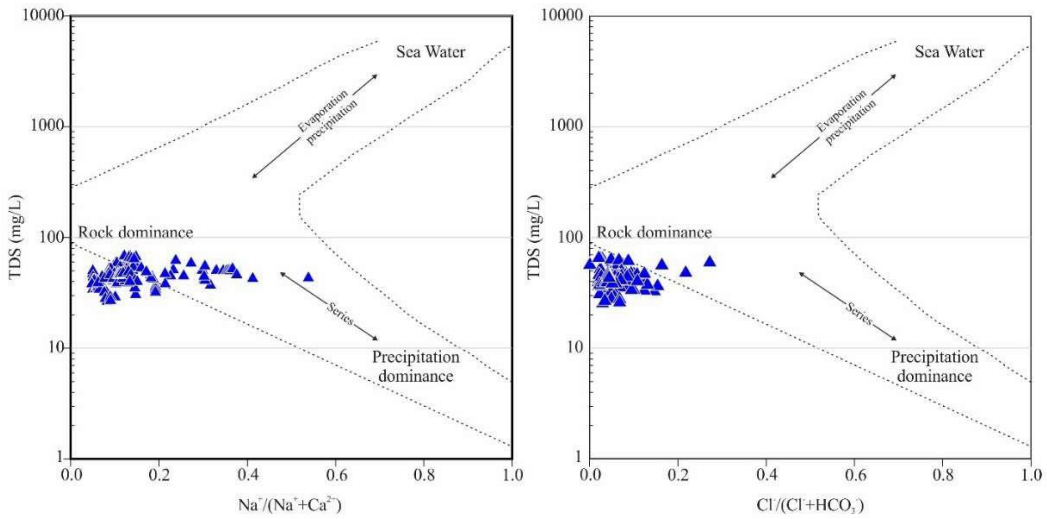


Figure 4-13: 2021 Gibb's Diagram

4.5.2 Bivariate Na-normalized molar ratios mixing diagram

Bivariate Na-normalized molar mixing diagram is plotted to understand the weathering controlled (silicate and carbonate weathering) in water chemistry. The diagram is plotted against Mg^{2+}/Na^+ vs Ca^{2+}/Na^+ and HCO_3^-/Na^+ vs Ca^{2+}/Na^+ . The calcium-sodium (Ca^{2+}/Na^+) ratios in the waters of the Himalayan streams exhibit considerable diversity. For instance, Krishnaswami and Singh (1999) reported an average Ca^{2+}/Na^+ ratio of 0.7, whereas Jacobson et al. (2002a) estimated it to be 0.18 for the Raikhot watershed within the Himalayan region. In our current investigation, the mixing diagram is plotted against all required ion concentration in mg/L as shown in **Figure 4-14, 4-15**. The broad spectrum of Ca^{2+}/Na^+ ratios in the Himalayan region can be ascribed to variations in the geological composition of both the Higher and Lesser Himalayan regions. The precise quantification of Ca^{2+} and Na^+ contributions from rocks remains a challenge, as pointed out by Krisnaswami and Sunil Singh (2005).

In the present study, Bivariate Na-normalized molar mixing diagram was plotted as shown in the **Figure 4-14, 4-15**, which reveals that the ion concentration for pre-monsoon and post-monsoon for both the year is primarily controlled by the mixing of carbonate and silicate weathering. It can be understood that the main controlling factor of the hydrochemistry of the study area, Teesta River is of geogenic weathering, which is carbonate and silicate weathering

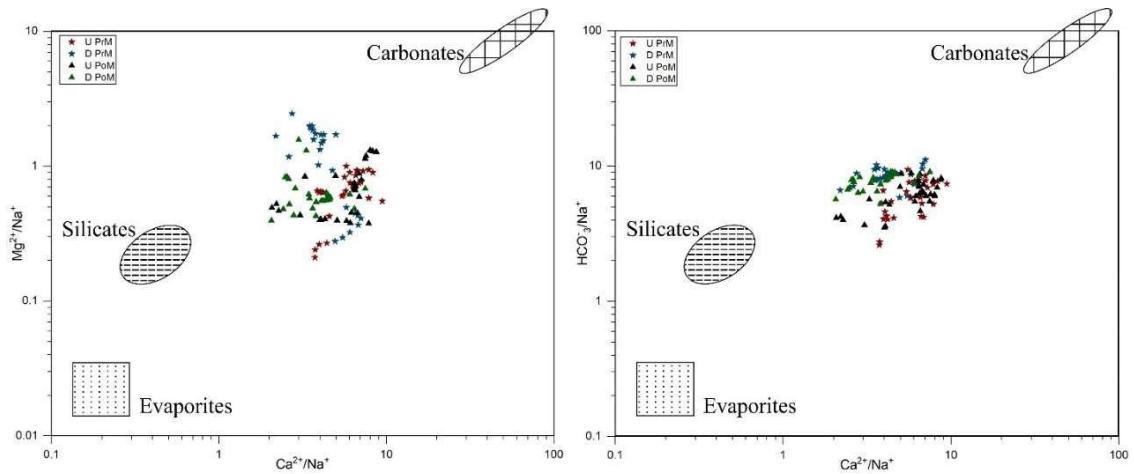


Figure 4-14: Bivariate Na-normalized molar ratios mixing diagram for 2019.

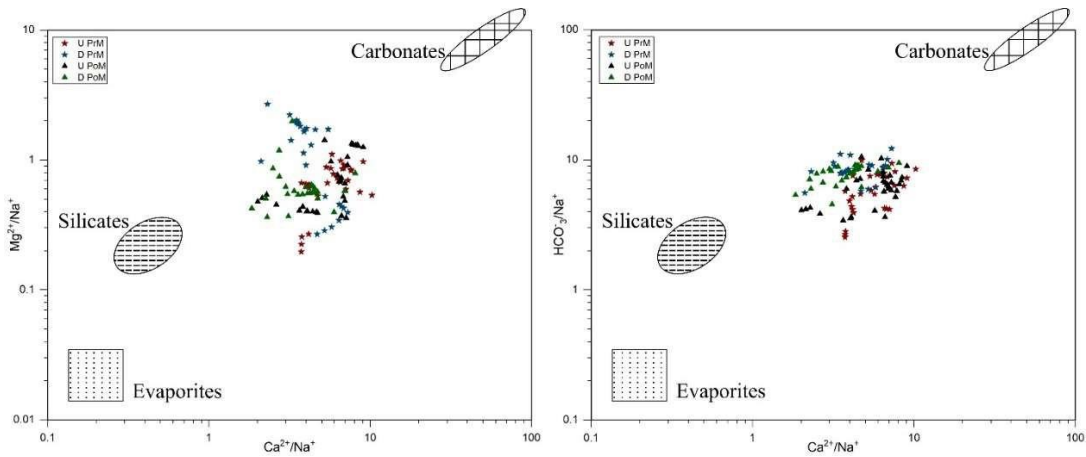


Figure 4-15 Bivariate Na-normalized molar ratios mixing diagram for 2021.

4.5.3 Influenced of weathering of silicate and carbonate.

- **Silicates weathering:**

The predominant bedrock within the Teesta River watershed basin is silicate rocks. In aquatic settings, carbonate rocks weather more quickly than silicate rocks. In this research, silicate weathering is thought to contribute to the presence of Na⁺ and K⁺ in river water. The dissolution of Na⁺ from silicates (Na_{sil}) may be estimated as follows:

$$Na_{sil} \approx Na_r - Cl_r$$

where Na_r & Cl_r are the Na^+ and Cl^- concentrations in the river flow. The average Na/Cl ratio in all waterways was found to be 6.8. This suggests that silicate weathering is the main source of Na^+ within the Teesta River.

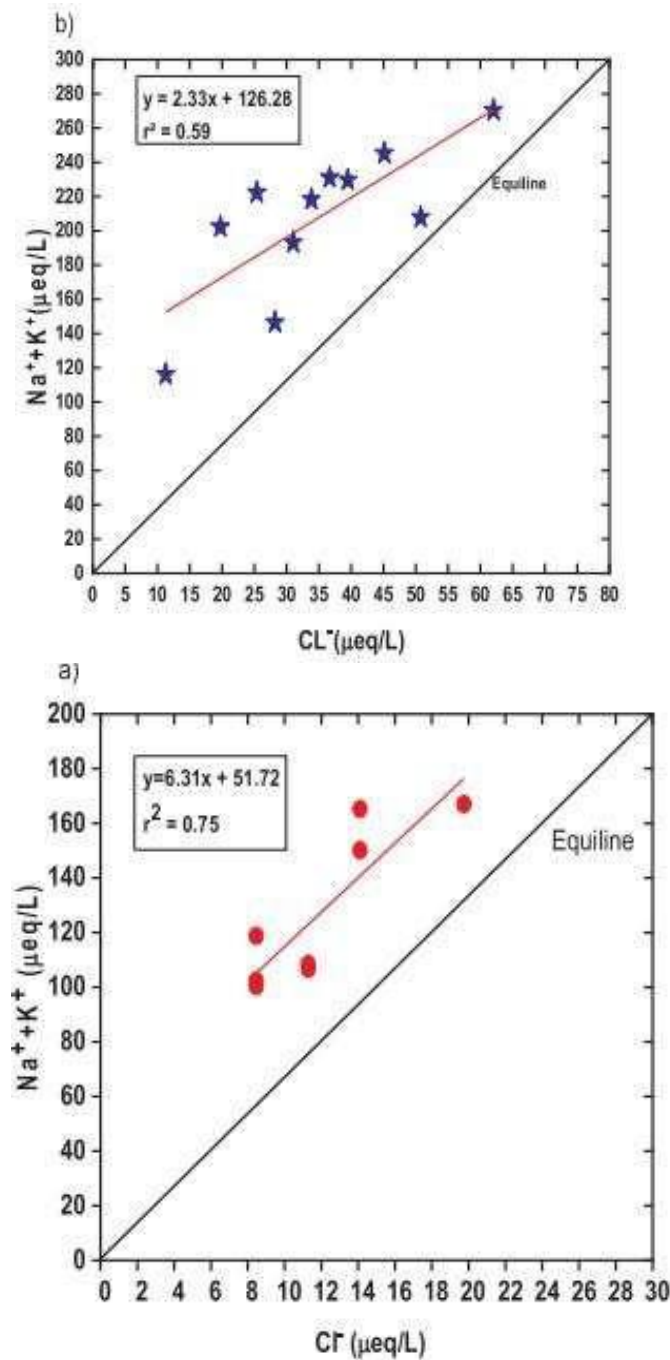
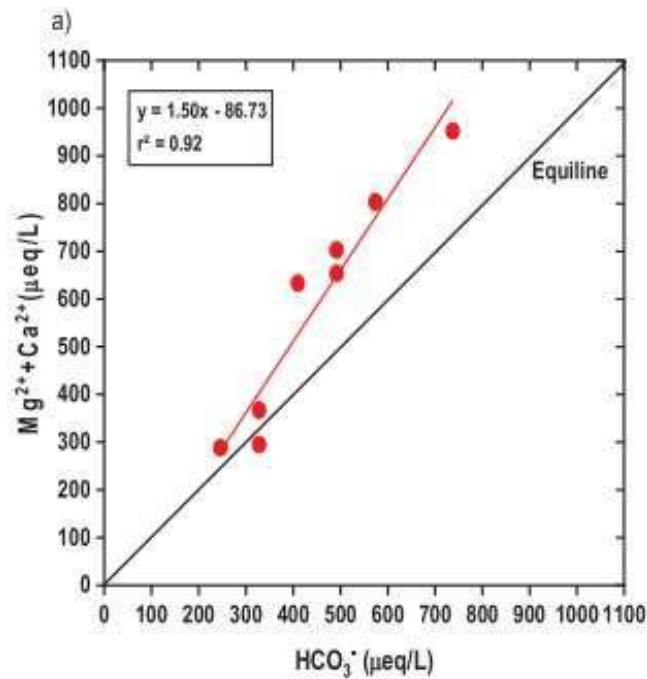


Figure 4-16 : Scatter plot of Cl^- vs $Na^+ + K^+$ in a) upstream and b) downstream for all waters

- **Carbonate weathering:**

The geology of the examined watershed revealed the distribution of large carbonate minerals in TSS rock units as well as carbonate intercalations with Silicates are the inGHS as well as LHS. Although carbonates constitute only 1% of the GHS, they provide 82% of the HCO_3^- to the rivers exhausting GHS rocks, revealing that over 90percent of HCO_3^- as well as Ca^{2+} is derived coming from weathering of carbonate in the glaciated Himalayas, despite the fact that carbonates constitute only 1% of the fresh glacial till.



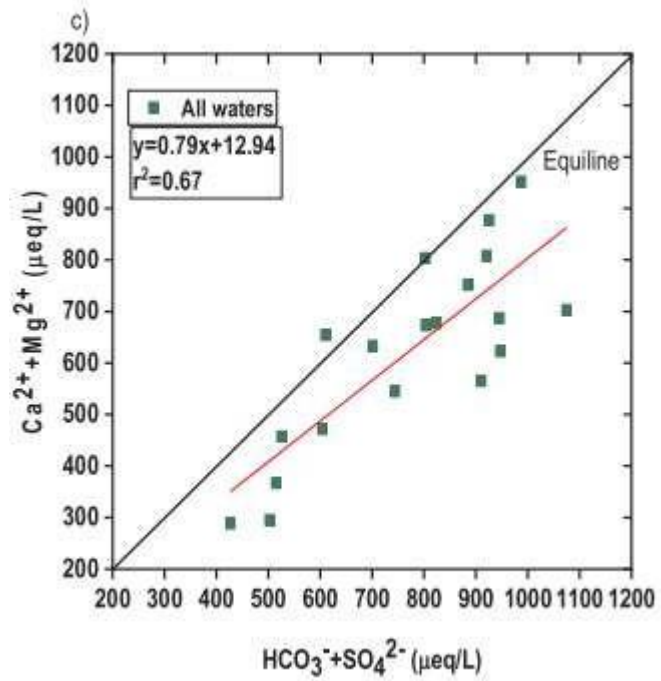
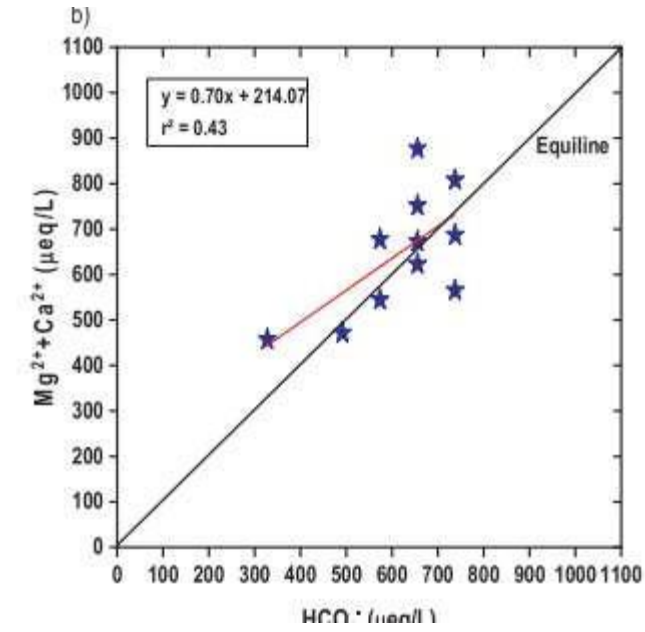


Figure 4-17: Scatter plot of HCO_3^- vs $Mg^{2+}+Ca^{2+}$ in a) upstream b) downstream c) $HCO_3^-+SO_4^{2-}$ vs $Ca^{2+}+Mg^{2+}$ for all waters.

4.6 WATER QUALITY ASSESMENT

4.6.1 Water Quality Index (Drinking purposes):

The Water Quality Index, also known as the WQI, provides a representation of the total water quality by combining the effects of physio-chemical concentration. The computation was done using the weighted arithmetic indexing approach. Variations in the water's quality state that are relevant to the appropriateness for water quality with respect to major ions and water physical parameters. In this study, the parameters used are represented in Table 16, all the major ion concentration are taken in mg/L. In this study, the status water quality index and water quality range/value given by (Chatteriji and Raziuddin, 2002). The water quality and status explained that 0-25 is excellent water quality, 26-50 is good water quality, 51-75 is poor water quality, 76-100 is very poor water quality and >100 is considered as unsuitable for drinking.

Table 16: Concentration of ions, standard limit and weight index for WQI

Parameter	Min Conc. (mg/L)	Mean Conc. (mg/L)	Max Conc. (mg/L)	Standard limit (Si) BSI (2012)	Weight (wi)
pH	6.38	7.29	8.56	8.5	4
TDS	34	47	62	500	4
Ca	5.2	11.51	18.87	75	2
Mg	0.47	2.21	6.7	30	1
Na	1.44	2.29	3.35	200	1
K	0.45	1.79	5.6	12	1
Alkalinity	6.10	16.11	24.4	200	3
NO ₃	0.18	1.67	6.18	45	5
SO ₄	5.92	8.86	15.6	200	4
Cl	0.1	1.14	6.84	250	4

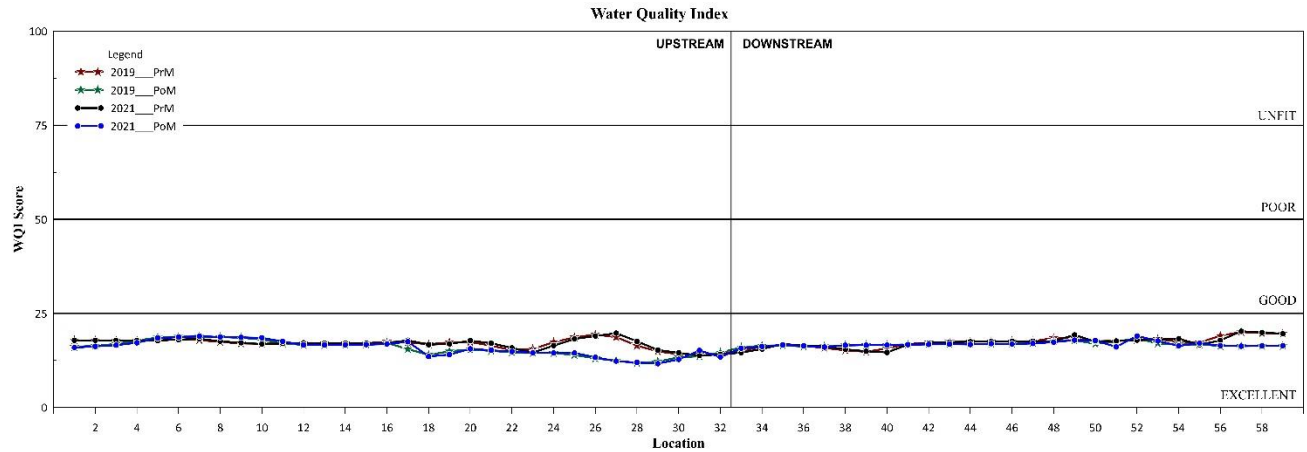


Figure 4-18: WQI index of the study area.

The table 17 shows the major ions and pH and TDS concentration parameters considered for water quality index (drinking purpose) analysis. These parameters, including pH, TDS, calcium (Ca), magnesium (Mg), sodium (Na), potassium (K), alkalinity, nitrate (NO₃), sulfate (SO₄), and chloride (Cl), are assessed in terms of their minimum, mean, and maximum concentrations, along with the standard limits and associated weights given to each parameter depending on their importance for drinking purpose.

The Water Quality Index of the study area shown in Figure 4:18, water quality index for pre-monsoon and post monsoon for 2019 and 2021, Figure 4-19, water quality map for 2019 and Figure 4:20, water quality map for 2021 indicates that all the sample location of the study area falls under excellent range (0-25).

From this index it can be understood that water quality for Teesta River is excellent for drinking purpose with respect to major ion concentration.

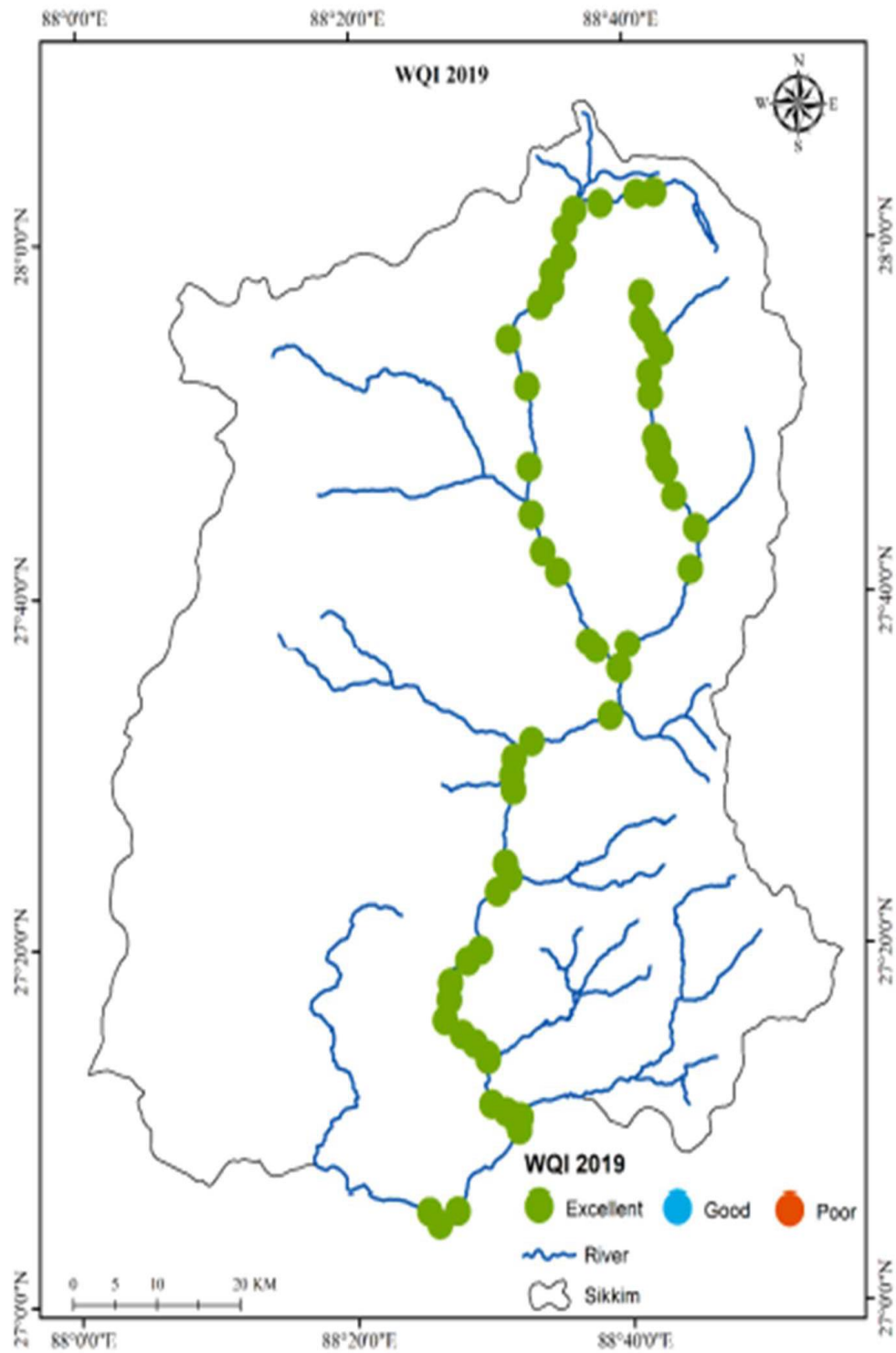


Figure 4-19: WQI in 2019 of the study area

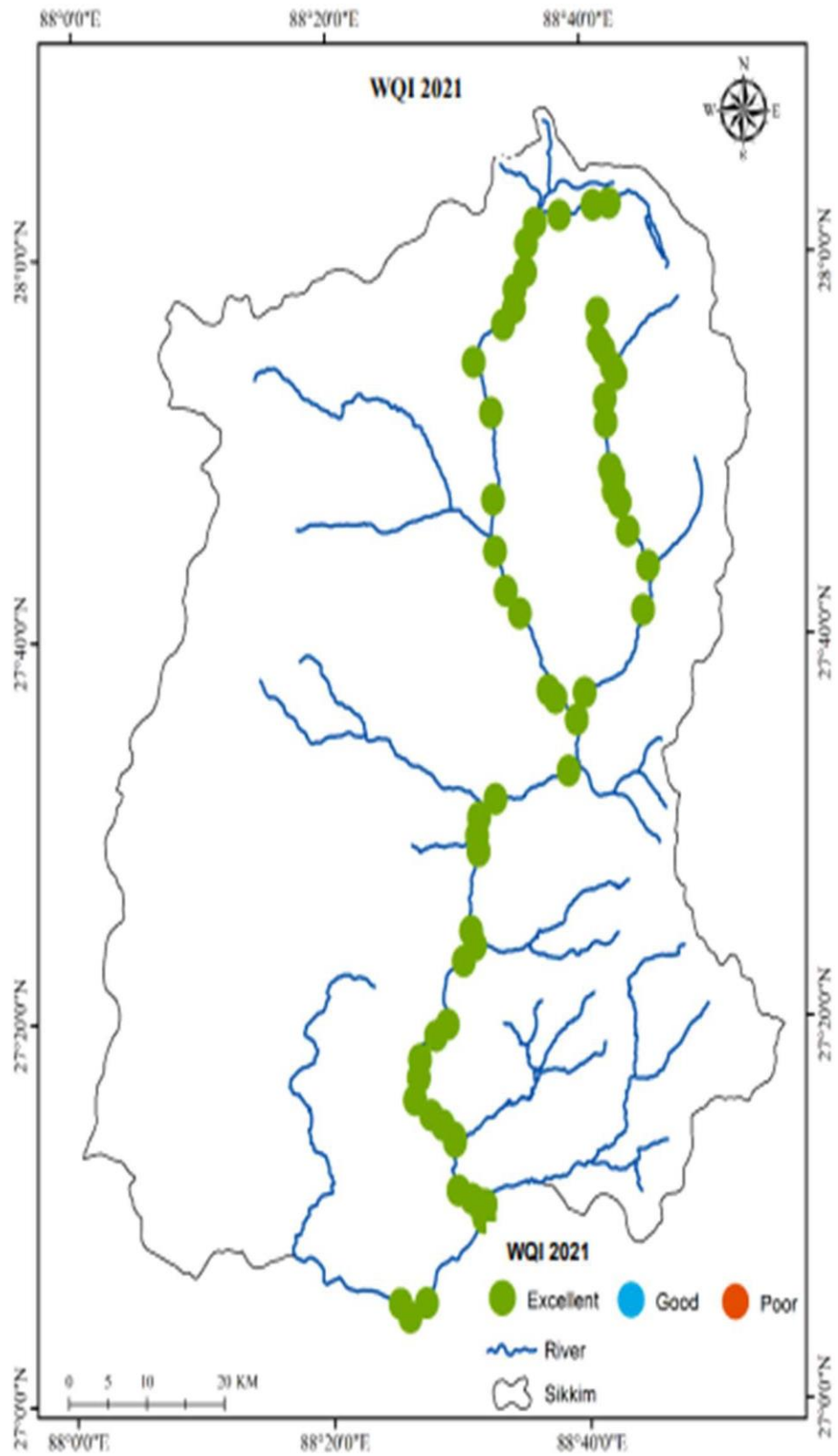


Figure 4-20: WQI in 2021 of the study area

4.6.2 WILCOX DIGRAM (Irrigation purposes):

Electrical conductivity (EC) and sodium percentage (Na%) are crucial parameters for assessing water quality in irrigation which is plotted in Wilcox Diagram (Wilcox 1955). Elevated salinity levels can create a physiological drought condition, leading to reduced plant growth due to decreased soil permeability (Ayers & Westcot, 1985). All ion values are measured in milliequivalents per liter (meq/l).

The Na% value quantifies the proportion of Na ions relative to the combined Ca and Mg ions in the water. High salinity's impact on agricultural productivity is a critical consideration for sustainable irrigation practices. Diligent water resource management, including monitoring and controlling EC and Na% levels, is imperative to ensure successful crop cultivation (Ayers & Westcot, 1985). The Bureau of Indian Standards (BIS) recommends a Na% value of approximately 60% as suitable for irrigation (BIS, 1982). In the present study area Na% of pre-monsoon and post-monsoon season for the year 2019 and 2021 ranges with a minimum of 9.61 to 30.81 of maximum. The study indicates that all the samples in the study area falls under excellent to good for irrigation purpose presented in Figure 4-21 and Figure 4-22.

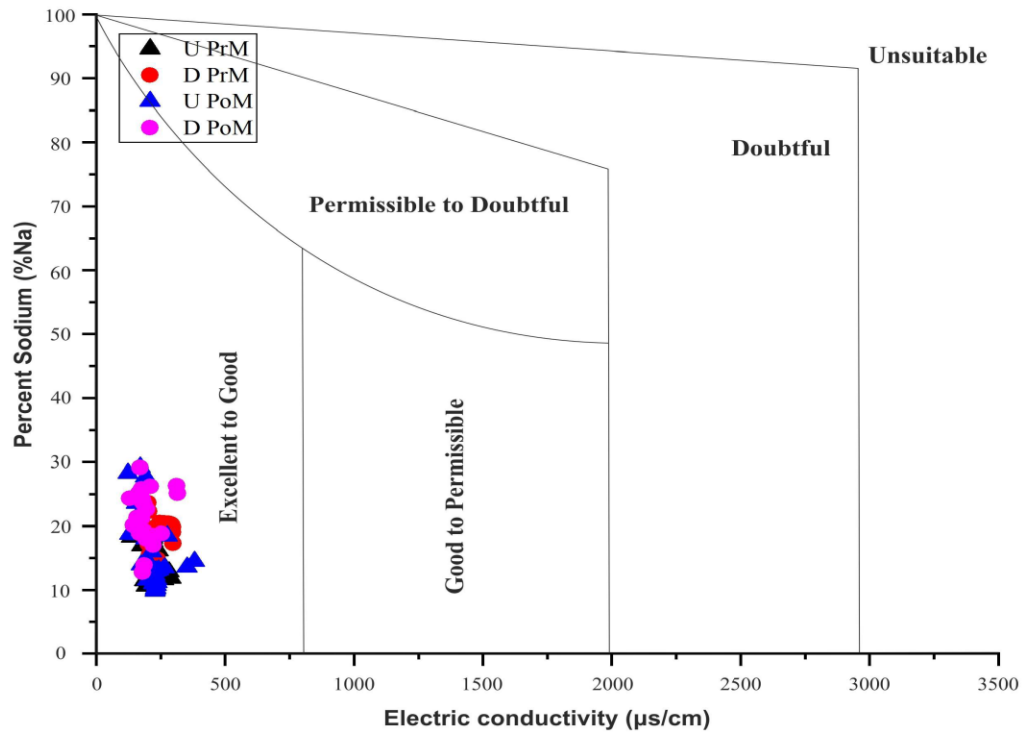


Figure 4-21: Graphical representation of Wilcox diagram showing the relationship between %Na vs EC in the Teesta River basin (2019)

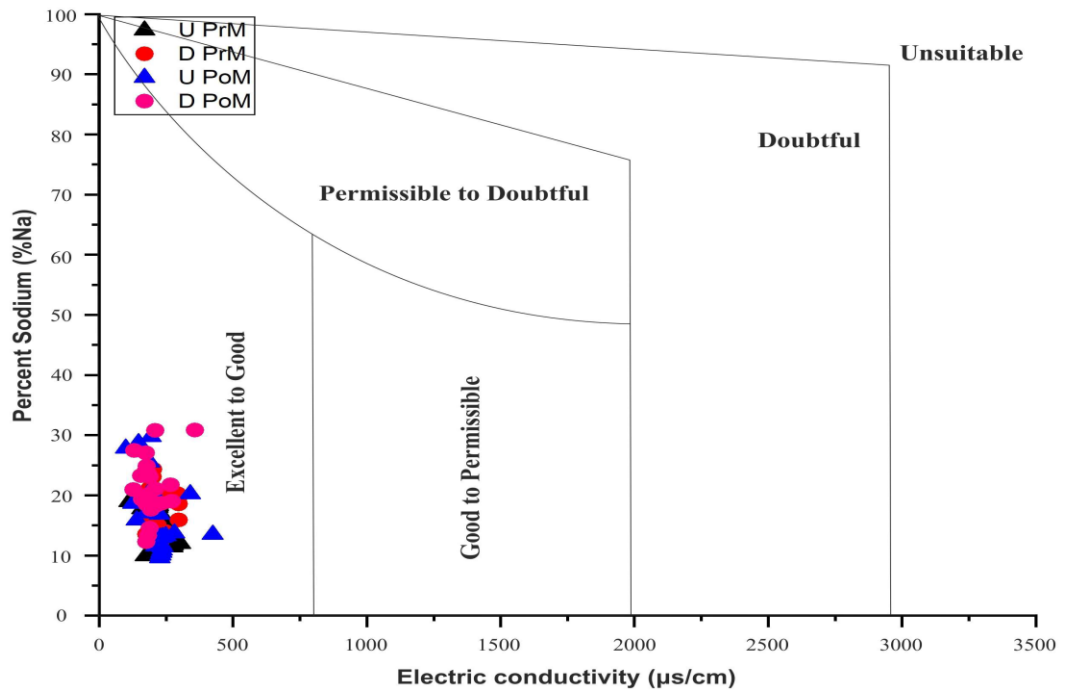


Figure 4-22: Graphical representation of Wilcox diagram showing the relationship between %Na vs EC in the Teesta river basin (2021)

4.6.3 Residual Sodium Carbonate:

The Residual Sodium Carbonate (RSC) index is a vital tool for assessing the alkalinity hazard of irrigation water on soil. Elevated levels of dissolved sodium relative to dissolved calcium and magnesium can have detrimental consequences. This situation may cause the soil to swell and disperse, leading to a substantial decrease in its water infiltration capacity (Karanth, 1989). To quantify this effect, the Residual Sodium Carbonate (RSC) was employed, following the methodology developed by (Eaton 1950).

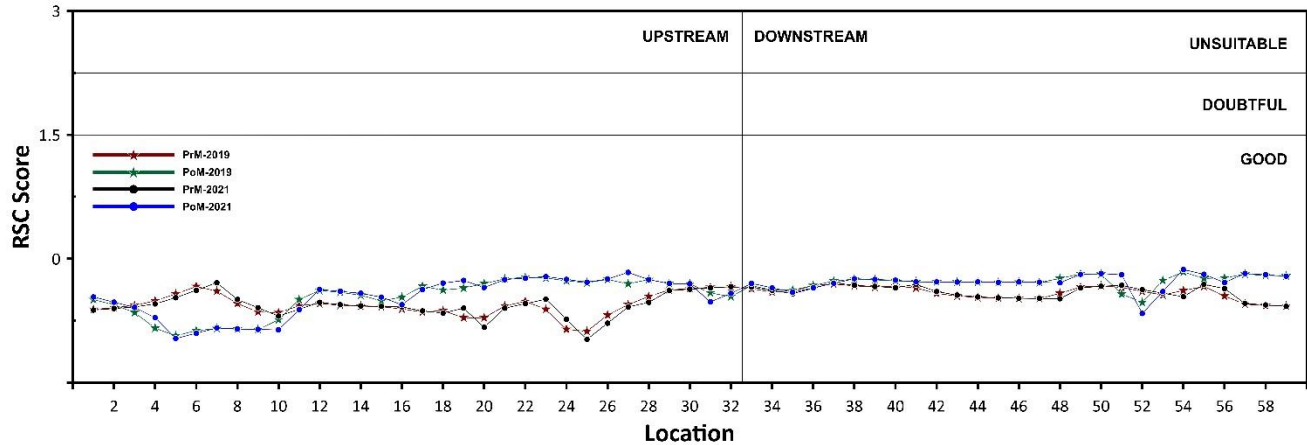


Figure 4-23: RSC score of the study area

Where all ionic concentrations are expressed in milliequivalents per liter (meq/l). The calculated RSC values for all the studied rivers ranged from -0.88 to -0.31 meq/l during the Pre-Monsoon (PrM) season, and from -0.93 to -0.16 meq/l during the Post-Monsoon (PoM) season for the year 2019. In the subsequent year, 2021, RSC values varied from -0.975 to -0.29 meq/l in the PrM season and from -0.964 to -0.13 meq/l in the PoM season as presented in **Figure 4-23**.

Interpretation of these results reveals that all RSC values obtained were below 1.25

meq/l, categorizing the river water as excellent in terms of water quality. Consequently, the study's findings indicate that all river water samples analyze in the study area are well-suited for irrigation purposes, a graphical representation is shown in **Figure 4-23**.

4.6.4 Permeability Index:

Water having more concentrations of HCO₃ and CO₃ ions undergo reactions with Ca²⁺ and Mg²⁺ ions within the soil solution. This leads to the precipitation of these cations in the form of calcite and magnesite, contributing to the adsorption of sodium onto clay surfaces. Consequently, the sodium hazard is amplified, giving rise to various adverse soil conditions, including reduced permeability and hindered root penetration (Todd and Mays, 2005).

The permeability index (PI) is a crucial metric that aids in quantifying these adverse effects on soil permeability. It is computed using the following equation:

$$PI = \frac{Na^+ + \sqrt{HCO_3^-}}{(Ca^{2+} + Mg^{2+} + Na^+)} \times 100$$

The PI value serves as an indicator of the soil's susceptibility to reduced permeability and associated challenges. Accurate assessment of the PI allows for informed decisions regarding irrigation practices and soil management, ultimately contributing to sustainable agriculture. As outlined by (Doneen 1964), the Permeability Index (PI) can be classified into three distinct categories: Class I (with a suitability of 75% or more), Class II (ranging from 25% to 75%, denoted as good), and Class III (less than 25%, considered unsuitable). It is advisable to utilize water falling into either Class I or Class II for irrigation purposes.

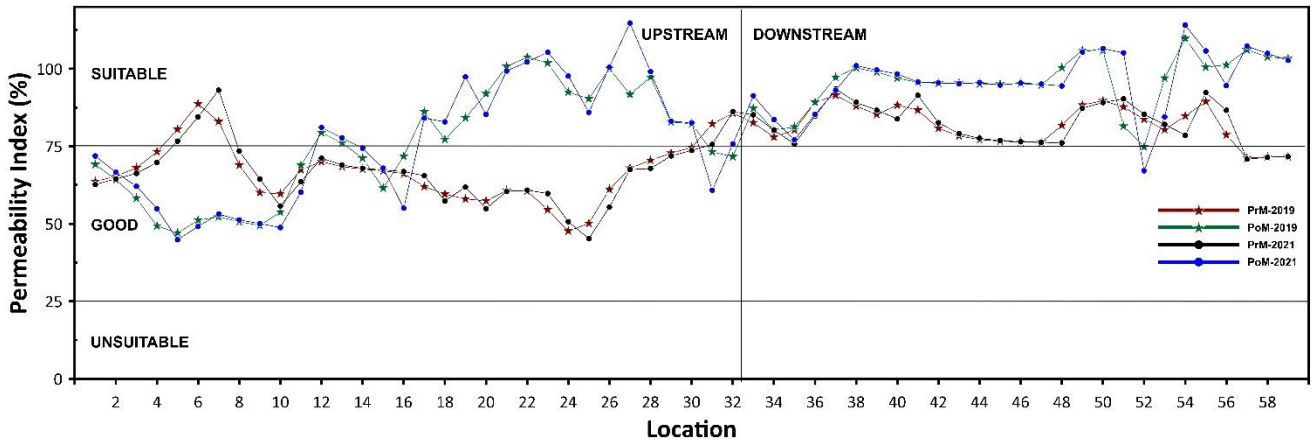


Figure 4-24: Permeability Index of the study area

The **Figure 4-24** demonstrates that the PI of the study area for pre and post monsoon seasons for 2019 and 2021. The PI data for the study area during the pre-monsoon season of 2019 showed that 49.15% fell into Class I, and 50.85% fell into Class II, while in the post-monsoon season of the same year, 71.19% was categorized as Class I, and 28.81% as Class II. Similarly, during the pre-monsoon season of 2021, 49.15% belonged to Class I, and 50.85% to Class II, while in the post-monsoon season of 2021, 72.88% was classified as Class I, and 27.12% as Class II. These results collectively indicate that the water samples from the study area are suitable to good for irrigation purposes.

4.6.4 Kelly's Index:

Kelly's ratio is a critical parameter used to determine the suitability of water for agricultural irrigation. It serves as an indicator of the sodium hazard present in groundwater. In the context of Kelly's ratio, if the value exceeds 1, it signifies an excess level of sodium ions in the water, rendering it unsuitable for irrigation (Kelly, 1963). High sodium levels can lead to soil degradation and reduced crop productivity.

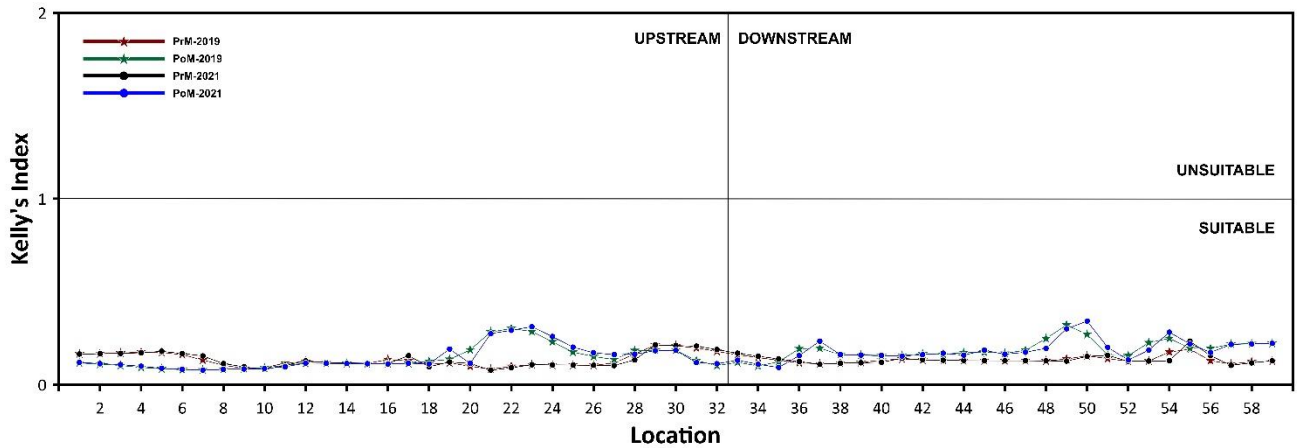


Figure 4-25: Kelly's Index of the study area

In this research, the evaluation of Kelly's ratio was conducted for water samples collected during both the pre-monsoon and post-monsoon seasons in the years 2019 and 2021 within the Teesta River region. The significant outcome was the consistency in the results ranges from 0.08 to 0.21 during the Pre-Monsoon (PrM) season, and from 0.08 to 0.23 during the Post-Monsoon (PoM) season for the year 2019. In the subsequent year, 2021, KI Index varied from 0.08 to 0.32 in the PrM season and from 0.08 to 0.34 in the PoM season, all of the samples, across the different seasons and years, exhibited Kelly's ratio values that remained below the critical threshold of 1 (**Figure 4-25**), which is under suitable condition for irrigation purpose.

The study in the present research area indicated by **Figure 4-25**, that the water quality in the Teesta River region is suitable for irrigation purposes

4.7 ASSESMENT OF HEAVY METALS OF TEESTA RIVER

Throughout history, the progress of human societies has been deeply intertwined with our mastery of metallurgy. This remains true in the contemporary world, where metals are indispensable in almost every aspect of our daily lives, enabling us to carry out a multitude of tasks. The very foundation of our industries and industrialization hinges on the extraction and utilization of metals. However, as we engage in these processes, the pressing issue of environmental contamination emerges.

Human activities have fundamentally altered the natural cycles of metallic elements on a global scale. In the natural environment, including plant and animal tissues, the background levels of most metals are typically very low. Yet, when the concentration of these metals surpasses a certain threshold, referred to as the "tolerable level" or "toxic level," it signifies a state of "metal pollution."

When delving into the realm of metal pollution research, one encounters terms like "heavy metals," "trace metals," "trace elements," and "toxic elements." These terms are often used interchangeably, giving the impression that they are synonyms. However, this is not always the case.

In fact, "heavy metals" are metals with a density of 5.0 or higher, while "trace metals" typically denote metals that occur in the environment at extremely low concentrations. Furthermore, "trace elements" encompass metals, metalloids, or non-metals that are found in trace amounts in the environment. Lastly, "toxic elements" are those that can pose a threat to living organisms even at trace levels.

In this research, we focus on several elements, namely, Chromium (Cr), Manganese

(Mn), Iron (Fe), Nickel (Ni), Copper (Cu), Arsenic (As), Barium (Ba) and Uranium (U).

However, considering their densities, each of these elements falls into the category of "heavy metals." Therefore, the term "heavy metal" is employed in this context.

According to Adriano (1986), the sources of trace elements and heavy metals can be categorized as follows: rocks, inorganic fertilizers, liming materials, sewage sludge, animal waste, pesticides, irrigation waters, coal combustion residues, metal smelting industries, automobile emissions, and various other sources. It is worth noting that, with the exception of rocks, all these sources are of anthropogenic origin.

Table 17: Descriptive statistical representation for concentration of Heavy Metals in the Teesta River basin (2019)

		Cr	Mn	Fe	Ni	Cu	Zn	As	Ba	U
PrM 2019	Min	1.49	2.78	66.82	1.05	1.14	7.52	1.43	1.25	1.00
	Max	16.93	101.04	9312.66	9.10	14.77	239.17	5.04	73.00	6.46
	Mean	4.90	25.49	2271.46	3.49	4.36	44.75	2.74	16.65	2.59
	Median	4.19	15.01	902.23	2.80	3.24	30.87	2.44	8.79	2.58
	SD	2.98	27.55	2932.22	2.01	3.21	44.70	0.88	18.42	1.05
PoM 2019	Min	1.01	1.12	180.02	1.03	1.05	3.54	0.60	3.17	1.07
	Max	9.25	72.26	2761.71	6.31	5.68	18.92	8.10	42.86	4.00
	Mean	2.52	17.38	1044.12	2.29	2.37	9.61	3.08	10.23	2.25
	Median	1.74	14.78	795.74	1.43	2.02	7.67	2.73	8.52	2.23
	SD	1.92	13.96	697.43	1.49	1.26	4.44	1.79	7.78	0.82

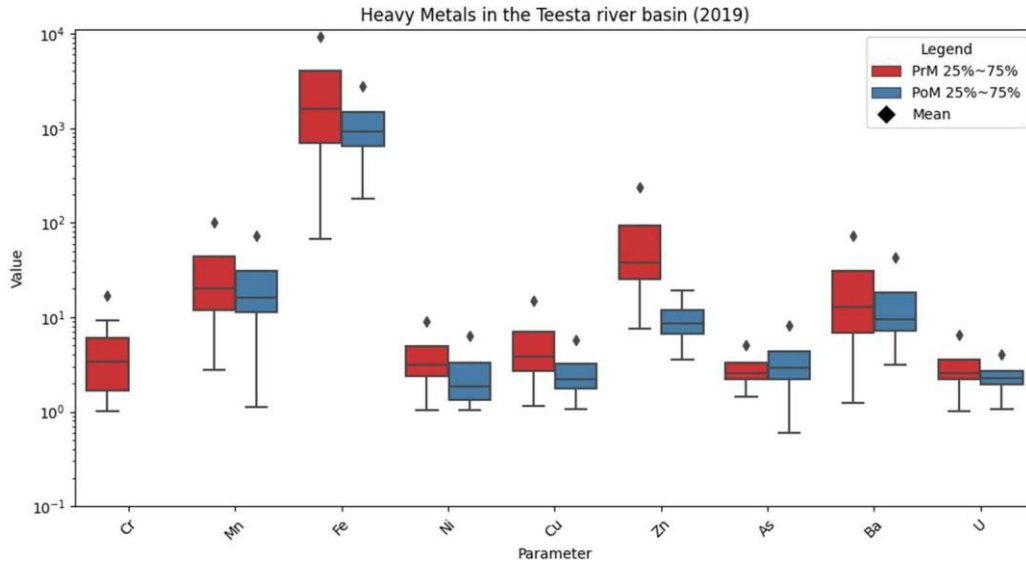


Figure 4-26: Box plot graphical representation of Heavy Metals in Teesta Basin River in 2019

The concentrations of trace metals in PrM (Pre-Monsoon) as well as PoM (Post-Monsoon) water samples taken in 2019 are shown in the table (Table 17) and graph (Figure 4-26). The levels of several trace metals were measured and examined. The data presents metal concentrations' minimum, maximum, mean, median, as well as standard deviation. The metal concentrations in PrM vary widely, from 1.489 to 16.930 for Chromium, 2.780 to 101.044 for Manganese, and 66.825 to 9312.662 for Iron. PoM also shows metal concentrations with lowest and maximum values for each metal. The mean and median values show metal concentrations' average amounts in each water source. The standard deviation figures also show the metal concentrations' dispersion around their averages, revealing the data's unpredictability. The descriptive statistical representation shows that spatio-temporal variation for premonsoon and postmonsoon of 2019 trace element concentrations in the study area

Table 18: Descriptive statistical representation for concentration of Heavy Metals in the Teesta River basin (2021)

		Cr	Mn	Fe	Ni	Cu	Zn	As	Ba	U
PrM 2021	Min	1.12	2.27	56.09	1.11	1.07	7.5	1.34	1.22	1.02
	Max	20.29	91.86	9731.67	9.91	15.59	263.15	5.98	61.12	3.89
	Mean	4.86	24.61	2206.19	3.59	4.34	44.56	2.77	15.77	2.61
	Median	4.16	14.82	1025.97	2.88	3.2	29.89	2.49	8.96	2.66
	SD	3.4	26.64	2809.48	2.05	3.48	48.4	0.95	17.57	0.74
PoM 2021	Min	1.01	2.03	132.21	1.01	1.01	3.41	1.02	1.87	1.13
	Max	6.98	58.72	2681.15	4.81	7.03	19.14	6.38	19.61	4.16
	Mean	2.19	16.08	1011.94	1.91	2.16	8.33	2.9	7.98	2.35
	Median	1.6	14.67	789.1	1.46	1.91	7.03	2.73	8.35	2.46
	SD	1.37	10.08	623.01	0.94	1.26	4	1.1	3.39	0.78

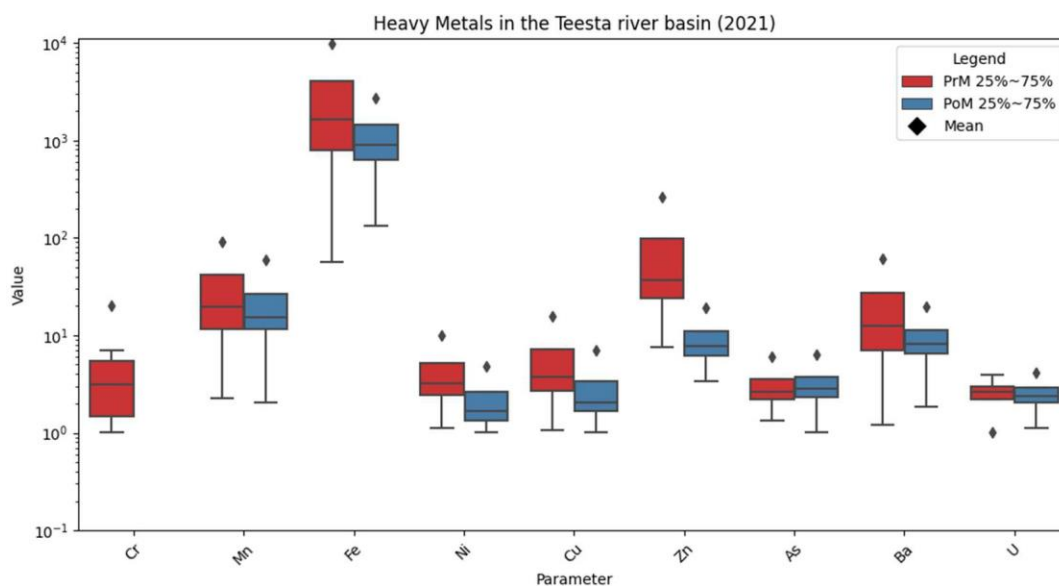


Figure 4-27: Box plot graphical representation of Heavy Metals in Teesta Basin River in 2019

From the above table (Table 18) and graph (Figure 4-27) it is observable that the trace metal concentrations in 2021 water samples from PrM (Pre-Monsoon) and PoM (Post-Monsoon). PrM values vary from 1.12 for Chromium, 2.27 for Manganese, and 56.09 for Iron to 20.29, 91.86, and 9731.67. Mean concentrations, such as 4.86 for Chromium, 24.61 for Manganese, and 2206.19 for Iron, show average levels, while medians and standard deviations show central tendency and data dispersion. PoM has identical mean concentrations for Chromium (2.19), Manganese (16.08), and Iron (1011.94). Median

values of 1.60 for Chromium, 14.67 for Manganese, and 789.10 for Iron, coupled with standard deviations of 1.37, 10.08, and 623.01, give more insights. The descriptive statistical representation shows that spatio-temporal variation for premonsoon and postmonsoon of 2021 trace element concentrations in the study area

4.7.1 Heavy Metal Pollution Index:

The Heavy Metal Pollution Index (HPI) is a scientifically robust methodology that plays a critical role in assessing the comprehensive impact of heavy metals on water quality. This approach, initially introduced by Mohan et al. in 1996, employs a systematic ranking (0-19 is low, 20-38 is medium and 38 and above considered as high ranking) technique to quantitatively evaluate individual heavy metals' contributions to overall water quality. It provides a rigorous and data-driven means of comprehending the cumulative influence of heavy metals in aquatic ecosystems.

The HPI offers valuable insights into the environmental health of water bodies, particularly in regions where heavy metal contamination is a concern. By aggregating the effects of various heavy metals, the index enables researchers, environmental scientists, and policymakers to gain a holistic understanding of the water quality, identify potential areas of concern, and develop targeted strategies for remediation and conservation. This scientifically grounded approach empowers decision-makers to make well-informed choices regarding the protection and sustainable management of precious water resources.

The following table (Table 19) represents the heavy metals concentrations in ppb in Min, Max, Mean and standard limit given by BIS (2012) and WHO (2011) which is employed in analyzing HPI, Contamination Index (CI) and Heavy metal Evaluation Index (HEI) for the study area.

Table 19: Heavy Metal concentration with permissible limit of BIS and WHO

Parameters	Conc.ppb			BIS	WHO
	Min	Max	Mean	2012 (ppb)	2011 (ppb)
Cr	1.12	20.29	4.86	50	50
Mn	2.27	91.86	24.61	300	400
Fe	56.09	9731.67	2206.19	300	300
Ni	1.11	9.91	3.59	70	70
Cu	1.07	15.59	4.34	1500	2000
Zn	7.5	263.15	44.56	15000	NA
As	1.34	5.98	2.77	50	10
Ba	1.22	61.12	15.77	700	NA
U	1.02	3.89	2.61	15	NA

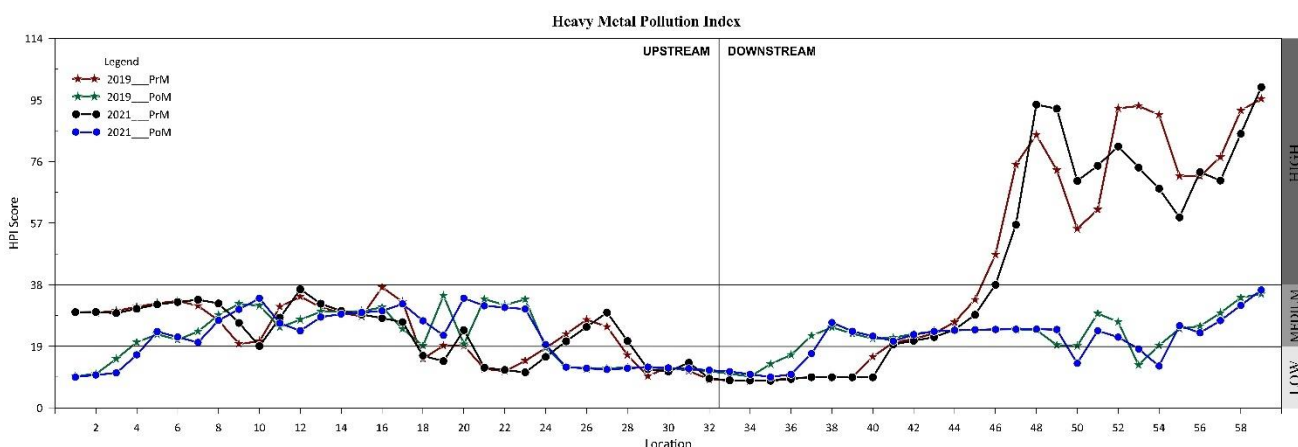


Figure 4-28: Heavy Pollution Index of the study area

In the present research the HPI graphical representation (Figure 4:28) shows an abrupt increase HPI of the river water samples at the lower portion (Sample location 46-59) comprising 14 sample locations, of the study area during pre-monsoon for both the year 2019 and 2021, indicating a high range category in HPI within the river over this period, 18 sample locations fall under low range category and 27 sample locations fall under medium range category during premonsoon of 2019 and 2021 respectively., during post-monsoon of 2019 and 2021 the HPI falls for low and medium range respectively for

16 sample locations (Low range) and 43 sample locations (Medium)

The heavy metal pollution index which show high range in the lower portion of Teesta River in the study area may be due to cause of anthropogenic and landcover changes in those areas or maybe due to the geological conditions and industrial operations.

4.7.2 Contamination Factor/Index:

The Contamination Index (CI) is a pivotal concept in the realm of water quality assessment. Its development, serves as a scientific cornerstone for comprehending the multifaceted impact of various quality factors on water quality. This index is instrumental in offering a consolidated perspective on the extent of heavy metal pollution and its implications for aquatic environments (Backman et al.1998) with a ranking of less than 0 is low, 0-3 is medium and above 3 is high .

By synthesizing the combined effects of different quality parameters, the CI provides a valuable quantitative estimate of the level of heavy metal pollution in a given water body. It offers a comprehensive view of the environmental stressors and challenges associated with heavy metal contamination.

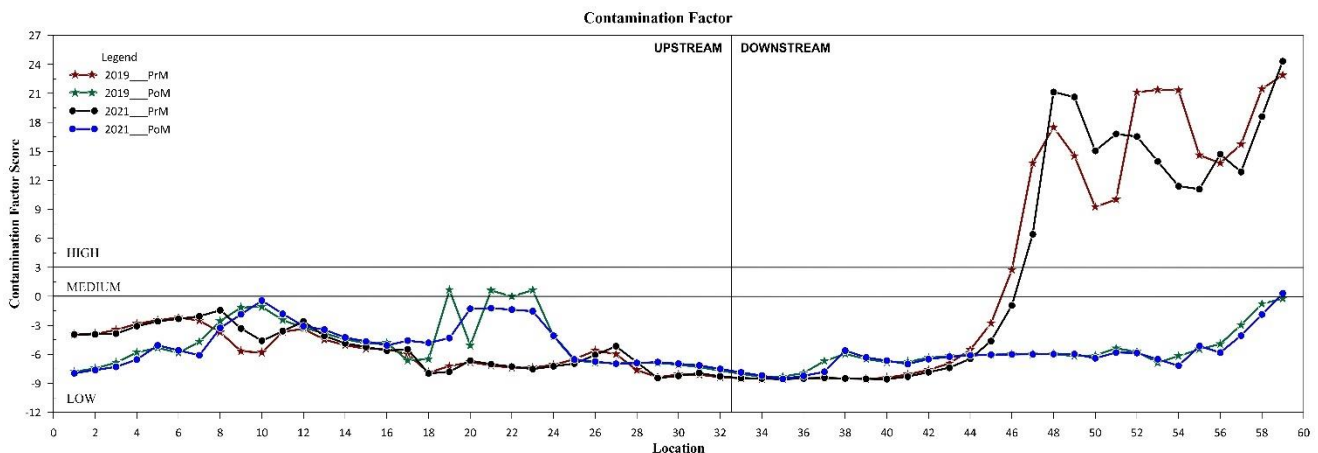


Figure 4-29: Contamination factor representation of the study area

In the course of our present research, the graphical representation of the CI, as depicted in (Figure 4:29), presents a spatio-temporal observation. It reveals a substantial elevation in the CI values for the river water samples collected from the lower reaches (Sample location 46-59) comprising 14 sample locations, of the study area during pre-monsoon for both the year 2019 and 2021, indicating a high range category in CI within the river over this period, 18 sample locations fall under low range category and 27 sample locations fall under medium range category during premonsoon of 2019 and 2021 respectively., during post-monsoon of 2019 and 2021 the CI falls for low and medium range respectively for 16 sample locations (Low range) and 43 sample locations (Medium)

Explanation could be linked to anthropogenic activities and alterations in land cover patterns occurring in these particular regions. The discharge of pollutants and changes in land use may have significantly contributed to the observed increase in contamination. Alternatively, geological factors and industrial operations within this geographical zone might also play a role in influencing the CI values. This finding underscores the complex interplay of natural and human-induced factors affecting water.

4.7.3 Heavy Metal Evaluation Index:

The Heavy Metal Evaluation Index (HEI), represents a critical advancement in the realm of water quality assessment. This index is specifically designed to offer a comprehensive evaluation of water quality by taking into account heavy metal concentrations. It provides a unified and scientifically grounded metric for assessing (less than 9 is low, 10-20 is medium and more than as high ranking) the environmental impact of heavy metals within aquatic ecosystems (Edet and Offiong 2002).

The HEI is instrumental in consolidating information from multiple heavy metal parameters and translating this data into a holistic assessment of water quality. By assigning a numerical value that reflects the overall impact of heavy metals, it facilitates a more precise understanding of the environmental health of water bodies. In essence, the HEI serves as a fundamental tool in the field of environmental science, supporting efforts to safeguard and preserve the quality of our precious water resources.

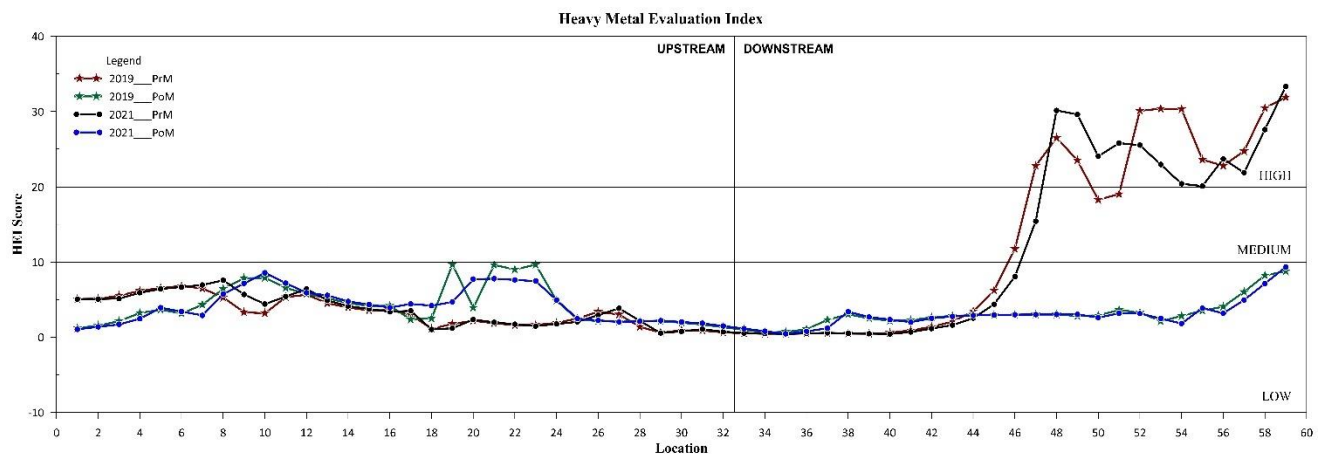


Figure 4-30 : Heavy Metal Evaluation Index of the study area

In the current research HEI has been depicted graphically (Figure 4:30). This representation serves as a critical visualization tool, shedding light on the dynamic trends and fluctuations in the HEI of the river water samples. Notably, there is a stark and sudden upsurge in HEI observed in the lower section at the lower portion (Sample location 46-59) comprising 14 sample locations, of the study area during pre-monsoon for both the year 2019 and 2021, indicating a high range category in HEI within the river over this period, 18 sample locations fall under low range category and 27 sample locations fall under medium range category during premonsoon of 2019 and 2021 respectively., during post-monsoon of 2019 and 2021 the HEI falls for low and medium range respectively for

16 sample locations (Low range) and 43 sample locations (Medium)

Several factors may contribute to this phenomenon. It could be attributed to anthropogenic activities and changes in land cover within these regions, indicating the influence of human interventions on water quality. Additionally, geological conditions and industrial operations in the lower part of the study area might also play a role in this observed surge in heavy metal contamination. The HEI graphical representation thus serves as a critical indicator of the complex interplay of environmental factors and human activities on the water quality dynamics of the river, offering valuable insights for further research and environmental management efforts.

4.8 COMPARISON OF LU/LC IN RANI KHOLA WATERSHED

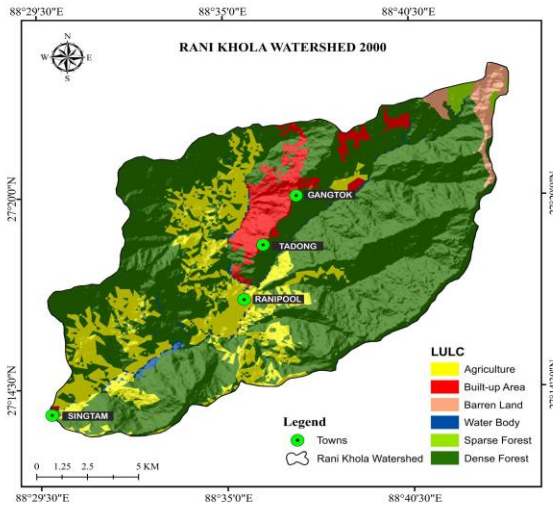


Figure 4-31: RANI KHOLA WATERSHED in 2000

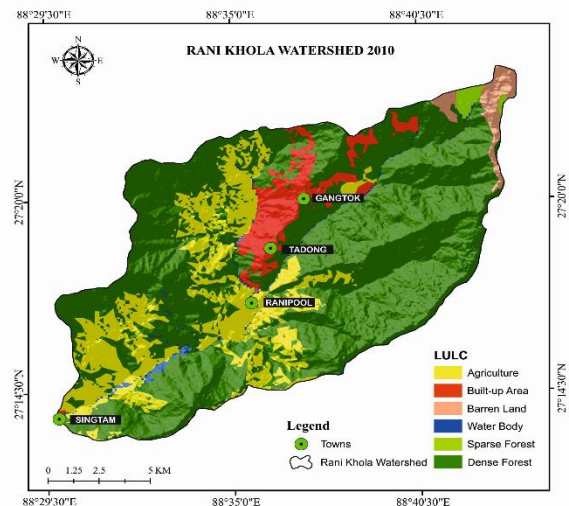


Figure 4-32: RANI KHOLA WATERSHED in 2010

This graphic shows the dramatic shifts in LULC that occurred in the Sikkim Himalayan Rani Khola watershed between the years 2000 and 2010. Agriculture, urban areas, bare terrain, thick forest, open forest, and bodies of water are all included in the LULC categories evaluated. Notable transformations in the watershed during this period include a remarkable 16.40% increase in dense forest (41.76 km²), a 2.13% expansion in built-up areas (5.41 km²), and a 0.11% rise in water bodies (0.28 km²). Conversely, there was a significant 13.98% reduction in open forest (35.59 km²), a 2.83% decrease in agriculture (7.22 km²), and a 1.82% decline in barren land (4.64 km²).

The surge in dense forest and decrease in open forest strongly suggest a process of afforestation in the Rani Khola watershed, likely influenced by a combination of factors including government-driven afforestation programs, heightened awareness of the vital role of forests, and natural forest regeneration. Population and economic growth in the watershed are blamed for the expansion of urban areas, while the rise in water bodies may be linked to climate change or other factors leading to increased precipitation and runoff.

In general, the shifts in LULC in the Rani Khola watershed are encouraging, signaling a shift towards a more forested landscape and a reduction in agricultural land. These changes are likely to yield numerous benefits, such as enhanced water quality, decreased soil erosion, and greater biodiversity. It is important to note, however, that the diagram solely illustrates the overarching alterations in LULC without pinpointing specific locations or the underlying causes driving these changes.

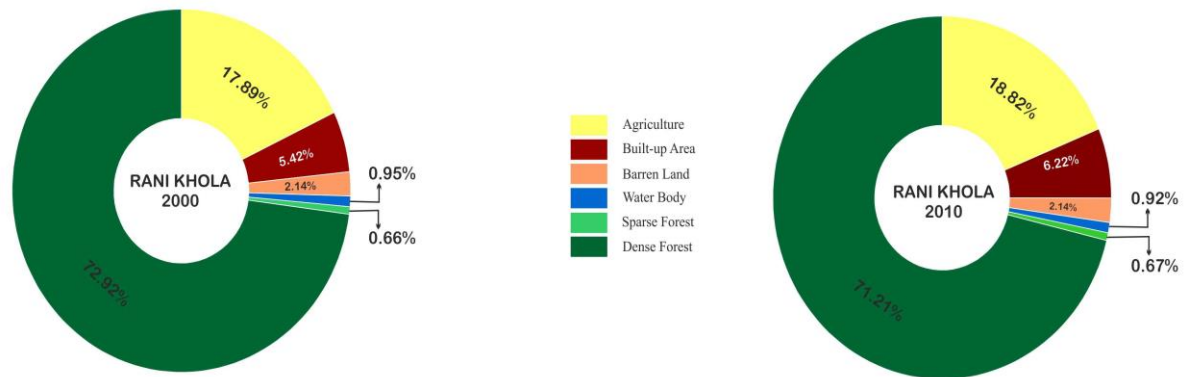


Figure 4-33: Graphical representation of LULC within Rani Khola watershed from 2000 to 2010

LULC in the Sikkim Himalayan Rani Khola watershed saw significant changes from 2000 to 2010. Key transformations include a notable 16.40% increase in dense forest, a 2.13% growth in built-up areas, and a minor 0.11% rise in water bodies. Conversely, open forest decreased by 13.98%, agriculture by 2.83%, and barren land by 1.82%.

The increase in dense forest and the decrease in open forest imply afforestation in the Rani Khola watershed, likely influenced by government initiatives, growing awareness of forests' importance, and natural regeneration. Urban area expansion is attributed to population and economic growth, while increased water bodies may be due to factors like climate change.

These LULC trends reflect a shift towards a more forested landscape and reduced agricultural land, promising benefits like improved water quality, reduced erosion, and greater biodiversity. However, it's important to note that the diagram provides an overview of LULC changes without specific locations or detailed drivers.

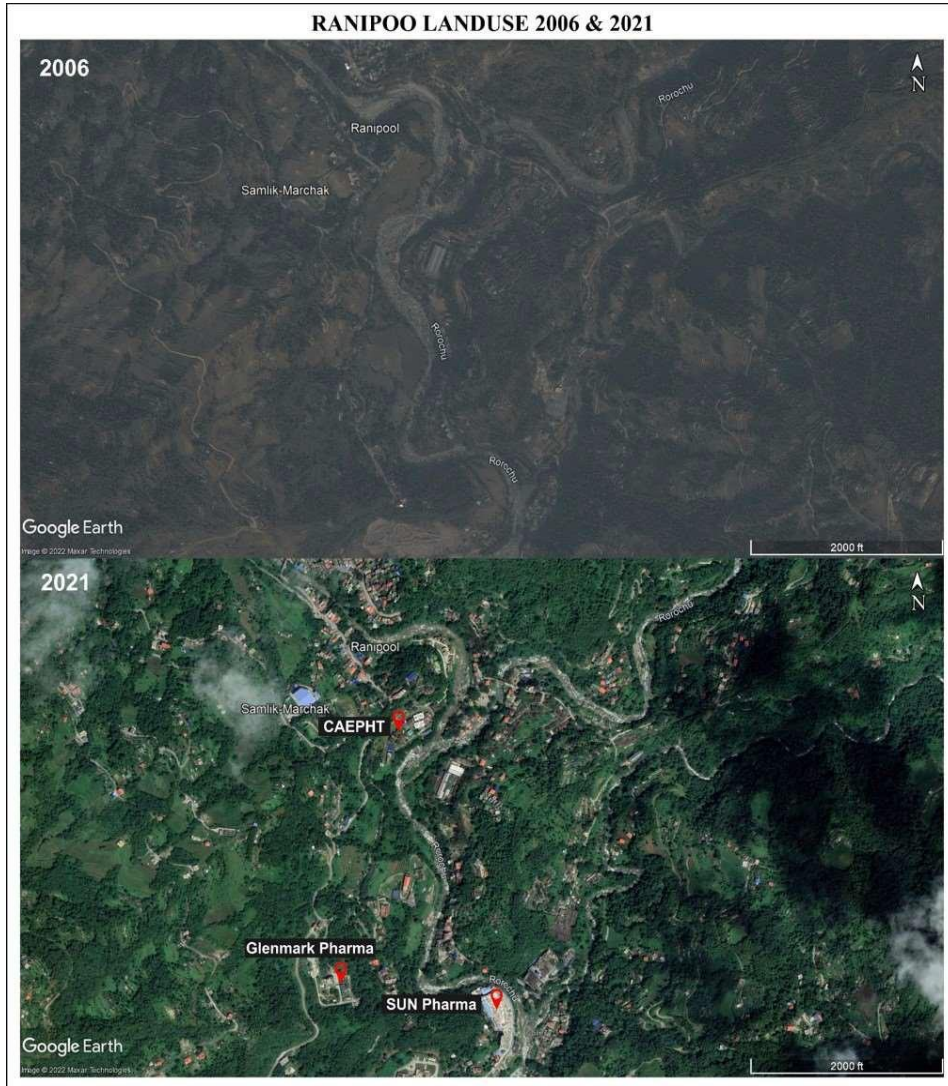


Figure 4-34 : Comparison of Ranipool Landuse Map using Google Earth in 2006 & 2021

The Ranipool land-use maps from 2006 and 2021 (Figure 34) was obtained from Google Earth, offer a thorough overview of the changes in the Ranipool area of the study area during a 15-year period. Ranipool's major land use in 2006 was agricultural, with areas of

woodland, scrublands, and less percentage of built-up area. However, significant changes have happened by 2021, the establishment of newly developed zones of industry in the area to the north, as well as the huge rise of the Samlik Marchak hamlet, signaled a large increase in urbanization. Furthermore, a new residential neighborhood has been created in Ranipool's southern region. These changes were followed by the transformation of agricultural fields into industrial as well as residential spaces, signifying a shift in the socioeconomic dynamics of the region

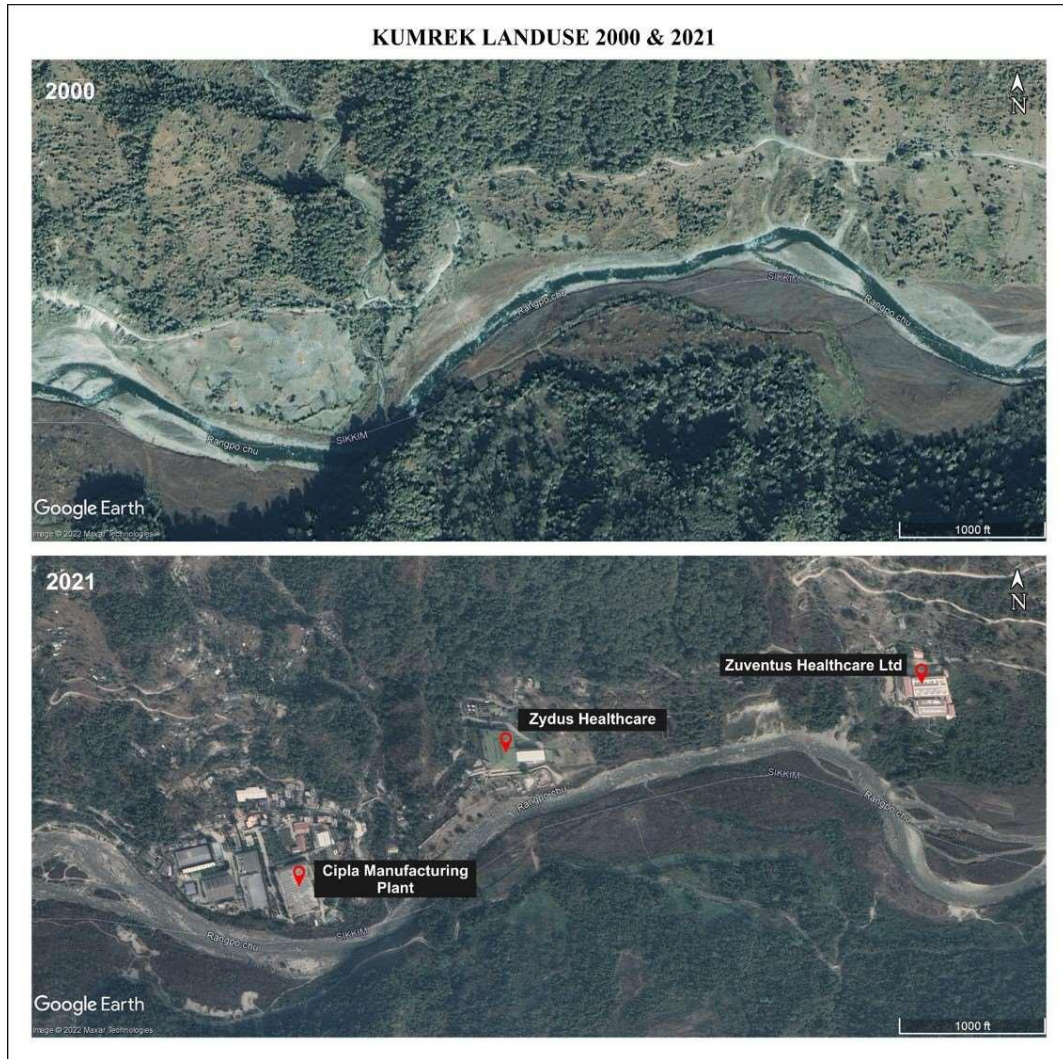


Figure 4-35: Comparison of Kumrek Landuse Map using Google Earth in 2006 & 2021

The Kumrek area in the study area had significant changes in land use during a 21-year period, from 2000 to 2021 was obtained from Google Earth, as represented in the Kumrek land-use maps (Figure 4:35). Kumrer is located in the lower part of Teesta River in the study area. As depicted in the google earth image of Kumrek for 2000 the locality was dominant with farmlands and sparse vegetation cover, intermingled by woodlands, scrublands, and less built up area. However, by 2021, there was a considerable movement towards

urbanization along with establishment of new small-scale industries and improvement of built up area in the region, due these certain development in the area may change the water chemistry of the study area due sewage discharge and domestic discharge from these newly established small scale industries and may lead as an anthropogenic pollutant in the study area. The heavy metal pollutant indices also confirm the presence of high metal pollution in Kumrek location of the study area.



Figure 4-36 : Majitar Landuse Map in 2006 & 2021

According to Majitar Land Use maps, Majitar region's land use changed significantly from 2006 to 2021 (Figure 4-36) which was obtained from Google Earth image, Majitar

is located in the lower part of the Teesta river in the study area. From 2006 image it can be observed that the area is covered with higher percentage of vegetation and agriculture along with scanty built-up area. Whereas comparing the 2006 image 2021 it can be observed that the area increases in built-up with new establishment of small-scale industries such as Alembic Pharmaceuticals Ltd., Aristo Pharma, Alkem Health Sc. Pvt. Ltd., and Intas Pharmaceuticals as shown in Figure 4-36. The new development of the region may change the chemical composition of the study area due sewage discharge and domestic discharge from these newly established small-scale industries and may lead as an anthropogenic pollutant in the study area. The heavy metal pollutant indices also confirm the presence of high metal pollution in Majitar region of the study area

4.9 MULTIVARIATE STATISTICAL ANALYSIS OF TEESTA RIVER

4.9.1 Pearson Correlation for physio-chemical ions (2019)

Pearson's correlation matrix builds relationships between components by determining how well the variation of each component can be explained by correlation with each other. To understand the coefficient correlation, correlated variables must have a shared origin and a comparable distribution. A correlation coefficient around -1 or 1 represents the most negative and strongest positive association between two variables, while a coefficient near 0 suggests no linear relationship among variables.

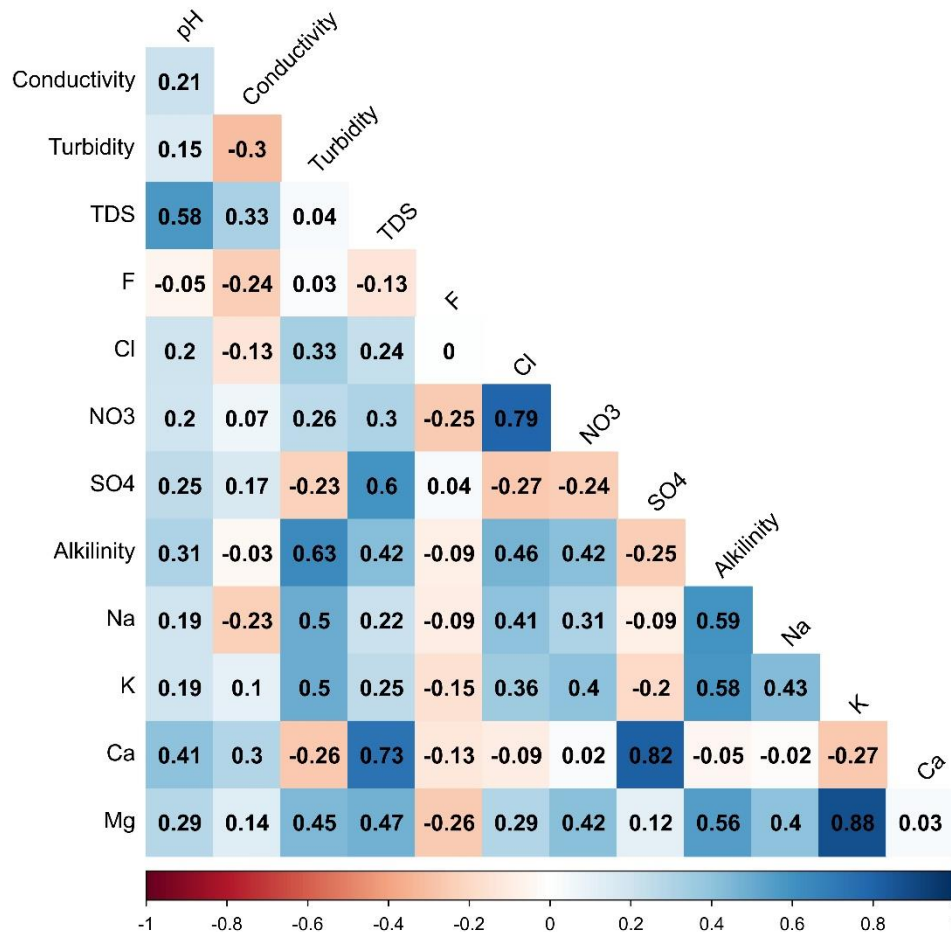


Figure 4-37: Correlation matrix heatmap of 2019 major ions.

The above correlation matrix (Figure 4-36) represents the relationships between

various water quality parameters. Each cell in the matrix contains a correlation coefficient that quantifies the degree and which way a linear connection between two variables points. pH has positive correlations with TDS, Ca, Mg, and Alkalinity. This suggests that as pH levels increase, these parameters tend to increase as well. In contrast, pH has a negative correlation with F, indicating that as pH increases, fluoride levels tend to decrease. Conductivity has positive correlations with TDS, Ca, and Mg, indicating that higher conductivity is associated with higher levels of these substances in the water. On the other hand, it has a negative correlation with Turbidity, suggesting that higher conductivity is associated with lower water turbidity. Alkalinity, NO₃, Na, K, and Mg all tend to rise in tandem with a rise in turbidity, suggesting a positive relationship between the two. It has a negative correlation with Conductivity, implying that higher turbidity is associated with lower conductivity. TDS exhibits positive correlations with pH, Conductivity, Turbidity, SO₄, Alkalinity, Na, K, and Ca, suggesting that as TDS levels increase, these parameters tend to increase as well. TDS has a negative correlation with F and Cl. F has a negative correlation with many parameters, including pH, Conductivity, Cl, NO₃, SO₄, Alkalinity, Na, K, Ca, and Mg, indicating that higher fluoride levels are associated with lower levels of these substances. Cl has strong positive correlations with NO₃ and SO₄, indicating that higher chloride levels are associated with higher levels of nitrate and sulfate. It also has positive correlations with Conductivity, Turbidity, Alkalinity, Na, K, Ca, and Mg. NO₃ shows positive correlations with Cl, SO₄, Alkalinity, Na, K, Ca, and Mg. Higher nitrate levels are associated with higher levels of these substances in the water. SO₄ is positively correlated with TDS, Alkalinity, Na, K, Ca, and Mg. This suggests that higher sulfate levels are associated with higher levels of these parameters. Alkalinity exhibits positive correlations with Turbidity, NO₃, SO₄, Na, K, Ca,

and Mg, indicating that higher alkalinity is associated with higher levels of these substances. Na, K, Ca, and Mg are positively correlated with each other, indicating that changes in the levels of one of these ions tend to be associated with similar changes in the others. These elements are also positively correlated with several other parameters, as mentioned above.

4.9.2 Pearson Correlation for major ions, pH, Conductivity, Turbidity and TDS (2021)

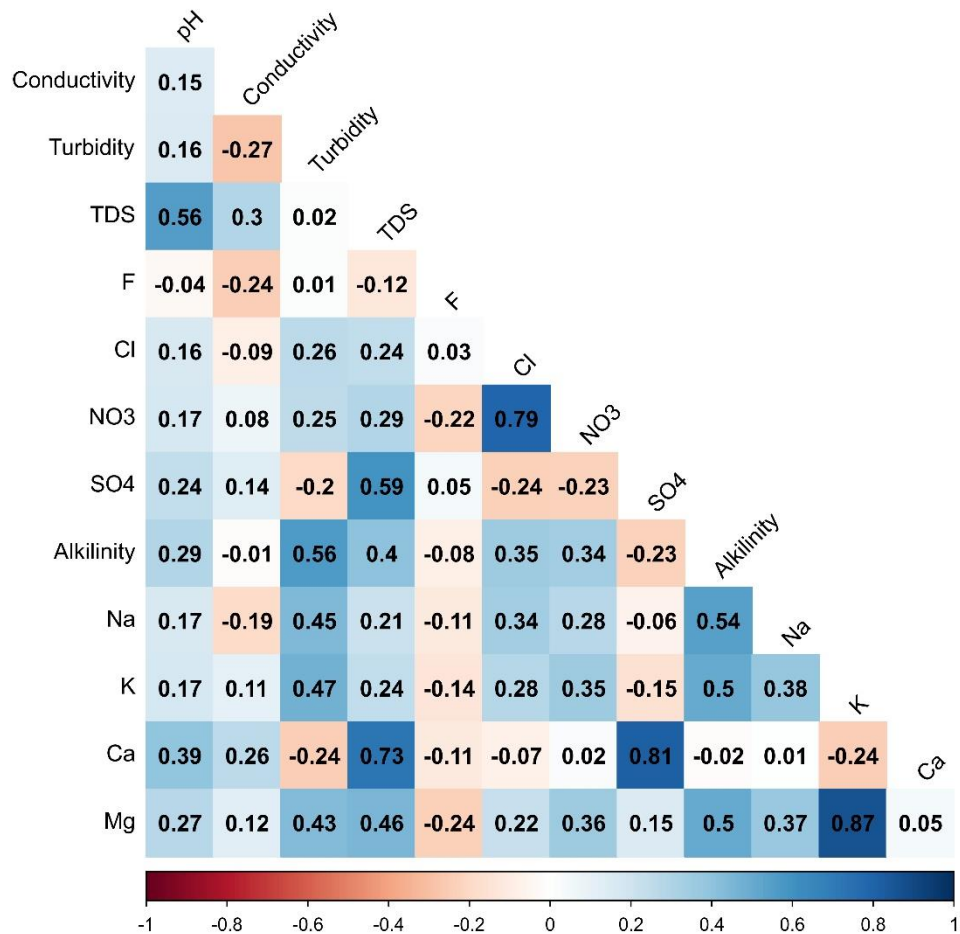


Figure 4-38: Correlation matrix heatmap of 2021 major ions.

The above correlation matrix reveals the relationships between various water quality parameters. Each cell in the matrix contains a correlation coefficient that quantifies the degree and which way a linear connection between two variables points. pH has positive correlations with TDS, Ca, Alkalinity, Na, K, and Cl. This suggests that

as pH levels increase, these parameters tend to increase as well. In contrast, pH has a negative correlation with F, indicating that as pH increases, fluoride levels tend to decrease. Conductivity has a positive correlation with TDS, implying that higher conductivity is associated with higher levels of total dissolved solids in the water. It also has positive correlations with Cl and SO₄, indicating that higher conductivity tends to be linked to higher levels of chloride and sulfate ions. Turbidity shows a positive correlation with Alkalinity, NO₃, Na, K, and Mg, suggesting that as turbidity increases, these parameters tend to increase as well. It has a negative correlation with Conductivity, implying that higher turbidity is associated with lower conductivity. TDS exhibits positive correlations with pH, Conductivity, Alkalinity, Na, K, Ca, and Mg, suggesting that higher TDS levels are associated with higher levels of these substances in the water. It also has a positive correlation with Cl and SO₄. F has negative correlations with many parameters, including pH, Conductivity, TDS, Cl, NO₃, SO₄, Alkalinity, Na, K, Ca, and Mg, indicating that higher fluoride levels are associated with lower levels of these substances. Cl has a strong positive correlation with NO₃ and SO₄, indicating that higher chloride levels are associated with higher levels of nitrate and sulfate. It also has positive correlations with Conductivity, Turbidity, Alkalinity, Na, K, Ca, and Mg. NO₃ shows positive correlations with Cl, SO₄, Alkalinity, Na, K, Ca, and Mg. Higher nitrate levels are associated with higher levels of these substances in the water. SO₄ is positively correlated with TDS, Alkalinity, Na, K, Ca, and Mg. This suggests that higher sulfate levels are associated with higher levels of these parameters. Alkalinity exhibits positive correlations with Turbidity, NO₃, SO₄, Na, K, Ca, and Mg, indicating that higher alkalinity is associated with higher levels of these substances. Na, K, Ca, and Mg are

positively correlated with each other, indicating that changes in the levels of one of these ions tend to be associated with similar changes in the others.

4.9.3 Pearson Correlation matrix for trace elements (2019)

Pearson's correlation matrix builds relationships between components by determining how well the variation of each component can be explained by correlation with each other. To understand the coefficient correlation, correlated variables must have a shared origin and a comparable distribution. A correlation coefficient around -1 or 1 represents the most negative and strongest positive association between two variables, while a coefficient near 0 suggests no linear relationship among variables.

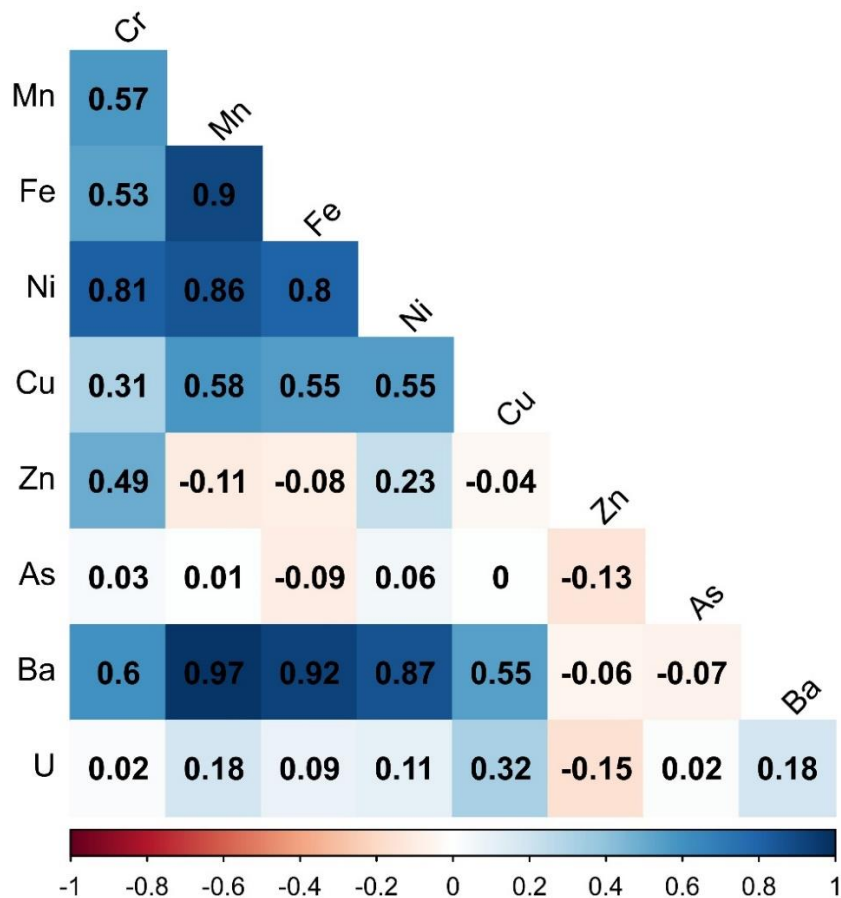


Figure 4-39: Correlation matrix heatmap of 2019 trace elements

The above figure shows the correlation matrix of the trace ions. The degree and

direction of a linear link between two variables are quantified by the correlation coefficient, which takes values between -1 and 1. This figure shows that Cr has a moderate positive correlation with Ni and Cu, a moderate positive correlation with Fe and Ba, and a moderate negative correlation with As. There is a moderate positive correlation between Mn and Fe, Ni, and Ba; a moderate positive correlation between Mn and Cr; and a moderate negative correlation between Mn and Zn. Fe has a moderately positive correlation with Mn, Ni, and Ba, a moderately negative correlation with Zn and As, and a weak positive correlation with Cr. Ni has a modest positive correlation with Cr and Mn and a weak negative correlation with As and Cu. Ni and Cu have a positive correlation, whereas Cr and Mn have a weak positive correlation, and Zn and As have a weak negative correlation. Weakly positive correlation exists between Zn and Ni, while slight negative correlation exists between Zn and Fe, Mn, Cu, and Ba. There is a little positive correlation between As and Ni, and a slight negative correlation between As and Fe, Cu, and Ba. There is a moderate positive correlation between Ba and Mn and Ni, a moderate positive correlation between Ba and Cr, Fe, and Cu, and a moderate negative correlation between Ba and Zn and As. U shows weak positive correlations with Cu, Ba, and Mn.

4.9.4 Pearson Correlation Matrix for trace elements 2021

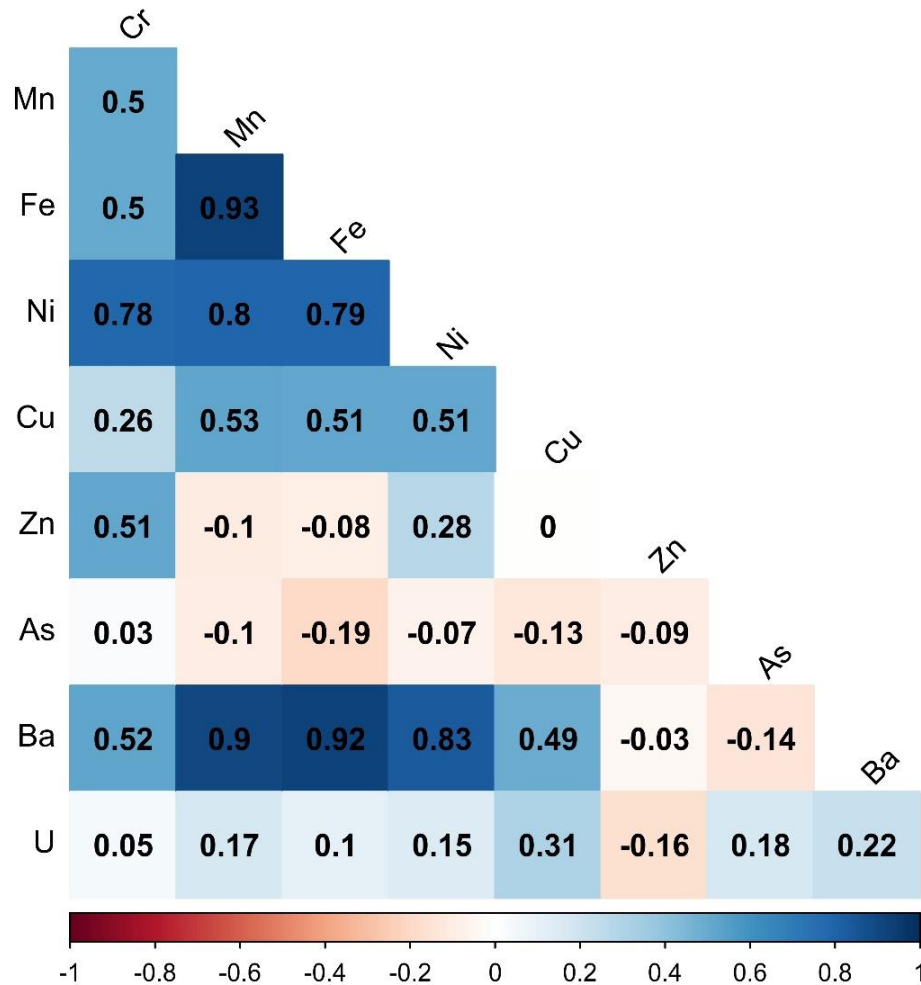


Figure 4-40: Correlation matrix heatmap of 2021 trace elements.

The above figure shows the correlation matrix of the trace ions. The degree and direction of a linear link between two variables are quantified by the correlation coefficient, which takes values between -1 and 1. As shown in the above diagram, Cr has a positive correlation with the elements Ni, Cu, Zn, and Ba. The associations with Mn and U are weakly positive, whereas those with Fe and As are negligible at best. The elements Fe, Ni, and Ba are all positively associated with Mn. It's weakly correlated positively with Cr and negatively with Zn and As. In general, Fe tends to go hand in hand with Mn, Ni, and even Ba. It's weakly correlated positively with Cr and negatively with Zn and As. Ni's relationships with Cr, Mn, Cu, and Ba

are all favorable. It's weakly correlated positively with Fe and negatively with As. The elements Cr, Mn, Ni, and Ba all have a positive correlation with Cu. It is inversely correlated with Zn and As and has extremely modest positive associations with Fe. Weakly positive correlation exists between Zn and Ni, while slight negative correlation exists between Zn and Fe, Mn, Cu, and Ba. The correlations between As and the other elements are extremely weak; they are either weakly positive with U or weakly negative with Cr, Mn, Fe, Cu, Zn, and Ba. When paired with Cr, Mn, Ni, or Cu, Ba has a positive correlation. The connections with Zn and As are quite modest, while the relationships with Fe and U are very poor. The positive connections between U and Cr, Mn, Fe, Ni, Cu, Zn, and As are quite modest. It has a weak positive correlation with Ba.

4.9.5 PRINCIPAL COMPONENT ANALYSIS FOR HYDRO-CHEMICAL DATA.

Principal Component Analysis (PCA) is a widely utilized method for multivariate data analysis, appreciated for its simplicity in algebra and straightforward interpretability. This exploratory, multivariate statistical technique is particularly valuable for assessing data variability. Unlike univariate techniques, which may entail errors from repeated statistical testing, multivariate methods, like PCA, can concurrently consider numerous factors influencing data variability (Boruvka 2005).

Environmental applications of PCA are diverse and pervasive, with applications extending to surface and groundwater studies (Chen et al. 2007; Kuppusamy and Grirdhar 2006), soil investigations (Boruvka et al. 2005; Zhang 2006), and biota assessments (Yawei et al. 2005). PCA has historically been employed to analyze the spatial distribution of contaminants. An advantage of PCA is that it relies solely on eigen value of the correlation or covariance matrix, imposing no specific data constraints like normality (Meglin 1991). Moreover, it has gained prominence for discerning contaminant sources (Mudge and Duce 2005) and identifying key variables in environmental monitoring (Carlton et al. 2001).

PCA facilitates the transformation of a large data matrix into smaller matrices that capture the majority of the original data's information. The resulting data matrices comprise Principal Component (PC) scores and loadings. These PC scores (S) are linear combinations of the normalized data (x), where the loadings (l) serve as coefficients:

$$[S = \sum(x * l).]$$

Each PC score effectively consolidates information from all the chemical measurements into a single numerical value, while the loadings elucidate each element's relative contribution to that score. Loadings are normalized to eigenvalues (l^*) with the notation $l^* =$

1\1. The Bartlett's sphericity test conducted on the correlation matrix of variables demonstrated a calculated $\chi^2=1865.09$, significance (Sig.) value=0.0000 and degree of freedom (df)=231 for Premonsoon 2019, $\chi^2=1884.49$, Sig. value=0.0000 and df =231 for Postmonsoon 2019, $\chi^2=1577.84$ and Sig. value=0.0000 and df =231 for Premonsoon 2021, $\chi^2=1444.31$ Sig. value=0.0000 and df =231 for Postmonsoon 2021, surpassing the critical value of $\chi^2 =260.78$ at a significance level of $p = 0.0005$ and 153 degrees of freedom shown in Table No 20, 22, 24 and 26. The result for KMO and Bartlett's test suggests that PCA can achieve a significant reduction of the dimensionality of the original dataset in the study area (Sing et. al. 2005).

To tabulate and graphically represent the hydrochemical characteristics of river water for both the pre-monsoon and post-monsoon seasons in the years 2019 and 2021, PCA was employed. An initial examination of the river water chemistry dataset indicated interdependencies among the primary components. To verify the appropriateness of utilizing PCA, Bartlett's sphericity test, which evaluates the independence of variables, was conducted on the correlation matrix (R). The results revealed a probability value of 0.000, significantly lower than the 0.05 threshold, aligning with the prerequisites for implementing PCA (Fung and Le, 1987; Feng, 2003; He and Meng, 2002; Mrklas et al., 2006). The eigenvalues (λ) of the R matrix represent the variance associated with each component

4.9.6 PCA Analysis for major ions and Trace elements for pre-monsoon 2019

Table 20: KMO and Bartlett's test for PrM hydro-chemistry data 2019

KMO and Bartlett's Test		
Kaiser-Meyer-Olkin Measure of Sampling Adequacy.		0.587
Bartlett's Test of Sphericity	Approx. Chi-Square	1865.098
	df	231
	Sig.	0.000

Table 21: Loadings of experimental variables on the first 5 PCs for PrM hydro-chemistry data 2019.

Rotated Component Matrix ^a					
Parameters	Component				
	1	2	3	4	5
pH	0.234	0.496	0.514	0.062	-0.109
EC	-0.218	0.873	-0.074	-0.069	-0.148
Turbidity	0.812	-0.188	0.126	0.155	0.184
TDS	0.055	0.771	0.298	0.225	0.255
F	-0.136	-0.038	-0.055	0.401	0.787
Cl	0.232	-0.003	0.019	0.935	0.064
NO3	0.374	0.042	0.031	0.860	0.191
SO4	-0.490	0.050	0.677	-0.256	-0.173
Alkalinity	0.608	0.540	0.021	0.166	0.357
Na	0.338	0.131	0.664	0.018	0.080
K	0.857	0.384	-0.040	0.105	-0.094
Ca	-0.627	0.248	0.588	-0.076	0.187
Mg	0.853	0.380	0.118	0.048	-0.101
Cr	0.660	-0.392	-0.306	-0.074	-0.101
Mn	0.929	-0.008	0.148	0.189	0.177
Fe	0.923	0.001	0.102	0.254	0.150
Ni	0.942	0.008	-0.142	0.121	0.077
Cu	0.469	0.198	0.030	-0.095	0.785
Zn	-0.117	-0.198	-0.754	-0.233	-0.071
As	-0.307	-0.385	0.608	-0.153	-0.312
Ba	0.936	0.047	0.086	0.206	0.127
U	0.123	0.698	0.417	-0.303	0.199
Total	7.813	3.176	2.905	2.311	1.854
% of Variance	35.515	14.438	13.204	10.506	8.425
Cumulative %	35.515	49.954	63.158	73.663	82.088
Extraction Method: Principal Component Analysis.					
Rotation Method: Varimax with Kaiser Normalization.					
a. Rotation converged in 7 iterations.					

As depicted in the Table 21, the initial five components exhibit eigenvalues (λ) greater than 1, cumulative % explains 82.08% of the overall variance observed in the original variables. Our comprehension of the chemical attributes of the water samples hinges on the interpretation of these first five principal components. In the first component (PC1), Turbidity, Alkalinity, K, Mg, Cr, Mn, Fe, Ni and Ba exhibit the positive loadings and Ca as a negative loading, characterized by the most substantial absolute coefficients within this component. PC1 accounts for 35.52% of the total variance, signifying a more conventional water source. Therefore, PC1 can be defined as a natural water component from the mineralization of geogenic components. This process encompasses salinization, ion-exchange and dissolution (Singh et al. 2010). PC2, responsible for elucidating 14.44% of the total variance. It is characterized by a positive loading of EC, TDS, Alkalinity and U indicating the weathering and dissolution significantly controlled these chemical constituents in water. PC3 explaining total variance 13.20% with the positive loading of pH, SO₄, Na, Ca and As, while negative loading by Zn indicating also rationalized natural weathering. PC1, PC2 and PC3 all are significantly characterized by weathering and dissolution however all three components are independent to each other denote different source attribution. PC4 is explain by 10.50% of the total variance with a positive loading of Cl and NO₃ indicating anthropogenic (urban drainage and septic discharge). PC5 is explained 8.43% of the total variance with the positive loading of F and Cu indicating weathering and leaching of fluoride containing rocks.

4.9.7 PCA analysis for major and trace elements for post-monsoon 2019

Table 22: KMO and Bartlett's test for PoM hydro-chemistry data 2019

KMO and Bartlett's Test		
Kaiser-Meyer-Olkin Measure of Sampling Adequacy.		0.578
Bartlett's Test of Sphericity	Approx. Chi-Square	1884.490
	df	231
	Sig.	0.000

Table 23: Loadings of experimental variables on the first 5 PCs for PoM hydro-chemistry data 2019.

Rotated Component Matrix ^a					
Parameters	Component				
	1	2	3	4	5
pH	-0.112	0.253	0.434	0.016	0.694
EC	0.070	-0.453	0.181	-0.401	0.440
Turbidity	0.351	0.720	0.018	-0.349	-0.090
TDS	0.061	0.213	0.912	-0.008	0.285
F	0.195	-0.311	-0.044	0.656	0.359
CL	-0.069	0.887	-0.070	0.102	0.232
NO3	-0.002	0.735	-0.052	-0.264	0.375
SO4	0.136	-0.258	0.929	0.128	-0.035
Alkalinity	0.169	0.871	0.069	-0.114	0.086
Na	0.250	0.876	0.005	0.190	-0.059
K	0.718	0.486	-0.066	-0.142	0.197
Ca	-0.054	-0.078	0.954	-0.031	0.155
Mg	0.708	0.368	0.538	-0.021	0.057
Cr	0.924	-0.108	0.041	0.226	0.103
Mn	0.903	0.167	0.023	0.297	0.079
Fe	0.452	-0.001	0.198	0.420	-0.179
Ni	0.838	-0.073	0.010	0.456	-0.120
Cu	0.524	0.230	0.098	0.677	-0.094
Zn	0.378	0.118	-0.293	0.644	0.024
As	0.230	-0.273	0.243	0.755	-0.046
Ba	0.926	0.214	-0.028	0.191	0.103
U	0.212	0.210	0.120	0.070	0.843
Total	5.262	4.501	3.347	2.887	1.962
% of Variance	23.919	20.457	15.213	13.121	8.919
Cumulative %	23.919	44.376	59.589	72.710	81.629

As presented in the table 23, the initial five components feature eigenvalues (λ) greater than 1, collectively explaining 81.63% of the total cumulative variance observed in the original variables. Our understanding of the chemical properties of the water samples is contingent upon the interpretation of these first five principal components.

In the PC1, K, Mg, Cr, Mn, Ni, Cu and Ba exhibit positive loadings. These components possess the most substantial absolute coefficients within PC1, which accounts for 23.92% of the total variance. This suggests a more conventional water source, and PC1 can be characterized as a natural water component resulting from the mineralization of geological components. This mineralization process encompasses ion-exchange, dissolution and rock water interaction. In PC2, which elucidates 20.46% of the total variance with a positive loading of Turbidity, Cl, NO₃, Alkalinity and Na indicating both geogenic and anthropogenic (domestic discharge) significantly contributed these chemical constituents into the river water system. PC3, responsible for 15.21% of the total variance with a positive loading of SO₄, Ca and Mg indicating weathering and dissolution of calcium and magnesium containing sulphate minerals such as gypsum. PC4, accounting for 13.12% of the total variance which is characterized by a positive loading of F, Cu, Zn and As indicating natural rock weathering and leaching. Finally, PC5, explaining 8.92% of the total variance with a positive loading of pH and U indicating alkaline environment supports uranium dissolution and mobilization in river water.

4.9.8 PCA Analysis for major ions and Trace elements for pre-monsoon 2021

Table 24: KMO and Bartlett's test for PrM hydro-chemistry data 2021.

KMO and Bartlett's Test		
Kaiser-Meyer-Olkin Measure of Sampling Adequacy.		0.620
Bartlett's Test of Sphericity	Approx. Chi-Square	1577.846
	df	231
	Sig.	0.000

Table 25 : Loadings of experimental variables on the first 6 PCs for PrM hydro-chemistry data 2021.

Rotated Component Matrix^a						
Parameters	Component					
	1	2	3	4	5	6
pH	0.283	0.419	-0.006	0.595	0.095	-0.111
EC	-0.174	0.787	-0.099	0.257	-0.291	-0.173
Turbidity	0.832	-0.316	0.040	0.233	-0.059	0.151
TDS	0.072	0.774	0.294	0.260	0.128	0.189
F	-0.156	-0.003	0.417	-0.027	-0.082	0.765
CL	0.158	0.001	0.952	0.052	-0.066	0.041
NO3	0.327	0.039	0.890	0.041	-0.057	0.156
SO4	-0.428	0.077	-0.223	0.428	0.567	-0.157
Alkalinity	0.620	0.485	0.060	0.162	-0.131	0.314
Na	0.317	0.224	0.044	0.183	0.671	0.095
K	0.838	0.399	0.082	-0.104	-0.065	-0.130
Ca	-0.558	0.268	-0.055	0.473	0.410	0.200
Mg	0.835	0.412	0.033	-0.038	0.100	-0.116
Cr	0.534	-0.180	-0.002	-0.686	0.140	-0.059
Mn	0.950	-0.050	0.146	0.114	0.016	0.145
Fe	0.900	-0.030	0.252	0.108	-0.073	0.135
Ni	0.908	0.060	0.101	-0.295	-0.034	0.068
Cu	0.449	0.171	-0.090	0.036	-0.093	0.781
Zn	-0.182	-0.151	-0.181	-0.732	-0.331	-0.053
As	-0.270	-0.128	-0.124	0.001	0.785	-0.266
Ba	0.922	0.097	0.205	-0.015	0.015	0.082
U	0.171	0.845	-0.120	0.073	0.342	0.187
Total	7.350	3.019	2.246	2.150	1.978	1.687
% of Variance	33.410	13.723	10.209	9.771	8.992	7.670
Cumulative %	33.410	47.133	57.342	67.113	76.106	83.776
Extraction Method: Principal Component Analysis.						
Rotation Method: Varimax with Kaiser Normalization.						
a. Rotation converged in 8 iterations.						

As illustrated in the table 25, the initial five components boast eigenvalues (λ) exceeding 1, collectively elucidating 83.77% of the total cumulative variance observed in the original variables for six principal components. Our comprehension of the chemical properties of the water samples hinges on the interpretation of these first five principal components. Within PC1, positive loadings are attributed to Turbidity, Alkalinity, K, Ca, Mg, Cr, Mn, Fe, Ni and Ba. These components exhibit the most substantial absolute coefficients within PC1, which accounts for 33.41% of the total variance. This pattern suggests a more conventional water source, and PC1 can be characterized as a natural water component from weathering and mineralization. In PC2, which elucidates 13.72% of the total variance, the component is marked by positive loadings of EC, TDS and U and moderate loading of pH indicating mobilization. In the PC3, responsible for explaining 10.21% of the total variance, which is characterized by positive loadings of Cl and NO₃ indicating significant contribution of anthropogenic inputs such as urban domestic and septic discharge. PC4, accounting for 9.77% of the total variance with a positive loading of pH, Cr and Zn indicating independent mixed source. PC5, accounting for 8.99% of the total variance with a positive loading of SO₄, Na and As indicating geogenic weathering. Lastly, PC5, explaining for 7.67% of the total variance with a positive loading of F and Cu indicating weathering and leaching of fluoride containing rocks.

4.9.9 PCA Analysis for major ions and Trace elements for post-monsoon 2021

Table 26: KMO and Bartlett's test for PoM hydro-chemistry data 2021.

KMO and Bartlett's Test		
Kaiser-Meyer-Olkin Measure of Sampling Adequacy.		0.514
Bartlett's Test of Sphericity	Approx. Chi-Square	1444.312
	df	231
	Sig.	0.000

Table 27: Loadings of experimental variables on the first 7 PCs for PoM hydro-chemistry data 2021

Rotated Component Matrix ^a							
Parameters	Component						
	1	2	3	4	5	6	7
pH	0.138	-0.030	0.312	0.829	-0.018	-0.129	-0.032
EC	-0.178	-0.008	0.106	0.097	-0.117	-0.076	0.919
Turbidity	0.762	0.045	-0.035	0.049	-0.195	-0.251	-0.174
TDS	0.199	0.123	0.851	0.404	-0.109	-0.004	0.051
F	-0.190	0.158	0.009	0.168	0.884	-0.083	-0.130
CL	0.746	-0.057	-0.115	0.266	-0.175	0.427	-0.054
NO3	0.726	-0.273	-0.064	0.214	-0.182	0.047	0.145
SO4	-0.156	0.232	0.939	-0.026	0.059	-0.086	0.059
Alkalinity	0.748	0.055	0.009	0.258	-0.172	0.179	-0.187
Na	0.847	0.115	-0.041	0.020	0.027	0.067	-0.264
K	0.788	0.112	-0.007	-0.085	0.217	-0.282	0.250
Ca	-0.063	-0.010	0.960	0.196	-0.063	-0.006	0.068
Mg	0.629	0.301	0.542	-0.042	0.215	-0.296	0.046
Cr	-0.123	0.915	0.051	0.052	0.107	-0.004	0.129
Mn	0.162	0.826	0.040	0.096	0.238	-0.124	-0.228
Fe	0.021	0.933	0.050	0.091	0.027	-0.097	-0.012
Ni	-0.022	0.834	0.189	-0.283	-0.017	0.258	0.109
Cu	0.526	0.464	0.296	-0.226	0.206	0.330	0.024
Zn	-0.013	0.003	-0.018	-0.039	-0.012	0.906	-0.063
As	-0.105	0.056	0.679	-0.034	0.522	0.260	-0.061
Ba	0.414	0.663	0.231	0.297	-0.337	0.021	-0.143
U	0.228	0.162	0.098	0.726	0.352	0.125	0.228
Total	4.664	4.064	3.604	1.893	1.662	1.593	1.258
% of Variance	21.199	18.473	16.383	8.605	7.554	7.242	5.717
Cumulative %	21.199	39.672	56.055	64.661	72.214	79.456	85.173
Extraction Method: Principal Component Analysis. Rotation Method: Varimax with Kaiser Normalization.							

The table 27 illustrates that the initial seven components have eigenvalues (λ) exceeding 1, collectively explaining 85.17% of the total cumulative variance. Our understanding of the chemical attributes of the water samples relies on the interpretation of these first five principal components. PC1 accounted for 21.19% of the total variance with a positive loading of Turbidity, Cl, NO₃, Alkalinity, Na, K, Mg and Cu indicating both natural and anthropogenic processes are significantly involved and controlling ions chemistry. PC 2 accounted for 18.47% of the total variance with a positive loading of Cr, Mn, Fe, Ni and Ba indicating dissolution of aforementioned minerals. PC3, which explains 16.38% of the total variance with a positive loading of TDS, SO₄, Ca, Mg and As. PC3 also accounted for natural weathering and dissolution. PC4, accounted for 8.60% of the total variance with a positive loading of pH and U indicating alkaline environment supports uranium dissolution and mobilization in river water. PC5 accounted for 7.45% of the total variance with the positive loading of F and As indicating the co-occurrence of F and As in alkaline environment. PC6, explaining 7.24% of the total variance and PC7 explained 5.72% of the variance with a positive loading of Zn and EC respectively showing lack of interdependence and exhibit an almost arbitrary association.

4.10 DISCUSSION

This study presents a comprehensive examination of the geochemical characteristics and the controlling processes that influence the chemical composition of the Teesta River, situated in the Sikkim Himalaya region. The focus is particularly on the segments of the river that are nourished by glacial sources.

In this research, a combination of analytical methods is employed. Firstly, morphometric parameters are analyzed, and these are complemented with the integration of land use and land cover (LU/LC) data. The objective is to precisely identify areas that are prone to erosion, which, in turn, has a discernible impact on the river's hydrochemical composition, whether directly or indirectly.

In terms of the river's chemical makeup, it is observed that specific major ions dominate, with a distinct order of prevalence. Cations are primarily represented by $\text{Ca}^{2+} > \text{Na}^{+} > \text{Mg}^{2+} > \text{K}^{+}$, while anions exhibit a hierarchy of $\text{HCO}_3^{-} > \text{SO}_4^{2-} > \text{NO}_3^{-} > \text{Cl}^{-}$.

The hydrochemical attributes, which encompass a range of parameters reflecting the chemical composition of water, exhibit substantial variations that are evident in both spatial and temporal dimensions. These variations in the water's chemical characteristics are not static; they evolve and shift over geographical locations and time periods. To effectively capture and communicate these dynamic changes, graphical representations serve as invaluable tools. In this study, one of the key means of representation is a set of bar graphs. These graphs provide a visual portrayal of how the concentrations of major cations and ions fluctuate across different points in the geographical landscape as well as how they change over distinct periods of time. The bar graphs allow for a quick and comprehensive assessment of the alterations in the water's chemical constituents, making it easy to

identify trends, anomalies, and the impact of various factors on the hydrochemical composition. This method not only aids in recognizing spatial disparities in water quality but also reveals the influence of temporal factors such as seasonal variations or long-term trends. As such, it enhances our understanding of the complex interplay between geological, environmental, and anthropogenic factors that influence the chemical characterization of the water, ultimately contributing to a more comprehensive assessment of the region's hydrochemistry.

To assess the hydrochemical facies, we utilized major cations and anions, including Ca^{2+} , Na^+ , Cl^- , SO_4^{2-} , and HCO_3^- , expressed in mg/L, and represented them in Piper diagrams and Durov Plot for each year in both seasons. This analytical approach provides insights into the prevailing chemical processes within the current lithological environment and the overall geochemical conditions.

The major ion chemistry analysis, as visualized in the Piper diagrams for the Teesta River, consistently indicates that the water exhibits a dominant Ca- HCO_3 type (85.23%), followed by a Mixed Ca-Mg-Cl type (14.77%) in both seasons for each year.

The comprehensive analysis of major ion chemistry, visualized through the Durov Plot for the Teesta River, consistently reveals a predominant water type characterized by Infiltration waters of HCO_3 -Ca (43.12%). This suggests that a significant portion of the water's composition can be attributed to the influence of infiltrating sources rich in bicarbonates and calcium. Additionally, the analysis indicates the presence of Calcite Gypsum water type (29.56%), signifying the influence of geological processes related to the dissolution of calcite and gypsum in the region. Furthermore, a noteworthy proportion of the water is indicative of Mixing reactions from various sources (24.32%). This highlights the complex interplay of

multiple origins contributing to the overall hydrochemical composition of the Teesta River, offering valuable insights into the water's characteristics and sources.

The Water Quality Index for domestic purpose based major ions indicates that the present study is fit for domestic purpose.

Furthermore, an evaluation of the Water Quality Index for domestic various indices, Permeability Index, Kelly's Index, Wilcox Diagram, Residual Sodium Carbonate Index, for irrigation purpose, all based on major ions, reveals that the river's water quality is categorized as excellent to good, making it suitable for both irrigation purposes.

To gain insight into the factors influencing water quality, the Gibbs Diagram and a Na-normalized molar ratios mixing diagram are employed. The primary determinant of the ionic composition in water bodies is the prevalent presence of particular rock types. In the specific study area, prolonged interactions between water and the underlying rock, encompassing processes like percolation and the passage through geological formations, have resulted in a substantial elevation in solute concentration and led to carbonate and silicate weathering. This increased solute concentration plays a pivotal role in shaping the overall water quality of the region.

Additionally, an analysis of Heavy Metal Pollution Indices, including HPI, CF, and HEI, highlights contamination with heavy metals, particularly in the lower section of the study area, underscoring the environmental challenges faced in the region. This research offers a comprehensive understanding of the complex interactions between geological, hydro-chemical, natural processes, and land use changes in the Teesta River Basin, providing valuable insights for effective environmental management, resource conservation, and a deeper appreciation of the

unique Himalayan ecosystem.

A parallel investigation of land use and land cover patterns between 2010 and 2021 reveals significant shifts. Agriculture has seen an increase of 0.93%, and Built-up Areas have expanded by 0.8%, while Water bodies and Forested areas have experienced declines of 0.03% and 1.7%, respectively also Google Earth image comparison for few locations in the study area (Ranipool, Kumrek and Majitar) was performed which indicates that the increase in small scale industries and settlement may have cause the water pollution with respect to heavy metal pollution indices due to anthropogenic pollutants (industrial and domestic discharge).

The PCA analysis conducted reveals that the hydrochemical parameters in the study area are mainly influenced by both natural and anthropogenic factors. Natural processes like erosion and weathering contribute to the release of various solutes into the water bodies, shaping their composition. Simultaneously, anthropogenic activities, including industrial processes and land use changes, introduce pollutants and modify the water's natural composition. This intricate interplay of natural and human-induced influences collectively controls the hydrochemistry.

CHAPTER 5

CONCLUSION

Based on the data presented in the result and discussion, some conclusions are made in this final chapter. Numerous techniques and strategies were successfully used to the environmental samples and data and arrived in these conclusions. The key objectives of this research study have determined the following conclusion.

- Morphometric parameters analysis along with LU/LC of the study area helps in finding soil erosion susceptibility zone which may contributes to hydro-chemical characteristics.
- Hydro-chemical attributes exhibit perceptible spatio-temporal variations in the study area as indicated by descriptive statistical analysis.
- The order of dominance of major ions follows $\text{Ca}^{2+} > \text{Na}^+ > \text{Mg}^{2+} > \text{K}^+$ for cations, and $\text{HCO}_3^- > \text{SO}_4^{2-} > \text{NO}_3^- > \text{Cl}^-$ for anions.
- Piper Diagram and Durov Plot classified the different types of water in the study area. The Piper diagram classified that Ca-HCO₃ type at the downstream during pre-monsoon and post-monsoon followed by a Mixed Ca-Mg-Cl type and Ca-HCO₃ at upstream during pre-monsoon and post-monsoon. Durov plot indicates the hydro-chemical facies of calcite-gypsum dissolution and infiltration water of Ca-HCO₃ types during pre-monsoon and post-monsoon at the downstream of the river. Whereas, mixing reactions from various origins and calcium-gypsum type during pre-monsoon and post-monsoon at the upstream of the river water.
- Gibbs Diagram and Na-normalized molar ratios mixing diagram which depicted the factors controlling the hydrochemistry in the study area shows that the water chemistry is controlled by rock weathering.

- The Water Quality Index (drinking purpose) results indicate that the water quality is excellent for domestic use in terms of major ion concentration.
- The water quality assessment of the Teesta River reveals a spectrum that spans from excellent to suitable for agricultural purposes, as evidenced by the outcomes of multiple comprehensive indices. These indices, including the Permeability Index, Kelly's Index, Wilcox Diagram, and Residual Sodium Carbonate, collectively provide a thorough evaluation of the Teesta River in the context of agriculture.
- Heavy Metal Pollution Index (HPI) is a comprehensive metric that amalgamates the influence of individual heavy metals, on the overall water quality. Similarly, the Contamination Factor (CF) and Heavy Metal Evaluation Index (HEI) offer additional dimensions of assessment. The results derived from these indices reveal that certain samples from the lower Teesta River exhibit noteworthy variations in heavy metal pollution levels during the pre-monsoon season.
- The analysis of LU/LC patterns within the Rani Khola watershed, situated within the study area, unveils significant changes over the decade from 2010 to 2021. Notably, there is a discernible increase in the extent of Agricultural and Built-up Areas by 0.93% and 0.8%, respectively. In contrast, there has been a marginal reduction in Water Bodies and a more substantial decline in Forest Area, shrinking by 0.03% and 1.7%, respectively, during this period. A closer examination through Google Earth image comparisons for areas such as Ranipool, Kumrek, and Majitar at the lower region of Teesta River brings transformations in land use. These changes are particularly evident in the emergence of new small-scale industrial

ventures within the region. The development of these industries raises concerns as they have the potential to introduce pollutants into the water chemistry of the area.

- The PCA analysis indicates that hydrochemical parameters in the study area result from the interplay of natural and anthropogenic factors. Natural processes, such as erosion and weathering, release solutes into the water, influencing its composition. Anthropogenic activities, such as industrial processes and land use changes, introduce pollutants and alter the water's natural attributes. This complex interaction of natural and human-induced factors collectively dictates the hydrochemistry of the area.

REFERENCES

- A.P.H.A. (2005) Standard methods of analysis of water, waste water, American Public Health Association, USA, 14th ed., Washington DC, 1457 pp.
- Adhikari, S., & Kamle, S. (2021). Governance and Management of Teesta River Water Resources: A Geopolitical Appraisal BT - Resource Management, Sustainable Development and Governance: Indian and International Perspectives (B. Thakur, R. Thakur, S. Chattopadhyay, & R. K. Abhay (eds.); pp. 249–266). Springer International Publishing. https://doi.org/10.1007/978-3-030-85839-1_15
- Ahmed, F. T., Khan, A. H. A. N., Khan, R., Saha, S. K., Alam, M. F., Dafader, N. C., Sultana, S., Elius, I. Bin, & Mamum, S. Al. (2021). Characterization of arsenic contaminated groundwater from central Bangladesh: Irrigation feasibility and preliminary health risks assessment. *Environmental Nanotechnology, Monitoring and Management*, 15(February). <https://doi.org/10.1016/j.enmm.2021.100433>
- Ahmed, Z., Alam, R., Ahmed, M. N. Q., Ambinakudige, S., Almazroui, M., Islam, M. N., Chowdhury, P., Kabir, M. N., & Mahmud, S. (2022). Does anthropogenic upstream water withdrawal impact on downstream land use and livelihood changes of Teesta transboundary river basin in Bangladesh? *Environmental Monitoring and Assessment*, 194(2). <https://doi.org/10.1007/s10661-021-09726-3>
- Akhter, S., Eibek, K. U., Islam, S., Towfiqul Islam, A. R. M., Chu, R., & Shuanghe, S. (2019). Predicting spatiotemporal changes of channel morphology in the reach of Teesta River, Bangladesh using GIS and ARIMA modeling. *Quaternary International*, 513(May), 80–94. <https://doi.org/10.1016/j.quaint.2019.01.022>

- Ali, S. N., Sharma, A., Agrawal, S., Yadava, M. G., Jani, R. A., Dubey, J., & Altaf, S., Meraj, G. & Romshoo, S.A. (2014) Morphometry and land cover based multi-criteria analysis for assessing the soil erosion susceptibility of the western Himalayan watershed. *Environ Monit Assess* 186, 8391–8412. <https://doi.org/10.1007/s10661-014-4012-2>
- Amin, A. R., Zafar, M. A., Abbas, M. S., Badruzzaman, M., & Hoshan, I. (2020). An assessment of vital water quality parameters of Teesta River closest to barrage region in Lalmonirhat district of Bangladesh. *International Journal of Fisheries and Aquatic Studies*, 8(6), 92–95. <https://doi.org/10.22271/fish.2020.v8.i6b.2365>
- Ansari, Z., & Ahmad, S. (2019). Hydro-geochemical characteristics of the Himalayan Streams. *Journal of Applied Geochemistry*, 21(2), 225–237. <https://search.proquest.com/docview/2213055378/fulltextPDF/D4F1209954324B5BPQ/1?accountid=14816>
- Ayers, R. S., & Westcot, D. W. (1985). *Water quality for agriculture* (Vol. 29). Food and Agriculture Organization of the United Nations.
- Backman, B., Bodiš, D., Lahermo, P., Rapant, S., Tarvainen, T. (1998). Application of a groundwater contamination index in Finland and Slovakia. *Environ. Geol.* 36 (1-2), 55–64. doi: 10.1007/s002540050320 , 1998/11/01 .
- Bishwakarma, K., Wang, G. xing, Zhang, F., Adhikari, S., Karki, K., & Ghimire, A. (2022). Hydrochemical characterization and irrigation suitability of the Ganges Brahmaputra River System: review and assessment. *Journal of Mountain Science*, 19(2), 388–402. <https://doi.org/10.1007/s11629-021-6834-z>
- Boruvka L, Veccek, O Jehlicka, J, (2005) Principal component analysis as a tool to indicate

the origin of potentially toxic elements in soil. *Geoderma* 128: 289–300.

Carlson C, Critto A, Marcomini A, Nathanail P, (2001) Risk based characterization of contaminated industrial site using multivariate and geostatistical tools. *Environ Pollut* 111: 417–427.

Chakrabarty, M., Panja, S., & Homechaudhuri, S. (2023). Predictive Modeling of a Fish-Based Index of Biotic Integrity in Assessing Environmental Degradation in the Lower Teesta River Basin of Eastern Himalayan Foothills, India. *Proceedings of the Zoological Society*, 76(1), 22–35. <https://doi.org/10.1007/s12595-023-00464-7>

Chatterjee and Raziuddin, C. Chatterjee, M. Raziuddin, (2002) Determination of Water Quality Index(WQI) of a degraded river in Asansol industrial area(West Bengal) *Nature, Environment and pollution technology*, 1 (2) (2002), pp. 181-189

Coplen, T.B.; Herczeg, A.L.; Barnes, C. Isotope engineering (2000): Using stable isotopes of the water molecule to solve practical problems. In *Environmental Tracers in Subsurface Hydrology*; Cook, P.G., Herczeg, A.L., Eds.; Kluwer Academic Publishers: Boston, MA, USA.

Das, S., Datta, P., Sharma, D., & Goswami, K. (2022). Trends in Temperature, Precipitation, Potential Evapotranspiration, and Water Availability across the Teesta River Basin under 1.5 and 2° C Temperature Rise Scenarios of CMIP6. *Atmosphere*, 13(6), 1–22. <https://doi.org/10.3390/atmos13060941>

Das, S., Tripathy, G. R., Rai, S. K., Danish, M., Thakur, D., Dutt, S., & Sarangi, S. (2021). The Role of Sulfuric Acid in Continental Weathering: Insights From Dissolved Major Ions and Inorganic Carbon Isotopes of the Teesta River, Lower Brahmaputra System.

Geochemistry, Geophysics, Geosystems, 22(4), e2020GC009324.

<https://doi.org/https://doi.org/10.1029/2020GC009324>

Doneen, L. D. (1964). Notes on water quality in agriculture. *Publications in Climatology*, 17(1), 1-28.

Eaton, F. M. (1950). Significance of carbonates in irrigation waters. *Soil Science*, 69(2), 123-133

Edet, A., Offiong, O. (2002). Evaluation of water quality pollution indices for heavy metal contamination monitoring. A study case from Akpabuyo-Odukpani area, Lower Cross River Basin (southeastern Nigeria). *GeoJournal* 57 (4), 295–304 .

Feng, W., Zhao, Q., Shi, J., & Liu, H. (2003). Principal component analysis and its application in seismology. *Earthquake*, 23(3), 1-9.

Fung, R. Y. K., & Le, C. Y. (1987). Principal component analysis with instrumental variables and its application to microwave multi-spectral scanning data. *IEEE Transactions on Geoscience and Remote Sensing*, 25(6), 676-683.

G. S. (2013). Water Quality Index with Missing Parameters. *International Journal of Research in Engineering and Technology*, 02(04), 609–614. <https://doi.org/10.15623/ijret.2013.0204035>

Ghimire, N. P., Adhikari, N., Pant, R. R., & Thakuri, S. (2021). Characterizations Of Water Quality In West-Seti and Tamor River Basins, Nepal. *Scientific World*, 14(14), 106–114. <https://doi.org/10.3126/sw.v14i14.35021>

Ghosh, K., & Chakraborty, T. (2022). Impact of human intervention structures on the

rivers: An investigation of the spatiotemporal variation of grain size in the Tista River, eastern Himalayas. *Earth Surface Processes and Landforms*, 47(9), 2245–2265.
<https://doi.org/https://doi.org/10.1002/esp.5374>

Giri, M. (2020). Assessment of Water Quality Index of River Teesta in East District.

Gupta, S., Nayek, S., & Chakraborty, D. (2016). Hydrochemical evaluation of Rangit river, Sikkim, India: using Water Quality Index and multivariate statistics. *Environmental Earth Sciences*, 75(7). <https://doi.org/10.1007/s12665-015-5223-8>

Gupta, V., Chauhan, N., Penna, I., Hermanns, R., Dehls, J., Sengupta, A., & Bhasin, R. K. (2022). Geomorphic evaluation of landslides along the Teesta river valley, Sikkim Himalaya, India. *Geological Journal*, 57(2), 611–621.
<https://doi.org/https://doi.org/10.1002/gj.4377>

Han, X., Pan, B., Liu, Z., Hou, B., Li, D., & Li, M. (2022). Relationship among water quality and hydrochemical indices reveals nutrient dynamics and sources in the most sediment- laden river across the continent. *Journal of Environmental Chemical Engineering*, 10(1), 107110.
<https://doi.org/https://doi.org/10.1016/j.jece.2021.107110>

He, L. J., & Meng, W. H. (2002). Principal component analysis for the variance covariance matrix. *Science in China Series A: Mathematics*, 45(5), 616-626.

Hoefs, J. *Stable Isotope Geochemistry*, 4th ed.; Springer: Berlin, Germany, (1997).

Horton RK (1965) An index system for rating water quality. *J Water Pollut Control Fed* 37:300–306

- Horton, R. E. (1932). Drainage basin characteristics. *Transactions American Geophysical Union*, 13, 350–361. <https://doi.org/10.1029/TR013i001p00350>
- Horton, R. E. (1945). Erosional development of streams and their drainage basins: Hydrophysical approach to quantitative morphology. *Bulletin of the Geological Society of America*, 56, 275–370. [https://doi.org/10.1130/0016-7606\(1945\)56\[275:EDOSAT\]2.0.CO;2](https://doi.org/10.1130/0016-7606(1945)56[275:EDOSAT]2.0.CO;2)
- Islam, A. R. M. T., Shen, S., Haque, M. A., Bodrud-Doza, M., Maw, K. W., & Habib, M. A. (2018). Assessing groundwater quality and its sustainability in Joypurhat district of Bangladesh using GIS and multivariate statistical approaches. *Environment, Development and Sustainability*, 20(5), 1935–1959. <https://doi.org/10.1007/s10668-017-9971-3>
- Islam, M. J., Hossain, A. M., Rahman, M. S., Khandoker, M. H., & Zahan, M. N. (2019). Hydrogeochemistry and Usability of Groundwater at the Tista River Basin in Northern Bangladesh. *Indian Journal of Science and Technology*, 12(47), 1–12. <https://doi.org/10.17485/ijst/2019/v12i47/147961>
- Islam, M., Islam, M., Islam, M., Kabir, M., & Meghla, N. (2015). Status of Water Quality in the Tista River at Kaunia Point and its Impact on Aquatic Environment. *Journal of Environmental Science and Natural Resources*, 8(1), 29–33. <https://doi.org/10.3329/jesnr.v8i1.24660>
- Jacobson, A.D., Blum, J.D., Chamberlain, C.P., Poage, M.A., Sloan, V.F., (2002a). Ca/Sr and Sr isotope systematics of a Himalayan glacial chronosequence: Carbonate versus silicate weathering rates as a function of landscape surface age. *Geochim.*

Cosmochim. Acta 66 (1), 13–27. [https://doi.org/10.1016/S0016-7037\(01\)00755-4](https://doi.org/10.1016/S0016-7037(01)00755-4).

Jana, K., Sengupta, D., & Rudra, K. (2016). Correction of bifurcated river flow measurements from historical data: Paving the way for the Teesta water sharing treaty. *Annals of Applied Statistics*, 10(3), 1757–1775. <https://doi.org/10.1214/16-AOAS958>

Jiang. (2020). Hydrochemical Characteristics and Water Quality Evaluation of Rivers in Different Regions of Cities.pdf.

July, 1475–1483.

Karant, K. R. (1989). *Groundwater Assessment, Development, and Management*. Tata McGraw-Hill Education.

Kashyap, A., & Behera, M. D. (2023). Geomorphic response of bedrock landslides induced landscape evolution across the Teesta catchment, Eastern Himalaya. *Environmental Earth Sciences*, 82(8), 193. <https://doi.org/10.1007/s12665-023-10859-6>

Kaushik, H., Soheb, M., Biswal, K., Ramanathan, A. L., Kumar, O., & Patel, A. K. (2023). Understanding the hydrochemical functioning of glacierized catchments of the Upper Indus Basin in Ladakh, Indian Himalayas. *Environmental Science and Pollution Research*, 30(8), 20631–20649. <https://doi.org/10.1007/s11356-022-23477-9>

Kelly, W. P. (1963) Use of saline irrigation water. *Soil Science* 95 (4),355–391.

Khan, I., & Ali, M. (2019). Potential Changes to the Water Balance of the Teesta River Basin Due to Climate Change. *American Journal of Water Resources*, 7(3), 95–105. <https://doi.org/10.12691/ajwr-7-3-2>

Khatri, K., Gurung, S., Jha, B. R., Sthapit, M., & Khadka, U. R. (2023). Major Ion

- Chemistry of the Bheri (Snow-Fed) and the Babai (Rain-Fed) River Systems in Western Nepal: Implication on Water Quality. *Environment and Natural Resources Journal*, 21(4), 299–311. <https://doi.org/10.32526/enrj/21/202200273>
- Krishnaswami, S., 1999. Silicate weathering in the Himalaya: role in contributing to major ions and radiogenic Sr to the Bay of Bengal. *Ocean Science*.
- Krisnaswami, Sunil Singh, (2005). Chemical weathering in the river basins of the Himalaya, India. *Curr. Sci.* 89 (5), 841–849.
- Kuppusamy MR, Grirdhar VV, (2006) Factor analysis of water quality characteristics including trace metal speciation in the coastal environmental system of Chennai Ennore. *Environ Int* 32: 174–179.
- Lü, J., & An, Y. (2023). Hydrochemical Characteristics and Risk Assessment of Tongzi River, Guizhou Province, Southwest China. *Water (Switzerland)*, 15(4), 1–15. <https://doi.org/10.3390/w15040802>
- M. S. A. (2018). Hydrochemistry, water quality and land use signatures in an ephemeral tidal river: implications in water management in the southwestern coastal region of Bangladesh. *Applied Water Science*, 8(2), 1–16. <https://doi.org/10.1007/s13201-018-0706-x>
- Ma, L., Huang, T., Qiu, H., Yang, Z., He, X., & Qian, J. (2021). Hydrogeochemical characteristic evaluation and irrigation suitability assessment of shallow groundwater in Dangshan County, China. *Geosciences Journal*, 25(5), 731–748. <https://doi.org/10.1007/s12303-020-0064-1>
- Mandal, S. P., & Chakrabarty, A. (2016). Flash flood risk assessment for upper Teesta river

basin: using the hydrological modeling system (HEC-HMS) software. *Modeling Earth Systems and Environment*, 2(2), 1–10. <https://doi.org/10.1007/s40808-016-0110-1>

Meglin RR (1991) Examining large databases: a chemometric approach using principal component analysis', *J. Chemomet*, 5: 163-179.

Milana, P., Dragan, D., Ugljesa, S., & Igor, L. (2013). Correlation Analysis of Impact of Natural Parameters on Water quality of the river Danube Near Nori Sad for the period 2004-2011,. *Geographica Pannonica* , 17 (3), 74-78.

Mishra, A. K., & Rai, S. C. (2019). Assessment of spatio-temporal variability of temperature using geo-statistical techniques: a case study of Upper Teesta River Basin, India. *Environmental Sustainability*, 2(1), 43–54. <https://doi.org/10.1007/s42398-019-00049-1>

Mohan, S.V., Nithila, P., Reddy, S.J., (1996). Estimation of heavy metals in drinking water and development of heavy metal pollution index. *J. Environ. Sci. Health Part A* 31 (2), 283–289.

Mondal, M. S. H., Murayama, T., & Nishikizawa, S. (2020). Assessing the flood risk of riverine households: A case study from the right bank of the Teesta River, Bangladesh. *International Journal of Disaster Risk Reduction*, 51, 101758. <https://doi.org/https://doi.org/10.1016/j.ijdrr.2020.101758>

Morthekai, P. (2020). Oxygen and deuterium isotope characteristics of Teesta river catchment from Sikkim Himalaya, India: Implications of different moisture sources. *Geochemical Journal*, 54(5), 327–336. <https://doi.org/10.2343/GEOCHEMJ.2.0604>

- Mrklas, L., De Long, D., & Gauch, H. G. (2006). Canonical correlation analysis and its use in ecological studies. *Canadian Journal of Botany*, 84(4), 559-570.
- Mudgal, K. D., Kumari, M., & Sharma, D. K. (2009). Hydrochemical analysis of drinking water quality of Alwar district, Rajasthan. *Nature and Science*, 7(2), 30–39.
- Mudge SM, Duce CE,(2005) Identifying the source, transport path and sinks of sewage derived organic matter, *Environ Pollut* 136: 209–220.
- Pal, R., Biswas, S. S., Mondal, B., & Pramanik, M. K. (2016). Landslides and Floods in the Tista Basin (Darjeeling and Jalpaiguri Districts): Historical Evidence, Causes and Consequences. *J. Ind. Geophys. Union*, 20(2), 66–72.
- Pant, R. R., Chalaune, T. B., Dangol, A., Dhital, Y. P., Sharma, M. L., Pal, K. B., Shah, S. T. H., Shrestha, A. K., & Thapa, L. B. (2021). Hydrochemical assessment of the Beeshazar and associated lakes in Central Nepal. *SN Applied Sciences*, 3(1), 38. <https://doi.org/10.1007/s42452-020-03983-6>
- Paul, K., Sharma¹, D., Singh², E., Paul³, K., & Mukherjee⁴, S. (2019). Assessment of hydromorphological conditions of upper and lower dams of river Teesta in Sikkim. Article in *Journal of Spatial Hydrology*, 15(2), 1–22. <https://www.researchgate.net/publication/338768061>
- Rahman, S. (2023). Predictions of Land Use and Land Cover (LULC) and Runoff of the Rai, N., & Khawas, V. (2023). Climate change and Hydropower Development in the Eastern Himalaya: Emerging conflicts in the Upper Tista Catchment of Sikkim, India. *Journal of Geography & Natural Disasters*, 1–16.
- Refat Nasher, N. M., & Humayan Ahmed, M. (2021). Groundwater geochemistry and

hydrogeochemical processes in the Lower Ganges-Brahmaputra-Meghna River Basin areas, Bangladesh. *Journal of Asian Earth Sciences*: X, 6, 100062. <https://doi.org/10.1016/j.jaesx.2021.100062>

Ribinu, S. K., Prakash, P., Khan, A. F., Bhaskar, N. P., & Arunkumar, K. S. (2023). Hydrogeochemical characteristics of groundwater in Thoothapuzha River Basin, Kerala, South India. *Total Environment Research Themes*, 5(December 2022), 100021. <https://doi.org/10.1016/j.totert.2022.100021>

Roy, K., Karim, M. R., Akter, F., Islam, M. S., Ahmed, K., Rahman, M., Datta, D. K., & Khan, Saha, S. (2022). Hydrogeochemistry and multivariate statistical analysis of groundwater quality of Tista alluvial fan, Bangladesh. *Arabian Journal of Geosciences*, 15(13), 1195. <https://doi.org/10.1007/s12517-022-10444-4>

Saha, S., Reza, A. H. M. S., & Roy, M. K. (2019). Hydrochemical evaluation of groundwater quality of the Tista floodplain, Rangpur, Bangladesh. *Applied Water Science*, 9(8), 1–12. <https://doi.org/10.1007/s13201-019-1085-7>

Saha, S., Reza, Ahms., Selim Reza, A., & Kanti Roy, M. (2019). Analysis of Physiochemical Parameters to Evaluate the Water Quality of the Tista-Brahmaputra River, Rangpur Division, Bangladesh. *IOSR Journal of Applied Geology and Geophysics*, 7(4), 27–35. <https://doi.org/10.9790/0990-0704012735>

Schneider, P., & Avellan, T. (2019). Water Security and Sustainability. In *Encyclopedia of Sustainability in Higher Education*. https://doi.org/10.1007/978-3-319-63951-2_473-1

Schumm, S. A. (1956). Evolution of drainage systems and slopes in Bad Lands at Perth

- Amboy, New Jersey. Geological Society of America Bulletin, 67, 597–646.
[https:// doi. org/ 10. 1130/ 0016-](https://doi.org/10.1130/0016-)
- Seth, R., Mohan, M., Singh, P., Singh, R., Dobhal, R., Singh, K., et al. (2014). Water Quality Evaluation of Himalayan rivers of Kumaun region, Uttarakahnd, India. Applied Water Science, DOI 10.1007/s13201-014-0213-7
- Sharma, A., & Goyal, M. K. (2020). Assessment of the changes in precipitation and temperature in Teesta River basin in Indian Himalayan Region under climate change. Atmospheric Research, 231(June 2019), 104670.
<https://doi.org/10.1016/j.atmosres.2019.104670>
- Sharma, B. B., & Sarma, H. P. (2011). Major Ion Chemsitry of Tenga River at Dahung, Arunachal Pradesh, India. Archives of Applied Science Research , 3 (6), 141-146.
- Shit, P. K., Bhunia, G. S., Bhattacharya, M., & Patra, B. C. (2019). Assessment of Domestic Water Use Pattern and Drinking Water Quality of Sikkim, North Eastern Himalaya, India: A Cross-sectional Study. Journal of the Geological Society of India, 94(5), 507–514. <https://doi.org/10.1007/s12594-019-1348-9>
- Sikkim, E. (2020). Spatial Analysis of Water Quality Parameters in River Teesta Using Arc-
- Singh KP, Malik A, Singh VK, Mohan D, Sinha S (2005) Chemometric analysis of groundwater quality data of alluvial aquifer of Gangetic plain, North India. Analytica Chimica Acta 550: 82–91.
- Singh, K. K., Tewari, G., Bisht, M., Tiwary, R. K., Kumar, S., Patni, K., Gangwar, A., & Kanyal, B. (2023). Hydrogeochemical characteristics and multivariate statistical approach for monitoring groundwater quality scenario in the vicinity of industrial area

- of western Himalaya, India. *Chemistry and Ecology*, 39(6), 611–639.
<https://doi.org/10.1080/02757540.2023.2224794>
- Song, Y., Zhang, X. (Yvon), Bouchez, J., Chetelat, B., Gaillardet, J., Chen, J. Bin, Zhang, T., Cai, H., Yuan, W., & Wang, Z. (2021). Deciphering the signatures of weathering and erosion processes and the effects of river management on Li isotopes in the subtropical Pearl River basin. *Geochimica et Cosmochimica Acta*, 313, 340–358.
<https://doi.org/10.1016/j.gca.2021.08.015>
- Sonker, I., Tripathi, J. N., Swarnim, & Singh, A. K. (2023). Morphometric and neotectonic study of Upper Teesta River basin, Sikkim Himalaya using geospatial techniques. *Journal of Applied Geophysics*, 212, 104978.
<https://doi.org/https://doi.org/10.1016/j.jappgeo.2023.104978>
- Strahler, A. N. (1964). Part II. Quantitative geomorphology of drainage basins and channel networks. (pp. 4–39). *Handbook of Applied Hydrology*: McGraw-Hill, New York.
- Su, C., Liu, Y., Cheng, Z., Wang, W., & Zheng, Z. (2022). Hydrochemical process and controls on the hydrochemistry of river water in the Muling-Xingkai Plain, Northeast China. *Frontiers in Environmental Science*, 10(October), 1–11.
<https://doi.org/10.3389/fenvs.2022.1010367>
- Talukdar, S., Eibek, K. U., Akhter, S., Ziaul, S., Towfiqul Islam, A. R. M., & Mallick, J. (2021). Modeling fragmentation probability of land-use and land-cover using the bagging, random forest and random subspace in the Teesta River Basin, Bangladesh. *Ecological Indicators*, 126. <https://doi.org/10.1016/j.ecolind.2021.107612>
- Talukdar, S., Ghose, B., Shahfahad, Salam, R., Mahato, S., Pham, Q. B., Linh, N. T. T.,

- Costache, R., & Avand, M. (2020). Flood susceptibility modeling in Teesta River basin, Bangladesh using novel ensembles of bagging algorithms. *Stochastic Environmental Research and Risk Assessment*, 34(12), 2277–2300. <https://doi.org/10.1007/s00477-020-01862-5>
- Teesta River Basin under Different Emission and Socioeconomic Scenarios. 1–37.
- Tiwari, A. K., Singh, A. K., Giri, S., & Mahato, M. K. (n.d.). Major ion chemistry and hydrochemical processes controlling water composition of Teesta River catchment, Sikkim Himalaya, India. *International Journal of Environmental Analytical Chemistry*, 1–19. <https://doi.org/10.1080/03067319.2021.1992402>
- Todd, D. K., & Mays, L. W. (2005). *Groundwater hydrology*. John Wiley & Sons.
- Tsering, T., Abdel Wahed, M. S. M., Iftekhar, S., & Sillanpää, M. (2019). Major ion chemistry of the Teesta River in Sikkim Himalaya, India: Chemical weathering and assessment of water quality. *Journal of Hydrology: Regional Studies*, 24(January), 100612. <https://doi.org/10.1016/j.ejrh.2019.100612>
- WHO, 2011. *Guidelines for Drinking-Water Quality*. 4th Edn., WHO, Geneva
- Wiejaczka, Ł., Prokop, P., Kozłowski, R., & Sarkar, S. (2018). Reservoir's Impact on the Water Chemistry of the Teesta River Mountain Course (Darjeeling Himalaya). *Ecological Chemistry and Engineering S*, 25(1), 73–88. <https://doi.org/10.1515/eces-2018-0005>
- Wilcox, L. V. (1955). *Classification and use of irrigation waters*. US Department of Agriculture, Washington, DC, 19(2), 1-19.

- Yawei W, Lina L, Jianbo S, Guibin J (2005) Chemometrics methods for the investigation of methylmercury and total mercury contamination in mollusks samples collected from coastal sites along the Chinese Bohai Sea. *Environ Pollut* 135: 457–467.
- Zhang C (2006) Using multivariate analyses and GIS to identify pollutants and their spatial patterns in urban soils in Galway, Ireland, *Environ Pollut* 142: 501–511.
- Zhang, F., Xiao, X., Wang, L., Zeng, C., Yu, Z., Wang, G., & Shi, X. (2021). Chemical weathering and CO₂ consumption in the glaciated Karuxung River catchment, Tibetan Plateau. *Hydrological Processes*, 35(8). <https://doi.org/10.1002/hyp.14330>

APPENDIX

Water Quality Data (Physio – chemical parameters)

Major ions 2019 PrM (mg/L)											
ID	TDS	pH	F	Cl	NO3	SO4	Alkalinity	Na	K	Ca	Mg
1	48	7.42	0.11	1.48	2.62	10.79	12.58	3.12	1.74	13.10	1.99
2	49	7.41	0.10	1.44	2.52	10.68	13.34	3.13	1.75	12.95	2.01
3	50	7.40	0.08	1.39	2.37	10.52	14.49	3.14	1.77	12.72	2.03
4	52	7.39	0.05	1.28	2.08	10.18	16.78	3.17	1.80	12.26	2.09
5	54	7.46	0.03	1.14	1.90	9.40	19.83	3.01	1.70	11.89	1.92
6	57	7.60	0.05	0.98	1.93	8.27	22.88	2.64	1.45	11.75	1.51
7	57	7.50	0.04	0.83	1.76	8.55	21.35	2.27	1.40	12.57	1.38
8	56	7.25	0.03	0.73	1.50	9.82	16.78	1.97	1.51	13.89	1.51
9	55	7.08	0.02	0.66	1.32	10.66	13.73	1.78	1.59	14.77	1.59
10	55	7.05	0.07	0.62	1.23	10.71	13.73	1.87	1.58	14.67	1.76
11	54	7.14	0.18	0.60	1.24	9.96	16.78	2.25	1.49	13.59	2.02
12	54	7.19	0.22	0.58	1.23	9.32	18.30	2.41	1.36	13.57	2.00
13	53	7.20	0.21	0.56	1.20	8.92	18.30	2.36	1.23	14.35	1.78
14	52	7.21	0.20	0.55	1.18	8.72	18.30	2.34	1.16	14.74	1.67
15	52	7.23	0.20	0.55	1.17	8.59	18.30	2.32	1.12	15.00	1.60
16	56	7.38	0.10	0.28	0.90	9.61	18.30	2.83	1.22	15.38	1.70
17	51	7.47	0.01	0.20	0.58	11.59	15.25	2.63	1.11	15.08	1.72
18	45	7.47	0.02	0.44	0.53	12.31	12.20	2.08	0.87	13.65	1.77
19	51	7.42	0.02	0.47	0.42	12.86	15.25	2.60	1.05	15.01	2.60
20	50	7.51	0.03	0.39	0.24	12.63	15.25	2.20	1.12	15.97	2.02
21	44	7.50	0.04	0.30	0.19	11.39	10.68	1.44	0.99	13.63	0.79
22	37	7.11	0.03	0.26	0.19	10.84	7.62	1.46	0.97	11.46	0.84
23	38	7.08	0.04	0.45	0.41	11.68	7.62	1.82	1.00	12.49	1.36
24	45	7.43	0.04	0.88	0.84	13.93	10.68	2.52	1.08	16.74	2.35
25	50	7.84	0.04	1.14	1.25	13.46	14.28	2.70	1.13	18.13	2.51
26	51	8.32	0.04	1.21	1.64	10.25	18.43	2.36	1.15	16.65	1.85
27	48	8.21	0.04	1.20	1.89	8.23	16.90	2.24	0.99	14.18	1.52
28	39	7.52	0.04	1.10	1.99	7.39	9.70	2.34	0.66	10.69	1.00
29	34	7.03	0.04	0.95	1.71	7.23	6.10	2.34	0.48	8.75	0.49
30	35	6.74	0.04	0.77	1.04	7.76	6.10	2.22	0.46	8.35	0.53
31	36	6.55	0.03	0.68	0.62	7.93	9.15	2.25	0.50	8.94	0.59
32	37	6.44	0.04	0.86	1.32	7.60	12.20	2.23	0.51	9.84	0.60
33	38	6.57	0.09	1.64	2.34	7.65	12.20	2.09	0.50	10.33	0.58
34	44	6.94	0.16	2.81	2.80	8.21	12.20	2.02	0.54	11.09	0.60
35	47	7.18	0.21	2.78	2.56	8.30	13.73	1.87	0.58	11.32	0.60
36	43	7.27	0.23	1.53	1.62	7.93	16.78	1.62	0.63	11.03	0.59
37	41	7.14	0.19	0.81	1.15	7.67	16.78	1.51	0.68	10.63	0.62
38	38	6.87	0.11	0.65	1.13	7.56	14.49	1.52	0.72	10.25	0.66
39	38	6.70	0.06	0.55	1.12	7.49	12.96	1.53	0.74	10.00	0.68

ID	TDS	pH	F	Cl	NO3	SO4	Alkalinity	Na	K	Ca	Mg
40	46	6.94	0.03	0.74	1.22	7.51	15.25	1.76	0.94	10.19	0.87
41	52	7.27	0.03	0.96	1.30	7.52	18.30	2.08	1.82	9.90	1.93
42	51	7.27	0.03	0.95	1.25	7.47	18.30	2.20	2.88	9.02	3.26
43	50	7.27	0.02	0.94	1.23	7.44	18.30	2.26	3.41	8.57	3.92
44	50	7.27	0.02	0.94	1.22	7.42	18.30	2.30	3.67	8.35	4.26
45	50	7.28	0.02	0.93	1.22	7.41	18.30	2.31	3.80	8.24	4.42
46	50	7.28	0.02	0.93	1.21	7.41	18.30	2.32	3.87	8.18	4.51
47	50	7.29	0.02	0.93	1.21	7.41	18.30	2.32	3.91	8.15	4.56
48	51	7.44	0.02	1.41	2.37	7.12	21.35	2.27	3.90	7.93	4.53
49	49	7.33	0.06	2.24	3.90	6.38	21.35	2.21	2.83	8.13	3.48
50	45	7.40	0.08	1.86	3.28	6.01	18.30	2.24	1.75	8.80	2.28
51	43	7.58	0.09	0.96	1.94	6.47	21.35	2.25	2.54	9.05	2.99
52	42	7.45	0.11	0.77	1.64	7.05	22.88	2.24	3.80	8.08	4.45
53	43	7.50	0.06	0.74	1.73	7.44	19.83	2.25	4.64	6.16	5.53
54	40	7.46	0.03	1.03	1.52	7.54	18.30	2.77	3.57	6.06	4.64
55	39	7.44	0.03	1.23	1.39	7.26	21.35	3.01	2.55	7.89	3.54
56	52	7.45	0.13	3.98	3.85	7.06	21.35	2.38	3.01	9.99	3.67
57	60	7.40	0.20	5.51	5.56	7.24	19.83	2.24	3.32	11.19	3.85
58	57	7.35	0.16	2.85	4.32	7.60	22.88	2.68	3.95	11.31	4.59
59	56	7.34	0.15	2.19	4.00	7.69	23.64	2.78	4.10	11.34	4.78

Major ions 2019 PoM (mg/L)											
ID	TDS	pH	F	Cl	NO3	SO4	Alkalinity	Na	K	Ca	Mg
1	43	7.19	0.25	0.25	0.75	11.16	12.20	1.86	0.92	12.53	0.83
2	46	7.22	0.24	0.27	0.70	12.27	12.20	1.93	0.98	13.28	1.14
3	51	7.26	0.24	0.29	0.63	13.94	12.20	2.03	1.06	14.40	1.60
4	61	7.35	0.23	0.34	0.50	17.27	12.20	2.23	1.22	16.65	2.53
5	67	7.45	0.22	0.37	0.39	19.29	13.73	2.28	1.30	18.25	3.00
6	68	7.52	0.20	0.39	0.37	18.90	16.78	2.13	1.26	18.46	2.71
7	67	7.54	0.18	0.59	0.39	18.93	16.78	2.07	1.36	18.08	2.62
8	66	7.52	0.17	0.88	0.42	19.26	14.49	2.10	1.53	17.36	2.70
9	65	7.50	0.16	1.08	0.44	19.49	12.96	2.12	1.64	16.88	2.76
10	58	7.55	0.17	1.06	0.59	16.97	12.20	1.97	1.46	14.92	2.35
11	46	7.68	0.21	0.84	0.87	11.72	12.20	1.67	0.97	11.47	1.47
12	40	7.75	0.24	0.70	0.97	9.10	11.82	1.53	0.75	9.84	1.04
13	41	7.78	0.24	0.65	0.91	9.10	11.06	1.55	0.79	10.01	1.07
14	43	7.82	0.24	0.58	0.82	9.12	9.91	1.58	0.85	10.27	1.10
15	45	7.89	0.25	0.43	0.64	9.14	7.62	1.64	0.97	10.79	1.17
16	48	7.89	0.26	0.37	0.66	9.20	12.20	1.73	1.09	11.17	1.29
17	41	7.24	0.25	0.37	0.52	8.25	12.20	1.40	0.90	9.15	0.93
18	36	6.55	0.18	0.29	0.32	7.79	9.15	1.53	0.90	9.45	0.69
19	38	6.75	0.16	0.25	0.40	8.24	12.20	1.75	1.95	8.69	1.48
20	37	7.07	0.25	0.38	0.29	8.29	12.20	2.15	2.36	7.04	1.80

ID	TDS	pH	F	Cl	NO3	SO4	Alkalinity	Na	K	Ca	Mg
21	35	7.03	0.31	0.57	0.18	8.33	12.20	2.89	1.90	6.38	1.51
22	33	6.88	0.30	0.69	0.21	8.13	12.20	2.95	1.84	6.12	1.45
23	31	6.92	0.27	0.65	0.22	7.88	10.68	2.68	1.54	6.11	1.25
24	30	7.17	0.21	0.43	0.19	7.59	7.63	2.08	1.03	6.36	0.90
25	28	6.84	0.18	0.34	0.19	7.16	9.15	1.77	0.76	7.62	0.72
26	34	5.93	0.18	0.40	0.22	6.59	15.25	1.75	0.74	8.88	0.69
27	33	5.48	0.18	0.43	0.27	6.50	15.25	1.72	0.73	9.98	0.68
28	28	5.50	0.17	0.44	0.35	6.91	9.15	1.70	0.72	6.91	0.68
29	28	5.88	0.18	0.45	0.37	7.02	6.10	1.70	0.72	6.91	0.68
30	26	6.61	0.19	0.45	0.32	6.84	6.10	1.73	0.73	6.97	0.69
31	27	6.52	0.19	0.39	0.28	6.61	9.15	1.68	0.71	10.22	0.64
32	34	6.78	0.17	0.32	0.37	7.10	12.20	1.56	0.71	12.23	0.58
33	41	7.56	0.15	0.31	0.47	7.78	12.20	1.45	0.84	9.36	0.70
34	44	7.70	0.12	0.33	0.45	7.84	12.20	1.35	1.02	10.08	0.92
35	44	7.56	0.11	0.71	0.68	7.25	12.20	1.64	1.85	9.91	1.01
36	41	7.13	0.11	1.46	1.17	6.00	12.20	2.33	3.35	8.86	1.00
37	39	7.26	0.15	1.14	1.04	6.26	15.25	2.35	2.82	8.52	1.14
38	40	7.58	0.20	0.51	0.66	7.16	18.30	2.02	1.52	8.83	1.28
39	42	7.55	0.20	0.66	0.66	7.18	18.30	2.03	1.47	9.07	1.25
40	44	7.54	0.20	0.88	0.67	7.21	18.30	2.04	1.41	9.43	1.19
41	46	7.53	0.20	1.18	0.70	7.21	18.30	2.10	1.38	9.65	1.18
42	47	7.53	0.20	1.47	0.74	7.19	18.30	2.21	1.43	9.61	1.23
43	47	7.54	0.20	1.42	0.73	7.19	18.30	2.20	1.42	9.62	1.22
44	47	7.55	0.20	1.72	0.78	7.17	18.30	2.31	1.46	9.58	1.27
45	48	7.57	0.20	1.81	0.79	7.16	18.30	2.35	1.48	9.56	1.29
46	47	7.60	0.20	1.62	0.76	7.18	18.30	2.27	1.45	9.59	1.26
47	48	7.67	0.20	2.20	0.85	7.13	18.30	2.50	1.53	9.51	1.36
48	48	7.81	0.22	2.43	0.90	6.95	21.35	3.36	1.68	9.41	1.45
49	44	7.60	0.16	2.62	2.07	6.14	24.40	4.31	2.05	8.88	1.70
50	42	7.16	0.14	1.98	1.98	6.15	24.40	3.65	1.92	8.85	1.76
51	44	7.18	0.25	1.06	1.08	8.89	21.35	2.85	4.05	9.48	3.70
52	45	7.30	0.25	1.30	1.31	9.45	19.83	3.07	5.40	9.19	4.80
53	44	7.22	0.16	1.67	1.04	6.45	22.87	3.32	3.02	8.25	2.75
54	42	7.27	0.14	1.69	1.22	6.06	24.40	3.21	1.88	8.45	1.67
55	40	7.38	0.17	1.26	1.19	7.21	21.35	2.66	1.71	9.25	1.53
56	45	7.20	0.17	1.03	0.74	6.85	21.35	2.62	1.68	9.01	1.62
57	48	7.00	0.16	1.09	0.64	6.73	24.40	2.94	1.97	8.43	2.01
58	46	7.01	0.15	1.12	0.65	7.29	24.40	3.07	2.15	8.02	2.46
59	46	7.01	0.14	1.12	0.66	7.44	24.40	3.10	2.19	7.91	2.57

Major ions 2021 PrM (mg/L)											
ID	TDS	pH	Na	K	Ca	Mg	Alkalinity	F	Cl	NO3	SO4
1	48	7.43	3.11	1.73	13.18	1.98	12.20	0.11	1.49	2.66	10.85
2	49	7.41	3.12	1.74	13.02	2.00	12.96	0.10	1.46	2.57	10.74
3	49	7.40	3.13	1.76	12.87	2.02	13.73	0.09	1.42	2.47	10.63
4	51	7.40	3.15	1.78	12.57	2.05	15.25	0.07	1.35	2.28	10.40
5	53	7.39	3.19	1.83	11.95	2.12	18.30	0.03	1.21	1.89	9.96
6	56	7.53	2.82	1.58	11.82	1.71	21.35	0.04	1.06	1.91	8.83
7	58	7.67	2.46	1.32	11.68	1.30	24.40	0.05	0.90	1.94	7.70
8	57	7.34	2.07	1.47	13.45	1.47	18.30	0.03	0.76	1.59	9.39
9	56	7.17	1.88	1.55	14.33	1.55	15.25	0.03	0.70	1.41	10.24
10	55	7.00	1.68	1.62	15.22	1.63	12.20	0.02	0.63	1.23	11.08
11	55	7.10	2.06	1.53	14.13	1.89	15.25	0.12	0.61	1.24	10.33
12	54	7.19	2.44	1.44	13.05	2.14	18.30	0.23	0.59	1.25	9.58
13	53	7.20	2.38	1.27	14.09	1.85	18.30	0.21	0.57	1.21	9.05
14	53	7.20	2.35	1.18	14.61	1.71	18.30	0.20	0.56	1.19	8.79
15	52	7.22	2.33	1.14	14.87	1.64	18.30	0.20	0.55	1.18	8.65
16	52	7.24	2.32	1.10	15.12	1.56	18.30	0.19	0.54	1.17	8.52
17	59	7.52	3.35	1.35	15.63	1.83	18.30	ND	0.01	0.64	10.70
18	42	7.42	1.92	0.88	14.52	1.62	12.20	0.02	0.38	0.52	12.49
19	48	7.51	2.24	0.87	12.79	1.93	12.20	0.02	0.50	0.53	12.13
20	53	7.33	2.97	1.23	17.23	3.28	18.30	0.02	0.45	0.30	13.60
21	47	7.69	1.44	1.00	14.72	0.77	12.20	0.04	0.33	0.18	11.66
22	41	7.30	1.45	0.98	12.54	0.82	9.15	0.04	0.28	0.19	11.11
23	34	6.91	1.47	0.97	10.37	0.87	6.10	0.03	0.23	0.20	10.56
24	42	7.26	2.17	1.04	14.62	1.85	9.15	0.04	0.67	0.63	12.81
25	49	7.60	2.87	1.12	18.87	2.84	12.20	0.05	1.10	1.05	15.06
26	51	8.08	2.53	1.14	17.39	2.18	16.35	0.04	1.18	1.45	11.85
27	52	8.56	2.19	1.16	15.92	1.52	20.50	0.04	1.25	1.84	8.65
28	43	7.87	2.29	0.82	12.43	1.52	13.30	0.04	1.15	1.94	7.81
29	34	7.17	2.40	0.49	8.95	0.47	6.10	0.04	1.05	2.04	6.96
30	35	6.88	2.28	0.47	8.55	0.51	6.10	0.04	0.86	1.37	7.50
31	35	6.59	2.16	0.45	8.15	0.55	6.10	0.04	0.68	0.70	8.03
32	36	6.50	2.34	0.55	9.74	0.63	12.20	0.03	0.68	0.53	7.82
33	38	6.38	2.12	0.48	9.95	0.57	12.20	0.05	1.05	2.11	7.37
34	38	6.76	2.05	0.52	10.71	0.59	12.20	0.13	2.22	2.57	7.93
35	50	7.13	1.99	0.56	11.47	0.61	12.20	0.20	3.40	3.02	8.49
36	44	7.22	1.74	0.61	11.18	0.60	15.25	0.22	2.16	2.09	8.12
37	41	7.31	1.50	0.65	10.88	0.59	18.30	0.25	0.91	1.16	7.75
38	40	6.96	1.52	0.71	10.38	0.64	15.25	0.14	0.71	1.14	7.60
39	36	6.79	1.52	0.73	10.13	0.67	13.73	0.09	0.60	1.13	7.53

ID	TDS	pH	Na	K	Ca	Mg	Alkalinity	F	Cl	NO3	SO4
40	39	6.61	1.53	0.76	9.88	0.70	12.20	0.03	0.50	1.12	7.46
41	52	7.27	1.99	1.12	10.50	1.05	18.30	0.03	0.97	1.32	7.56
42	51	7.27	2.16	2.53	9.31	2.82	18.30	0.03	0.95	1.27	7.49
43	51	7.27	2.24	3.23	8.72	3.70	18.30	0.03	0.94	1.24	7.45
44	50	7.27	2.28	3.58	8.42	4.15	18.30	0.02	0.94	1.23	7.43
45	50	7.27	2.31	3.76	8.28	4.37	18.30	0.02	0.93	1.22	7.42
46	50	7.28	2.32	3.85	8.20	4.48	18.30	0.02	0.93	1.22	7.41
47	50	7.29	2.32	3.89	8.17	4.53	18.30	0.02	0.93	1.21	7.41
48	50	7.30	2.33	3.94	8.13	4.59	18.30	0.02	0.93	1.21	7.41
49	52	7.58	2.21	3.86	7.72	4.47	24.40	0.01	1.89	3.52	6.83
50	45	7.07	2.21	1.81	8.55	2.50	18.30	0.11	2.59	4.28	5.92
51	44	7.73	2.26	1.70	9.06	2.06	18.30	0.05	1.13	2.28	6.09
52	42	7.42	2.24	3.39	9.04	3.92	24.40	0.14	0.79	1.60	6.85
53	43	7.48	2.25	4.22	7.12	4.99	21.35	0.08	0.76	1.69	7.24
54	43	7.53	2.25	5.06	5.20	6.07	18.30	0.03	0.73	1.78	7.63
55	37	7.39	3.28	2.09	6.92	3.21	18.30	0.03	1.34	1.27	7.45
56	41	7.48	2.74	3.01	8.86	3.87	24.40	0.04	1.12	1.51	7.06
57	62	7.42	2.02	3.01	11.13	3.47	18.30	0.21	6.84	6.18	7.06
58	59	7.38	2.46	3.64	11.25	4.22	21.35	0.18	4.18	4.94	7.42
59	55	7.33	2.89	4.26	11.36	4.96	24.40	0.14	1.52	3.69	7.78

Major ions 2021 PoM (mg/L)											
ID	TDS	pH	Na	K	Ca	Mg	Alkalinity	F	Cl	NO3	SO4
1	41	7.17	1.83	0.90	12.15	0.68	12.20	0.25	0.25	0.77	10.61
2	44	7.20	1.90	0.95	12.90	0.99	12.20	0.25	0.26	0.73	11.72
3	48	7.23	1.96	1.00	13.65	1.30	12.20	0.24	0.28	0.68	12.83
4	54	7.29	2.09	1.11	15.15	1.91	12.20	0.24	0.31	0.59	15.05
5	67	7.41	2.36	1.33	18.15	3.15	12.20	0.23	0.37	0.40	19.49
6	68	7.49	2.20	1.28	18.36	2.86	15.25	0.21	0.38	0.38	19.10
7	68	7.56	2.05	1.24	18.56	2.57	18.30	0.19	0.39	0.36	18.71
8	66	7.53	2.09	1.47	17.60	2.68	15.25	0.17	0.78	0.41	19.15
9	65	7.51	2.11	1.59	17.12	2.73	13.73	0.16	0.98	0.43	19.38
10	64	7.49	2.12	1.70	16.64	2.79	12.20	0.15	1.17	0.46	19.60
11	52	7.62	1.82	1.21	13.19	1.91	12.20	0.19	0.95	0.73	14.35
12	40	7.74	1.52	0.73	9.75	1.03	12.20	0.24	0.73	1.00	9.09
13	41	7.77	1.54	0.77	9.92	1.06	11.44	0.24	0.68	0.94	9.10
14	42	7.79	1.56	0.81	10.10	1.08	10.68	0.24	0.63	0.88	9.11
15	44	7.84	1.60	0.89	10.44	1.13	9.15	0.24	0.53	0.76	9.12
16	47	7.94	1.68	1.06	11.14	1.22	6.10	0.25	0.33	0.52	9.16
17	48	7.84	1.79	1.13	11.20	1.37	18.30	0.27	0.41	0.81	9.24
18	34	6.63	1.02	0.68	7.09	0.49	6.10	0.22	0.33	0.24	7.25
19	38	6.46	2.04	1.12	7.80	0.89	12.20	0.14	0.25	0.39	8.34
20	38	7.04	1.45	2.78	7.58	2.06	12.20	0.19	0.25	0.41	8.15

ID	TDS	pH	Na	K	Ca	Mg	Alkalinity	F	Cl	NO3	SO4
21	36	7.10	2.86	1.94	6.50	1.54	12.20	0.31	0.50	0.17	8.43
22	34	6.95	2.92	1.87	6.25	1.48	12.20	0.31	0.63	0.20	8.23
23	32	6.80	2.98	1.80	5.99	1.42	12.20	0.30	0.76	0.23	8.03
24	31	7.05	2.38	1.29	6.24	1.08	9.15	0.24	0.54	0.20	7.74
25	29	7.29	1.78	0.77	6.49	0.73	6.10	0.18	0.32	0.18	7.45
26	27	6.38	1.76	0.75	7.75	0.70	12.20	0.18	0.37	0.21	6.87
27	32	5.47	1.74	0.73	8.21	0.68	18.30	0.18	0.43	0.24	6.30
28	28	5.49	1.71	0.72	7.94	0.68	12.20	0.18	0.44	0.31	6.71
29	29	5.51	1.68	0.72	6.88	0.68	6.10	0.17	0.45	0.39	7.11
30	27	6.24	1.72	0.73	6.94	0.69	6.10	0.19	0.45	0.34	6.93
31	35	6.97	1.75	1.73	10.00	1.70	7.10	0.20	0.75	0.70	7.75
32	38	6.07	1.61	0.68	11.45	0.57	12.20	0.19	0.33	0.27	6.46
33	39	7.49	1.51	0.75	9.00	0.60	12.20	0.16	0.31	0.48	7.75
34	43	7.63	1.40	0.93	9.72	0.81	12.20	0.13	0.32	0.46	7.81
35	46	7.77	1.29	1.11	10.44	1.02	12.20	0.11	0.33	0.44	7.87
36	43	7.35	1.99	2.60	9.39	1.00	12.20	0.11	1.09	0.93	6.62
37	39	6.92	2.68	4.10	8.33	0.99	12.20	0.11	1.84	1.41	5.38
38	39	7.59	2.02	1.54	8.71	1.30	18.30	0.20	0.43	0.66	7.15
39	41	7.56	2.02	1.49	8.95	1.26	18.30	0.20	0.58	0.66	7.17
40	43	7.55	2.03	1.45	9.19	1.23	18.30	0.20	0.73	0.66	7.19
41	46	7.53	2.04	1.36	9.67	1.16	18.30	0.20	1.03	0.67	7.23
42	47	7.53	2.16	1.41	9.63	1.21	18.30	0.20	1.33	0.72	7.20
43	47	7.54	2.27	1.45	9.59	1.26	18.30	0.20	1.62	0.76	7.18
44	46	7.54	2.12	1.39	9.64	1.19	18.30	0.20	1.23	0.70	7.21
45	48	7.55	2.50	1.53	9.51	1.36	18.30	0.20	2.20	0.85	7.13
46	47	7.58	2.20	1.42	9.62	1.22	18.30	0.20	1.42	0.73	7.19
47	48	7.63	2.35	1.48	9.56	1.29	18.30	0.20	1.81	0.79	7.16
48	49	7.72	2.65	1.59	9.46	1.42	18.30	0.21	2.59	0.91	7.09
49	46	7.90	4.07	1.77	9.36	1.48	24.40	0.23	2.27	0.88	6.80
50	42	7.30	4.55	2.33	8.40	1.93	24.40	0.08	2.96	3.25	5.47
51	41	7.02	2.75	1.51	9.29	1.58	24.40	0.20	1.01	0.72	6.84
52	46	7.34	2.95	6.58	9.66	5.82	18.30	0.30	1.11	1.44	10.95
53	45	7.26	3.19	4.21	8.72	3.78	21.35	0.21	1.48	1.18	7.95
54	43	7.18	3.44	1.84	7.78	1.73	24.40	0.11	1.85	0.91	4.95
55	40	7.35	2.97	1.93	9.12	1.62	24.40	0.17	1.54	1.53	7.17
56	40	7.40	2.35	1.49	9.38	1.45	18.30	0.17	0.99	0.85	7.25
57	49	6.99	2.88	1.88	8.64	1.78	24.40	0.17	1.07	0.63	6.45
58	47	7.00	3.01	2.06	8.22	2.23	24.40	0.16	1.10	0.65	7.01
59	45	7.01	3.13	2.24	7.81	2.68	24.40	0.14	1.13	0.66	7.58

Water Quality Data (Heavy metals parameters)

Heavy metals 2019 PrM (ppb)									
ID	Cr	Mn	Fe	Ni	Cu	Zn	As	Ba	U
1	3.260	19.005	1394.266	2.178	3.385	8.001	2.427	12.865	2.809
2	2.614	20.072	1410.266	2.191	3.397	8.107	2.543	12.915	2.793
3	2.328	22.124	1534.948	2.244	2.950	7.855	2.918	13.420	2.691
4	2.698	23.174	1723.146	2.281	2.521	7.523	3.136	13.935	2.602
5	2.834	22.565	1838.328	2.388	2.775	7.702	2.886	14.583	2.583
6	2.993	21.248	1919.757	2.629	3.239	8.009	2.356	15.860	2.537
7	3.616	21.054	1822.505	3.145	3.250	22.497	2.194	16.142	2.303
8	3.639	18.829	1473.971	3.099	2.650	32.227	2.009	13.812	1.830
9	3.143	13.915	914.870	2.610	1.671	37.353	1.538	9.510	1.096
10	3.422	15.193	864.926	2.547	1.400	42.788	1.678	8.403	1.439
11	3.933	22.198	1462.106	2.514	2.057	34.197	2.329	10.848	3.072
12	3.684	22.849	1541.943	2.319	5.687	30.874	2.573	11.061	3.819
13	2.928	18.571	1213.813	2.051	10.639	32.332	2.452	9.546	3.715
14	2.550	16.433	1049.748	1.918	13.115	33.061	2.392	8.789	3.663
15	2.298	15.007	940.371	1.829	14.766	33.547	2.351	8.284	3.628
16	2.641	16.830	882.010	1.614	8.332	26.580	3.359	8.938	6.457
17	2.359	13.240	726.126	1.216	ND	23.742	3.804	6.807	5.590
18	1.767	6.557	258.642	1.051	ND	34.265	3.666	3.808	1.659
19	4.814	8.742	404.013	2.249	ND	31.945	5.044	4.611	2.447
20	4.925	7.593	539.921	2.077	ND	28.808	4.717	4.577	2.029
21	1.927	5.862	516.820	ND	1.156	30.466	3.423	3.590	ND
22	1.489	6.177	444.091	ND	ND	23.115	3.357	3.215	ND
23	1.627	8.171	429.434	ND	ND	19.524	3.635	3.472	1.004
24	2.341	11.846	472.849	1.299	ND	19.692	4.256	4.362	2.131
25	2.637	13.966	627.409	1.506	ND	18.735	3.985	5.844	2.948
26	2.514	14.532	893.115	1.512	ND	16.652	2.824	7.919	3.454
27	3.553	11.678	783.500	1.995	ND	31.410	2.837	7.060	3.036
28	5.753	5.405	298.563	2.956	ND	63.008	4.025	3.267	1.693
29	10.212	2.780	81.291	3.587	ND	95.806	4.209	1.415	ND
30	16.930	3.805	131.684	3.890	1.137	129.803	3.389	1.504	ND
31	10.975	3.297	168.912	2.443	ND	81.118	3.325	1.700	ND
32	2.221	2.838	150.401	ND	ND	16.137	4.094	1.534	ND
33	2.367	3.287	114.759	ND	ND	16.376	4.171	1.247	ND
34	1.536	3.064	104.559	ND	ND	15.451	3.480	1.306	ND
35	2.144	3.092	102.406	1.324	ND	29.067	2.830	2.483	ND
36	4.191	3.369	108.299	2.639	1.230	57.225	2.221	4.778	ND
37	5.341	4.124	98.554	3.191	1.430	119.266	1.802	5.605	ND
38	5.531	5.048	79.516	3.034	1.288	191.208	1.632	5.124	ND
39	5.658	5.665	66.825	2.929	1.193	239.170	1.518	4.804	ND
40	5.249	5.093	73.369	2.804	1.455	167.790	1.817	5.108	1.889
41	4.806	4.792	154.257	2.767	1.793	72.081	2.169	5.995	3.041

ID	Cr	Mn	Fe	Ni	Cu	Zn	As	Ba	U
42	4.863	5.950	290.252	2.840	1.852	71.387	2.164	6.842	3.035
43	4.949	7.686	494.245	2.950	1.939	70.346	2.157	8.113	3.025
44	5.122	11.159	902.230	3.169	2.115	68.265	2.142	10.655	3.007
45	5.467	18.106	1718.201	3.608	2.465	64.102	2.111	15.739	2.970
46	6.156	31.998	3350.144	4.487	3.167	55.775	2.051	25.907	2.895
47	7.536	59.784	6614.028	6.244	4.569	39.123	1.929	46.242	2.746
48	8.501	63.760	7712.478	7.287	5.446	30.696	1.916	48.924	2.654
49	6.804	66.374	6865.738	5.941	6.911	29.390	1.434	39.916	1.596
50	4.853	51.479	5368.573	4.152	7.717	20.828	ND	20.158	ND
51	7.210	55.660	5533.159	5.130	6.204	19.157	1.525	34.237	1.325
52	10.286	76.979	8774.159	7.486	6.000	24.023	2.431	57.629	2.264
53	11.310	99.144	8805.741	9.099	7.182	27.935	2.788	73.004	2.388
54	8.501	101.044	8837.323	7.900	6.941	26.896	2.410	53.803	1.643
55	6.062	86.915	6873.779	6.265	6.062	31.881	2.263	45.127	1.164
56	6.502	68.918	6636.105	6.030	5.203	28.995	2.006	43.054	1.710
57	6.748	63.634	7217.610	6.001	4.885	22.488	1.909	47.356	1.953
58	8.123	79.167	8893.651	7.157	5.874	31.207	3.048	56.529	2.004
59	8.466	83.050	9312.662	7.446	6.122	33.387	3.332	58.823	2.016

Heavy metals 2019 PoM (ppb)									
ID	Cr	Mn	Fe	Ni	Cu	Zn	As	Ba	U
1	ND	5.423	334.246	ND	1.262	12.153	3.624	3.173	ND
2	ND	7.752	429.832	ND	1.266	11.172	3.992	3.848	ND
3	ND	11.246	573.210	1.028	1.272	9.700	4.544	4.862	1.124
4	1.135	18.234	859.968	1.107	1.284	6.757	5.648	6.888	1.914
5	1.369	21.063	978.813	1.186	1.430	4.776	6.194	7.775	2.365
6	1.304	17.404	834.160	1.241	1.705	4.741	5.815	6.848	2.216
7	2.201	18.303	1179.585	2.152	2.585	6.439	4.992	9.359	1.986
8	3.596	22.397	1806.210	3.479	3.698	9.012	4.042	13.822	1.752
9	4.526	25.126	2223.961	4.363	4.440	10.728	3.409	16.797	1.597
10	4.568	19.902	2260.565	3.679	3.767	10.702	2.683	14.180	1.226
11	3.721	6.724	1916.024	1.426	1.678	8.935	1.866	5.973	ND
12	3.085	7.604	1657.618	1.062	1.241	7.610	1.873	5.573	1.364
13	2.556	15.513	1442.279	1.641	1.631	6.505	2.294	9.077	2.746
14	2.079	16.173	1248.475	1.367	1.304	5.511	2.299	8.778	3.290
15	1.762	16.613	1119.272	1.185	1.086	4.848	2.303	8.578	3.653
16	1.692	17.822	1121.054	1.169	1.131	4.623	2.460	8.974	3.997
17	1.735	9.452	595.602	1.247	1.537	4.952	2.467	5.161	3.402
18	1.645	7.354	665.139	1.547	2.671	5.397	3.847	4.844	1.888
19	4.290	36.668	2739.766	3.636	4.759	12.676	7.269	21.351	1.422
20	5.599	48.887	983.393	5.149	5.677	17.540	8.099	21.928	1.477
21	4.164	38.117	2722.464	4.782	5.145	16.167	7.124	21.448	1.219
22	4.058	36.248	2539.861	4.607	4.658	17.807	7.301	20.371	1.174

ID	Cr	Mn	Fe	Ni	Cu	Zn	As	Ba	U
23	3.248	28.651	2761.706	3.734	3.627	15.037	6.492	16.169	1.066
24	1.733	15.326	1387.999	2.163	2.051	7.856	4.697	8.844	ND
25	1.388	8.368	662.553	2.035	1.586	7.983	3.575	5.018	ND
26	2.212	7.778	585.367	3.352	2.231	15.419	3.126	4.691	ND
27	2.172	7.927	567.796	3.287	2.238	16.242	2.765	4.474	ND
28	1.267	8.815	609.841	1.841	1.607	10.453	2.490	4.366	ND
29	ND	8.975	606.200	1.074	1.184	7.322	2.299	4.217	ND
30	ND	8.406	556.875	ND	ND	6.850	2.192	4.026	ND
31	ND	7.615	482.212	ND	ND	6.552	1.578	3.223	ND
32	ND	6.602	382.211	ND	ND	6.428	0.876	5.479	ND
33	ND	5.589	282.210	ND	ND	6.304	0.688	7.579	ND
34	ND	4.576	182.209	ND	ND	6.180	0.596	5.853	ND
35	ND	3.086	180.018	ND	ND	6.575	0.623	5.042	1.114
36	ND	1.119	275.637	ND	ND	7.489	0.768	5.145	1.721
37	1.216	7.384	612.423	ND	ND	8.859	1.783	7.033	2.631
38	1.458	13.659	804.721	1.117	1.167	8.254	2.726	8.519	3.057
39	1.282	12.200	659.702	ND	1.055	5.976	2.727	7.996	2.785
40	1.165	11.227	563.023	ND	ND	4.457	2.728	7.647	2.604
41	1.082	11.799	585.500	ND	1.274	7.223	2.834	7.747	2.635
42	1.046	13.388	691.726	1.116	1.771	12.509	2.992	8.158	2.819
43	1.028	14.182	744.839	1.230	2.019	15.153	3.072	8.364	2.910
44	1.019	14.579	771.396	1.286	2.144	16.474	3.111	8.466	2.956
45	1.015	14.777	784.674	1.315	2.206	17.135	3.131	8.518	2.979
46	1.012	14.877	791.313	1.329	2.237	17.466	3.141	8.543	2.991
47	1.011	14.943	795.739	1.338	2.258	17.686	3.148	8.560	2.998
48	ND	15.272	803.012	1.416	4.648	12.096	2.904	8.642	2.995
49	ND	15.698	775.803	1.179	4.820	7.665	2.640	9.810	1.644
50	ND	15.567	804.082	ND	1.813	6.428	2.609	9.774	1.422
51	9.251	72.265	819.883	6.312	3.533	18.918	3.004	42.786	3.756
52	9.094	70.598	737.297	6.208	3.610	18.790	2.475	42.856	3.158
53	ND	10.306	616.870	ND	1.246	3.539	1.009	8.852	ND
54	ND	12.266	800.427	ND	1.684	6.528	1.102	9.610	1.304
55	1.068	15.069	969.730	1.116	1.562	7.671	1.813	9.434	2.441
56	1.461	16.828	1129.639	1.192	2.016	6.106	1.861	9.612	2.241
57	2.233	23.875	1710.077	1.840	2.780	6.900	1.627	12.892	1.907
58	2.808	32.804	2357.456	2.775	2.435	7.671	1.242	17.370	1.604
59	2.951	35.037	2519.301	3.008	2.348	7.863	1.146	18.490	1.528

Heavy metals 2021 PrM (ppb)									
ID	Cr	Mn	Fe	Ni	Cu	Zn	As	Ba	U
1	3.305	18.990	1389.218	2.168	3.378	8.002	2.481	12.815	2.816
2	3.214	19.020	1399.314	2.188	3.392	8.000	2.372	12.914	2.801
3	2.014	21.124	1421.218	2.193	3.401	8.213	2.714	12.915	2.784
4	2.642	23.124	1648.678	2.294	2.498	7.497	3.121	13.925	2.598
5	2.754	23.224	1797.613	2.268	2.543	7.548	3.151	13.945	2.606
6	2.914	21.907	1879.043	2.509	3.007	7.856	2.621	15.222	2.560
7	3.073	20.589	1960.472	2.749	3.471	8.163	2.091	16.498	2.514
8	4.159	21.519	2151.205	3.541	3.028	36.831	2.296	15.785	1.676
9	3.120	16.140	1613.404	2.656	2.271	27.623	1.722	11.839	1.257
10	3.166	11.690	1266.336	2.563	1.071	47.083	1.353	7.180	ND
11	3.677	18.695	1513.516	2.530	1.728	38.493	2.004	9.625	1.944
12	4.188	25.700	1760.696	2.497	2.385	29.902	2.654	12.070	3.888
13	3.180	19.997	1323.190	2.141	8.988	31.846	2.493	10.051	3.750
14	2.676	17.146	1104.436	1.962	12.290	32.818	2.412	9.042	3.680
15	2.424	15.720	995.060	1.873	13.940	33.304	2.371	8.537	3.646
16	2.172	14.294	885.683	1.784	15.591	33.790	2.331	8.032	3.611
17	3.109	15.366	916.337	1.443	1.073	19.370	4.387	9.843	3.302
18	1.609	5.113	235.914	ND	ND	28.114	3.220	3.770	1.878
19	1.924	8.001	281.370	1.114	ND	40.415	4.111	3.846	1.440
20	7.704	9.482	526.656	3.384	ND	23.475	5.977	5.376	3.453
21	2.146	5.704	553.185	ND	1.359	34.141	3.456	3.777	ND
22	1.708	6.019	480.456	ND	ND	26.791	3.390	3.402	ND
23	1.270	6.334	407.726	ND	ND	19.440	3.324	3.027	ND
24	1.984	10.009	451.141	ND	ND	19.608	3.945	3.917	1.348
25	2.698	13.683	494.556	1.503	ND	19.776	4.566	4.807	2.695
26	2.576	14.249	760.262	1.509	ND	17.694	3.405	6.882	3.201
27	2.453	14.815	1025.968	1.515	ND	15.611	2.243	8.956	3.707
28	4.653	8.542	541.031	2.476	ND	47.209	3.431	5.163	2.364
29	6.853	2.268	56.094	3.436	ND	78.807	4.619	1.370	1.021
30	13.571	3.293	106.487	3.739	ND	112.805	3.799	1.459	ND
31	20.289	4.317	156.880	4.041	1.230	146.802	2.979	1.548	ND
32	1.660	2.277	180.943	ND	ND	15.434	3.671	1.851	ND
33	2.782	3.398	119.859	ND	ND	16.839	4.516	1.217	ND
34	1.952	3.176	109.659	ND	ND	15.914	3.825	1.276	ND
35	1.121	2.953	99.459	ND	ND	14.988	3.134	1.335	ND
36	3.168	3.230	105.352	1.648	ND	43.146	2.525	3.630	ND
37	5.214	3.507	111.245	3.296	1.525	71.304	1.916	5.925	ND
38	5.468	4.740	85.862	3.087	1.335	167.228	1.689	5.285	ND
39	5.594	5.357	73.171	2.982	1.240	215.189	1.575	4.964	ND
40	5.721	5.973	60.479	2.877	1.145	263.151	1.461	4.644	ND
41	4.777	4.213	86.259	2.730	1.764	72.428	2.172	5.571	3.044
42	4.834	5.371	222.254	2.803	1.822	71.734	2.167	6.418	3.038

ID	Cr	Mn	Fe	Ni	Cu	Zn	As	Ba	U
43	4.892	6.528	358.249	2.876	1.881	71.040	2.162	7.266	3.032
44	5.007	8.844	630.240	3.023	1.998	69.653	2.152	8.960	3.019
45	5.237	13.475	1174.221	3.316	2.232	66.877	2.132	12.350	2.994
46	5.697	22.737	2262.182	3.901	2.699	61.326	2.091	19.128	2.945
47	6.616	41.260	4438.105	5.073	3.634	50.225	2.010	32.685	2.846
48	8.455	78.307	8789.951	7.415	5.504	28.021	1.848	59.799	2.647
49	8.547	75.213	8635.005	7.159	5.387	33.371	1.983	58.048	2.661
50	5.060	57.534	7096.470	4.722	8.435	25.409	ND	21.783	ND
51	4.646	45.424	7640.675	3.581	6.998	16.247	ND	18.532	ND
52	9.774	65.896	7425.642	6.679	5.409	22.067	2.252	49.941	2.202
53	10.798	78.061	6622.675	8.293	6.591	25.979	2.609	55.316	2.326
54	11.822	90.226	5819.708	9.906	7.773	29.891	2.966	60.691	2.450
55	5.180	91.861	5854.937	5.893	6.108	23.900	1.854	26.915	ND
56	6.943	81.968	6892.621	6.637	6.016	39.861	2.672	43.339	1.492
57	6.060	55.867	6379.589	5.423	4.390	18.128	1.340	42.769	1.927
58	7.435	71.400	8055.631	6.579	5.380	26.848	2.479	51.943	1.978
59	8.810	86.933	9731.672	7.735	6.369	35.567	3.617	61.116	2.029

Heavy metals 2021 PoM (ppb)									
ID	Cr	Mn	Fe	Ni	Cu	Zn	As	Ba	U
1	ND	4.258	286.453	ND	1.260	12.644	3.440	2.835	ND
2	ND	6.587	382.039	ND	1.264	11.663	3.808	3.511	ND
3	ND	8.917	477.625	ND	1.268	10.682	4.176	4.186	ND
4	ND	13.576	668.796	ND	1.276	8.719	4.912	5.537	1.220
5	1.402	22.893	1051.139	1.159	1.292	4.794	6.384	8.239	2.440
6	1.337	19.234	906.487	1.214	1.568	4.759	6.005	7.312	2.291
7	1.271	15.574	761.834	1.268	1.843	4.723	5.625	6.384	2.141
8	3.131	21.033	1597.335	3.037	3.327	8.155	4.359	12.334	1.830
9	4.061	23.762	2015.086	3.921	4.069	9.870	3.725	15.309	1.675
10	4.991	26.491	2432.836	4.805	4.811	11.586	3.092	18.284	1.519
11	4.144	13.246	2088.295	2.403	2.406	9.819	2.275	10.077	ND
12	3.297	ND	1743.753	ND	ND	8.052	1.457	1.869	ND
13	2.874	15.039	1571.482	1.748	1.203	7.168	2.290	9.277	1.917
14	2.238	15.936	1313.076	1.421	ND	5.842	2.297	8.878	2.876
15	1.921	16.385	1183.873	1.258	ND	5.180	2.301	8.678	3.355
16	1.603	16.833	1054.670	1.094	ND	4.517	2.305	8.478	3.834
17	1.780	18.810	1187.437	1.243	1.284	4.729	2.615	9.469	4.159
18	1.690	ND	1173.766	1.250	1.790	5.175	2.319	ND	2.645
19	1.600	14.613	1326.512	1.843	2.552	5.620	3.375	8.834	1.131
20	6.980	58.722	2153.020	2.428	2.965	6.732	2.162	7.868	1.713
21	4.217	39.051	2213.766	1.869	2.388	5.347	3.035	8.987	1.241
22	4.111	37.182	2171.163	2.194	1.902	6.987	2.713	8.410	1.197
23	4.005	35.313	2128.559	2.519	1.415	8.627	2.390	7.832	1.152

ID	Cr	Mn	Fe	Ni	Cu	Zn	As	Ba	U
24	2.003	21.988	1414.853	1.948	1.339	6.446	3.095	6.507	ND
25	ND	8.663	701.146	1.377	1.263	4.265	3.799	5.181	ND
26	1.312	8.073	623.960	2.694	1.909	11.701	3.351	4.855	ND
27	2.624	7.483	546.774	4.010	2.554	19.137	2.902	4.528	ND
28	1.312	8.371	588.819	2.564	1.923	13.348	2.627	4.420	ND
29	ND	9.259	630.863	1.118	1.291	7.558	2.352	4.312	ND
30	ND	8.690	581.538	ND	ND	7.086	2.245	4.121	ND
31	ND	8.121	532.212	ND	ND	6.614	2.138	3.930	ND
32	ND	7.108	432.211	ND	ND	6.490	1.018	2.516	ND
33	ND	6.095	332.211	ND	ND	6.366	ND	8.442	ND
34	ND	5.082	232.210	ND	ND	6.242	ND	6.716	ND
35	ND	4.069	132.209	ND	ND	6.118	ND	4.990	ND
36	ND	2.035	227.828	ND	ND	7.032	ND	5.094	ND
37	ND	ND	323.446	ND	ND	7.946	ND	5.197	1.619
38	1.575	14.632	901.400	1.243	1.242	9.773	2.725	8.868	3.238
39	1.341	12.686	708.042	ND	ND	6.736	2.727	8.171	2.876
40	1.223	11.713	611.362	ND	ND	5.217	2.727	7.822	2.694
41	1.106	10.740	514.683	ND	ND	3.698	2.728	7.473	2.513
42	1.058	12.858	656.318	ND	1.134	10.747	2.940	8.021	2.758
43	1.034	13.917	727.135	ND	1.701	14.272	3.045	8.295	2.880
44	1.022	14.447	762.543	ND	1.985	16.034	3.098	8.432	2.941
45	1.016	14.711	780.248	1.007	2.126	16.915	3.125	8.501	2.971
46	1.013	14.844	789.100	1.175	2.197	17.355	3.138	8.535	2.987
47	1.012	14.910	793.526	1.259	2.233	17.576	3.144	8.552	2.994
48	1.010	14.976	797.952	1.343	2.268	17.796	3.151	8.569	3.002
49	ND	15.567	808.071	1.489	7.028	6.396	2.656	8.714	2.988
50	ND	15.829	743.534	ND	2.611	8.933	2.623	10.905	ND
51	1.057	15.305	864.629	ND	1.014	3.922	2.595	8.643	2.543
52	1.445	19.224	782.043	1.637	6.052	3.913	3.412	7.929	2.969
53	ND	11.973	699.457	ND	1.169	3.667	1.298	8.783	1.272
54	ND	8.640	534.284	ND	1.323	3.411	ND	8.922	ND
55	1.160	15.892	1066.569	1.221	2.045	9.644	1.724	10.298	2.458
56	ND	14.246	872.891	1.011	1.078	5.697	1.902	8.570	2.423
57	1.946	19.410	1386.387	1.373	2.953	6.515	1.819	10.653	2.058
58	2.521	28.340	2033.767	2.308	2.608	7.286	1.435	15.131	1.755
59	3.095	37.269	2681.146	3.242	2.262	8.056	1.050	19.609	1.452
ND: Non detected									

PUBLICATION:

1. Paolenmang Haokip, Md. Abdullah Khan, Pandurang Choudhari, Luc Cimusa Kulimushi & Ibodullo Qaraev (2020). *Identification of erosion-prone areas using morphometric parameters, land use land cover and multi-criteria decision-making method: geo-informatics approach*. Environment, Development and Sustainability volume 24, pages 527–557 <https://doi.org/10.1007/s10668-021-01452-7>

SEMINAR/CONFERENCE:

1. Presented an oral presentation at International Conference on the topic “**Morphometric analysis of Lower and Middle Teesta Basin, Sikkim Himalaya using Geographical Information System Techniques.**” organized by Department of Geology Sikkim University, Gangtok, Sikkim, 8th – 9th October, 2020.
2. Presented an oral presentation at International Conference on the topic “**Water Quality Assessment of Teesta River, Sikkim Himalaya**” organized by Research Committee & Department of Computer Application, Patna Women’s College, Patna University, 5th – 7th May, 2022



Identification of erosion-prone areas using morphometric parameters, land use land cover and multi-criteria decision-making method: geo-informatics approach

Paolenmang Haokip¹ · Md. Abdullah Khan¹ · Pandurang Choudhari² ·
Luc Cimusa Kulimushi³ · Ibodullo Qaraev⁴

Received: 17 September 2020 / Accepted: 18 April 2021 / Published online: 4 May 2021
© The Author(s), under exclusive licence to Springer Nature B.V. 2021

Abstract

Soil erosion is the main driving force of several devastating natural hazards in the complex mountainous terrain of the Himalayas where the Teesta River basin is located. The present study focused on GIS-based multi-criteria analytical approach (MCA) that integrates morphometric parameters with land cover categories for identification of erosion hotspot areas through sub-watersheds prioritization. The general character of the eight sub-watersheds was derived from the linear, areal and relief aspects, while seven land cover types derived from maximum likelihood classification were evaluated in the MCA. Before combination of the studied parameters in MCA, each parameter was individually ranked and compound value (Cp) was calculated which produced four classes: low, medium, high and very high priority. Later, these ranks were integrated into MCA to give eight major classes classified from 1 to 8. Lowest Cp ranked 1 gets very high priority, while the highest Cp is ranked 8, i.e., lowest priority. The results revealed a predominance of dense forest account for 31.73% of the total area, the basin is a sixth-order river dominated by high relief and marginal slope, elongated in shape, and mean bifurcation ratio (Rb) was 3.879 which indicates an undistorted natural drainage system. Final MCA priority ranking indicated that: SW-4 and 5 having lowest Cp values (3.39 and 4) ranked 1 and 2 suggest very high erosion susceptibility, SW-8 and 3 (4.22 and 4.39) rated 3 and 4, i.e., high priority; SW-6 and 7 ranked 5 and 6, i.e., medium priority; and SW-1 and SW-2 ranked 7 and 8 because of their highest Cp (5.39 and 5.67), i.e., least priority. The prioritization result identified critical areas that are indispensable for sustainable use and management of water and land resources.

Keywords Morphometry · Land cover · Erosion susceptibility · Middle and Lower Teesta River basin · Geographic information system · Remote sensing · Sikkim

✉ Pandurang Choudhari
choudharipp79@gmail.com

Extended author information available on the last page of the article



Certificate of Participation

THIS IS TO CERTIFY THAT

Paolenmang Haakip, Sikkim University

PARTICIPATED IN


**ONLINE INTERNATIONAL CONFERENCE ON
“RECENT DEVELOPMENTS AND CHALLENGES IN
EARTH & ENVIRONMENTAL SCIENCES, NATURAL RESOURCE MANAGEMENT,
& CLIMATE CHANGE WITH SPECIAL FOCUS ON EASTERN HIMALAYAS”,**

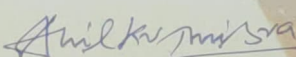
AS

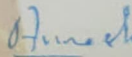
CHAIRMAN OF SESSION / CO-CHAIRMAN OF SESSION / INVITED SPEAKER / POSTER OR ORAL PRESENTATION / VOLUNTEER

Organized By

Department of Geology, Sikkim University from 8th to 9th October, 2020


Dr. Nishchal Wanjari
Organizing Secretary


Dr. Anil Kumar Misra
Convener & Head of Department


Prof. Avinash Khare
Vice Chancellor



Online International Conference

Empowering Smart Future through Scientific Development and Technology



Co-sponsored and Co-Chaired by MOL2NET, Switzerland,
Co-hosted and Co-sponsored by USEDAT- USA- Europe Data Analysis Congress Series

Certificate of Paper Presentation

Conferred To

Mr. Paolenmang Haokip

**Research Scholar , Sikkim University, Gangtok,
Sikkim**



for successfully presenting a paper entitled:

Water Quality Assessment of Teesta River, Sikkim Himalaya

during the Online International Conference on *Empowering Smart Future Through Scientific Development and Technology*, held from 5th - 7th May 2022, organized by the Research Committee & Department of Computer Applications (MCA), Patna Women's College (Autonomous), Patna University.



Dr. Sister M. Rashmi A.C.
CONFERENCE CHAIR
PRINCIPAL
PATNA WOMEN'S COLLEGE



Dr. Debjani Sarkar Ghose
SESSION CHAIR
Head, Department of Geography,
Patna Women's College



Dr. Bhawna Sinha
CONVENER
RESEARCH COORDINATOR &
HEAD, DEPARTMENT OF MCA,
PATNA WOMEN'S COLLEGE



Ms. Sushmita Chakraborty
ORGANIZING SECRETARY
ASST. PROFESSOR,
DEPARTMENT OF MCA
PATNA WOMEN'S COLLEGE